



Western Michigan University
ScholarWorks at WMU

Dissertations

Graduate College

5-2010

High-Throughput Screening Studies of Inhibition of Human Carbonic Anhydrase II and Bacterial Flagella Antimicrobial Activity

Albert A. Barrese III
Western Michigan University

Follow this and additional works at: <https://scholarworks.wmich.edu/dissertations>



Part of the Biochemistry, Biophysics, and Structural Biology Commons, and the Biology Commons

Recommended Citation

Barrese, Albert A. III, "High-Throughput Screening Studies of Inhibition of Human Carbonic Anhydrase II and Bacterial Flagella Antimicrobial Activity" (2010). *Dissertations*. 500.
<https://scholarworks.wmich.edu/dissertations/500>

This Dissertation-Open Access is brought to you for free and open access by the Graduate College at ScholarWorks at WMU. It has been accepted for inclusion in Dissertations by an authorized administrator of ScholarWorks at WMU. For more information, please contact wmu-scholarworks@wmich.edu.



HIGH-THROUGHPUT SCREENING STUDIES OF INHIBITION OF HUMAN
CARBONIC ANHYDRASE II AND BACTERIAL FLAGELLA
ANTIMICROBIAL ACTIVITY

by

Albert A. Barrese III

A Dissertation
Submitted to the
Faculty of The Graduate College
in partial fulfillment of the
requirements for the
Degree of Doctor of Philosophy
Department of Biological Sciences
Advisor: Brian C. Tripp, Ph.D.

Western Michigan University
Kalamazoo, Michigan
May 2010

UMI Number: 3410393

All rights reserved

INFORMATION TO ALL USERS

The quality of this reproduction is dependent upon the quality of the copy submitted.

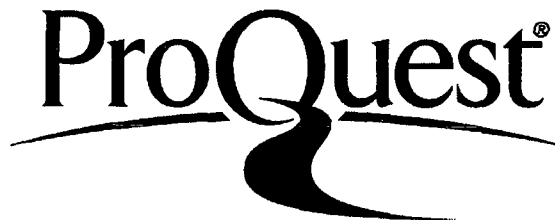
In the unlikely event that the author did not send a complete manuscript and there are missing pages, these will be noted. Also, if material had to be removed, a note will indicate the deletion.



UMI 3410393

Copyright 2010 by ProQuest LLC.

All rights reserved. This edition of the work is protected against unauthorized copying under Title 17, United States Code.



ProQuest LLC
789 East Eisenhower Parkway
P.O. Box 1346
Ann Arbor, MI 48106-1346

HIGH-THROUGHPUT SCREENING STUDIES OF INHIBITION OF HUMAN CARBONIC ANHYDRASE II AND BACTERIAL FLAGELLA ANTIMICROBIAL ACTIVITY

Albert A. Barrese III, Ph.D.

Western Michigan University, 2010

Carbonic anhydrase (CA) enzymes catalyze the reversible hydration of carbon dioxide to form bicarbonate and release a proton. There are currently five known CA structural families, α -, β -, γ -, δ -, and ζ -classes, as reviewed in Chapter One.

In Chapter Two, the hypothesis that a high-throughput screen (HTS) of diverse biologically active compounds could yield new structural insights into CA inhibition and identify new inhibitors for this enzyme was experimentally tested. Human CA II was screened against 960 structurally diverse, biologically active small molecules. The assay monitored CA II esterase activity against the substrate 4-nitrophenyl acetate (4-NPA) in a format allowing high-throughput screening. The assay proved to be robust and reproducible with a hit rate of <2%.

Chapter Three examines the functional mechanism of thioxolone. Analytical chemistry and biochemical methods were used to investigate the fate of thioxolone upon binding to CA II. When thioxolone binds in the active site of CA II it is cleaved and forms 4-mercaptobenzene-1,3-diol which then binds to the zinc active site via the thiol group, and is therefore the active CA inhibitor.

The preliminary development and validation of a novel methodology for the

high-throughput screening of antimicrobial compounds and inhibitors of bacterial motility is described in Chapter Four. Two basic techniques were combined to enable rapid screening for motility inhibitors; the classical bacterial swarming agar motility assay and the use of 96-well microplates common to HTS drug discovery techniques with a standard absorbance microplate reader. The feasibility of screening the *Salmonella typhimurium* SJW1103 strain, which is wild-type for flagellar motility and has peritrichously arranged flagella, was examined.

The non-physiological substrate, 4-nitrophenyl acetate, does not react with all known isozymes of α -class CAs or the γ -class CA from *M. thermophila*. Preliminary studies describing the subcloning and expression CA I and a truncated, soluble form of CA IV, are described in Chapter Five. This chapter also details the preliminary exploration of several alternative pH absorbance assays for measuring the catalytic activity of CAs. Finally, some possible directions for future research, based on the experimental results presented in Chapters 2-5, are discussed in Chapter Six.

Copyright by
Albert A. Barrese III
2010

ACKNOWLEDGMENTS

I would like to thank Dr. Tripp for his guidance, support, dedication and patience with me during my graduate study at Western Michigan University. He was a great mentor and I feel that the skills that I learned from him will start my scientific career off in a successful way.

I would also like to thank my committee members; Dr. John Geiser, Dr. James Kiddle, and Dr. Wendy Ransom-Hodgkins. Their suggestions and thoughtful insights have given me the opportunity to critically think about my work and at times see a new direction for my work to proceed in.

Lastly I would like thank my family and friends for their support and patience without them this work would not have been possible.

Albert A. Barrese III

TABLE OF CONTENTS

ACKNOWLEDGMENTS	ii
LIST OF TABLES.....	vii
LIST OF FIGURES	ix
CHAPTER	
I. OVERVIEW OF CARBONIC ANHYDRASE ENZYMES, INHIBITORS, AND BACTERIAL FLAGELLIN PROTEINS	1
Introduction.....	1
Carbonic Anhydrase Enzyme Classification, Protein Structures, and Catalytic Mechanisms.....	1
Inhibitors of Carbonic Anhydrase.....	15
Medical Applications of Carbonic Anhydrase Inhibitors	17
Bacterial Flagellin Protein	19
References.....	25
II. CA II INHIBITION STUDIES WITH THE GENESIS PLUS AND NCI DIVERSITY SET COMPOUND LIBRARIES	37
Introduction.....	37
Experimental Procedures	38
Compound Libraries	39
Esterase Activity Screening Assay	41
Inhibitor IC ₅₀ Measurement	42

Table of Contents-Continued

CHAPTER

Inhibitor K_d Measurement	45
Results.....	47
GenPlus Compound Library: Preliminary Identification of Hits	47
Reproducibility	55
Signal to Noise Characteristics	57
Enzyme and Substrate Stability	59
Hit Confirmation.....	60
I. Sulfonamide CAIs	60
II. Non-Sulfonamide CAIs.....	63
Hit Characterization.....	67
Results of IC_{50} Assays with 1 μ M CA II	68
Results of IC_{50} Assay with 5 μ M CA II.....	68
Hill Slope as an Indicator of Promiscuity	69
Results of IC_{50} Assay with 1 μ M CA II and Triton X-100.....	70
Dissociation Constant Assay Results.....	72
Comparison of IC_{50} and K_d Values	77
NCI Compound Library	79
Discussion	90

Table of Contents-Continued

CHAPTER

Limitations of 4-NPA Esterase Assay	90
Esterase vs. Fluorescence Screening Assays	92
References	94
III. MECHANISTIC STUDIES OF HUMAN CARBONIC ANHYDRASE II INHIBITION BY THIOXOLONE.....	101
Introduction.....	101
Experimental Procedures	104
Enzyme Expression and Purification	104
Materials	106
Preparation of 4-mercaptobenzene-1,3-diol (Compound 3) by acid hydrolysis of thioxolone (Compound 1)	106
Carbonic Anhydrase 4-NPA Esterase Inhibition Studies	109
Michaelis–Menten Enzyme Kinetic Studies.....	110
Liquid Chromatography–Mass Spectroscopic Studies	113
Results.....	115
Structure-Activity Relationship Study	115
Enzyme Kinetic Studies.....	129
Liquid Chromatography–Mass Spectroscopy Analysis of Thioxolone and Hydrolysis Products.....	136
Discussion	138
References.....	143

Table of Contents-Continued

CHAPTER

IV.	A HIGH-THROUGHPUT SCREENING ASSAY FOR DETECTING INHIBITION OF FLAGELLAR MOTILITY	148
	Introduction.....	148
	Experimental Procedures	149
	Results and Discussion	152
	References.....	166
V.	CARBONIC ANHYDRASE SUBCLONING, EXPRESSION, AND CO ₂ HYDRATION ACTIVITY ASSAY DEVELOPMENT...	168
	Carbonic Anhydrase Isozyme Subcloning and Expression	168
	Expression and Purification of γ -class Carbonic Anhydrase (Cam).....	192
	Sodium Bicarbonate pH Assay	196
	References.....	217
VI.	FUTURE WORK.....	219
	Reference	224
APPENDIX		
	Recombinant DNA Biosafety Approval	225

LIST OF TABLES

2.1. Potential carbonic anhydrase II inhibitor compounds identified in initial screen of Genesis Plus compound library, as confirmed by two statistical criteria.	49
2.2. Summary of IC ₅₀ values and K _d values for Genesis Plus hit compounds and model sulfonamide compounds	74
2.3 Carbonic anhydrase II inhibitor compounds identified in a screen of the NCI Diversity set compound library	83
3.1. Structures and apparent IC ₅₀ values for inhibition of human carbonic anhydrase II by thioxolone analogs.	119
3.2. Michaelis-Menten kinetic parameters determined for concentration-dependence of thioxolone inhibition of 4-nitrophenyl acetate hydrolysis by carbonic anhydrase II	131
3.3. Mechanism-based enzyme inactivation parameters determined for thioxolone inhibition of 4-nitrophenyl acetate hydrolysis by carbonic anhydrase II.....	136
4.1. Complete list of antibacterial compounds detected in screen of Genesis Plus library with offset motility detection method	161
5.1. Mammalian α -class carbonic anhydrase clone vector and sequence information	170
5.2. Sequencing results for the pET28c-CA I and pET28c-CA IV	176
5.3. Partial blastx search results with CA I DNA sequence results.	177
5.4. Partial blastx search results with CA IV DNA sequence results.	178
5.5. The translated peptide sequence for the subcloned carbonic anhydrase I and IV genes in the pET 28c-CA I and pET 28c-CA IV plasmids.....	179

List of Tables-Continued

5.6.	Comparison of the translated CA I pET28c-CA I plasmid DNA sequence to the wild-type protein sequence	180
5.7.	Comparison of pEt 28c-CA I V plasmid DNA sequence to the wild-type CA IV sequence	181
5.8.	Results of non-linear fit of standard CA II esterase assay IC ₅₀ data using Graph Pad Prism 4.0 sigmoidal dose-response model/curve fit.	206
5.9.	Results of non-linear fit for microplate format CA II CO ₂ hydration pH assay IC ₅₀ data using Graph Pad Prism 4.0 sigmoidal dose-response model/curve fit.....	206
5.10.	Statistical results of fluorescein MultiDrop 8-channel peristaltic test for three successive dispensing operations into 96-well microplates.....	209
5.11.	The concentration of reagents right after mixing the aqueous solution of sulphuric acid, cobalt sulphate, and potassium dihydrogen phosphate with an aqueous solution of sodium bicarbonate	210
5.12.	CA II carbonic acid dehydrating to CO ₂ pH assay. Assay components and concentrations.	212
5.13.	Comparison of standard 4-nitrophenyl acetate CA II esterase assay vs. CA II carbonic acid dehydrating to CO ₂ pH assay	213

LIST OF FIGURES

1.1. Ribbon diagram of human alpha-class carbonic anhydrase II enzyme structure.....	5
1.2. The active site of HCA II with the active site residues as labeled and the zinc atom shown as a grey sphere.	6
1.3. An example of β -carbonic anhydrase from the dicotyledonous plant <i>Pisum sativum</i>	9
1.4. γ -carbonic anhydrase from <i>Methanosarcina thermophila</i> , with the zinc ions as grey spheres and the three histidine residues that coordinate the zinc (His 81, His 117, and His 122) shown in stick form.....	12
1.5. The first ζ -class of carbonic anhydrase (CDCA1), from the marine diatom <i>Thalassiosira weissflogii</i>	14
1.6. Chemical structure of acetazolamide, a sulfonamide inhibitor of carbonic anhydrase II, molecular formula $C_4H_6N_4O_3S_2$	15
1.7. Complete structure of flagellin protein from <i>Salmonella typhimurium</i>	20
1.8. Bacterial flagella fibers and flagellin protein.....	21
2.1. Plot of example 4-NPA esterase IC_{50} data fit to Eq. 2.1 for two sulfonamide and two non-sulfonamide compounds identified as carbonic anhydrase inhibitors in the Genesis Plus compound library.	44
2.2. Initial results of screening the Genesis Plus 960 compound library for inhibitors of human CAII.....	48
2.3. Analysis of assay quality for each of the 12 compound plates in the Genesis Plus collection that were screened for inhibition of carbonic anhydrase 4-NPA esterase activity.....	56
2.4. Example of raw kinetic absorbance data simultaneously collected for eight compounds (column 8, plate 1) during initial screen of compound library for CA II inhibitors.	58

List of Figures-Continued

2.5.	Proposed reaction mechanism of thioxolone cleavage by CA II, based on crystallographic studies.....	65
2.6.	A possible pro-drug reaction mechanism for NCI compound NSC 320870-G, which involves ester bond hydrolysis to release an active terminal sulfonamide group.	90
3.1.	Chemical structure of thioxolone, a novel CA II inhibitor identified in a screen of the 960 compound Genesis Plus compound library.	101
3.2.	A view of the atomic arrangement of thioxolone, determined by X-ray diffraction, showing the atom-numbering scheme and 50% probability displacement ellipsoids.	102
3.3.	SDS polyacrylamide gel showing preinduction whole cell lysate and three hour post-induction whole cell lysate of CA II expression.	105
3.4.	SpectraMax raw data plot, showing the time range used to calculate initial enzyme velocity from the absorbance measurements at 348 nm wavelength of the colorimetric 4-NPA esterase reaction catalyzed by CA II.	111
3.5.	IC ₅₀ plots of 2-mercaptophenol (2-hydroxythiophenol, compound 4) and benzenethiol (compound 5) inhibition of CA II 4-NPA esterase activity.	117
3.6.	Crystal structure of CA II complexed with 2-hydroxythiophenol (compound 4).	124
3.7.	Crystal structure of CA II soaked with thioxolone..	125
3.8.	Kinetics studies of thioxolone inhibition of CA II esterase activity.....	132
3.9.	Time-dependence of thioxolone inhibition of CA II as monitored by apparent second order rate constant, k' , as a function of inhibitor incubation time.	134

List of Figures-Continued

3.10. Plot of CA II activity loss versus thioxolone concentration.	135
3.11. LC-MS of thioxolone products generated in the absence and presence of CA II.	138
3.12. Proposed reaction mechanism of thioxolone cleavage by CA II, based on crystallographic studies.....	139
4.1. Comparison of motile and non-motile bacterial growth patterns in 96-well plate formatted motility agar.....	153
4.2. Comparison of average absorbance readings for motile and non-motile <i>S. typhimurium</i> bacterial cells.....	155
4.3. Growth curves for motile and non-motile <i>S. typhimurium</i> bacterial cells inoculated in 96-well plate-formatted motility agar.	157
4.4. Plot of average Z' values and average absorbance (OD ₅₅₀) values for positive and negative controls for each of the 12 Genesis Plus library compound plates, using the offset-inoculation method.	159
4.5. Scatter plot of results of screening the Genesis Plus library of 960 compounds for inhibitors of microbial growth and motility, using the offset-inoculation method.	160
4.6. Enlarged images showing three types of growth patterns observed for <i>S. typhimurium</i> cells center-inoculated in the larger wells of the 24-well tissue culture plate.....	165
5.1. Agarose gel electrophoresis analysis of Pfu Turbo PCR product for the subcloned CA IV gene.....	173
5.2. Plasmid map of pET28c-CA I, showing the CA I gene, the kanamycin resistance gene, and the lac I gene.	182

List of Figures-Continued

5.3. Plasmid map of pET28c-CA IV, showing the CA IV gene, the kanamycin resistance gene, and the lac I gene	183
5.4. SDS-PAGE analysis of CA I and CA IV protein expression using the BL21-AI strain of <i>E. coli</i>	186
5.5. Plot of the initial FPLC purification run of CA IV protein using the ÄKTA™ FPLC instrument with the FPLC UNICORN™ software.	190
5.6. Plot of the FPLC purification run of CA I protein using the ÄKTA™ FPLC instrument with the FPLC UNICORN™ software and a 50 ml SP Sepharose FF column..	191
5.7. Plot of the first step of the FPLC purification of Cam protein using the ÄKTA™ FPLC instrument with the FPLC UNICORN™ software..	195
5.8. Plot of the second step of the FPLC purification of Cam protein via hydrophobic interaction chromatography.	196
5.9. Bicarbonate dehydration kinetic absorbance assay results for CA II - 10 mM NaHCO ₃ pH assay.....	198
5.10. Bicarbonate dehydration kinetic assay results for CA II - 60 mM NaHCO ₃ pH assay.....	200
5.11. Bicarbonate dehydration kinetic assay results for Cam - 60 mM NaHCO ₃ pH assay with serial dilution of Cam inhibitors.....	202
5.12. Comparison of CA II microplate format CO ₂ hydration pH assay IC ₅₀ vs. standard IC ₅₀ esterase assay with 1:2 diluted acetazolamide.....	205
5.13. Average fluorescein fluorescence emission value for each column.	209
5.14. IC ₅₀ plots for A. acetazolamide, B. sulfanilamide, and C. ethoxyzolamide using the CA II carbonic acid dehydrating to CO ₂ pH assay.....	214

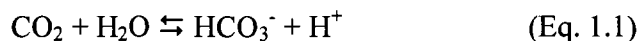
CHAPTER I

OVERVIEW OF CARBONIC ANHYDRASE ENZYMES, INHIBITORS, AND BACTERIAL FLAGELLIN PROTEINS

Introduction

Carbonic Anhydrase Enzyme Classification, Protein Structures, and Catalytic Mechanisms

Carbonic anhydrase (CA)¹ enzymes (EC 4.2.1.1) catalyze the reversible hydration of carbon dioxide to form bicarbonate and release a proton.



CAs use a two-step “ping-pong” mechanism¹⁻⁴ that typically involves a zinc ion cofactor functioning as a Lewis acid to ionize a water molecule, although other metal ion co-factors are known⁵⁻⁷. CAs are found in most eukaryotic and many microbial organisms^{8,9}. There are currently five known CA structural families, the structurally characterized α -, β -, and γ -classes and the more recently discovered δ - and ζ -classes^{1,6,7,10-13}.

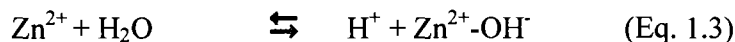
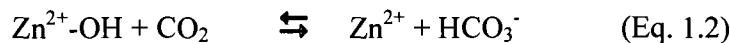
α -Class Carbonic Anhydrase

The α -class family of CA is found both in mammals and in bacteria. The mammalian α -class CA is represented by carbonic anhydrase II (CA II), which is the most studied of the α -carbonic anhydrases. First isolated and characterized in 1933, CA II was first reported by Meldrum and Roughton when they discovered an enzyme

in erythrocytes that catalyzed the reaction in equation 1.1^{14,15}. There are a total of 16 mammalian isozymes in this family designated as CA I, CA II, CA III, CA IV, CA VA, CA VB, CA VI, CA VII, CA VIII, CA IX, CA X, CA XI, CA XII, CA XIII, CA XIV, and CA XV^{10,16-20}. Thirteen of these isozymes have varying rates of measurable CO₂ hydration activity. CA II is the most active of the known α -class isozymes with a near diffusion-limited CO₂ hydration rate (k_{cat}) of 10^6 sec^{-1} at 25 °C^{2,4, 21,22}. Three mammalian α -class CA isozymes are catalytic inactive and have been labeled as CA-related proteins (CA-RPs): CA VIII, CA X, and CA XI¹⁷. In addition to the mammalian α -class CAs, α -CAs are also found in bacteria. These are structurally similar to the mammalian α -class CA II and are found in *Neisseria gonorrhoeae*²³⁻²⁵ and *Helicobacter pylori*²⁵⁻²⁷. Furthermore, several recent papers describe α -CAs that are found in the malaria parasite *Plasmodium falciparum*²⁸. At least three isozymes within this new α -class that have been identified²⁹. There is some evidence that inhibiting CA in this parasite with standard sulfonamide CA inhibitors can prevent the growth of *Plasmodium falciparum*²⁸⁻³⁰, and consequently, could have potential for the therapeutic treatment of malaria, a major human health problem in many tropical regions of the world.

All of the catalytically active α -class CAs share a strong degree of sequence conservation in their active sites. Any differences in their catalytic rates are due to the small differences in amino acid composition of the active site³¹. They all contain a zinc (II) (Zn²⁺) ion, which functions as a Lewis acid in the two-step reaction mechanism¹. The active species in the reaction mechanism are the zinc ion cofactor

and a hydroxide ion formed by the ionization of a water molecule.



X-ray crystallography studies of the CA II structure (Fig. 1.1) revealed a deep conical shape active site cavity (15 Å deep) with a zinc ion that is tetrahedrally coordinated to three histidines (His 94, His 96, and His 119) and a hydroxide ion³²⁻³⁸. The active site is divided between a cluster of hydrophobic amino acid residues (Val 121, Val 143, Leu 198, Val 207, and Trp 209) which form a hydrophobic pocket (Figure 1.2) near the zinc-bound hydroxide, and on the other side of the zinc, the surface is lined with hydrophilic residues Tyr 7, Asn 62, His 64, and Asn 67³²⁻³⁹. It is within this hydrophobic pocket of the active site where the CO₂ substrate is thought to bind and it is the linear binding orientation of CO₂ that makes the carbon of CO₂ more susceptible to nucleophilic attack^{32-34,39,40}. The actual binding of CO₂ in this region was only recently observed by X-ray crystallography studies with CO₂ under high pressure³⁹. The distance from Zn-OH to the CO₂ is about 3 Å for each of the oxygen atoms and 2.8 Å for the carbon, which is within a feasible distance for a nucleophilic attack from the zinc bound hydroxide^{33,41}. Crystallographic studies have also shown that a water molecule (the “deep water”) is positioned near the mouth of the hydrophobic pocket and is stabilized by the amide nitrogen of Thr 199 and the zinc-bound hydroxide. Consequently, it has been proposed that this water is displaced upon binding of CO₂ in the hydrophobic pocket^{32-34,39,40}.

Two mechanisms have been suggested for the release of the bicarbonate product after the nucleophilic attack of the hydroxide on the bound CO₂ molecule. The first, called the Lipscomb mechanism, suggests a Zn-HCO₃⁻ intermediate where a proton rapidly moves from the original Zn-OH⁻ to one of the oxygen atoms of the HCO₃⁻ ^{39,42}. The Lindskog mechanism is the second possibility and it proposes a Zn-HCO₃⁻ intermediate that requires one of the oxygen atoms of the original CO₂ molecule to coordinate directly with the zinc^{39,43}. There was a prior mutation study performed by Xue et al., where a T200H variant showed a higher affinity for HCO₃⁻ than wild-type CA II. This amino acid substitution allowed the variant to be crystallized with a bicarbonate in the active site, which showed support for the Lindskog mechanism after it was shown the CO₂ substrate exists in the same plane as HCO₃⁻ product^{39,44}.



Figure 1.1. Ribbon diagram of human alpha-class carbonic anhydrase II enzyme structure. The grey sphere shows the active site zinc ion coordinated to imidazole groups of three histidine residues. The PDB file 2AX2 was used with PyMol software to generate the figure.

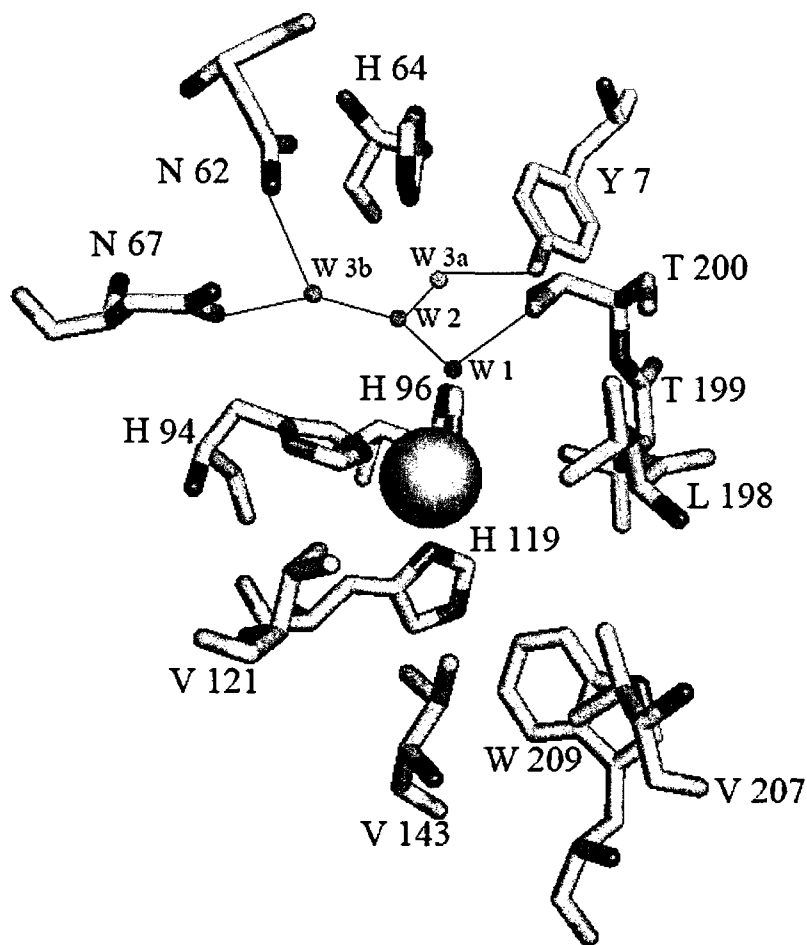


Figure 1.2. The active site of HCA II with the active site residues as labeled and the zinc atom shown as a grey sphere. The waters are shown as small grey spheres, labeled for their role in the transport of the proton from the zinc to the bulk solvent. Black lines are inferred hydrogen bonds⁴⁵. The PDB file 2AX2 was used with PyMol software to generate the figure.

Residue His 64 is located near the entrance of the CA II active site, approximately 8-12 Å from the active site zinc. This histidine residue has been shown by site-directed mutagenesis and chemical rescue experiments to be important for the high catalytic rate of CA II; the transfer of a proton from His 64 to bulk solvent appears to be the rate-limiting step^{38,46-48}. Furthermore, the side chain of this residue has been shown to have two distinct conformations in various X-ray crystal structures, one termed “in”, pointing inward toward the active site, and one termed “out”, pointing outward away from the active site. It is this apparent flexibility of His 64 which is essential to its function as an efficient proton shuttle^{35,45,49,50}. When His 64 adopts the “in” orientation it has an average distance of 7.5 Å from the Zn ion and when in the “out” orientation it is between 11 – 12 Å from the Zn ion³⁵.

The zinc-bound hydroxide ion functions as the catalyst in the interconversion of CO₂ to HCO³⁻ (Eq. 1.2), followed by binding of another neutral water molecule to the zinc. A proton is then transferred from the water ligand to the imidazole ring of His 64 via a “proton wire” composed of a well-defined network of hydrogen-bonded water molecules, and is ultimately transferred to the bulk solvent to regenerate the zinc bound hydroxide (Eq. 1.3). It has been shown by crystallographic studies that there is an intramolecular water wire consisting of 2-4 hydrogen-bonded water molecules 8-10 Å in the active site of CA II^{35-37,45,50-55}. These water molecules facilitate the transport of a proton from the enzyme active site to the solvent, via a Grotthus proton wire mechanism, and are stabilized by interactions with active site residues Tyr 7, Asn 62, Asn 67, Thr 199, and Thr 200 (Figure 1.2)^{35,45,50}. Thr 199

forms a hydrogen bond with the Zn bound solvent, which, in turn, is hydrogen bonded to water 1 (W1). W1 is further stabilized by Thr 200 and the next solvent in the chain, water 2 (W2). The solvent network then branches as W2 is hydrogen bonded to both water three 3a and water 3b (W3a and W3b). W3a is further coordinated by the hydroxyl group of Tyr 7, whereas W3b is stabilized by Asn 62 and Asn 67. This solvent network localizes W2, W3a, and W3b all in close proximity to His 64, when in the inward conformation (Figure 1.2)^{45,50}.

β -Class Carbonic Anhydrase

The β -class family of carbonic anhydrase (Figure 1.3) is found in plants, thermophilic Archaea, cyanobacteria, bacteria, algae, and marine diatoms^{8,11,56-62}. The β -CAs do not exhibit any sequence homology to any of the other classes of carbonic anhydrase and are high molecular mass, multimeric proteins that also contain Zn^{2+} as their metal ion^{56,60}. Unlike α - or γ -CA's the Zn^{2+} is coordinated by two cysteine residues and one histidine residue, in addition to the active site water molecule^{56,60}.



Figure 1.3. An example of β -carbonic anhydrase from the dicotyledonous plant *Pisum sativum*. The molecule is an octamer with a novel dimer of dimers of dimers arrangement⁶³. The zinc ions are shown as black spheres. The PDB file 1EKJ was used with PyMol software to generate the figure.

The β -CAs are mostly located in the chloroplast in plants and in a few different cellular locations in cyanobacteria and green algae, depending on the physiological function of the CA protein⁶¹. For example, in the green alga *Chlamydomonas reinhardtii*, CAs are expressed in the periplasmic space, the mitochondria, and the thylakoid lumen⁶¹.

CsoSCA (formerly CsoS3) is a bacterial carbonic anhydrase from *Halothiobacillus neapolitanus* and is localized in the carboxysome^{11,64}. It was first identified as a novel class of carbonic anhydrase (ϵ) because of its lack of homology at the primary structural level and its size (57 kDa, twice that of other CA's)^{11,64} but a recent crystal structure has revealed that it is actually a new sub-class of β -carbonic anhydrase. The crystal structure showed that CsoSCA contains three domains and is composed mostly of four α -helices, while the catalytic domain resembles other β -carbonic anhydrases⁶⁴. However, its lack of active site pairing is why it is considered to be a new sub-group of β -carbonic anhydrase⁶⁴. A more typical β -carbonic anhydrase maintains a pair of active sites within a two-fold homodimer or a pair of fused, homologous domains⁶⁴.

γ -Class Carbonic Anhydrase

The γ -class of carbonic anhydrase is found in Eubacteria, Archaea, and has recently been discovered in photosynthetic Eukaryotic organisms (plants and green algae)⁶⁵. The first known carbonic anhydrase enzyme in this class was isolated from the archaeon *Methanosarcina thermophila* and was termed Cam (Figure 1.4)⁶⁶. Cam

is a trimer, unlike the α -class CAs. It is composed of a left-handed β -helical structure and was only the second “hexapeptide repeat” protein with this novel secondary structure motif to have its structure determined by X-ray crystallography. It has three active sites, each located between two of the beta-helical domains. The metal ion species is thought to be either iron or zinc^{5,67}. The reason for the ambiguity of metal species is due to the organism from which it was first identified from, *Methanosarcina thermophila*. *M. thermophila* is an anaerobic moderate extremeophile that grows at 50 °C, and consequently, requires specialized anaerobic culture methods. When Cam was expressed in *Escherichia coli*, the enzyme could incorporate zinc (II) into the three-histidine active site to yield a catalytically active CA⁶⁷. However, iron was also frequently observed as a contaminant in this protein. A subsequent metal substitution study by Tripp, et al. (2004)⁵ indicated that the iron (II) form was significantly more active in catalyzing the CO₂-hydration reaction than the zinc (II) form, in the absence of oxygen, but this activity rapidly decreased in the presence of oxygen. In a more recent paper by the J.G. Ferry research group, the *in vivo* incorporation of iron in the Cam active site instead of zinc was reported⁶⁷. The use of a recombinant protein overproduction system was developed in *Methanosarcina acetivorans* to characterize oxygen-sensitive metalloenzymes from anaerobic species in the *Archaea* domain and this was used to overproduce Cam. The overproduced Cam was oxygen sensitive, and had fully incorporated iron (II) in its active site⁶⁷. These studies indicate that Cam evolved to use iron II as a Lewis acid catalyst instead of the more commonly used zinc II ion. While Cam is structurally

different at the level of tertiary and quaternary structure from the α -class CAs, it still performs the same catalytic function of reversible carbon dioxide hydration⁶⁸. This would suggest that the different structural classes of carbonic anhydrase evolved by convergent evolution⁶⁸. However, unlike CA II, Cam does not have any esterase activity with 4-NPA⁶⁹.



Figure 1.4. γ -carbonic anhydrase from *Methanosarcina thermophila*, with the zinc ions as grey spheres and the three histidine residues that coordinate the zinc (His 81, His 117, and His 122) shown in stick form. The PDB file 1THJ was used with PyMol software to generate the figure.

δ-Class Carbonic Anhydrase

The δ-class of CA was first isolated from the marine diatom *Thalassiosira weissflogii* and the protein discovered was a 27 kDa zinc metalloprotein (TWCA1)^{1,56,70}. The sequence analysis of TWCA1 indicates that it has less than 10% sequence homology to other known classes of CAs and none of the conserved regions defining α-, β-, and γ-CAs^{56,70}. This class of CA has also been found in a wide variety eukaryotic phytoplankton^{60,71}. No structure has been deposited in the protein data bank for this protein, as of June 2009.

ζ-Class Carbonic Anhydrase

The marine diatom *Thalassiosira weissflogii*, which was the source of the first known δ-class carbonic anhydrase, is also the organism from which the first ζ-class of carbonic anhydrase was isolated (CDCA1, Figure 1.5)⁶. CDCA1 is composed of three nearly identical repeats yielding a functional enzyme of roughly 66 kDa molecular mass. However, in the marine diatom *Thalassiosira pseudonana*, the CDCA1 protein appears to be a monomer of 26 kDa and is referred to as CDCA_{TP}⁶⁰. This new class is different from the other known structural classes of CA because it is the first class to use cadmium as the metal ion in the active site in the native form of the protein^{6,72,73}. A further study of marine phytoplankton reveals that CDCA1 is found exclusively in many of the marine diatom species^{60,72}. Because it has been shown that cadmium plays an important role in marine diatoms and is cycled thru the water column as a nutrient for marine diatoms, it is thought that this is an adaptation

of diatom species to limited availability of essential metals in ocean waters^{72,73}.

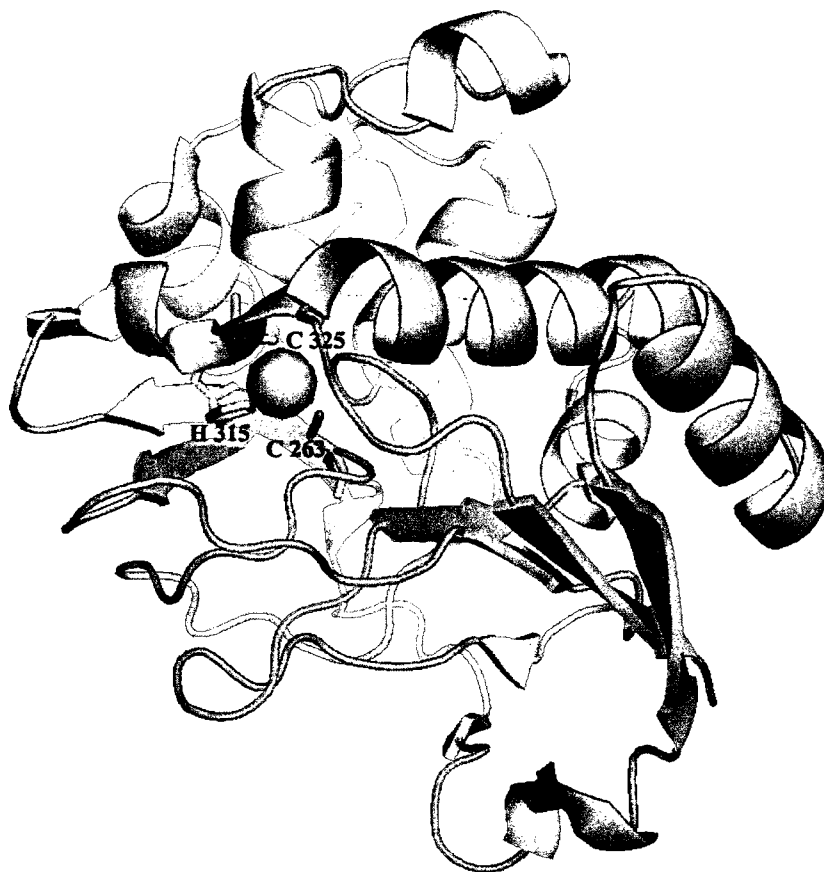


Figure 1.5. The first ζ -class of carbonic anhydrase (CDCA1), from the marine diatom *Thalassiosira weissflogii*. The cadmium ion is shown as a grey sphere. The cadmium is coordinated by three invariant residues in the CDCA isozymes of all diatom species⁷³: Cys 263, His 315, and Cys 325. The figure shows the second domain of CDCA1. The PDB file 3BOB was used with PyMol software to generate the figure.

Inhibitors of Carbonic Anhydrase

Given that most medically relevant CA isoforms are members of the α -class, the great majority of therapeutic inhibitors are targeted to one or more isozymes in the α -class. The classic CA inhibitors have been sulfonamides ($R-C-SO_2NH_2$). A few examples of classic CA inhibitors are acetazolamide (Figure 1.6), ethoxzolamide, and methazolamide^{17,74}.

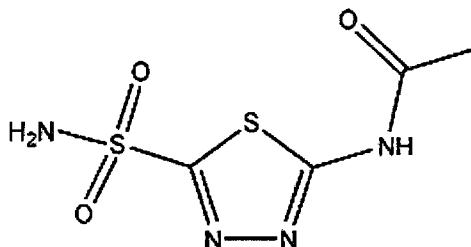


Figure 1.6. Chemical structure of acetazolamide, a sulfonamide inhibitor of carbonic anhydrase II, molecular formula $C_4H_6N_4O_3S_2$.

Other known α -class CA inhibitors include various anions (Cl^-), imidazole, phenol, hydroxyurea, carboxylates, organic phosphates, and phosphonates^{3,10,75}. The first organic CA inhibitor discovered was sulfanilamide, a sulfonamide compound⁷⁶. Furthermore, variations on the sulfonamide structure have yielded additional CA inhibitors; for example, sulfamates ($R-OSO_2-NH_2$), hydroxysulfonamides ($R-SO_2NH(OH)$), and hydroxamates ($R-CO-NH-OH$)^{10,17,18,77}. To date, therapeutic CA inhibitors have been based on sulfonamide, sulfamate, and hydroxamate functional groups that coordinate to the active site zinc ion^{17,77-80}. However, new classes of CA

inhibitors are being pursued by various research groups around the world, with one main objective of higher specificity for particular isozymes involved in particular infections, other disease states, or types of cancer. Other possible objectives include the generation of inhibitors without the potentially allergenic sulfonamide group, or that have novel mechanisms of action, such as activation in the cell or by the enzyme itself. A recent study by Maresca, et al.⁸¹ described the discovery and characterization of a novel coumarin CA inhibitor with a suicide inhibitor type of activation mechanism by the research group of Prof. Claudio T. Supuran in Italy. Another study described the activation of a CA inhibitor based on reduction of thiols inside the cell⁸². One of the earliest examples of a novel CA suicide inhibitor, thioxolone, was originally identified by the research group of Prof. B.C. Tripp at Western Michigan University, via high-throughput screening (HTS) of a library of biologically active compounds⁷⁴. A more detailed description of this study and a follow-up study of the mechanism of action in collaboration with the research groups of Prof. Robert McKenna and Prof. David N. Silverman at the University of Florida are described in detail as part of this thesis.

Thioxolone as a Novel Class of Carbonic Anhydrase Inhibitor

Thioxolone represents an example of a new class of CA inhibitor that does not have a sulfonamide or sulfamate group. This novel CA inhibitor was discovered during a high-throughput screen of 960 biologically active compounds, along with a number of known carbonic anhydrase inhibitors, in a study by Iyer et al.⁷⁴. An

expanded description of screening studies with two separate compound libraries is presented in Chapter Two of this thesis.

Thioxolone is proposed to be a pro-drug inhibitor that is cleaved via a CA II zinc-hydroxide mechanism known to catalyze the hydrolysis of esters. When thioxolone binds in the active site of CA II, it is cleaved and forms 4-mercaptobenzene-1,3-diol, via the intermediate S-(2,4-thiophenyl)hydrogen thiocarbonate. The esterase cleavage product binds to the zinc active site via the thiol group, and is therefore postulated to be the active CA inhibitor, while the intermediate is located at the rim of the active-site cavity. Because this type of pro-drug inhibitor mechanism depends on cleavage of ester bonds, this class of inhibitor may have advantages over sulfonamides in determining isozyme specificity. Thioxolone is an example of a CA inhibitor that could potentially be used without the undesirable side effect of allergic reactions that a significant number of people have to sulfonamide-based drugs. However, there have been studies that suggest thioxolone may have toxicity in some people and it has been linked to contact dermatitis⁸³⁻⁸⁵. The reader is referred to Chapter Three of this thesis for a detailed mechanistic study of the fate of thioxolone upon binding to CA II.

Medical Applications of Carbonic Anhydrase Inhibitors

Mammalian α -CAs have important physiological functions including pH control, bicarbonate metabolism, gluconeogenesis, lipogenesis, ureagenesis and regulation of intracellular osmotic pressure^{20,86}. Consequently, a number of α -class CA isozymes, e.g., CA II and CA IV, are the intended targets of drugs that function

as CA inhibitors. CA inhibitors are commonly used as diuretics for the treatment of symptoms of hypertension^{79,87}, as antiglaucoma drugs^{75,79}, and for the treatment of high altitude sickness, gastric and duodenal ulcers, epilepsy, memory function, and osteoporosis^{19,75,79,88}. More recently CA inhibitors have been shown to have potential as anti-obesity drugs. For example the anti-epileptic drug Topiramate was shown to reduce energy and fat gain in lean and obese Zucker rats²⁰. The CA IX and CA XII isozymes are also being investigated as potential targets of sulfonamide compounds for the treatment of certain types of cancers such as gliomas, papillary/follicular carcinomas, carcinomas of the bladder, nasopharyngeal carcinoma, head and neck, breast, squamous/basal cell carcinomas, and kidney tumors^{16,20,79,89}. Other uses being explored include treatment of osteoporosis and as a diagnostic tool in magnetic resonance imaging (MRI) and photon emission tomography (PET)⁷⁵. Furthermore, other α -class CA isozymes that may be therapeutically targeted by CA inhibitors are found in the prokaryotic mammalian pathogens *Neisseria gonorrhoeae*²³⁻²⁵, *Helicobacter pylori*^{26,27,90}, and the eukaryotic malarial parasite *Plasmodium falciparum*²⁸⁻³⁰. There is some evidence that inhibiting CA in this parasite with standard sulfonamide CA inhibitors affects the growth of *Plasmodium falciparum*²⁸⁻³⁰. There is also Rv1284 (β -class CA) from *Mycobacterium tuberculosis* that appears to have a vital role in the survival of *Mycobacterium tuberculosis* and could be therapeutically targeted by CA inhibitors⁶².

Effective intraocular pressure reduction in the treatment of glaucoma requires large doses of sulfonamide drugs. These drugs often have poor specificity for the

targeted isozyme, which is CA IV, resulting in a wide array of undesirable side effects including altered taste, malaise, fatigue, depression, and anorexia⁹¹⁻⁹⁴. Furthermore, a significant fraction of the human population has demonstrated an allergic reaction towards some sulfonamide-based drugs⁹⁵⁻⁹⁷. Because of the many different roles that CAs have in the physiological function of various diseases, it would be useful to develop therapeutic inhibitors to CAs that can be used by people without the complication of an allergic reaction to sulfonamide drugs. Thus, the discovery of new classes of non-sulfonamide CA inhibitors, potentially with more controlled specificity for different CA isozymes, could lead to the development of useful alternatives to existing drugs.

Bacterial Flagellin Protein

Bacterial flagella are protein nanotubes with an inner diameter of 2-3 nm and outer diameter of about 20 nm, with lengths of up to 15 μm ⁹⁸. These fibers are primarily composed of a globular bacterial protein termed flagellin (Figure 1.7)⁹⁸. Bacterial flagellin monomers self-assemble into helical flagella bundles (Figure 1.8) through non-covalent interactions between N- and C-terminal α -helical coiled-coil domains to form the flagellar fiber⁹⁸. Flagellin also has solvent-accessible D2 and D3 domains located on the surface of the flagellar fiber that form the “knobs” on the surface of the flagellar fiber⁹⁸.

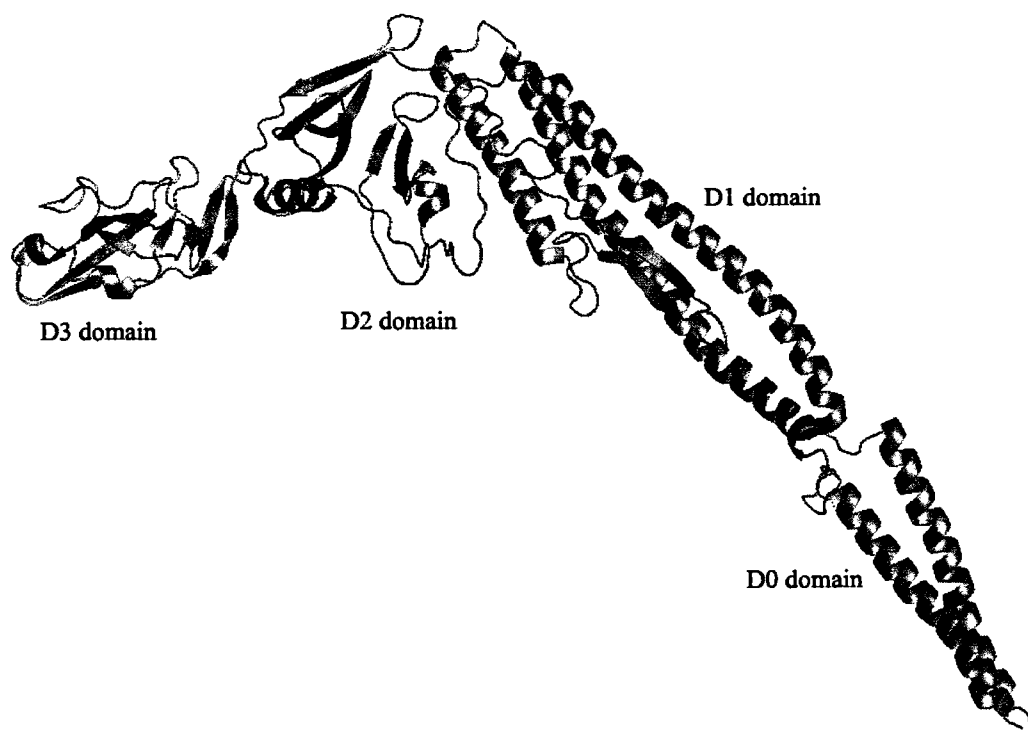


Figure 1.7. Complete structure of flagellin protein from *Salmonella typhimurium*. The PDB file 1UCU was used with PyMol software to generate the figure.

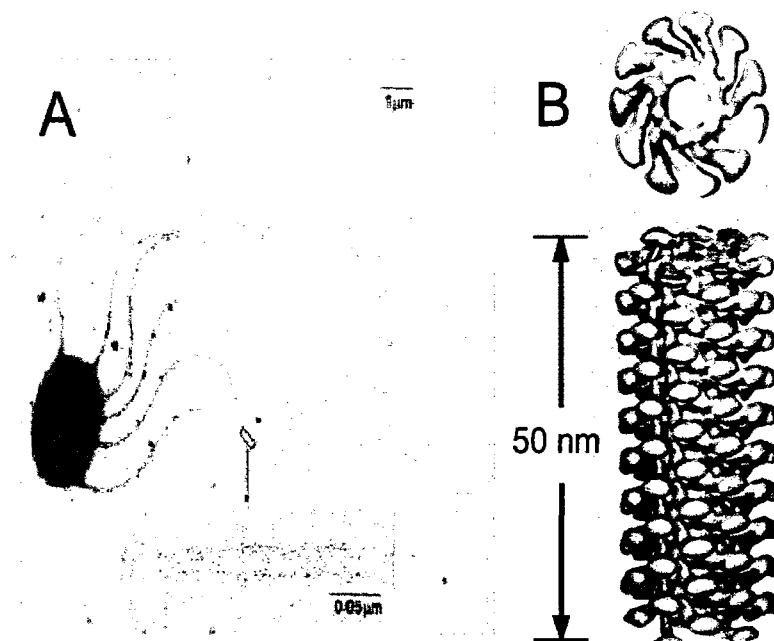


Figure 1.8. Bacterial flagella fibers and flagellin protein. **A.** Electron micrograph of negatively stained bacterium of *Salmonella typhimurium*. **B.** Three-dimensional structure of the helical flagellar filament of *Salmonella typhimurium* determined by X-ray fiber diffraction. Cross-sectional view (top) image shows the 20-30 Å central pore. The side-view (bottom) shows the multivalent display of the hypervariable, solvent-exposed central domains on surface of flagella. The figure was adapted from a photograph by K. Namba⁹⁹.

Antibiotic resistance in bacteria is currently a growing, major public health problem because bacteria may soon evolve resistance to all known antibiotics¹⁰⁰⁻¹⁰². Bacterial signal transduction components, efflux pumps, and genes involved in motility and biofilm formation represent some of the possible targets for antibiotic drug discovery research^{103,104}. Bacterial motility frequently involves the chemotaxis-controlled rotation of flagella,^{105,106} which are also involved in evasion of host

immunity,¹⁰⁷ host colonization, and biofilm formation.¹⁰⁸ Thus, the bacterial flagellar system represents a possible target for antimicrobial drugs. Motility inhibitors could potentially be used with other antimicrobial compounds to prevent the spread of infectious pathogens in the environment or the host organism. An HTS assay for detecting inhibition of flagellar motility or other types of bacterial motility, e.g. pili-mediated motility, could be used for screening compounds for antimicrobial activity and also in fundamental structure-function studies of genes and proteins involved in motility. In Chapter Four a detailed study and development of a novel HTS screening assay for antimicrobial and antimotility is presented.

The following chapters of this thesis describe several experimental investigations into the molecular function and mechanism of inhibition of a mammalian carbonic anhydrase enzyme, a bacterial flagellin protein, and their interactions with a library of small molecules. The following chapters describe results in further detail that were previously presented in three peer reviewed publications^{41,74,109}.

In Chapter Two, the hypothesis that a high-throughput screen of diverse biologically active compounds could yield new structural insights into CA inhibition and identify new inhibitors for this enzyme was experimentally tested. A colorimetric assay for the 4-NPA esterase activity¹¹⁰ was adapted to a high-throughput format and used to screen the Genesis Plus library of compounds. This strategy of screening biologically characterized compounds (i.e., “old” drugs on “new” targets) has been described previously¹¹¹. This chapter describes the use of HTS to test ligand

interaction with CA II, resulting in the identification of at least two novel classes of CA inhibitors. Also in Chapter Two, CA II was screened against the NCI Diversity set, which is a collection of 1990 compounds (more information on the Diversity set can be found in Chapter Two's experimental section). Approximately 40 compounds were identified in the initial screen as possible inhibitors of CA II. Subsequently, IC_{50} studies of those hits were performed to confirm the initial screening results and determine relative potencies of inhibition. Chapter Three examines the functional mechanism of thioxolone, a compound identified as a weak inhibitor of human carbonic anhydrase II by Iyer et al.,⁷⁴ as described in detail in Chapter Two of this thesis. Thioxolone lacks sulfonamide, sulfamate, or hydroxamate functional groups that are typically found in therapeutic CA inhibitors, such as acetazolamide. Analytical chemistry and biochemical methods were used to investigate the fate of thioxolone upon binding to CA II, including Michaelis-Menten kinetics of 4-nitrophenyl acetate esterase cleavage, liquid chromatography-mass spectrometry (LC-MS), oxygen-18 isotope exchange studies and X-ray crystallography, in collaboration with the research groups of Prof. Robert McKenna and Prof. David N. Silverman, at the University of Florida.

A high-throughput screening (HTS) assay for detecting inhibition of flagellar motility or other types of bacterial motility, e.g. pili-mediated motility, could be used for screening compounds for antimicrobial activity and also in fundamental structure-function studies of genes and proteins involved in motility. The preliminary development and validation of a novel methodology for the high-throughput

screening of antimicrobial compounds and inhibitors of bacterial motility is described in Chapter Four. Two basic techniques were combined to enable rapid screening for motility inhibitors; the classical bacterial swarming agar motility assay and the use of 96-well microplates common to HTS drug discovery techniques with a standard absorbance microplate reader. Different versions of motility assays have been used for the chemotaxis experiments on both prokaryotic¹¹² and eukaryotic cells. The feasibility of screening the *Salmonella typhimurium* SJW1103 strain¹¹³, which is wild-type for flagellar motility and has peritrichously arranged flagella, was examined. For the non-motile control, the *S. typhimurium* SJW134 strain¹¹⁴ that has both the *fliC* and *fljB* flagellin genes knocked out and cannot produce flagella fibers was used.

The colorimetric absorbance assay used for HTS and inhibition studies of the CA II enzyme in Chapters 2 and 3 are not applicable to all isozymes. The non-physiological substrate, 4-nitrophenyl acetate, does not react with all known isozymes of α -class CAs or the γ -class CA from *M. thermophila*, Cam. Preliminary studies describing the subcloning and expression of several other CA isozymes, CA I and a truncated, soluble form of CA IV, are described in Chapter Five. This chapter also details the preliminary exploration of several alternative pH absorbance assays for measuring the catalytic activity of CAs. Finally, some possible directions for future research, based on the experimental results presented in Chapters 2-5, are discussed in Chapter Six.

References

1. Tripp, B.; Smith, K.; Ferry, J. Carbonic anhydrase: new insights for an ancient enzyme. *Journal of Biological Chemistry* 2001, 276, 48615-48618.
2. Lindskog, S.; Silverman, D. N. The catalytic mechanism of mammalian carbonic anhydrases. *Exs* 2000, 175-95.
3. Lindskog, S. Structure and mechanism of carbonic anhydrase. *Pharmacol. Ther.* 1997, 74, 1-20.
4. Khalifah, R. G. Reflections on Edsall's carbonic anhydrase: paradoxes of an ultra fast enzyme. *Biophysical Chemistry* 2003, 100, 159-170.
5. Tripp, B.; Bell, C.; Cruz, F.; Krebs, C.; Ferry, J. A Role for iron in an ancient carbonic anhydrase. *Journal of Biological Chemistry* 2004, 279, 6683-6687.
6. Lane, T. W.; Saito, M. A.; George, G. N.; Pickering, I. J.; Prince, R. C.; Morel, F. M. Biochemistry: a cadmium enzyme from a marine diatom. *Nature* 2005, 435, 42.
7. Lane, T. W.; Morel, F. M. Regulation of carbonic anhydrase expression by zinc, cobalt, and carbon dioxide in the marine diatom *Thalassiosira weissflogii*. *Plant Physiol.* 2000, 123, 345-52.
8. Smith, K. S.; Jakubzick, C.; Whittam, T. S.; Ferry, J. G. Carbonic anhydrase is an ancient enzyme widespread in prokaryotes. *Proc Natl Acad Sci U S A* 1999, 96, 15184-9.
9. Smith, K. S.; Ferry, J. G. Prokaryotic carbonic anhydrases. *FEMS Microbiol Rev* 2000, 24, 335-66.
10. Supuran, C. T.; Scozzafava, A.; Conway, J. Carbonic anhydrase: its inhibitors and activators. CRC Press: New York, 2004; Vol. 1, p 363.
11. So, A. K.; Espie, G. S.; Williams, E. B.; Shively, J. M.; Heinhorst, S.; Cannon, G. C. A novel evolutionary lineage of carbonic anhydrase (epsilon class) is a component of the carboxysome shell. *J Bacteriol* 2004, 186, 623-30.

12. Cox, D.; Hunt, J.; Compher, K.; Fierke, C.; Christianson, D. Structural influence of hydrophobic core residues on metal binding and specificity in carbonic anhydrase II. *Biochemistry* 2000, 39, 13687-13694.
13. Zimmerman, S. A.; Ferry, J. G.; Supuran, C. T. Inhibition of the archaeal beta-class (Cab) and gamma-class (Cam) carbonic anhydrases. *Curr. Top. Med. Chem.* 2007, 7, 901-8.
14. Stadie, W. C.; O'Brien, H. The catalysis of the hydration of carbon dioxide and dehydration of carbonic acid by an enzyme isolated from red blood cells. *J. Biol. Chem.* 1933, 103, 521-529.
15. Meldrum, N.; Roughton, F. Carbonic Anhydrase: Its preparation and properties. *Journal of Physiology* 1933, 80, 113-141.
16. Saarnio, J. Distribution of carbonic anhydrase isoenzyme IX, MN/CA IX, in normal and neoplastic gastrointestinal and hepatobiliary tissues. Its potential value as a new biomarker and comparison of its expression with that of isoenzymes I, II, IV, V, and VI. University of Oulu, Oulu, Finland, 2000.
17. Supuran, C. T.; Scozzafava, A.; Casini, A. Carbonic anhydrase inhibitors. *Medicinal Research Reviews* 2003, 23, 146-189.
18. Supuran, C. T.; Vullo, D.; Manole, G.; Casini, A.; Scozzafava, A. Designing of novel carbonic anhydrase inhibitors and activators. *Curr. Med. Chem.* 2004, 2, 49-68.
19. Pastorekova, S.; Parkkila, S.; Pastorek, J.; Supuran, C. T. Carbonic anhydrases: current state of the art, therapeutic applications and future prospects. *J. Enzyme Inhib. Med. Chem.* 2004, 19, 199-229.
20. Supuran, C. T. Carbonic anhydrases: novel therapeutic applications for inhibitors and activators. *Nat Rev Drug Discov* 2008, 7, 168-81.
21. Khalifah, R. The carbon dioxide hydration activity of carbonic anhydrase: stop-flow kinetic studies on the native human isozymes B and C. *Journal of Biological Chemistry* 1971, 246, 2561-2573.

22. Sly, W.; Hu, P. Human carbonic anhydrases and carbonic anhydrase deficiencies. *Annual Review of Biochemistry* 1995, 64, 375-401.
23. Sanders, E.; Maren, T. H. Inhibition of carbonic anhydrase in *Neisseria*: effects on enzyme activity and growth. *Mol. Pharmacol.* 1967, 3, 204-15.
24. Huang, S.; Xue, Y.; Sauer-Eriksson, E.; Chirica, L.; Lindskog, S.; Jonsson, B. H. Crystal structure of carbonic anhydrase from *Neisseria gonorrhoeae* and its complex with the inhibitor acetazolamide. *J Mol Biol* 1998, 283, 301-10.
25. Elleby, B.; Chirica, L. C.; Tu, C.; Zeppezauer, M.; Lindskog, S. Characterization of carbonic anhydrase from *Neisseria gonorrhoeae*. *Eur J Biochem* 2001, 268, 1613-9.
26. Nishimori, I.; Minakuchi, T.; Morimoto, K.; Sano, S.; Onishi, S.; Takeuchi, H.; Vullo, D.; Scozzafava, A.; Supuran, C. T. Carbonic anhydrase inhibitors: DNA cloning and inhibition studies of the alpha-carbonic anhydrase from *Helicobacter pylori*, a new target for developing sulfonamide and sulfamate gastric drugs. *J. Med. Chem.* 2006, 49, 2117-26.
27. Chirica, L. C.; Elleby, B.; Lindskog, S. Cloning, expression and some properties of alpha-carbonic anhydrase from *Helicobacter pylori*. *Biochim Biophys Acta* 2001, 1544, 55-63.
28. Krungkrai, J.; Scozzafava, A.; Reungprapavut, S.; Krungkrai, S. R.; Rattanajak, R.; Kamchonwongpaisan, S.; Supuran, C. T. Carbonic anhydrase inhibitors: inhibition of *Plasmodium falciparum* carbonic anhydrase with aromatic sulfonamides towards antimalarials with a novel mechanism of action. *Bioorg Med Chem* 2005, 13, 483-9.
29. Reungprapavut, S.; Krungkrai, S. R.; Krungkrai, J. *Plasmodium falciparum* carbonic anhydrase is a possible target for malaria chemotherapy. *Journal of Enzyme Inhibition and Medicinal Chemistry* 2004, 19, 249-256.
30. Sein, K. K.; Aikawa, M. The pivotal role of carbonic anhydrase in malaria infection. *Med Hypotheses* 1998, 50, 19-23.

31. Tu, C.; Qian, M.; Earnhardt, J. N.; Laipis, P. J.; Silverman, D. N. Properties of intramolecular proton transfer in carbonic anhydrase III. *Biophys J* 1998, 74, 3182-9.
32. Liang, J. Y.; Lipscomb, W. N. Binding of substrate CO₂ to the active site of human carbonic anhydrase II: a molecular dynamics study. *Proc Natl Acad Sci USA* 1990, 87, 3675-9.
33. Fierke, C. A.; Calderone, T. L.; Krebs, J. F. Functional consequences of engineering the hydrophobic pocket of carbonic anhydrase II. *Biochemistry* 1991, 30, 11054-63.
34. Alexander, R. S.; Nair, S. K.; Christianson, D. W. Engineering the hydrophobic pocket of carbonic anhydrase II. *Biochemistry* 1991, 30, 11064-72.
35. Maupin, C. M.; Voth, G. A. Preferred orientations of His64 in human carbonic anhydrase II. *Biochemistry* 2007, 46, 2938-47.
36. Eriksson, A. E.; Jones, T. A.; Liljas, A. Refined structure of human carbonic anhydrase II at 2.0 Å resolution. *Proteins* 1988, 4, 274-82.
37. Hakansson, K.; Carlsson, M.; Svensson, L. A.; Liljas, A. Structure of native and apo carbonic anhydrase II and structure of some of its anion-ligand complexes. *J Mol Biol* 1992, 227, 1192-204.
38. Jude, K. M.; Banerjee, A. L.; Haldar, M. K.; Manokaran, S.; Roy, B.; Mallik, S.; Srivastava, D. K.; Christianson, D. W. Ultrahigh resolution crystal structures of human carbonic anhydrases I and II complexed with "two-prong" inhibitors reveal the molecular basis of high affinity. *J Am Chem Soc* 2006, 128, 3011-8.
39. Domsic, J. F.; Avvaru, B. S.; Kim, C. U.; Gruner, S. M.; Agbandje-McKenna, M.; Silverman, D. N.; McKenna, R. Entrapment of carbon dioxide in the active site of carbonic anhydrase II. *J Biol Chem* 2008, 283, 30766-71.
40. Merz, K. CO₂ Binding to human carbonic anhydrase II. *Journal of the American Chemical Society* 1991, 113, 406-411.
41. Barrese, A. A., 3rd; Genis, C.; Fisher, S. Z.; Orwenyo, J. N.; Kumara, M. T.; Dutta, S. K.; Phillips, E.; Kiddle, J. J.; Tu, C.; Silverman, D. N.; Govindasamy,

- L.; Agbandje-McKenna, M.; McKenna, R.; Tripp, B. C. Inhibition of carbonic anhydrase II by thioxolone: a mechanistic and structural study. *Biochemistry* 2008, 47, 3174-84.
42. Liang, J. Y.; Lipscomb, W. N. Hydration of carbon dioxide by carbonic anhydrase: internal proton transfer of Zn²⁺-bound HCO₃⁻. *Biochemistry* 1987, 26, 5293-301.
 43. Lindskog, S. in *Zinc Enzymes*. Wiley: New York, 1983; p 77.
 44. Xue, Y.; Vidgren, J.; Svensson, L. A.; Liljas, A.; Jonsson, B. H.; Lindskog, S. Crystallographic analysis of Thr-200-->His human carbonic anhydrase II and its complex with the substrate, HCO₃⁻. *Proteins* 1993, 15, 80-7.
 45. Fisher, S. Z.; Tu, C.; Bhatt, D.; Govindasamy, L.; Agbandje-McKenna, M.; McKenna, R.; Silverman, D. N. Speeding up proton transfer in a fast enzyme: kinetic and crystallographic studies on the effect of hydrophobic amino acid substitutions in the active site of human carbonic anhydrase II. *Biochemistry* 2007, 46, 3803-13.
 46. Jackman, J. E.; Merz, K. M., Jr.; Fierke, C. A. Disruption of the active site solvent network in carbonic anhydrase II decreases the efficiency of proton transfer. *Biochemistry* 1996, 35, 16421-8.
 47. Tu, C. K.; Silverman, D. N.; Forsman, C.; Jonsson, B. H.; Lindskog, S. Role of histidine 64 in the catalytic mechanism of human carbonic anhydrase II studied with a site-specific mutant. *Biochemistry* 1989, 28, 7913-8.
 48. Qian, M.; Tu, C.; Earnhardt, J. N.; Laipis, P. J.; Silverman, D. N. Glutamate and aspartate as proton shuttles in mutants of carbonic anhydrase. *Biochemistry* 1997, 36, 15758-64.
 49. Nair, S. K.; Calderone, T. L.; Christianson, D. W.; Fierke, C. A. Altering the mouth of a hydrophobic pocket: structure and kinetics of human carbonic anhydrase II mutants at residue Val-121. *J. Biol. Chem.* 1991, 266, 17320-5.
 50. Fisher, Z.; Hernandez Prada, J. A.; Tu, C.; Duda, D.; Yoshioka, C.; An, H.; Govindasamy, L.; Silverman, D. N.; McKenna, R. Structural and kinetic

- characterization of active-site histidine as a proton shuttle in catalysis by human carbonic anhydrase II. *Biochemistry* 2005, 44, 1097-105.
51. Lesburg, C. A. a. C., David W. X-ray Crystallographic studies of engineered hydrogen bond networks in a protein-zinc binding site. *J. Am. Chem. Soc.* 1995, 117, 6838-6844.
 52. Toba, S.; Colombo, G.; Merz, K. M. J. Solvent dynamics and mechanism of proton transfer in human carbonic anhydrase II. *J. Am. Chem. Soc.* 1999, 121, 2290-2302.
 53. Lu, D., and Voth, G. A. Proton transfer in the enzyme carbonic anhydrase: an ab initio study. *J. Am. Chem. Soc.* 1988, 120, 4006-4014.
 54. Cui, Q.; Karplus, M. Is a "proton wire" concerted or stepwise: a model study of proton transfer in carbonic anhydrase. *J. Phys. Chem. B* 2003, 107, 1071-1078.
 55. Riccardi, D.; Schaefer, P.; Yang, Y.; Yu, H.; Ghosh, N.; Prat-Resina, X.; Konig, P.; Li, G.; Xu, D.; Guo, H.; Elstner, M.; Cui, Q. Development of effective quantum mechanical/molecular mechanical (QM/MM) methods for complex biological processes. *Journal of Physical Chemistry B* 2006, 110, 6458-69.
 56. Cox, E. H.; McLendon, G. L.; Morel, F. M.; Lane, T. W.; Prince, R. C.; Pickering, I. J.; George, G. N. The active site structure of *Thalassiosira weissflogii* carbonic anhydrase. *Biochemistry* 2000, 39, 12128-30.
 57. Harada, H.; Nakatsuma, D.; Ishida, M.; Matsuda, Y. Regulation of the expression of intracellular beta-carbonic anhydrase in response to CO₂ and light in the marine diatom *Phaeodactylum tricornutum*. *Plant Physiol* 2005, 139, 1041-50.
 58. Kitao, Y.; Harada, H.; Matsuda, Y. Localization and targeting mechanisms of two chloroplastic beta-carbonic anhydrases in the marine diatom *Phaeodactylum tricornutum*. *Physiol Plant* 2008, 133, 68-77.
 59. Badger, M. R.; Price, G. D. Carbonic anhydrase activity associated with the cyanobacterium *Synechococcus* PCC7942. *Plant Physiol* 1989, 89, 51-60.

60. McGinn, P. J.; Morel, F. M. Expression and regulation of carbonic anhydrases in the marine diatom *Thalassiosira pseudonana* and in natural phytoplankton assemblages from Great Bay, New Jersey. *Physiol Plant* 2008, 133, 78-91.
61. Tanaka, Y.; Nakatsuma, D.; Harada, H.; Ishida, M.; Matsuda, Y. Localization of soluble beta-carbonic anhydrase in the marine diatom *Phaeodactylum tricornutum*. sorting to the chloroplast and cluster formation on the girdle lamellae. *Plant Physiol* 2005, 138, 207-17.
62. Suarez Covarrubias, A.; Larsson, A. M.; Høgbom, M.; Lindberg, J.; Bergfors, T.; Björkelid, C.; Mowbray, S. L.; Unge, T.; Jones, T. A. Structure and function of carbonic anhydrases from *Mycobacterium tuberculosis*. *J Biol Chem* 2005, 280, 18782-9.
63. Kimber, M. S.; Pai, E. F. The active site architecture of *Pisum sativum* beta-carbonic anhydrase is a mirror image of that of alpha-carbonic anhydrases. *Embo J* 2000, 19, 1407-18.
64. Sawaya, M. R.; Cannon, G. C.; Heinhorst, S.; Tanaka, S.; Williams, E. B.; Yeates, T. O.; Kerfeld, C. A. The structure of beta-carbonic anhydrase from the carboxysomal shell reveals a distinct subclass with one active site for the price of two. *J Biol Chem* 2006, 281, 7546-55.
65. Parisi, G.; Perales, M.; Fornasari, M. S.; Colaneri, A.; Gonzalez-Schain, N.; Gomez-Casati, D.; Zimmermann, S.; Brennicke, A.; Araya, A.; Ferry, J. G.; Echave, J.; Zabaleta, E. Gamma carbonic anhydrases in plant mitochondria. *Plant Mol Biol* 2004, 55, 193-207.
66. Alber, B. E.; Ferry, J. G. A carbonic anhydrase from the archaeon *Methanosarcina thermophila*. *Proceedings of the National Academy of Sciences* 1994, 91, 6909-6913.
67. Macauley, S. R.; Zimmerman, S. A.; Apolinario, E. E.; Evilia, C.; Hou, Y. M.; Ferry, J. G.; Sowers, K. R. The archetype gamma-class carbonic anhydrase (Cam) contains iron when synthesized in vivo. *Biochemistry* 2009, 48, 817-9.

68. Alber, B. E.; Colangelo, C. M.; Dong, J.; Stalhandske, C. M.; Baird, T. T.; Tu, C.; Fierke, C. A.; Silverman, D. N.; Scott, R. A.; Ferry, J. G. Kinetic and spectroscopic characterization of the gamma-carbonic anhydrase from the methanoarchaeon *Methanosarcina thermophila*. *Biochemistry* 1999, 38, 13119-28.
69. Alber, B. E.; Ferry, J. G. Characterization of heterologously produced carbonic anhydrase from *Methanosarcina thermophila*. *J Bacteriol* 1996, 178, 3270-4.
70. Roberts, S. B. Carbonic anhydrase in the marine diatom *Thalassiosira weissflogii* (Bacillariophyceae). *J. Phycol* 1997, 33, 845-850.
71. Lapointe, M.; Mackenzie, T. D.; Morse, D. An external delta-carbonic anhydrase in a free-living marine dinoflagellate may circumvent diffusion-limited carbon acquisition. *Plant Physiol* 2008, 147, 1427-36.
72. Park, H.; Song, B.; Morel, F. M. Diversity of the cadmium-containing carbonic anhydrase in marine diatoms and natural waters. *Environ Microbiol* 2007, 9, 403-13.
73. Xu, Y.; Feng, L.; Jeffrey, P. D.; Shi, Y.; Morel, F. M. Structure and metal exchange in the cadmium carbonic anhydrase of marine diatoms. *Nature* 2008, 452, 56-61.
74. Iyer, R.; Barrese, A. A., 3rd; Parakh, S.; Parker, C. N.; Tripp, B. C. Inhibition profiling of human carbonic anhydrase II by high-throughput screening of structurally diverse, biologically active compounds. *J Biomol Screen* 2006, 11, 782-91.
75. Supuran, C. T.; Scozzafava, A. Carbonic anhydrase inhibitors and their therapeutic potential. *Expert Opinion on Therapeutic Patents* 2000, 10, 575-600.
76. Mann, B.; Keilin, D. Sulphanilamide as a specific inhibitor of carbonic anhydrase. *Nature* 1940, 146, 164-165.

77. Winum, J. Y.; Scozzafava, A.; Montero, J. L.; Supuran, C. T. New zinc binding motifs in the design of selective carbonic anhydrase inhibitors. *Mini Rev. Med. Chem.* 2006, 6, 921-36.
78. Scolnick, L.; Clements, M.; Liao, J.; Crenshaw, L.; Hellberg, M.; May, J.; Dean, T.; Christianson, D. Novel binding mode of hydroxamate: inhibitors to human carbonic anhydrase II. *Journal of the American Chemical Society* 1997, 119, 850-851.
79. Supuran, C.; Scozzafava, A. Applications of carbonic anhydrase inhibitors and activators in therapy. *Expert Opinion on Therapeutic Patents* 2002, 12, 217-241.
80. Winum, J. Y.; Scozzafava, A.; Montero, J. L.; Supuran, C. T. Sulfamates and their therapeutic potential. *Medicinal Research Reviews* 2005, 25, 186-228.
81. Maresca, A.; Temperini, C.; Vu, H.; Pham, N. B.; Poulsen, S. A.; Scozzafava, A.; Quinn, R. J.; Supuran, C. T. Non-zinc mediated inhibition of carbonic anhydrases: coumarins are a new class of suicide inhibitors. *J Am Chem Soc* 2009, 131, 3057-3062
82. De Simone, G.; Vitale, R. M.; Di Fiore, A.; Pedone, C.; Scozzafava, A.; Montero, J. L.; Winum, J. Y.; Supuran, C. T. Carbonic anhydrase inhibitors: hypoxia-activatable sulfonamides incorporating disulfide bonds that target the tumor-associated isoform IX. *J Med Chem* 2006, 49, 5544-51.
83. Camarasa, J. Contact dermatitis to thioxolone. *Contract Dermatitis* 1981, 7, 213-214.
84. Naher, H.; Frosch, P. J. Contact dermatitis to thioxolone. *Contact Dermatitis* 1987, 17, 250-1.
85. Villas Martinez, F.; Joral Badas, A.; Garmendia Goitia, J. F. Contact dermatitis from thioxolone. *Contact Dermatitis* 1993, 29, 96.
86. Maren, T.; Conroy, C. A new class of carbonic anhydrase inhibitor. *Journal of Biological Chemistry* 1993, 268, 26233-26239.

87. Maren, T. H. Carbonic anhydrase - chemistry physiology and inhibition. *Physiological Reviews* 1967, 47, 595-&.
88. Richalet, J. P.; Rivera, M.; Bouchet, P.; Chirinos, E.; Onnen, I.; Petitjean, O.; Bienvenu, A.; Lasne, F.; Moutereau, S.; Leon-Velarde, F. Acetazolamide: a treatment for chronic mountain sickness. *Am. J. Respir. Crit. Care Med.* 2005, 172, 1427-33.
89. Supuran, C. T.; Briganti, F.; Tilli, S.; Chegwidde, W. R.; Scozzafava, A. Carbonic anhydrase inhibitors: sulfonamides as antitumor agents? *Bioorganic & Medicinal Chemistry* 2001, 9, 703-714.
90. Nishimori, I.; Vullo, D.; Minakuchi, T.; Morimoto, K.; Onishi, S.; Scozzafava, A.; Supuran, C. T. Carbonic anhydrase inhibitors: cloning and sulfonamide inhibition studies of a carboxyterminal truncated alpha-carbonic anhydrase from *Helicobacter pylori*. *Bioorganic & Medicinal Chemistry Letters* 2006, 16, 2182-8.
91. Epstein, D. L.; Grant, W. M. Carbonic anhydrase inhibitor side effects: serum chemical analysis. *Archives of Ophthalmology* 1977, 95, 1378-1382.
92. Wallace, T.; Fraunfelder, F.; Petursson, G.; Epstein, D. Decreased libido-a side effect of carbonic anhydrase inhibitor. *Annals of Ophthalmology* 1979, 11, 1563-1566.
93. Lichter, P. R.; Newman, L. P.; Wheeler, N. C.; Beall, O. V. Patient tolerance to carbonic anhydrase inhibitors. *American journal of Ophthalmology* 1978, 85, 495-502.
94. Lichter, P. R. Reducing side effects of carbonic anhydrase inhibitors. *Ophthalmology* 1981, 88, 266-269.
95. Saxon, A.; Macy, E. Cross-reactivity and sulfonamide antibiotics. *New England Journal of Medicine* 2004, 350, 302-302.
96. Ray, W. Population-based studies of adverse drug effects. *New England Journal of Medicine* 2003, 349, 1592-1594.

97. Strom, B.; Schinnar, R.; Apter, A.; Margolis, D.; Lautenbach, E.; Hennessy, S.; Wilker, W.; Pettitt, D. Absence of cross-reactivity between sulfonamide antibiotics and sulfonamide nonantibiotics. *New England Journal of Medicine* 2003, 349, 1628-1635.
98. Macnab, R. M. How bacteria assemble flagella. *Annu Rev Microbiol* 2003, 57, 77-100.
99. Jones, C. J.; Aizawa, S. The bacterial flagellum and flagellar motor: structure, assembly and function. *Adv Microb Physiol* 1991, 32, 109-72.
100. Fishman, N. Antimicrobial stewardship. *Am J Med* 2006, 119, S53-61; discussion S62-70.
101. Tenover, F. C. Mechanisms of antimicrobial resistance in bacteria. *Am J Med* 2006, 119, S3-10; discussion S62-70.
102. Yoneyama, H.; Katsumata, R. Antibiotic resistance in bacteria and its future for novel antibiotic development. *Biosci Biotechnol Biochem* 2006, 70, 1060-75.
103. Danese, P. N. Antibiofilm approaches: prevention of catheter colonization. *Chem Biol* 2002, 9, 873-80.
104. Pages, J. M.; Masi, M.; Barbe, J. Inhibitors of efflux pumps in gram-negative bacteria. *Trends Mol Med* 2005, 11, 382-9.
105. Bardy, S. L.; Ng, S. Y.; Jarrell, K. F. Prokaryotic motility structures. *Microbiology* 2003, 149, 295-304.
106. Macnab, R. M. Type III flagellar protein export and flagellar assembly. *Biochim Biophys Acta* 2004, 1694, 207-17.
107. Andersen-Nissen, E.; Smith, K. D.; Strobe, K. L.; Barrett, S. L.; Cookson, B. T.; Logan, S. M.; Aderem, A. Evasion of toll-like receptor 5 by flagellated bacteria. *Proc Natl Acad Sci U S A* 2005, 102, 9247-52.
108. Costerton, J. W.; Stewart, P. S.; Greenberg, E. P. Bacterial biofilms: a common cause of persistent infections. *Science* 1999, 284, 1318-22.

109. Malapaka, V. R.; Barrese, A. A.; Tripp, B. C. High-throughput screening for antimicrobial compounds using a 96-well format bacterial motility absorbance assay. *J Biomol Screen* 2007, 12, 849-54.
110. Innocenti, A.; Casini, A.; Alcaro, M. C.; Papini, A. M.; Scozzafava, A.; Supuran, C. T. Carbonic anhydrase inhibitors: the first on-resin screening of a 4-sulfamoylphenylthiourea library. *J Med Chem* 2004, 47, 5224-9.
111. Wermuth, C. G. Selective optimization of side activities: another way for drug discovery. *J Med Chem* 2004, 47, 1303-14.
112. Adler, J. Chemotaxis in bacteria. *Science* 1966, 153, 708-16.
113. Yamaguchi, S.; Fujita, H.; Sugata, K.; Taira, T.; Iino, T. Genetic analysis of H2, the structural gene for phase-2 flagellin in *Salmonella*. *J Gen Microbiol* 1984, 130, 255-65.
114. Williams, A. W.; Yamaguchi, S.; Togashi, F.; Aizawa, S. I.; Kawagishi, I.; Macnab, R. M. Mutations in fliK and flhB affecting flagellar hook and filament assembly in *Salmonella typhimurium*. *J Bacteriol* 1996, 178, 2960-70.

CHAPTER II

CA II INHIBITION STUDIES WITH THE GENESIS PLUS AND NCI DIVERSITY SET COMPOUND LIBRARIES

Introduction

There are potential problems with currently approved sulfonamide drugs and related compounds; their lack of CA isozyme specificity may result in undesirable systemic side effects such as altered taste, malaise, fatigue, depression and anorexia¹⁻⁶. It is also well documented that a significant fraction of the human population has shown an allergic response to some of the therapeutic sulfonamides, including acetazolamide (Diamox®), furosemide (Lasix®), metolazone (Zaroxolyn®), and indapamide (Lozol®)⁷. Other newer drugs not originally classified as carbonic anhydrase inhibitors (CAIs), e.g. cyclooxygenase-2 (COX-2) inhibitors celecoxib and valdecoxib⁸, anti-convulsant drugs such as topiramate⁹ and zonisamide¹⁰, and antipsychotic drugs such as sulpiride¹¹ may have unexpected CAI activity, and consequently, both unforeseen novel uses and side effects. Thus, the discovery and development of non-sulfonamide CAIs could lead to the development of novel classes of therapeutically useful drugs for the treatment of various diseases and physiological conditions. The recent discovery of several novel inhibitors of CA II, such as the small, fluorinated aliphatic sulfonamide compound $\text{CF}_3\text{SO}_2\text{NH}_2$ ¹² and hydroxyurea¹³, implies that a comprehensive evaluation of other biologically-active chemical structures capable of binding and inhibition of CA II could still yield

additional information relating the structure activity relationship of α -CAs.

Human carbonic anhydrase II (CA II), a zinc metalloenzyme, was screened against two separate compound libraries comprising approximately 3000 compounds. The assay monitored inhibition of CA II esterase activity with the non-physiological, colorimetric substrate 4-nitrophenyl acetate (4-NPA) in a format allowing high-throughput screening in 96-well microplates. This assay was used to test the hypothesis that a high-throughput screen of structurally diverse compounds, with known biological activity, would yield new structural insights into CA inhibition and potentially yield new inhibitors for this class of enzyme. The colorimetric absorbance assay for 4-NPA esterase activity¹⁴ was used to screen both the Genesis Plus (GenPlus) library of 960 structurally diverse, biologically active compounds, as described in a published study¹⁵ and the NCI Diversity Set library of 1990 synthetic compounds available from the National Cancer Institute (NCI). This strategy of screening libraries of biologically characterized compounds, i.e., old drugs, against new pharmacological targets has been described previously in the context of drug discovery and is termed the Selective Optimization of Side Activities (SOSA) approach¹⁶.

Experimental Procedures

The CA II expression plasmid, pACA, was a generous gift from Dr. Carol Fierke, University of Michigan. This plasmid contains the mature form of human CA II under control of the T7 promoter¹⁷. The enzyme was expressed by growing *Escherichia coli* BL21 (DE3) cultures in Luria-Bertani media (1 L per flask), at 37 °C

shaken at 225 rpm to an optical density at 600 nm (OD₆₀₀) value of 0.5 to 0.8, followed by induction with 0.1 mM IPTG for 3 h. Cells were lysed in 20 mM, pH 7.5 MOPS buffer containing 1.0 mg/ml lysozyme, 5 µg/ml deoxyribonuclease I, and 5 mM MgSO₄, with stirring on ice for 30 min. The lysate was clarified by centrifugation at 8000 x g for 15 min and loaded onto an SP Sepharose 26/20 Fast Flow cation exchange column (~50 ml, 2.6 mm x 20 cm height, Amersham Biosciences, Piscataway, NJ). CA II was eluted with a 0 to 1.0 M linear NaCl gradient (over 10 column volumes), using a Fast Protein Liquid Chromatography (FPLC) system. Eluted fractions containing CA II were assessed to be > 95% pure by sodium dodecyl sulfate polyacrylamide gel electrophoresis. These CA II fractions were concentrated using a Centricon device with a YM-10 membrane (Millipore, Billerica, MA), then frozen in liquid nitrogen and stored at -80 °C until use. CA II protein concentration was determined via absorbance measurements at 280 nm, using a molar absorptivity of $5.4 \times 10^4 \text{ M}^{-1} \text{ cm}^{-1}$ ¹⁷.

Compound Libraries

The GenPlus collection of 960 biologically active compounds was purchased from MicroSource Discovery Systems (Gaylordsville, CT). Compounds were stored frozen at -80 °C until use. The complete list of compounds and structure-data file (SDF) format structure files for this library are available online at <http://www.msdiscovery.com/download.html>. This library consisted of individual compounds dissolved at 10 mM concentration in dimethyl sulfoxide (DMSO), pre-dispensed into 80 wells of 2 ml storage tubes in 96-well format storage racks. A

Perkin Elmer/CCS Packard PlateTrak robotic pipetting workstation with a P50 dispensing head was used to transfer and dilute compounds into 100% DMSO in Costar 3365 96-well polypropylene round-bottom storage plates (Corning, Acton, MA) at 2 mM final concentration for use as working “daughter” plates and 100% DMSO with no inhibitor added was used as a negative control (0% inhibition). All compound daughter plates used for both screening and follow-up assays were hand sealed with Costar 6570 aluminum self-adhesive lids and stored at –20 °C until use.

The NCI Diversity Set is a subset of 1,990 compounds chosen from over 140,000 open compounds to represent the unique array of pharmacophores present in the NCI compound repository. The library was derived from compounds that had at least a gram of material available. The compounds that met these two criteria were then reduced to the final number using Chem-X (Oxford Molecular Group) to create a finite set of pharmacophores. The Chem-X diverse subset generating function reads through a set of structures and for every structure, determines the acceptable conformations of that structure. For each acceptable conformation, it determines all the pharmacophores for that conformation. The pharmacophores for the current structure are compared to the set of all pharmacophores found in structures already accepted into the diverse subset. If the current structure has more than a preset number of new pharmacophores, it is added to the diverse subset. The requirements were set as 5 new pharmacophores and, additionally, 5 or fewer rotatable bonds. Because the selection procedure is order dependent, the order in which the structures were considered was randomized. This procedure resulted in the selection of 1990

compounds that were freely available for use by investigators in individual vials or 96-well plates. More information on the Diversity Set collection is available at:

http://dtp.nci.nih.gov/branches/dscb/diversity_explanation.html.

Esterase Activity Screening Assay

The catalytic activity of human CA II was monitored by its ability to catalyze the non-physiological esterase activity with the commercially available ester, 4-NPA¹⁸. This hydrolysis reaction releases acetate and nitrophenolate as products. The nitrophenolate product readily ionizes to give a bright yellow nitrophenolate anion which is readily detected by measuring its absorbance at 348-400 nm¹⁹ and can also be visually observed. This frequently used esterase assay was adapted for HTS format with a SpectraMax Plus³⁸⁴ UV-visible spectrophotometer (Molecular Devices Corp., Sunnyvale, CA) with 96-well microplate-reading capabilities. For initial screens, 100 μ l of assay solution containing 1 μ M purified CA II enzyme in 50 mM, pH 7.5 MOPS, 33 mM Na₂SO₄, 1.0 mM EDTA buffer was dispensed into flat-bottom polystyrene 96-well plates (Costar 3370) with a Matrix Impact² P1250 electronic programmable 8-channel pipettor (Matrix Technologies Corp., Hudson, NH) or a Finstruments Multidrop peristaltic pump 8-channel microplate dispenser (MTX Lab Systems Inc., Vienna, VA), when sufficient numbers of assays were performed on the same day. Each compound plate was screened in triplicate. Daughter compound plates containing 2 mM of each compound in 100% DMSO were thawed at room temperature followed by removal of the foil lid and storage in a desiccator. A PlateTrak pipetting workstation was then used to dispense 1 μ l of each compound

into the assay solution. Compounds were allowed to equilibrate with the enzyme for 15 min at room temperature prior to performing the assay, to facilitate formation of the enzyme-inhibitor complex. The well-known CA II inhibitor, acetazolamide, was included in duplicate on each assay plate at 100 μ M concentration as a positive control (100% inhibition) and 100% DMSO was included as a negative control (0% inhibition). A 10 μ l volume of 5 mM 4-NPA solution in 10% DMSO, 90% assay buffer was then rapidly added to each plate with a Multidrop dispenser and the data collection was started. The absorbance in each well was measured at 348 nm, the isobestic point of 4-nitrophenolate anion (product of 4-NPA hydrolysis), at intervals of 12-15 sec for a total period of 5 min with a SpectraMax Plus³⁸⁴ microplate spectrophotometer running SoftMax Pro software. These conditions give an initial substrate concentration of 450 μ M 4-NPA in each well and a final total volume of 111 μ l per well, resulting in an 18 μ M final compound concentration. The final DMSO concentration in this assay was 1.8% (v/v), which did not appear to interfere with CA II enzyme activity or specificity.

Inhibitor IC₅₀ Measurement

Potential inhibitor compounds identified in the initial screens were dissolved at 10 mM final concentration in DMSO and serially diluted 1:2 into DMSO in duplicate in round bottom 96-well polypropylene compound storage plates (Costar 3365). Each dilution series was continued from a first plate to a second plate to extend the concentration range of each compound. Dilution plates were hand sealed

with Costar 6570 aluminum self-adhesive lids and stored at $-20\text{ }^{\circ}\text{C}$ until use. The enzyme concentration ($1\text{ }\mu\text{M}$), assay plates, and buffer composition were identical to those used in the initial screen. One μl of each diluted compound was added to $100\text{ }\mu\text{l}$ of enzyme-assay buffer using a CCS PlateTrak and allowed to incubate for 15 min, followed by rapid addition of $10\text{ }\mu\text{l}$ 4-NPA substrate with a Multidrop 8 channel dispenser to give a final assay volume of $111\text{ }\mu\text{l}$ and immediate acquisition of kinetic esterase data with the SpectraMax Plus³⁸⁴ spectrophotometer. These conditions yielded a final inhibitor concentration ranging from 43.0 pM to $90.1\text{ }\mu\text{M}$. The final DMSO concentration in the 4-NPA assay was 1.8% (v/v). The IC_{50} assays for each compound of interest were determined in quadruplicate, using two duplicate rows of each plate for a compound, with two replicate assays performed for each plate.

Each “hit” inhibitor compound of interest identified in the GenPlus library was tested for non-specific promiscuous inhibition²⁰⁻²² in the presence and absence of 0.01% Triton X-100 to screen putative hits for promiscuous inhibition resulting from formation of colloidal aggregates of lipophilic compounds. The influence of CA II enzyme concentration on the Hill slope and IC_{50} values was also investigated using a 5-fold higher enzyme concentration ($1\text{ }\mu\text{M}$ vs. $5\text{ }\mu\text{M}$).

All 4-NPA esterase kinetic data were normalized to a scale of 0-100% inhibition with an MS Excel spreadsheet using the internal positive and negative controls on each plate: $10\text{ }\mu\text{M}$ acetazolamide as a positive control (100% inhibition) and pure DMSO as a negative control (0% inhibition). The reduced data was then fit to the 4-parameter non-linear sigmoidal dose-response model (Equation 2.1, i.e., the

Hill equation) via non-linear optimization to obtain the IC_{50} and Hill slope using GraphPad Prism version 4.0 software, as reviewed by Walters and Namchuk²³.

$$\%Inhibition = I_{min} + \frac{I_{max} - I_{min}}{1 + 10^{(LogIC_{50} - x) - Hillslope}} \quad (Eq. 2.1)$$

Where I_{min} is the minimum signal, I_{max} is the maximum signal, X is the concentration of inhibitor and Hill slope is the slope (Figure 2.1).

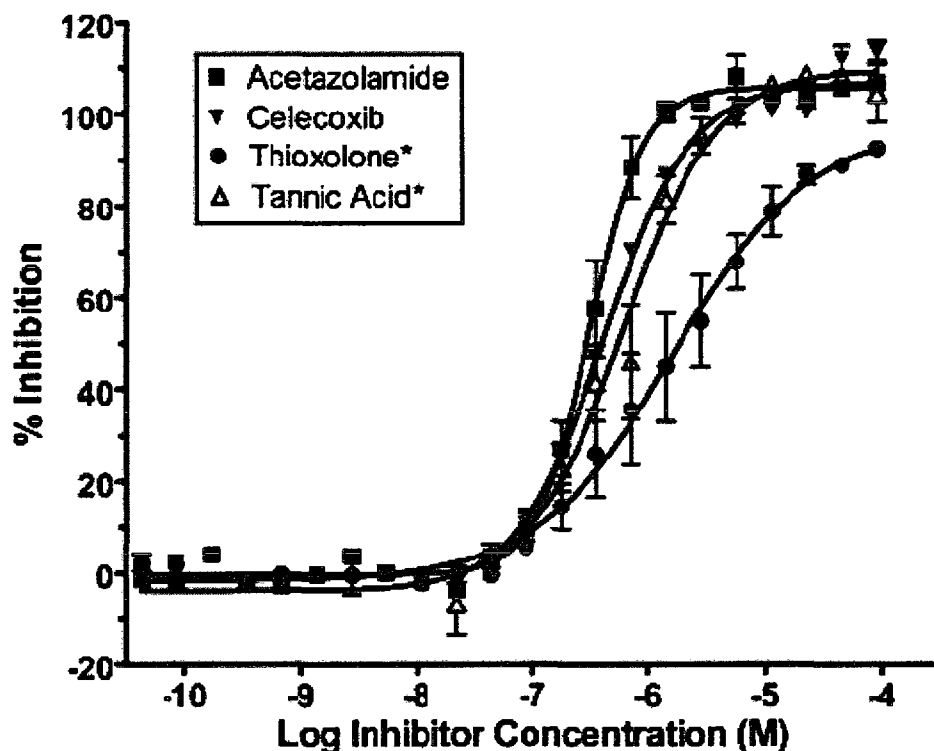


Figure 2.1. Plot of example 4-NPA esterase IC_{50} data fit to Eq. 2.1 for two sulfonamide and two non-sulfonamide compounds identified as carbonic anhydrase inhibitors in the Genesis Plus compound library.

Inhibitor K_d Measurement

The second biochemical assay used in this study relied on equilibrium binding displacement competition of a fluorescent CA-II inhibitor, dansylamide (DNSA), by other potential inhibitors. DNSA is virtually non-fluorescent when dissolved in aqueous solution. However, binding of DNSA to carbonic anhydrase is followed by an increase in fluorescence emission at 470 nm following excitation at 280 nm, as originally discussed by Chen and Kernohan²⁴. The interactions of this fluorescent probe with CA I and CA II isozymes were recently investigated by Banerjee, et al.²⁵. The equilibrium dissociation constants (K_d values) of CAIs were determined using essentially the same approach described by Baird, et al.²⁶, except that all assays were determined in microplate format instead of cuvettes, using black untreated polystyrene flat bottom 96-well plates (Corning Costar 3915) and a BMG Technologies Polarstar fluorescence microplate reader with 280 and 470 nm fixed wavelength band-pass optical filters. The buffer was the same as that used for the IC_{50} experiments. First, the K_d value for the fluorescent probe, DNSA, was determined by titrating 100 nM CA II with varying concentrations of DNSA, ranging from 96.7 nM to 99.0 μ M in a total assay volume of 101 μ l, resulting in an increase in the observed fluorescence intensity as the DNSA progressively binds the CA II active site. The equilibrium dissociation constant for DNSA (K_{DNSA}) was then determined by fitting the data to Eq. 2.2.

$$F_{tot} = \frac{F_{obs} - F_{ini}}{F_{end} - F_{ini}} = \frac{1}{1 + (K_{DNSA} / [DNSA])} \quad (\text{Eq.2.2})$$

where, F_{tot} is the fraction of total fluorescence, F_{ini} is initial fluorescence of CA II in the absence of DNSA and F_{end} is end-point fluorescence. The equilibrium dissociation constants for other CAI compounds were then determined by a competitive binding assay with DNSA, using a fixed concentration of 20 μM DNSA, 100 nM CA II and an inhibitor concentration that was varied from 47.2 pM to 99.0 μM , resulting in a decrease in the observed fluorescence intensity of DNSA as it was progressively displaced from the CA II active site by a competing compound. The K_d value of each inhibitor was then determined by fitting the data to Eq. 2.3.

$$F_{tot} = \frac{F_{obs} - F_{end}}{F_{ini} - F_{end}} = \frac{1}{1 + (K_{DNSA} / [DNSA]) (1 + [I] / K_d)} \quad (\text{Eq. 2.3})$$

Where F_{tot} is the fraction of total fluorescence, F_{obs} is the fluorescence signal at any concentration of inhibitor, F_{ini} is initial fluorescence of CA II in the absence of DNSA, F_{end} is end-point fluorescence, and $[I]$ is concentration of competing inhibitor compound.

Results

GenPlus Compound Library: Preliminary Identification of Hits

The CAI assay used for screening was a kinetic esterase assay using 4-NPA as the substrate. The assay was robust and able to identify known inhibitors, as demonstrated by the positive identification of acetazolamide and methazolamide, two sulfonamide compounds known to be CA II inhibitors (Table 2.1). The initial screen of 960 biologically active compounds in the GenPlus library yielded 19 lead compounds that appeared to function as CA II inhibitors, as defined using a minimum cut-off value of 48% inhibition (Figure 2.2, Table 2.1) and confirmed by visual inspection of the time course data for each compound, indicating an initial hit rate of 2.0%.

In addition to the 19 original hits, three additional compounds identified by the percent inhibition analysis were ruled out by visual inspection of the raw data, due to noise or inconsistent results: danazol (noisy data, very weak inhibition), cyclophosphamide hydrate (apparent artifact, no significant inhibition), and amphotericin B (high background absorbance, initial inhibition decreasing over time). The majority of the 19 hits were sulfonamides, although a number of non-inhibitory sulfonamide compounds were also identified during analysis of the screening results. Also of note was the detection of several novel CAIs that did not have any sulfonamide groups.

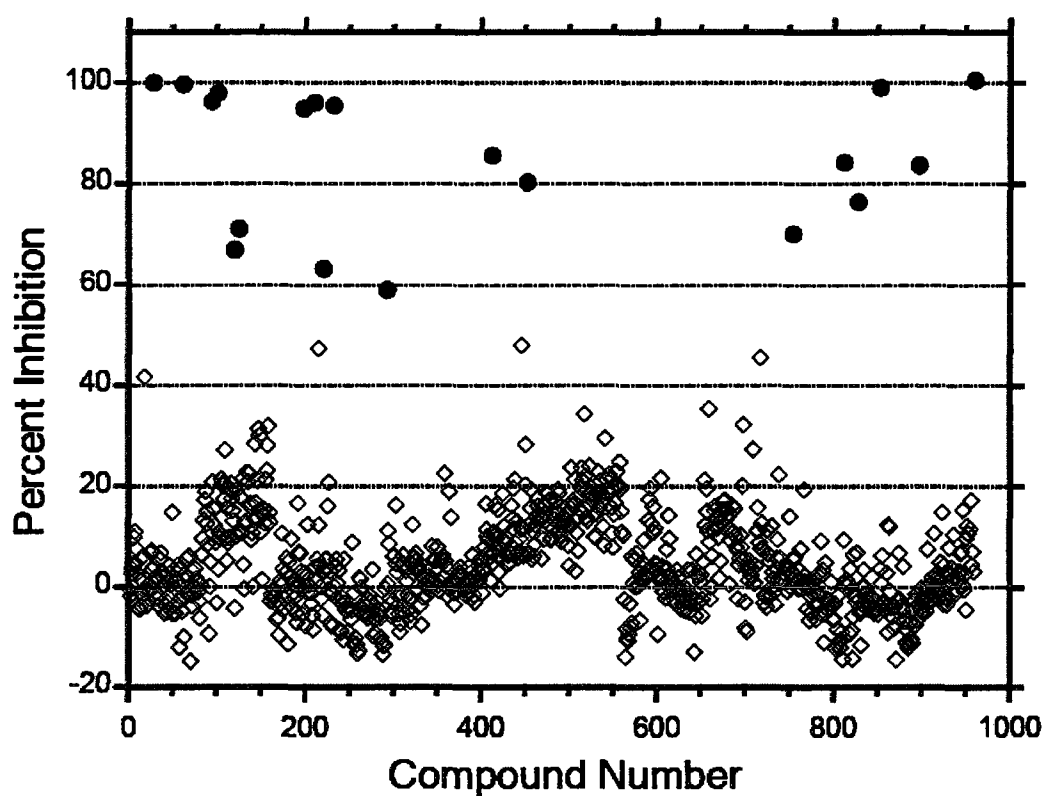


Figure 2.2. Initial results of screening the Genesis Plus 960 compound library for inhibitors of human CAII. The percent inhibition of each compound is plotted vs. the compound number. Each data point is the average of three separate experiments in which the rate of 4-NPA ester hydrolysis by CA II was measured in 96-well plates. Open diamonds are non-inhibitory compounds. Closed circles are strongly inhibitory compounds, as defined by the criteria of 48%-100% inhibition, with 10 μ M acetazolamide used as the 100% inhibition control.

Table 2.1. Potential carbonic anhydrase II inhibitor compounds identified in initial screen of Genesis Plus compound library, as confirmed by two statistical criteria ^a.

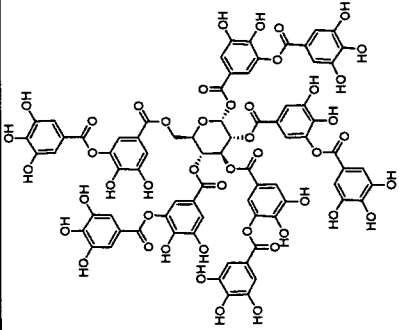
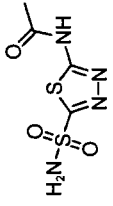
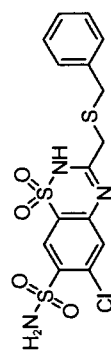
Compound	Structure	Mol. Mass (Da)	XlogP _b	Criteria 1: %Inhib. c	Criteria 2: Inhib. rate > 2σ ^d
1. Tannic acid ^e		1701.2	0.523	100.6%	(3X)
2. Acetazolamide		222.3	-0.224	100.1%	(3X)
3. Benzthiazide		431.9	2.918	99.8%	(3X)

Table 2.1. - Continued

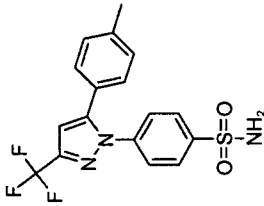
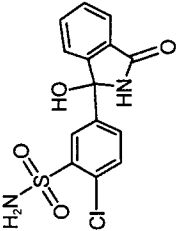
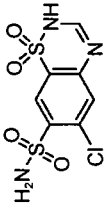
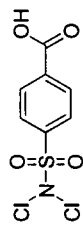
Compound	Structure	Mol. Mass (Da)	XlogP _b	Criteria 1: %Inhib. _c	Criteria 2: Inhib. rate > 2σ ^d
4. Celecoxib		381.4	4.157	99.2%	(3X)
5. Chlorthalidone		338.8	1.718	98.1%	(3X)
6. Chlorothiazide		295.7	0.549	96.4%	(3X)
7. Halazone		270.1	3.408	96.1%	(3X)

Table 2.1. - Continued

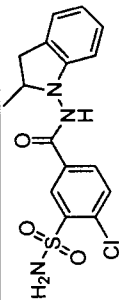
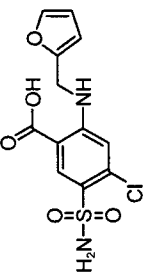
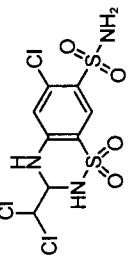
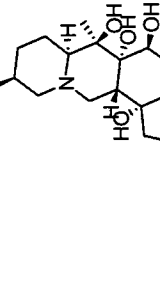
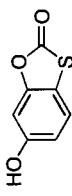
Compound	Structure	Mol. Mass (Da)	XlogP _b	Criteria 1: %Inhib. c	Criteria 2: Inhib. rate > 2σ ^d
8. Indapamide		365.8	3.121	95.6%	(3X)
9. Furosemide		330.7	1.514	95.0%	(3X)
10. Trichlormethiazide		380.7	1.023	85.7%	(3X)
11. Cevadine		591.7	0.164	84.3%	(3X)
12. Thioxolone		168.2	1.884	83.7%	(3X)

Table 2.1. - Continued

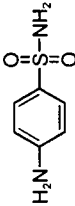
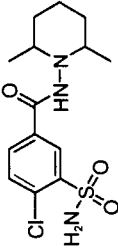
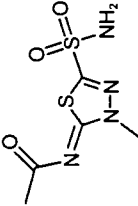
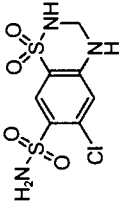
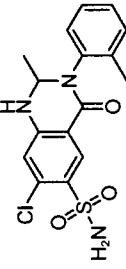
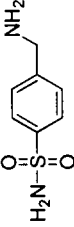
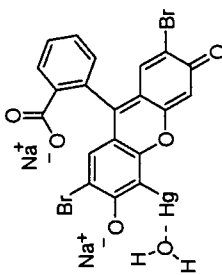
Compound	Structure	Mol. Mass (Da)	XlogP _b	Criteria 1: %Inhib. c	Criteria 2: Inhib. rate > 2σ ^d
13. Sulfanilamide		172.2	-0.201	80.4%	(3X)
14. Clopamide		345.9	2.290	76.5%	(3X)
15. Methazolamide		236.3	0.231	70.3%	(2X)
16. Hydrochlorothiazide		297.7	-0.268	63.2%	(3X)
17. Metolazone		365.8	2.784	59.0%	(3X)
18. Mafenide		186.2	-0.220	49.7%	(3X)

Table 2.1. - Continued

Compound	Structure	Mol. Mass (Da)	XlogP _b	Criteria 1: %Inhib. c	Criteria 2: Inhib. rate > 2σ ^d
19. Merbromin		751.7	n/a.	48.0%	(2X)

^a Inhibition of 4-NPA esterase activity measured in triplicate.

^b XlogP values were those listed for each compound in the NCBI PubChem Compound database at: <http://pubchem.ncbi.nlm.nih.gov/>

^c Criteria 1 uses the percent inhibition for each compound, as normalized by positive and negative controls on each plate.

^d Criteria 2 uses the an observed kinetic rate for CA II 4-NPA esterase activity that is less than 2 times the standard deviation from the mean kinetic rate for each plate of 80 compounds.

^e Compound is a heterogeneous mixture, computed properties are only approximate.

An alternative approach to analysis of the screening data was performed using a statistical analysis of the reaction rates. Reaction rates that were less than the mean plate value by 2 times the standard deviation ($< 2 \sigma$), for at least 2 out of three duplicate assays were identified as hits. This method yielded 25 hits, with a subset of 20 compounds that were consistently below the mean kinetic rate value by 2σ in three repeated runs (data not shown). The hit list included the same 19 strongly inhibitory compounds identified previously. However, there was significant variation in the weaker hits identified by this second analysis method. The six additional weak hits identified via the second "rate $< 2\sigma$ " criteria were: pyrvinium pamoate, tolazamide, reserpine, estradiol propionate, rifampin, and phenolphthalein. However further analysis of the data for these six compounds indicated that they all exhibited very low percentage inhibition values (12-23% inhibition). Thus, these compounds were not pursued further as potential hits. A more detailed statistical analysis of the data indicated other possible weak inhibitors. However, many of these compounds may have functioned as promiscuous inhibitors, as many of the structures indicate complex aromatic or polycyclic ring structures that may have amphiphilic, surface-active properties and a tendency to form enzyme denaturing colloidal aggregates²⁰⁻²². Comparison of the potential hit compounds obtained by the two different methods of data analysis suggests that the first method of computing and comparing the percent inhibition was more statistically robust than analyzing the raw data for statistical outliers. However, this analysis also highlighted the possibility of using visual inspection of the raw kinetic data to verify further whether a compound was truly

functioning as an inhibitor of the target enzyme.

Reproducibility

The reproducibility of the screening assays was assessed by using the frequently employed metric, the Z' factor^{23,27}, which has been defined in Eq. 2.4 as:

$$Z' = 1 - (3\sigma_{c+} + 3\sigma_{c-}) / (\mu_{c+} - \mu_{c-}) \quad (\text{Eq. 2.4})$$

Where, σ_{c+} is the standard deviation of the positive control for the assay, σ_{c-} is the standard deviation for the negative control and $(\mu_{c+} - \mu_{c-})$ define the mean values for the positive and negative controls. As stated by Zhang and coworkers, an enzymatic assay showing a $Z' > 0.5$ is deemed suitable for HTS and the closer to the value of Z' is to 1, the higher the quality of the assay²⁷. The Z' values for individual triplicate screens of all 12 plate sets used in the screening assay were 0.7 or higher (Figure 2.3) and the average Z' value for all 12 compound plates run in triplicate was 0.891 ± 0.084 . The triplicate repeat of each screening experiment and the use of kinetic absorbance data rather than endpoint data enabled this statistically robust approach and may have contributed to the quality of this screening data set.

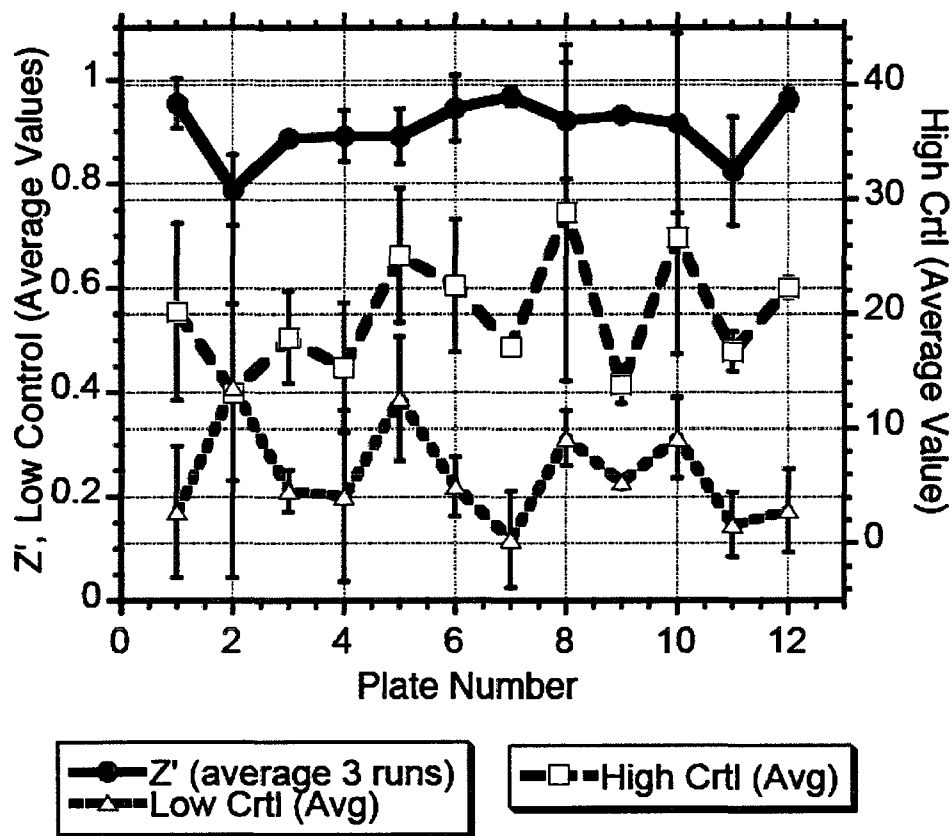


Figure 2.3. Analysis of assay quality for each of the 12 compound plates in the Genesis Plus collection that were screened for inhibition of carbonic anhydrase 4-NPA esterase activity. Left axis: average of Z' (filled circle symbol) and low (100% inhibition-10 mM acetazolamide) control values (open triangle symbol) for three experimental runs with each plate. Right axis: average of high control (0% inhibition-DMSO only) values (open square symbol) for three experimental runs with each compound plate.

Signal to Noise Characteristics

The signal to noise ratio was very high in this kinetic assay, as indicated by an average signal: baseline (S:B) ratio of 134 ± 194 mAbs₃₄₈ units min⁻¹ for all 12 GenPlus compound plates screened. This high S:B ratio was a result of the consistently large difference in the negative and positive controls on each plate (Figure 2.3), which had a negative control (0% inhibition) average kinetic rate value of 20.0 ± 7.53 mAbs₃₄₈ units min⁻¹ and a positive control (100% inhibition) average value of 0.241 ± 0.145 mAbs₃₄₈ units min⁻¹ for all plates screened. Strong CAIs could be readily identified by visual inspection of the assay plate or raw kinetic data as shown for the column of compounds on plate 1 that contains a known inhibitor, acetazolamide (Figure 2.4).

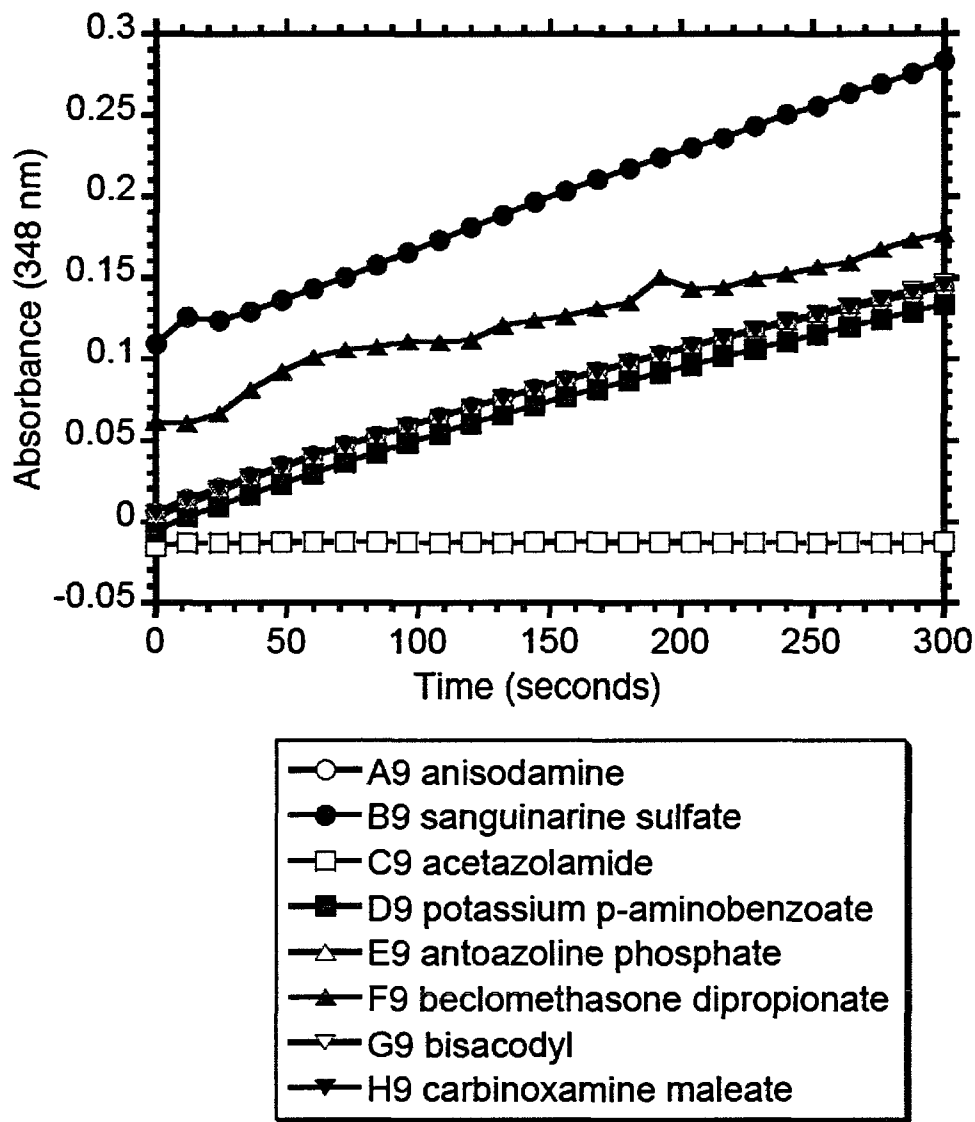


Figure 2.4. Example of raw kinetic absorbance data simultaneously collected for eight compounds (column 8, plate 1) during initial screen of compound library for CA II inhibitors. Although two of the compounds (B9, F9) had visible absorbance at the wavelength of 348 nm, the kinetic slopes were readily determined from the change in absorbance for each compound. Compound C9 (open squares) is acetazolamide, a known CA II inhibitor.

Enzyme and Substrate Stability

The CA II enzyme appeared to be stable and consistently active over a time course of several hours, as verified by the high rate of 4-NPA esterase activity observed in the negative controls on each plate that contained enzyme and DMSO but no inhibitor. This result indicated that the native CA II protein structure and activity were not significantly perturbed by the dilute (1.8% w/v) non-polar DMSO solvent present in the final assay buffer.

The 4-NPA ester substrate had a significant background rate of hydrolysis, despite the presence of 1.0 mM EDTA in the assay buffer, and required frequent replenishment every 15 min from a non-aqueous 100% DMSO stock solution to ensure the best assay quality. The background hydrolytic rate for the 4-NPA esterase reaction can be high under the best conditions, so a relatively high concentration of the CA II enzyme (1 μ M) was used in the screening assay to allow reliable measurement of its 4-NPA esterase activity at 348 nm. The initial 4-NPA substrate concentration used in this assay (450 μ M) was far in excess of the 1 μ M CA enzyme concentration and is well below published K_m values for the CA II enzyme-4-NPA substrate system. This substrate has relatively low solubility in aqueous solutions, so estimates of its K_m value vary in the literature, ranging from 4-22 mM^{19,28,29}. The substrate concentration used in this study was also within the typical range of 0.4–1.0 mM 4-NPA typically used in studies involving CA esterase assays^{9,26,30,31}.

Hit Confirmation

All 19 hit compounds that exhibited significant inhibition in the preliminary screen (Table 2.1) were further characterized by several different types of assays, first to verify their inhibitory function and second, to determine a more quantitative measure of their potency, i.e., their affinity for the CA II active site. The original 19 hit compounds (Table 2.1) were first retested at 18 μ M concentration for inhibition of the enzyme 4-NPA esterase activity, using the same assay buffer. Only one of the initial hit compounds, cevadine, consistently failed to exhibit substantial inhibition when retested. This compound was not further characterized.

I. Sulfonamide CAIs

The majority of strong inhibitors identified in the initial screen have a free sulfonamide end group, including the well-known therapeutic CAIs, acetazolamide and methazolamide. Little correlation was apparent between the percent inhibition and either the molecular mass or the compound hydrophobicity of inhibitory sulfonamides as quantified by the XlogP value. For example, acetazolamide had a very small, polar XlogP value of -0.224, while celecoxib had a higher, non-polar XlogP value of 4.157 (Table 2.1), yet both were strong CAIs (100% and 99% inhibition in the initial screen). These results reconfirm the general SAR “rule” that sulfonamide compounds often function as CAIs³², as first noted in 1940, when sulfanilamide was first described as a CAI by Mann and Keilin³³. Thus, the potential high affinity of a terminal sulfonamide functional group for the active site zinc ion in

a metalloenzyme should not be underestimated. The sulfonamide binding mechanism has been experimentally shown by X-ray crystallography to involve direct coordination of the ionized, negatively-charged form of the nitrogen atom to the active site zinc ion^{34,35}. This is further qualified in that only primary terminal sulfonamides efficiently bind to the active site of the CA II enzyme. A structural search of the GenPlus compound library database with the ChemFinder software (CambridgeSoft, Cambridge, MA) yielded approximately 40 secondary sulfonamide-linked compounds that did not interact with the enzyme. These non-inhibitory sulfonamide-like compounds included two compounds with smaller modified sulfonamide-like terminal groups, sulfacetamide ($-\text{SO}_2\text{NH}-\text{CO}-\text{CH}_3$) and thiothixene ($-\text{SO}_2-\text{N}(\text{CH}_3)_2$).

I.A. Diuretic Sulfonamides

Many of the CAI sulfonamide compounds, i.e., acetazolamide, benzthiazide, furosemide, chlorothiazide, chlorthalidone, hydrochlorothiazide, indapamide, metolozone, and trichlormethiazide, are categorized as diuretics³², a class of drugs long used therapeutically³⁶ and often recommended for the treatment of hypertension³⁷. Various reports have first implicated³⁸⁻⁴⁰ and more recently, demonstrated^{41,42} a primary role for CA inhibition in the physiological function of these diuretics, although they are not consistently classified as CAIs in the medical literature.

I.B. COX-2 Inhibitor Sulfonamides

Celecoxib is another sulfonamide compound recently identified as a CAI⁴³. This compound is primarily used therapeutically as a COX-2 inhibitor for the treatment of arthritic pain, but is also under evaluation as an anticancer drug⁸. Although highly speculative, the sulfonamide moiety might play a larger role than originally expected. Thus, this study possibly implies a possible number of “off-target” side effects or alternative therapeutic applications, e.g., diuretics, for some sulfonamide COX-2 inhibitors such as celecoxib⁴³.

I.C. Antibacterial Sulfonamides

Sulfanilamide and mafenide are two additional sulfonamide hits categorized as antibacterial compounds; indeed, sulfanilamide, a metabolite of the antibacterial prontosil⁴⁴, was the first CAI described in the literature³³. Halazone was another atypical sulfonamide derivative identified as a CAI in this study (Table 2.1). It is a chlorine-substituted sulfonamide that has historically been used as an antimicrobial agent to disinfect drinking water⁴⁵. Halazone is also known to prevent inactivation of sodium channels⁴⁶. A literature search of the PubMed database failed to yield any mention of this compound as a CAI. However, given that the function of this water disinfectant is to release chlorine, it is not clear if the chlorinated or chlorine-free sulfonamide form of this compound is actually inhibiting CA II. The free chloride anion is also a well-known inhibitor of CA II³². Thus it is possible that both free sulfonamide and chloride degradation products of this compound inhibit the enzyme.

II. Non-Sulfonamide CAIs

Perhaps the most intriguing result was the identification in the initial screen of four potential CAIs that did not possess any sulfonamide-related structural groups: tannic acid (100%), cevadine (84.3%), thioxolone (83.7%), and merbromin (48.0%). Cevadine failed to show significant inhibition in the initial hit confirmation studies, but the other three compounds continued to exhibit inhibition in the initial hit confirmation assay and were further characterized with respect to their potency.

II.A. Cevadine

This compound, also known as veratrine, has a complex, macrocyclic structure that may have amphiphilic, detergent-like properties. Although a consistent degree of significant inhibition (84% inhibition) was observed in the initial triplicate screen, a follow-up study with a separate stock of this compound obtained from the same commercial supplier failed to yield any significant inhibition in the 4-NPA esterase assay.

II.B. Tannic Acid

Tannic acid is a large molecular mass, heterogeneous, polyphenolic species and is described as a “nonspecific enzyme/receptor blocker” by the compound supplier. A significant degree of inhibition was consistently observed for this compound (100% inhibition) in the initial triplicate screen. The confirmatory 4-NPA esterase reaction with two different sources of compound also yielded significant inhibition. As noted above, phenol is a well-known inhibitor of CA II, thus terminal

phenolic subunits and hydrolysis products of this heterogeneous compound may have a specific inhibitory effect. However, anomalous results were observed for this compound in one of the secondary assays, suggesting a more nonspecific inhibition mechanism, as discussed below.

II.C. Thioxolone

The third non-sulfonamide CAI identified in the initial screen is thioxolone (84% inhibition). A search of the CAI literature in the NCBI PubMed database and the Chemical Abstracts database indicated that thioxolone had not previously been identified as a CAI or used therapeutically for the inhibition of CAs. Examination of the thioxolone structure (Table 2.1) suggested several possible modes of inhibition, as discussed later in Chapter 3. First, a benzene ring at one end of the molecule has a hydroxyl group that may interact with the active site zinc ion, similar to phenol, a known CAI⁴⁷. A second 5-membered 1,3-oxathiol-2-one ring at the other end of thioxolone has both ester and thioester groups that may interact with the CA II active site in some manner. The carbonyl oxygen and one of the ester groups may bind to the active site region, possibly directly to the zinc ion and the Thr 199 “gate-keeper” residue. This cyclic ester ring structure may mimic the transition state of the 4-NPA esterase reaction catalyzed by CA II and bind intact. Alternatively, one or both of the ester and thioester bonds may be subject to cleavage in the same reaction that cleaves the 4-NPA substrate, releasing a more potent phenolic and/or thiol inhibitor that then binds the active site zinc ion. A more detailed study of the mechanism of thioxolone inhibition was undertaken, as described in a recent publication and Chapter Three of

this thesis⁴⁸. The results indicate that thioxolone binds to the active site of CA II and is cleaved by successive hydrolysis of the thioester and ester bonds to form 4-mercaptobenzene-1,3-diol (Figure 2.5). The 4-mercaptobenzene-1,3-diol product then binds to the CA II active site zinc ion, displacing the zinc-bound hydroxide group. Thus, thioxolone is proposed to be a prodrug inhibitor that is cleaved via a CA II zinc-hydroxide mechanism known to catalyze the hydrolysis of esters²⁸.

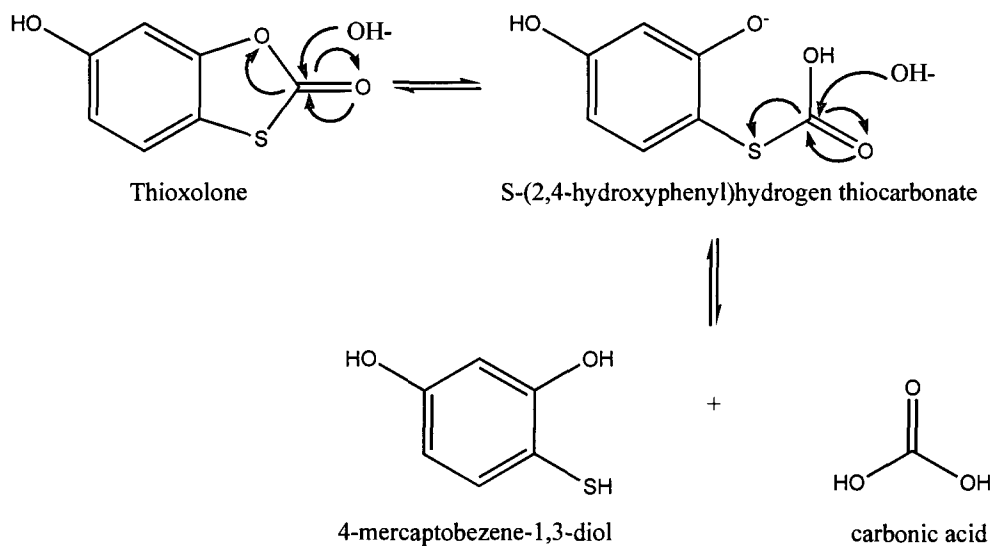


Figure 2.5. Proposed reaction mechanism of thioxolone cleavage by CA II, based on crystallographic studies. The less reactive ester bond is first enzymatically cleaved via nucleophilic attack by the active site Zn-bound hydroxide ion. A second nucleophilic attack by another activated hydroxide ion then cleaves the remaining, more reactive thioester bond, releasing the final inhibitor, 4-mercaptobenzene-1,3-diol and carbonic acid. The carbonic acid rapidly ionizes to form a bicarbonate ion (HCO_3^-) and CO_2 .

II.D. Merbromin

Also known as mercurichrome, merbromin is a fluorescein derivative that is used as a topical disinfectant. No mention of this compound functioning as a CAI was found during a literature search of the PubMed database. Merbromin contains a mercury ion that may coordinate to the imidazole side chain of residue His 64 in the CA II active site or the thiol side chain of Cys 206, located on the entrance to the CA II active site cavity; both residues were observed to bind Hg^{2+} metal ions in X-ray crystallography studies⁴⁹; the Cys 206 thiol is routinely labeled with Hg^{2+} ions in these studies for phase determination^{17,50-52}.

Hit Characterization

More detailed characterization studies were performed on the 18 confirmed hit compounds in Table 2.1 to further confirm that they were specific, competitive inhibitors of the CA II enzyme and determine their relative potencies. The results of these studies are summarized in Table 2.2. Two of the non-sulfonamide initial hit compounds were obtained from two different sources, Sigma-Aldrich (St. Louis, MO) and MicroSource Discovery Systems, and were tested to evaluate the influence of supply source on potency of inhibition. An additional “high affinity” CA II sulfonamide inhibitor, ethoxzolamide, and fluorescent but weak sulfonamide inhibitor, DNSA, were also included in these studies for comparison. The IC_{50} value and the equilibrium dissociation constant (K_d value) were experimentally determined for each hit compound (Table 2.2), using the 4-NPA esterase assay used in the initial screen and a competition binding assay using DNSA fluorescence. Two additional experiments were also performed to ensure that the compounds identified as hits in the assay were not acting by some non-specific or “promiscuous” mechanism, such as the formation of micelle-like colloidal aggregates from amphiphilic compounds that would adsorb and denature the enzyme^{20,22,53}. These secondary IC_{50} assays were performed either in the presence of 0.01% Triton X-100, a non-ionic detergent, or with a five-fold higher enzyme concentration of 5 μ M to test for non-specific, promiscuous inhibition (Table 2.2).

Results of IC₅₀ Assays with 1 μ M CA II

This detailed characterization of potency with 1 μ M CA II enzyme concentration indicated measurable CAI activity for the three confirmed non-sulfonamide hits, tannic acid, thioxolone, and merbromin. Tannic acid from two different sources yielded IC₅₀ values of 540 nM and 2.0 μ M, a 3.7-fold difference and Hill slope values of 1.1 and 0.69, values not significantly different from the ideal value of 1.0. Thioxolone obtained from two different sources consistently functioned as a moderate inhibitor, with less than a 3-fold difference in the measured IC₅₀ values of 1.8 μ M and 4.6 μ M and Hill slope values of 0.80 and 0.53 for the two different compound samples. Merbromin, the weakest of all 19 hits in the initial screen (48% inhibition, Table 2.1), yielded a large, relatively weak IC₅₀ value of 1.3 mM (Table 2.2) and a Hill slope of 0.48, a value less than 1.0. However, there is a large experimental uncertainty associated with this compound, due to the failure to attain 100% inhibition in the IC₅₀ assays.

Results of IC₅₀ Assay with 5 μ M CA II

The IC₅₀ experiments performed at a 5-fold higher enzyme concentration of (5 μ M) also indicated that none of the hit compounds were functioning in a promiscuous manner, including thioxolone and tannic acid. The measured IC₅₀ values (Table 2.2) generally increased when a higher enzyme concentration was used. The average IC₅₀ value for all compounds (Table 2.2) was 3.5-fold higher, including 3.3-fold and 6.0-fold higher values for the strong CA II inhibitors, acetazolamide and ethoxzolamide.

The Hill slopes were also statistically greater at the higher enzyme concentration of 5 μ M, with an average 2.6-fold (\pm 3.6-fold) increase in the Hill slope for all compounds.

This assay also indicated significant but decreased inhibition for two of the three non-sulfonamide hits. The IC_{50} values for both tannic acid samples increased by 5.7- and 5.4-fold to 3.1 μ M and 11 μ M when the enzyme concentration was increased by 5-fold, an increase only slightly higher than the 3.8-fold average increase in IC_{50} value observed for all compounds under the same conditions. The IC_{50} values of thioxolone increased by 2.6- and 2.4-fold to 4.5 μ M and 11 μ M at the higher enzyme concentration. In contrast to the other two compounds, the IC_{50} value of merbromin decreased by 27-fold from 1.3 mM to 49 μ M at the higher enzyme concentration, while the Hill slope increased to 9.0, suggesting some promiscuous behavior for this compound. However, as noted above, the IC_{50} values for this compound have a large inherent uncertainty. These results are not consistent with two of the three confirmed non-sulfonamide CAIs, thioxolone and tannic acid, functioning as promiscuous inhibitors.

Hill Slope as an Indicator of Promiscuity

Analysis of the IC_{50} data (Table 2.2) indicated that four therapeutic sulfonamide compounds with high affinity for CA II exhibited Hill slope values closer to 2.0 than 1.0: acetazolamide, benzthiazide, ethoxzolamide, and methazolamide. These four compounds had an average Hill slope of 2.15 ± 0.25 in

the 1 μ M CA II assay, 3.4 ± 0.50 in the 5 μ M CA II assay and 2.65 ± 0.67 in the presence of Triton X-100. Although these values are not a 10-fold deviation from 1.0, these observations contravene the traditional screening wisdom that a Hill slope deviating upwards from 1.0 is strictly indicative of a poor lead compound, false hit, or non-specific promiscuous inhibitor, as reviewed by Walters and Namchuck²³. This observation implies that a Hill slope value > 1.0 is a false lead does not apply in this case, as molecular co-crystals are available for some of these compounds, many or all of which are used therapeutically, and by definition are “good” drugs.

Results of IC₅₀ Assay with 1 μ M CA II and Triton X-100

Addition of 0.01% Triton X-100 non-ionic detergent has been suggested as a simple method for discriminating between productive and nonspecific promiscuous inhibitors²⁰, although a more recent study of promiscuous compounds used a higher concentration of 0.1% Triton X-100⁵³. The observed result of this hit confirmation assay was that most of the hits exhibited similar potency in the CA II 4-NPA assay, regardless of the presence or absence of Triton X-100, suggesting that most hits were not functioning in some promiscuous, non-specific manner. The IC₅₀ values of most strong CAIs increased by only a minor extent in the presence of this non-ionic detergent (Table 2.2). The one notable exception was tannic acid, which yielded an atypically large, 640-fold increase (four orders of magnitude) in the IC₅₀ value for one sample and a complete loss of detectable inhibition by the other sample. This anomalous result was perhaps the most definitive indication that this compound could be functioning as a non-specific, promiscuous inhibitor, as originally indicated by the

compound supplier. Excluding tannic acid, the average IC_{50} value for all compounds increased by 2.6-fold (\pm 2.1-fold) in the presence of the detergent. The average IC_{50} value for all sulfonamides, excluding halazone, increased by an average value of 2.2-fold (\pm 1.3-fold). Thus, even though some of the sulfonamide compounds are known to bind to the CA II active site with nanomolar affinities, addition of Triton X-100 still exerts a minor effect on these specific inhibitors. The addition of 0.01% Triton X-100 yielded 7.6- and 8.1-fold increases in thioxolone IC_{50} values of 13.4 μ M and 37.0 μ M. The 8-fold increase in the IC_{50} value is four times larger than that observed for sulfonamides. Although this increase is not nearly as large as that observed for tannic acid, it may hint at a possibly promiscuous interaction for this weakly-inhibitory compound and any possible products. The addition of Triton X-100 to merbromin yielded a 10-fold smaller IC_{50} value of 133 μ M and a Hill slope of 1.55. IC_{50} values measured at such high concentrations all have a large inherent uncertainty associated with them and so it is possible that the apparently lower IC_{50} could be due to errors in the estimated values, or even improvement in the apparent solubility of the compound, with Triton X-100 helping to solubilize merbromin at higher concentrations. A higher concentration of Triton X-100 may be required to distinguish between promiscuous and weak competitive inhibitors. These results are consistent with such Triton X-100 addition experiments helping to identify non-specific, promiscuous inhibitors and confirm the value of using the nonionic detergent in follow-up assays for validating hits.

Dissociation Constant Assay Results

The dissociation constants (K_d values) were determined for most of the potential hits via a competitive binding assay with a fluorescent sulfonamide, DNSA (Table 2.2). Ethoxzolamide yielded the smallest K_d value of 3.6 nM, followed by acetazolamide and celecoxib, which both yielded similar, 4-fold larger K_d values of 16 nM. This relative ranking was followed by benzthiazide (17 nM) and methazolamide (55 nM). The K_d values obtained in this study (Table 2.2) for previously characterized CAIs such as acetazolamide, sulfanilamide (13 μ M), and dansylamide (2.7 μ M) were slightly higher than, but similar in magnitude to, published K_d values for these same compounds (11 nM, 1.0 μ M, and 1.0 μ M, respectively)²⁶. These differences may reflect slightly different experimental conditions and potential protein or compound adsorption, as well as background fluorescence effects involving the use of polystyrene 96-well plates in this study. At least five of the hit compounds exhibited a significant degree of background fluorescence in the competitive binding assay with DNSA, potentially affecting accurate determination of the K_d value: bendroflumethiazide, celecoxib, ethoxzolamide, hydroflumethiazide, and trichlormethiazide. This issue might be overcome by using a longer excitation wavelength, e.g., 330 nm²⁵.

Both samples of tannic acid were inhibitory in this alternate competitive binding assay, yielding K_d values of 250 nM and 2.3 μ M (a 9.2-fold difference between samples) in the competitive binding assay with dansylamide (Table 2.2),

suggesting that this compound is a weak CAI. This assay also indicated a weak interaction of thioxolone with the CA II enzyme, yielding K_d values of 33 μM and 72 μM . The low potency of merbromin as a CAI observed in the initial screen was also confirmed in this assay by the measured K_d value of 380 nM. It should also be noted that no K_d value could be determined for metolazone (Table 2.2), one of the weakest inhibitors identified in the initial screen (59% inhibition, Table 2.1; 31 μM IC_{50} value, Table 2.2). The low affinity of this compound for CA II, combined with its strong autofluorescence, precluded measurement of binding in the presence of DNSA, unlike celecoxib, another autofluorescent compound with a relatively high affinity for CA II (99% inhibition, Table 2.1; 16 nM K_d value, 430 nM IC_{50} value, Table 2.3). These results suggest that this assay is acceptable for compound characterization, especially when used with non-fluorescent compounds, but will also function with autofluorescent compounds that have relatively high affinity for the CA active site.

Table 2.2. Summary of IC₅₀ values and K_d values for Genesis Plus hit compounds and model sulfonamide compounds^a.

Compound	K _d Value (μM)	K _i value (μM) (C-P Eq.)	1 μM CA II		Triton X-100		5 μM CA II	
			IC ₅₀ Value (μM)	Hill Slope	IC ₅₀ Value (μM)	Hill Slope	IC ₅₀ Value (μM)	Hill Slope
1. Acetazolamide	0.02							
	±							
	0.003	0.28	0.312	1.9	0.297	2.5	1.03	3.4
2. Benzenesulfonamide	1.44							
	±							
	0.19	0.473	0.526	0.78	1.63	1	2.87	1.7
3. Benzthiazide	0.167							
	±							
	0.003	0.241	0.268	2.4	0.377	3.6	1.39	3.4
4. Celecoxib ^b	0.016							
	±							
	0.004	0.386	0.429	1.2	0.604	1.2	1.28	1.7
5. Chlorothiazide	0.372							
	±							
	0.053	0.394	0.438	1.3	0.55	1	1.39	1.6
6. Chlorthalidone	0.119							
	±							
	0.019	0.234	0.26	1.4	0.434	1.5	1.33	2
7. Clopamide	14.6							
	±							
	3.37	2.34	2.6	0.83	7.88	0.79	9.08	1.3
8. Dansylamide	2.66							
	±							
	0.052	1.76	1.96	0.88	3.31	0.72	7.58	1.4

Table 2.2. - Continued

Compound	K_d Value (μM)	K_i value (μM) (C-P Eq.)	1 μM CA II		Triton X-100		5 μM CA II	
			IC ₅₀ Value (μM)	Hill Slope	IC ₅₀ Value (μM)	Hill Slope	IC ₅₀ Value (μM)	Hill Slope
	0.004							
9. Ethoxzolamide	\pm							
	0.001	0.188	0.209	2.3	0.292	2.5	1.25	2.8
	3.14							
10. Furosemide	\pm							
	0.52	0.716	0.796	1.1	1.29	1.2	3.96	1.5
	1.45							
11. Halazone	\pm							
	0.15	0.575	0.64	1.2	0.827	0.89	4.38	1.6
	7.19							
12.	\pm							
Hydrochlorothiazide	1.23	8.89	9.89	0.77	41.3	0.95	15.8	1.4
	1.42							
13. Indapamide	\pm							
	0.23	0.541	0.602	1.2	1.38	0.88	2.08	1.4
	0.379							
14. Merbromin ^b	\pm							
	0.061	1,200	1340	0.48	133	1.6	48.7	163
	0.055							
15. Methazolamide	\pm							
	0.013	0.262	0.29	2	0.317	2	2.04	4
16. Metolazone	ND ^c	27.6	30.7	0.64	22.1	1.3	50.9	2.7
	26.7							
17. Mafenide	\pm 3.1	10.6	11.8	0.73	59	0.52	17.1	1.3

Table 2.2. - Continued

Compound	K_d Value (μM)	K_i value (μM) (C-P Eq.)	1 μM CA II		Triton X-100		5 μM CA II	
			IC ₅₀ Value (μM)	Hill Slope	IC ₅₀ Value (μM)	Hill Slope	IC ₅₀ Value (μM)	Hill Slope
18. Sulfanilamide	13.2							
	± 1.8	2.44	2.71	0.66	10.8	0.84	10.1	1.2
	2.33							
19. Tannic acid	\pm							
	0.23	1.78	1.98	0.69	ND ^c	ND ^c	10.6	1.4
	0.246							
20. Tannic acid ^b	\pm							
	0.043	0.484	0.538	1.1	344	0.32	3.05	1.8
	32.7							
21. Thioxolone ^b	\pm							
	11.4	1.59	1.77	0.8	13.4	0.72	4.52	1.4
	71.8							
22. Thioxolone	\pm							
	23.9	4.12	4.58	0.53	37	0.72	10.9	1.5
	2.60							
23. Trichlormethiazide ^b	\pm							
	0.51	1.74	1.94	0.66	6.62	1.7	5.78	1.1

^a Error ranges for fitted IC₅₀ values and Hill slopes were defined as 95% confidence intervals.

^b Compounds denoted by this symbol were obtained from MicroSource Discovery Systems. All other compounds were obtained from Sigma-Aldrich.

^c ND (no data) indicates that the IC₅₀ or K_d value could not be reliably determined by the experimental method used in this assay.

^d Estimated K_i value for compounds computed with Cheng-Prusoff equation (Eq. 2.7) from 1 μM CA II IC₅₀ values using an assumed K_m value of 4.0 mM for the 4-NPA substrate.

Comparison of IC₅₀ and K_d Values

The experimentally determined K_d values had a much wider range of magnitude than the IC₅₀ values. A minimum K_d value of 3.6 nM was determined for ethoxzolamide and a maximum K_d value of 72 μM for thioxolone (Table 2.2), yielding a K_d max:min signal ratio of 20,000. This is in contrast to a minimum IC₅₀ value of 210 nM for ethoxzolamide and a maximum IC₅₀ value of 31 μM for metolazone, yielding an IC₅₀ max:min ratio of 150 (excluding the anomalous merbromin IC₅₀ data set, which had very poor fitting statistics). However, the relative rankings of the IC₅₀ values and K_d values determined by these two different assays were in good agreement. The compound with the smallest K_d value, ethoxzolamide, has previously been shown to have very high affinity for CA II^{26,54}. The measured K_d values for DNSA, acetazolamide, ethoxzolamide, and sulfanilamide were in reasonable agreement with those previously determined⁵⁴. The K_d values did not appear to correlate with the initially computed percent inhibition values (data not shown). However, a reasonable correlation was observed between the IC₅₀ values and the independently determined K_d values. A fit of IC₅₀ data and the K_d data to a power law Eq. 2.5 yielded fit parameter values of C = 0.000148 M and D = 0.359, with an R² value of 0.375 for the 1 μM CA II IC₅₀ data and values of C = 0.000185 M and D = 0.279, with an R² value of 0.547 for the 5 μM CA II IC₅₀ data.

$$IC_{50} = C * (K_d)^D \quad (Eq. 2.5)$$

However, a more established theoretical approach can be used to estimate K_i values. If the Michaelis constant, K_m , is known for an enzyme substrate, the IC_{50} value determined for an inhibitor with that same substrate can be used to estimate an apparent binding constant, K_i , by using the oft-cited Cheng–Prusoff equation⁵⁵.

$$K_i = IC_{50} / (1 + (S/K_m)) \quad (\text{Eq. 2.6})$$

where IC_{50} is the concentration of the competitive inhibitor producing a 50% inhibition, S is the substrate concentration used, and K_m is the Michaelis constant of the enzyme substrate. The Cheng-Prusoff K_i value was computed for all compounds using the IC_{50} data for 1 μ M CA II and the most recently published estimate of 4 mM for the K_m value of 4-NPA²⁹ (Table 2.2). The average overall computed K_i value for all compounds (excluding metolazone) at 1 μ M CA concentration was 150-fold higher than the experimentally determined average K_d value (Table 2.2). The IC_{50} value of 312 nM (Table 2.2) for acetazolamide yields a computed inhibition constant, K_i , of 280 nM, compared with an experimentally determined value of 16 nM. This represents a 17.5 fold higher K_i value by this method. The average computed K_i for all sulfonamide compounds (excluding halazone, merbromin, thioxolone, and tannic acid) was 7.5-fold higher than the experimental value, although this figure was biased by strong inhibitors acetazolamide, benzthiazide, celecoxib, ethoxzolamide, and methazolamide, for which 5–52 fold higher K_i values were estimated by this method than determined by the experimental DNSA K_d assay (Table 2.2). The weaker sulfonamide inhibitors exhibited an average K_i value of 0.66-fold lower than that of the experimentally determined K_d value, and halazone had similar results, with a K_i

value of 0.40-fold lower than the K_d value. The average K_i value for tannic acid was also 1.4-fold greater than the K_d value. In contrast, the average K_i value for thioxolone was 0.053-fold smaller than the K_d value. These results suggest that simple application of the Cheng-Prusoff equation tends to underestimate the equilibrium binding affinity for compounds that strongly inhibit CA II, although the K_m value of 4-NPA was not experimentally determined under the assay conditions used.

NCI Compound Library

Given the prior success of the screen of the GenPlus library in identifying novel CAIs, additional compound libraries were sought for screening via the previously validated 4-NPA assay. Discussions with other researchers indicated that the NCI Diversity Set of *ca.* 2000 compounds was also available upon request for academic research purposes. The NCI Diversity Set is a subset of 1,990 compounds chosen from over 140,000 open compounds to represent the unique array of pharmacophores present in significant quantities in the NIH National Cancer Institute (NCI repository). For a full description of the NCI compound library refer back the experimental procedure section earlier in this chapter. A short written compound request proposal was submitted to NCI and small amounts of each dissolved compound in 96-well plates were provided by NCI essentially for free, except for shipping costs. Subsequently, this second compound library was also screened for CAIs, using the same 4-NPA esterase assay described above.

The initial screen of the NCI Diversity Set library yielded 40 hit compounds that were identified as moderate to strong inhibitors of CA II esterase activity.

Additional samples of those 40 compounds were requested from the NCI Developmental Therapeutics Program and delivered as ~10 mg dry powder samples in individual vials. The compounds were then dissolved to a 10 mM concentration in 100% DMSO. These preliminary hit compounds were rescreened for inhibition of the 4-NPA esterase reaction with CA II. For the CA II and final inhibitor concentrations, please refer back to the IC₅₀ subsection of the experimental section found earlier in this chapter. This follow-up study indicated that only 34 of the initial 40 hits were confirmed as CA II inhibitors. These remaining 34 compounds were then further characterized for potency via the previously described IC₅₀ assay (Table 2.3).

Potential inhibitor compounds identified in the initial screens were dissolved at 10 mM final concentration in DMSO and serially diluted 1:2 into DMSO in duplicate in round bottom 96-well polypropylene compound storage plates (Costar 3365). Each dilution series was continued from a first plate to a second plate to extend the concentration range of each compound. Then 1 µl of each diluted compound was added to 100 µl of enzyme-assay buffer (50 mM, pH 7.5 MOPS, 33 mM Na₂SO₄, 1.0 mM EDTA buffer) using a CCS PlateTrak and allowed to incubate for 15 min, followed by rapid addition of 10 µl 4-NPA substrate with a Multidrop 8 channel dispenser to give a final assay volume of 111 µl and immediate acquisition of kinetic esterase data with the SpectraMax Plus³⁸⁴ spectrophotometer. These conditions yielded a final inhibitor concentration ranging from 43.0 pM to 90.1 µM. The IC₅₀ assays for each compound of interest were determined in quadruplicate, using two duplicate rows of each plate for a compound, with two replicate assays

performed for each plate.

Most of the hits were typical sulfonamide carbonic anhydrase inhibitors but there were two compounds that were not typical sulfonamides because they had internal sulfonamide groups (compounds **39** and **40** (Table 2.3)). Another hit that was not a typical sulfonamide was compound **13**, which contains a thiol group instead of a sulfonamide. Furthermore, there were three hit compounds with multiple sulfonamide groups: compounds **4** and **14** each have two sulfonamide groups and compound **2** has three sulfonamide groups.

The average IC_{50} value excluding the six compounds that did not inhibit CA II was 2.13 μM . There were 16 compounds (**2**, **3**, **4**, **14**, **16**, **19**, **22-28**, and **32-34**) with IC_{50} values below 1 μM , with the lowest IC_{50} value (0.4 μM) belonging to compound **19**. The highest IC_{50} value was observed for compound **35** (13.9 μM). The range of IC_{50} values for the 16 hit compounds below 1 μM was 0.4 to 0.99 μM and four of those compounds had IC_{50} values approaching the 0.312 μM IC_{50} value observed for the strong CA II inhibitor, acetazolamide (Table 2.2). For the remaining 18 compounds, the IC_{50} values were all below 5 μM , except for three compounds (**7**, **13**, and **35**).

Compounds **6**, **8**, **20**, and **30** are amphiphilic compounds and might have behaved as promiscuous inhibitors during the initial screening; however, no further CAII inhibition was observed for these compounds in follow-up assays. Compounds **1** and **9** may have bound via hydrophobic interactions to inhibit CA II during the initial screening of the NCI library.

Compound **40** contains an internal sulfonamide-like group, but does not have an exposed terminal sulfonamide group. It is strictly speculation at this point, but one hypothesis is that this compound is first cleaved by hydrolysis of the ester bond, to release a terminal sulfonamide group that can then bind to the CA II zinc ion. This proposed prodrug mechanism is similar to thioxolone, another prodrug⁴⁸, except that thioxolone cleavage by CA II yields a reactive thiol group, and there is no sulfonamide group in the final active inhibitor. A possible reaction mechanism for compound **40** is shown in Figure 2.6. The compound 4-methylbenzenesulfonamide (CAS 70-55-3), which is commercially available, can be used to test the proposed reaction mechanism for compound **40** by comparing the IC₅₀ results of 4-methylbenzenesulfonamide with the IC₅₀ value for compound **40** (Table 2.3).

Table 2.3. Carbonic anhydrase II inhibitor compounds identified in a screen of the NCI Diversity set compound library ^a.

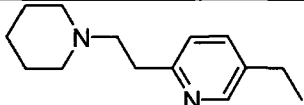
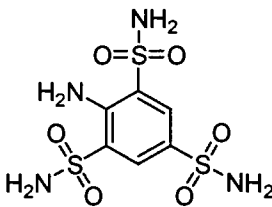
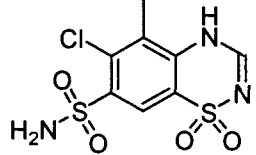
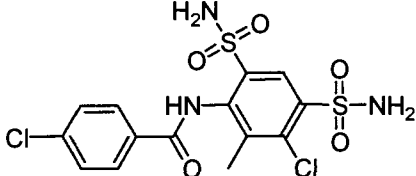
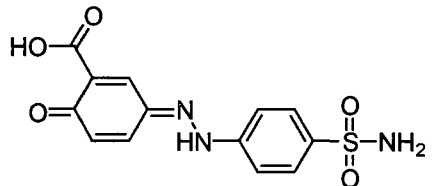
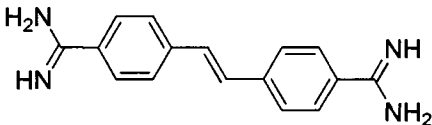
NCI Compound Number	Molecular Structure	Molecular Weight (Da)	CA II Inhibition (μ M) ^{b, c}
1. NSC 22819-L		218	No inhibition ^d
2. NSC 25857-N		330	0.81 (.77 – 84)
3. NSC 25861-R		310	0.99 (94 – 1.04)
4. NSC 25869-Z		438	0.47 (.44 – .51)
5. NCS 27236-M		321	1.39 (1.32 – 1.47)
6. NSC 35605-J	 HCl	337	No inhibition ^d

Table 2.3. - Continued

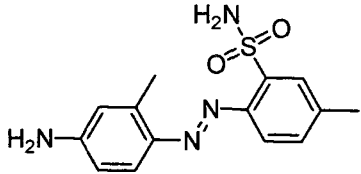
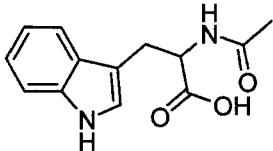
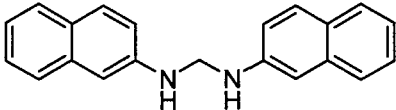
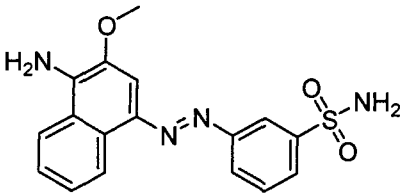
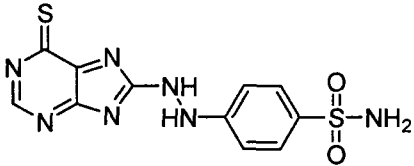
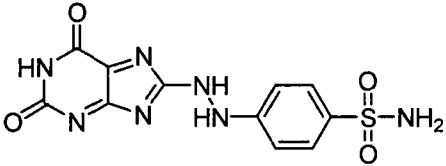
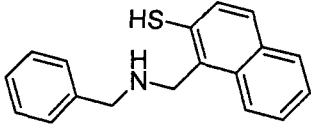
NCI Compound Number	Molecular Structure	Molecular Weight (Da)	CA II Inhibition (μ M) ^{b, c}
7. NSC 45527-S		304	8.1 (7.01 – 9.24)
8. NSC 49124-C		246	No inhibition ^d
9. NSC 57975-X		298	No inhibition ^d
10. NSC 65537-S		356	3.46 (3.21 – 3.64)
11. NSC 75140-H		335	2.08 (2.0 – 2.16)
12. NSC 77393-G		335	1.99 (1.91 – 2.07)
13. NSC 81747-N		279	5.68 (4.59 – 7.04)

Table 2.3. - Continued

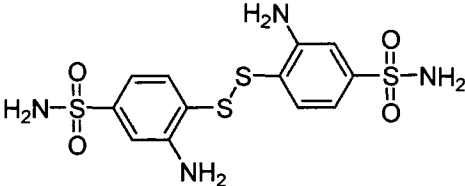
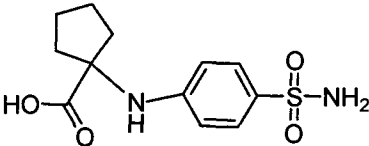
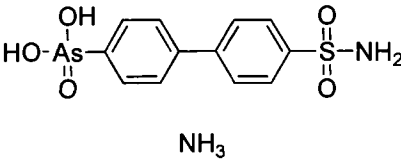
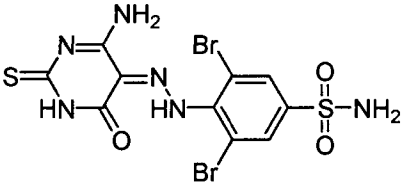
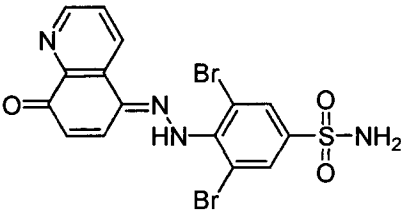
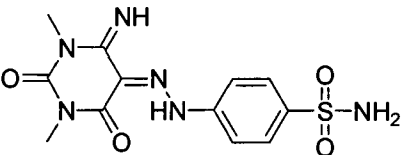
NCI Compound Number	Molecular Structure	Molecular Weight (Da)	CA II Inhibition (μ M) ^{b, c}
14. NCS 83217-L		407	0.57 (.53 – .61)
15. NSC 105432-J		284	1.77 (1.66 – 1.88)
16. NSC 108731-T		374	0.77 (.73 – .81)
17. NSC 114359-M		484	3.3 (3.16 – 3.45)
18. NSC 114381-L		486	2.41 (2.26 – 2.57)
19. NSC 114449-K		338	0.4 (.38 – .41)

Table 2.3. - Continued

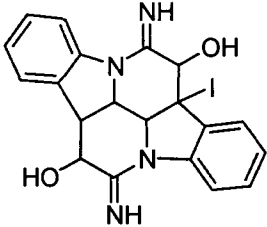
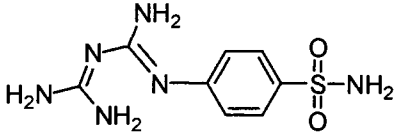
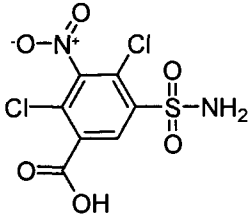
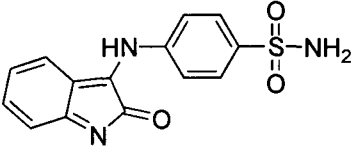
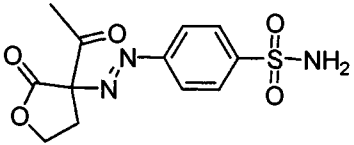
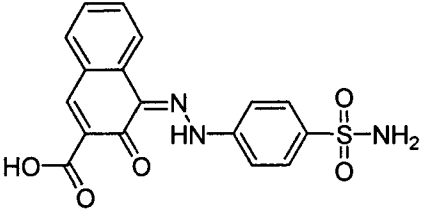
NCI Compound Number	Molecular Structure	Molecular Weight (Da)	CA II Inhibition (μM) ^{b, c}
20. NSC 118176-L		472	No inhibition ^d
21. NSC 125201-V		256	4.64 (4.4 – 4.9)
22. NSC 132073-Q		315	0.55 (.50 – .60)
23. NSC 133074-F		301	0.9 (.85 – .95)
24. NSC 134120-Q		311	0.88 (.82 – .93)
25. NSC 134137-K		371	0.63 (.59 – .67)

Table 2.3. - Continued

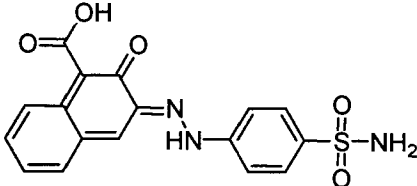
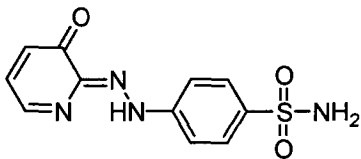
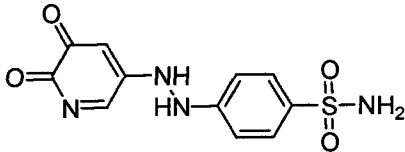
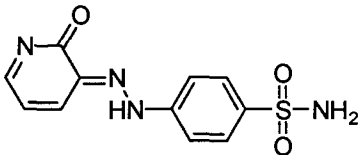
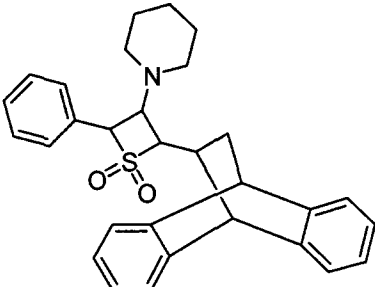
NCI Compound Number	Molecular Structure	Molecular Weight (Da)	CA II Inhibition (μ M) ^{b, c}
26. NSC 134148-V		371	0.7 (.63 – .78)
27. NSC 134149-W		278	0.91 (.85 – .98)
28. NSC 134159-J		294	0.65 (.60 – .70)
29. NSC 134196-X		278	2.11 (2.02 – 2.23)
30. NSC 135371-Z		470	No inhibition ^d

Table 2.3. - Continued

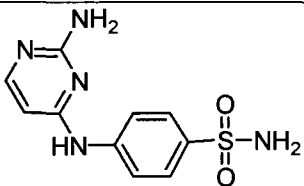
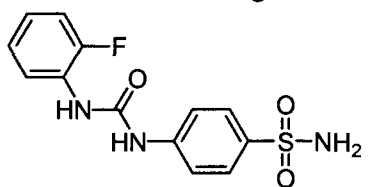
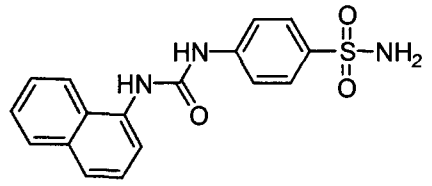
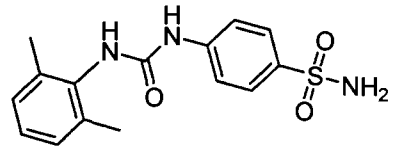
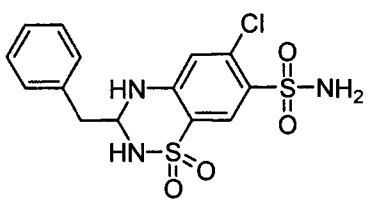
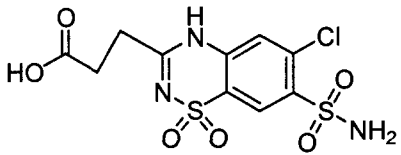
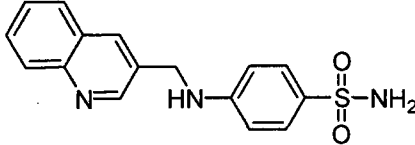
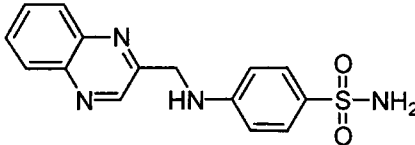
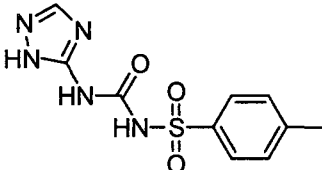
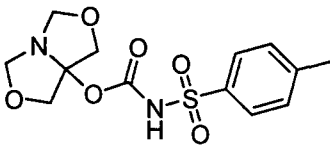
NCI Compound Number	Molecular Structure	Molecular Weight (Da)	CA II Inhibition (μ M) ^{b, c}
31. NCS 135784-Y		265	1.5 (1.38 – 1.63)
32. NCS 204667-W		309	0.64 (.62 – .67)
33. NSC 205628-R		341	0.58 (.55 – .61)
34. NSC 205842-Y		319	0.51 (.48 – .54)
35. NSC 263220-R		388	13.9 (11.15 – 17.28)
36. NCS 279835-A		368	3.05 (2.89 – 3.223.05)

Table 2.3. - Continued

NCI Compound Number	Molecular Structure	Molecular Weight (Da)	CA II Inhibition (μ M) ^{b, c}
37. NCS 299209-L		313	1.03 (.89 – 1.12)
38. NCS 299210-M		314	1.46 (1.23 – 1.74)
39. NSC 307711-A		281	2.34 (1.94 – 2.81)
40. NSC 320870-G		328	1.12 (.90 – 1.39)

^a http://dtp.nci.nih.gov/branches/dscb/diversity_explanation.html

^b IC₅₀ values for inhibition of 4-NPA esterase kinetic rate, determined by absorbance measurements at 348 nm and GraphPad Prism version 4.03 was used to fit the data.

^c Error range for fitted IC₅₀ value was defined as a 95% confidence interval.

^d No inhibition was observed upon rescreening this compound.

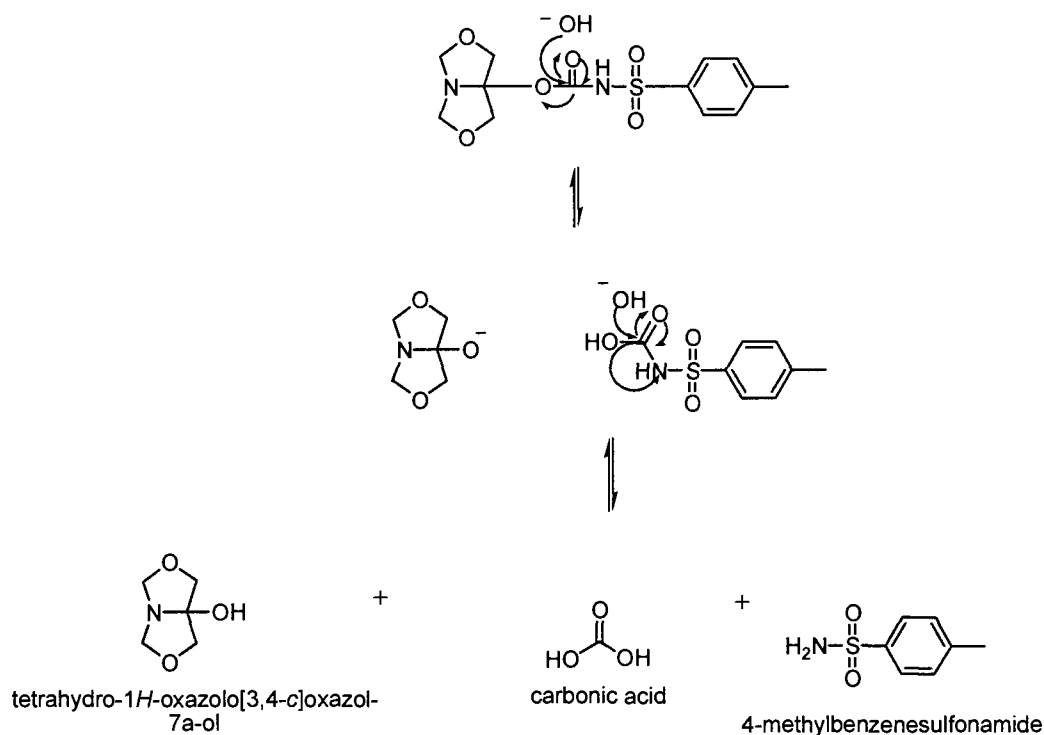


Figure 2.6. A possible pro-drug reaction mechanism for NCI compound NSC 320870-G, which involves ester bond hydrolysis to release an active terminal sulfonamide group.

Discussion

Limitations of 4-NPA Esterase Assay

The 4-NPA colorimetric assay could possibly be adapted to higher density homogeneous assay formats for screening CA II, e.g., 384 well and 1536 well plates to minimize reagent use and increase throughput. The screening assay relies on the biologically irrelevant yet fortuitous high rate of 4-NPA esterase activity of the CA II isozyme^{14,18}. The ability of different α -class CA isozymes to catalyze this esterase

reaction can vary greatly³⁴. For example, 4-NPA esterase activity is 150-fold lower for the CA IV isozyme than for CA II²⁶, and the CA III isozyme exhibits very little detectable esterase activity with this same substrate⁵⁶. Furthermore, the rate can be increased or decreased by site-directed mutagenesis of active site residues^{28,57,58}. The chemical structure and substitution position of the nitro group in the aromatic ring of the ester substrate can also have a profound influence on the observed esterase activity, e.g. 4-, 3-, and 2-nitrophenyl acetate and 4-nitrophenyl propionate exhibited different rates of hydrolysis with CA II²⁸. Thus, the 4-NPA substrate or a structurally similar one may be adapted for screening of inhibitor compounds with some α -CA isozymes, but it may not be applicable to other α -class CA isozymes that have much lower rates of 4-NPA esterase activity, e.g., CA III and other structurally unrelated CA isoforms such as γ -CA (Cam)⁵⁹, known to have much lower rates of 4-NPA esterase activity⁶⁰. However, it may be possible to obtain or synthesize other nitrophenol ester derivatives that may yield higher rates of hydrolysis with some CA isozymes as observed for mutants of CA II²⁸. Although the esterase screening assay is effective for identifying competitive inhibitors, it is probably not useful for identifying activators of the physiologically relevant CO₂ hydration/HCO₃³⁻ dehydration reaction in CA. The non-physiological 4-NPA hydrolysis reaction may not involve the same type of two-step ping-pong reaction observed for the CO₂ hydration reaction^{34,59}, including the rate-limiting proton transfer step, which is typically rescued by imidazole compounds⁶¹⁻⁶³. Alternatively, a colorimetric^{26,64} or fluorescence⁶⁵ pH indicator assay of the physiological catalytic activity could

potentially be adapted from single sample, stopped-flow format to HTS format. These stopped-flow assays directly monitor the intrinsic catalytic activity of CA isoforms by monitoring the pH change as the substrate, HCO_3^- , is catalytically dehydrated to yield CO_2 or the reverse reaction. However, either reaction will require a rapid injection and monitoring system, due to the short reaction time, roughly 90 sec or less, typically observed for the CO_2 hydration reaction in stopped-flow assays. An abstract by Hochman et al.⁶⁶ cited this approach and concluded that it may yield more biologically relevant inhibition parameters.

Esterase vs. Fluorescence Screening Assays

In this study, two mechanistically different assays were used to probe the CA II active site. First, the 4-NPA esterase assay originally described as a cuvette-based assay¹⁸ was adapted into a 96-well microplate HTS format. The 4-NPA esterase assay has been used in numerous studies to characterize the activity of CAs. This colorimetric absorbance assay is simple and robust, even if the test compounds have significant background absorbance at the measured wavelength. When measuring kinetic changes in absorbance, the higher background signal due to colored compound has little effect on the change in absorbance resulting from hydrolysis of the 4-NPA substrate.

A second, fluorescence intensity screening assay was also attempted with the GenPlus library, using the fluorescent probe DNSA, known to bind to CA II. This second assay monitored binding of the probe DNSA to the CA II active site by monitoring the increase in fluorescence upon binding to the hydrophobic pocket of

the active site²⁴⁻²⁶. Both types of assays used in this study require the addition of a molecular probe, either 4-NPA in the esterase assay or dansylamide in the binding assay. Although the second assay was performed under equilibrium conditions and thus avoids the complicated analysis of kinetics, it involves excitation of the probe at the wavelength of 280 nm. However, numerous test compounds, typically 3-5% of the compounds in each plate, were also observed to exhibit autofluorescence in this system, yielding extremely high background levels of fluorescence relative to the DNSA fluorescence intensity (unpublished data). This phenomenon appears to be a common fluorescence screening problem, as reviewed by Gribbon and Sewing⁶⁷. To address this issue, collection of multiple data sets at different gain settings was performed with each compound plate to allow sensitive in-range readings of all test compounds. Even after implementing this precaution, results were inconsistent with those of the 4-NPA esterase and the fluorescence intensity screening approach assay; some compounds may also quench fluorescence of the DNSA probe molecule, resulting in false hits by this method⁶⁷.

References

1. Lee, D. A.; Higginbotham, E. J. Glaucoma and its treatment: a review. *Am J Health Syst Pharm* 2005, 62, 691-9.
2. Sheth, R. D. Metabolic concerns associated with antiepileptic medications. *Neurology* 2004, 63, S24-9.
3. Epstein, D. L.; Grant, W. M. Carbonic anhydrase inhibitor side effects: serum chemical analysis. *Archives of Ophthalmology* 1977, 95, 1378-1382.
4. Wallace, T.; Fraunfelder, F.; Petursson, G.; Epstein, D. Decreased libido-a side effect of carbonic anhydrase inhibitor. *Annals of Ophthalmology* 1979, 11, 1563-1566.
5. Lichter, P. R.; Newman, L. P.; Wheeler, N. C.; Beall, O. V. Patient tolerance to carbonic anhydrase inhibitors. *American journal of Ophthalmology* 1978, 85, 495-502.
6. Lichter, P. R. Reducing side effects of carbonic anhydrase inhibitors. *Ophthalmology* 1981, 88, 266-269.
7. Slatore, C. G.; Tilles, S. A. Sulfonamide hypersensitivity. *Immunol Allergy Clin North Am* 2004, 24, 477-90, vii.
8. Supuran, C. T.; Innocenti, A.; Mastrolorenzo, A.; Scozzafava, A. Antiviral sulfonamide derivatives. *Mini Rev Med Chem* 2004, 4, 189-200.
9. Maryanoff, B.; McComsey, D.; Costanzo, M.; Hochman, C.; Smith-Swintosky, V.; Shank, R. Comparison of sulfamate and sulfamide groups for the inhibition of carbonic anhydrase-II by using topiramate as a structural platform. *Journal of Medicinal Chemistry* 2005, 48, 1941-1947.
10. Morgan, P. E.; Supuran, C. T.; Casey, J. R. Carbonic anhydrase inhibitors that directly inhibit anion transport by the human Cl⁻/HCO₃⁻ exchanger, AE1. *Mol Membr Biol* 2004, 21, 423-33.
11. Abbate, F.; Coetzee, A.; Casini, A.; Ciattini, S.; Scozzafava, A.; Supuran, C. T. Carbonic anhydrase inhibitors: X-ray crystallographic structure of the adduct of

- human isozyme II with the antipsychotic drug sulpiride. *Bioorg Med Chem Lett* 2004, 14, 337-41.
12. Maren, T. H.; Conroy, C. W. A new class of carbonic anhydrase inhibitor. *J Biol Chem* 1993, 268, 26233-9.
 13. Vullo, D.; Franchi, M.; Gallori, E.; Pastorek, J.; Scozzafava, A.; Pastorekova, S.; Supuran, C. T. Carbonic anhydrase inhibitors: inhibition of the tumor-associated isozyme IX with aromatic and heterocyclic sulfonamides. *Bioorg Med Chem Lett* 2003, 13, 1005-1009.
 14. Gould, S. M.; Tawfik, D. S. Directed evolution of the promiscuous esterase activity of carbonic anhydrase II. *Biochemistry* 2005, 44, 5444-52.
 15. Iyer, R.; Barrese, A. A., 3rd; Parakh, S.; Parker, C. N.; Tripp, B. C. Inhibition profiling of human carbonic anhydrase II by high-throughput screening of structurally diverse, biologically active compounds. *J Biomol Screen* 2006, 11, 782-91.
 16. Wermuth, C. G. Selective optimization of side activities: another way for drug discovery. *J Med Chem* 2004, 47, 1303-14.
 17. Nair, S. K.; Calderone, T. L.; Christianson, D. W.; Fierke, C. A. Altering the mouth of a hydrophobic pocket: structure and kinetics of human carbonic anhydrase II mutants at residue Val-121. *J. Biol. Chem.* 1991, 266, 17320-5.
 18. Pocker, Y.; Stone, J. T. The catalytic versatility of erythrocyte carbonic anhydrase. III: kinetic studies of enzyme-catalyzed hydrolysis of *p*-nitrophenyl acetate. *Biochemistry* 1967, 3, 668-678.
 19. Verpoorte, J. A.; Mehta, S.; Edsall, J. T. Esterase activities of human carbonic anhydrases B and C. *J Biol Chem* 1967, 242, 4221-9.
 20. McGovern, S. L.; Helfand, B. T.; Feng, B.; Shoichet, B. K. A specific mechanism of nonspecific inhibition. *J Med Chem* 2003, 46, 4265-72.
 21. McGovern, S. L.; Caselli, E.; Grigorieff, N.; Shoichet, B. K. A common mechanism underlying promiscuous inhibitors from virtual and high-throughput screening. *J Med Chem* 2002, 45, 1712-22.

22. Seidler, J.; McGovern, S. L.; Doman, T. N.; Shoichet, B. K. Identification and prediction of promiscuous aggregating inhibitors among known drugs. *J Med Chem* 2003, 46, 4477-86.
23. Walters, W. P.; Namchuk, M. Designing screens: how to make your hits a hit. *Nat Rev Drug Discov* 2003, 2, 259-66.
24. Chen, R.; Kernohan, J. Combination of bovine carbonic anhydrase with a fluorescent sulfonamide. *Journal of Biological Chemistry* 1967, 242, 5813-5823.
25. Banerjee, A. L.; Tobwala, S.; Ganguly, B.; Mallik, S.; Srivastava, D. K. Molecular basis for the origin of differential spectral and binding profiles of dansylamide with human carbonic anhydrase I and II. *Biochemistry* 2005, 44, 3673-82.
26. Baird, T. T., Jr.; Waheed, A.; Okuyama, T.; Sly, W. S.; Fierke, C. A. Catalysis and inhibition of human carbonic anhydrase IV. *Biochemistry* 1997, 36, 2669-78.
27. Zhang, J. H.; Chung, T. D.; Oldenburg, K. R. A simple statistical parameter for use in evaluation and validation of high-throughput screening assays. *J Biomol Screen* 1999, 4, 67-73.
28. Elleby, B.; Sjoblom, B.; Lindskog, S. Changing the efficiency and specificity of the esterase activity of human carbonic anhydrase II by site-specific mutagenesis. *Eur J Biochem* 1999, 262, 516-21.
29. Banerjee, A. L.; Swanson, M.; Roy, B. C.; Jia, X.; Haldar, M. K.; Mallik, S.; Srivastava, D. K. Protein surface-assisted enhancement for recombinant human carbonic anhydrase II. *Journal of the American Chemical Society* 2004, 126, 10875-10883.
30. Elleby, B.; Sjoblom, B.; Tu, C.; Silverman, D. N.; Lindskog, S. Enhancement of catalytic efficiency by the combination of site-specific mutations in a carbonic anhydrase-related protein. *Eur J Biochem* 2000, 267, 5908-5915.

31. Innocenti, A.; Casini, A.; Alcaro, M. C.; Papini, A. M.; Scozzafava, A.; Supuran, C. T. Carbonic anhydrase inhibitors: the first on-resin screening of a 4-sulfamoylphenylthiourea library. *J Med Chem* 2004, 47, 5224-9.
32. Supuran, C. T.; Scozzafava, A.; Conway, J. Carbonic anhydrase. its inhibitors and activators. CRC Press: New York, 2004; Vol. 1, p 363.
33. Mann, B.; Keilin, D. Sulphanilamide as a specific inhibitor of carbonic anhydrase. *Nature* 1940, 146, 164-165.
34. Lindskog, S. Structure and mechanism of carbonic anhydrase. *Pharmacol. Ther.* 1997, 74, 1-20.
35. Di Fiore, A.; De Simone, G.; Menchise, V.; Pedone, C.; Casini, A.; Scozzafava, A.; Supuran, C. T. Carbonic anhydrase inhibitors: X-ray crystal structure of a benzenesulfonamide strong CA II and CA IX inhibitor bearing a pentafluorophenylaminothioureido tail in complex with isozyme II. *Bioorg Med Chem Lett* 2005, 15, 1937-42.
36. Ponto, L. L.; Schoenwald, R. D. Furosemide (frusemide). A pharmacokinetic/pharmacodynamic review (Part I). *Clin Pharmacokinet* 1990, 18, 381-408.
37. Fuchs, F. D. Diuretics: drugs of choice for the initial management of patients with hypertension. *Expert Rev Cardiovasc Ther* 2003, 1, 35-41.
38. Brors, O.; Braut, G. S.; Braut, S.; Jacobsen, S. Interaction of hydroflumethiazide and 2,4-disulfamyl-5-trifluoromethylaniline with cyclic AMP phosphodiesterase and carbonic anhydrase. *Acta Pharmacol Toxicol (Copenh)* 1982, 51, 273-7.
39. Schaeffer, P.; Vigne, P.; Frelin, C.; Lazdunski, M. Identification and pharmacological properties of binding sites for the atypical thiazide diuretic, indapamide. *Eur J Pharmacol* 1990, 182, 503-8.
40. Goldfarb, D. S.; Chan, A. J.; Hernandez, D.; Charney, A. N. Effect of thiazides on colonic NaCl absorption: role of carbonic anhydrase. *Am J Physiol* 1991, 261, F452-8.

41. Puscas, I.; Coltau, M.; Baican, M.; Domuta, G.; Hecht, A. Vasodilatory effect of diuretics is dependent on inhibition of vascular smooth muscle carbonic anhydrase by a direct mechanism of action. *Drugs Exp Clin Res* 1999, 25, 271-9.
42. Puscas, I.; Coltau, M.; Baican, M.; Pasca, R.; Domuta, G. The inhibitory effect of diuretics on carbonic anhydrases. *Res Commun Mol Pathol Pharmacol* 1999, 105, 213-36.
43. Weber, A.; Casini, A.; Heine, A.; Kuhn, D.; Supuran, C. T.; Scozzafava, A.; Klebe, G. Unexpected nanomolar inhibition of carbonic anhydrase by COX-2-selective celecoxib: new pharmacological opportunities due to related binding site recognition. *J Med Chem* 2004, 47, 550-7.
44. Mitsuhashi, S. Drug resistance in bacteria: history, genetics and biochemistry. *J Int Med Res* 1993, 21, 1-14.
45. Hackenberg, H. W. Reduction of the microbial count of surface water with halazone and its mixture with chalk as a sedimentation accelerator. *Z Gesamte Hyg* 1964, 10, 241-51.
46. Rack, M.; Rubly, N.; Waschow, C. Effects of some chemical reagents on sodium current inactivation in myelinated nerve fibers of the frog. *Biophys J* 1986, 50, 557-64.
47. Khalifah, R. G. Reflections on Edsall's carbonic anhydrase: paradoxes of an ultra fast enzyme. *Biophysical Chemistry* 2003, 100, 159-170.
48. Barrese, A. A., 3rd; Genis, C.; Fisher, S. Z.; Orwenyo, J. N.; Kumara, M. T.; Dutta, S. K.; Phillips, E.; Kiddle, J. J.; Tu, C.; Silverman, D. N.; Govindasamy, L.; Agbandje-McKenna, M.; McKenna, R.; Tripp, B. C. Inhibition of carbonic anhydrase II by thioxolone: a mechanistic and structural study. *Biochemistry* 2008, 47, 3174-84.
49. Eriksson, A. E.; Jones, T. A.; Liljas, A. Refined structure of human carbonic anhydrase II at 2.0 Å resolution. *Proteins* 1988, 4, 274-82.

50. Scolnick, L.; Clements, M.; Liao, J.; Crenshaw, L.; Hellberg, M.; May, J.; Dean, T.; Christianson, D. Novel binding mode of hydroxamate inhibitors to human carbonic anhydrase II. *Journal of the American Chemical Society* 1997, 119, 850-851.
51. Stams, T.; Chen, Y.; Boriack-Sjodin, P. A.; Hurt, J. D.; Liao, J.; May, J. A.; Dean, T.; Laipis, P.; Silverman, D. N.; Christianson, D. W. Structures of murine carbonic anhydrase IV and human carbonic anhydrase II complexed with brinzolamide: molecular basis of isozyme-drug discrimination. *Protein Sci* 1998, 7, 556-63.
52. Duda, D.; Govindasamy, L.; Agbandje-McKenna, M.; Tu, C.; Silverman, D. N.; McKenna, R. The refined atomic structure of carbonic anhydrase II at 1.05 Å resolution: implications of chemical rescue of proton transfer. *Acta Crystallogr D Biol Crystallogr* 2003, 59, 93-104.
53. Feng, B. Y.; Shelat, A.; Doman, T. N.; Guy, R. K.; Shoichet, B. K. High-throughput assays for promiscuous inhibitors. *Nat Chem Biol* 2005, 1, 146-8.
54. Tu, C.; Qian, M.; Earnhardt, J. N.; Laipis, P. J.; Silverman, D. N. Properties of intramolecular proton transfer in carbonic anhydrase III. *Biophys J* 1998, 74, 3182-9.
55. Cheng, Y.; Prusoff, W. H. Relationship between the inhibition constant (K_i) and the concentration of inhibitor which causes 50 per cent inhibition (I_{50}) of an enzymatic reaction. *Biochem Pharmacol* 1973, 22, 3099-108.
56. Ren, X. L.; Jonsson, B. H.; Lindskog, S. Some properties of site-specific mutants of human carbonic anhydrase II having active-site residues characterizing carbonic anhydrase III. *Eur J Biochem* 1991, 201, 417-20.
57. Behravan, G.; Jonasson, P.; Jonsson, B. H.; Lindskog, S. Structural and functional differences between carbonic anhydrase isoenzymes I and II as studied by site-directed mutagenesis. *Eur J Biochem* 1991, 198, 589-92.

58. Krebs, J. F.; Fierke, C. A. Determinants of catalytic activity and stability of carbonic anhydrase II as revealed by random mutagenesis. *J Biol Chem* 1993, 268, 948-54.
59. Tripp, B.; Smith, K.; Ferry, J. Carbonic Anhydrase: New insights for an ancient enzyme. *Journal of Biological Chemistry* 2001, 276, 48615-48618.
60. Alber, B. E.; Ferry, J. G. Characterization of heterologously produced carbonic anhydrase from *Methanosarcina thermophila*. *J Bacteriol* 1996, 178, 3270-4.
61. Tu, C. K.; Silverman, D. N.; Forsman, C.; Jonsson, B. H.; Lindskog, S. Role of histidine 64 in the catalytic mechanism of human carbonic anhydrase II studied with a site-specific mutant. *Biochemistry* 1989, 28, 7913-8.
62. Tripp, B. C.; Ferry, J. G. A structure-function study of a proton transport pathway in the gamma-class carbonic anhydrase from *Methanosarcina thermophila*. *Biochemistry* 2000, 39, 9232-40.
63. Tu, C.; Rowlett, R. S.; Tripp, B. C.; Ferry, J. G.; Silverman, D. N. Chemical rescue of proton transfer in catalysis by carbonic anhydrases in the beta- and gamma-class. *Biochemistry* 2002, 41, 15429-35.
64. Khalifah, R. The carbon dioxide hydration activity of carbonic anhydrase: stop-flow kinetic studies on the native human isozymes B and C. *Journal of Biological Chemistry* 1971, 246, 2561-2573.
65. Shingles, R.; Moroney, J. V. Measurement of carbonic anhydrase activity using a sensitive fluorometric assay. *Anal Biochem* 1997, 252, 190-7.
66. Hochman, C. B., Smith-Swintosky, V.P., and Shank, R.P. . Carbonic anhydrase inhibitors: how should we assay them? *In. Society for Neuroscience Abstract Viewer and Itinerary Planner* 2003.
67. Gribbon, P.; Sewing, A. Fluorescence readouts in HTS: no gain without pain? *Drug Discov Today* 2003, 8, 1035-43.

CHAPTER III

MECHANISTIC STUDIES OF HUMAN CARBONIC ANHYDRASE II INHIBITION BY THIOXOLONE

This chapter reproduced with permission from *Biochemistry* 2008, 47, 3174-8; Copyright 2010, American Chemical Society.

Introduction

This chapter describes a preliminary investigation of human carbonic anhydrase II (CA II) inhibition by thioxolone (IUPAC name: 6-hydroxy-1,3-benzoxathiol-2-one, Figure 3.1). Thioxolone is a low molecular mass (mol mass: 168.2 g/mol), biologically-active compound with the chemical formula $C_7H_4O_3S$. It was originally identified as a weak inhibitor of human CA II in a high-throughput screen of the Genesis Plus library of 960 biologically-active compounds by Iyer et al¹.

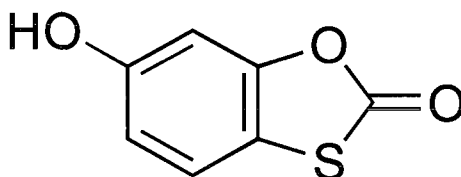


Figure 3.1. Chemical structure of thioxolone, a novel CA II inhibitor identified in a screen of the 960 compound Genesis Plus compound library.

As reviewed by Byres and Cox², thioxolone has been classified as an antiseborrheic agent³ and has been used in the treatment of skin conditions such as acne⁴ and dandruff. Some hair-care products such as shampoos have incorporated

thioxolone into their formulation as an antiseborrheic agent³. Other reported medically useful properties include cytostatic⁵, antipsoriatic, antibacterial, and antimycotic activity³; however, some toxicity issues involving contact dermatitis have also been reported for this compound⁶. The thioxolone structure is somewhat polar, with an XlogP value of 1.3 and has one hydrogen bond donor (a hydroxyl group) on one end and three hydrogen bond acceptors, including a carbonyl group on the other end, allowing for the formation of extensive hydrogen bonds². This structure lacks sulfonamide, sulfamate, or related functional groups that are typically a key structural feature of known CA inhibitors⁷⁻⁹. Thus, it potentially represents a new class of lead compound for further exploration and development as a non-sulfonamide therapeutic CA inhibitor. The structure of thioxolone was recently determined by X-ray diffraction (Figure 3.2)².

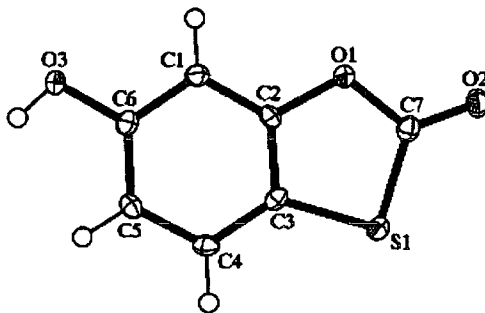


Figure 3.2. A view of the atomic arrangement of thioxolone, determined by X-ray diffraction, showing the atom-numbering scheme and 50% probability displacement ellipsoids. Adapted from Byres and Cox².

The preliminary characterization of thioxolone inhibition indicated that it was a relatively weak CA II inhibitor, relative to some therapeutic sulfonamide inhibitors,

both in a kinetic esterase assay with the substrate 4-NPA and in a competitive binding assay with the fluorescent probe, dansylamide. Thioxolone (compound **1**) yielded an IC_{50} value of 1.8 μ M and a K_d value of 33 μ M vs. an IC_{50} value of 0.31 μ M and a K_d value of 20 nM for acetazolamide (compound **2**), a therapeutic CA inhibitor¹ (All compound structures are listed in Table 3.1). The mechanism of CA II inhibition was not immediately obvious from the thioxolone structure (Figure 3.1). Phenol is a well-known CA inhibitor¹⁰⁻¹² and the C6 hydroxyl group of thioxolone could function in a phenol-like manner in binding to the zinc ion. The five-membered ring of thioxolone also contains both ester and thioester groups, which could mimic the transition state for the CA-catalyzed esterase reaction. Furthermore, either or both of the ester and thioester bonds could function as substrates for the well-known non-physiological esterase activity of CA II^{13,14}, which involves a zinc-hydroxide mechanism¹³⁻¹⁹.

Regardless of the mechanism, thioxolone represents a novel class of CA inhibitor that may function as the basis for new types of CA-specific drugs. Analytical chemistry and biochemical methods were used to investigate the fate of thioxolone upon binding to CA II, including Michaelis–Menten kinetics of 4-nitrophenyl acetate esterase cleavage, liquid chromatography–mass spectrometry (LC-MS), oxygen-18 isotope exchange studies, and X-ray crystallography, in collaboration with the research groups of Prof. Robert McKenna, and Prof. David N. Silverman, who are both at the University of Florida, Gainesville, FL.

Experimental Procedures

Enzyme Expression and Purification

The CA II expression plasmid, pACA, was a generous gift from Dr. Carol Fierke, University of Michigan. This plasmid contains the mature form of human CA II under control of the T7 promoter²⁰. The enzyme was expressed by growing *Escherichia coli* BL21 (DE3) cultures in Luria-Bertani (LB) media (1 L media per 2 L flask) at 37 °C, with shaking at 225 rpm to an OD₆₀₀ of 0.5 to 0.8, followed by induction with 0.1 mM IPTG for 3 h. Cells were lysed in 20 mM, pH 7.5 MOPS buffer containing 1.0 mg/ml lysozyme, 5 µg/ml deoxyribonuclease I, 5 mM MgSO₄, with stirring, on ice, for 30 min. The lysate was clarified by centrifugation at 8000 x g for 15 min and loaded onto an SP Sepharose 26/20 Fast Flow cation exchange column (~50 ml, 2.6 mm x 20 cm height, Amersham Biosciences, Piscataway, NJ). CA II was eluted with a 0 to 1.0 M linear NaCl gradient (over 10 column volumes), using a Fast Protein Liquid Chromatography (FPLC) system. Fractions containing CA II were pooled and concentrated using a Centricon device with a YM-10 membrane (10 kDa mol. mass cutoff) (Millipore, Billerica, MA), then aliquoted into Eppendorf 1.5 ml tubes and frozen in liquid nitrogen and stored at -80 °C until use. Samples of purified CA II were assessed to be >95% pure by sodium dodecyl sulfate polyacrylamide gel electrophoresis (SDS-PAGE), (Figure 3.3). The CA II protein concentration was determined via absorbance measurements at 280 nm using a published molar absorptivity for CA II of $5.4 \times 10^4 \text{ M}^{-1} \text{ cm}^{-1}$ ²⁰.

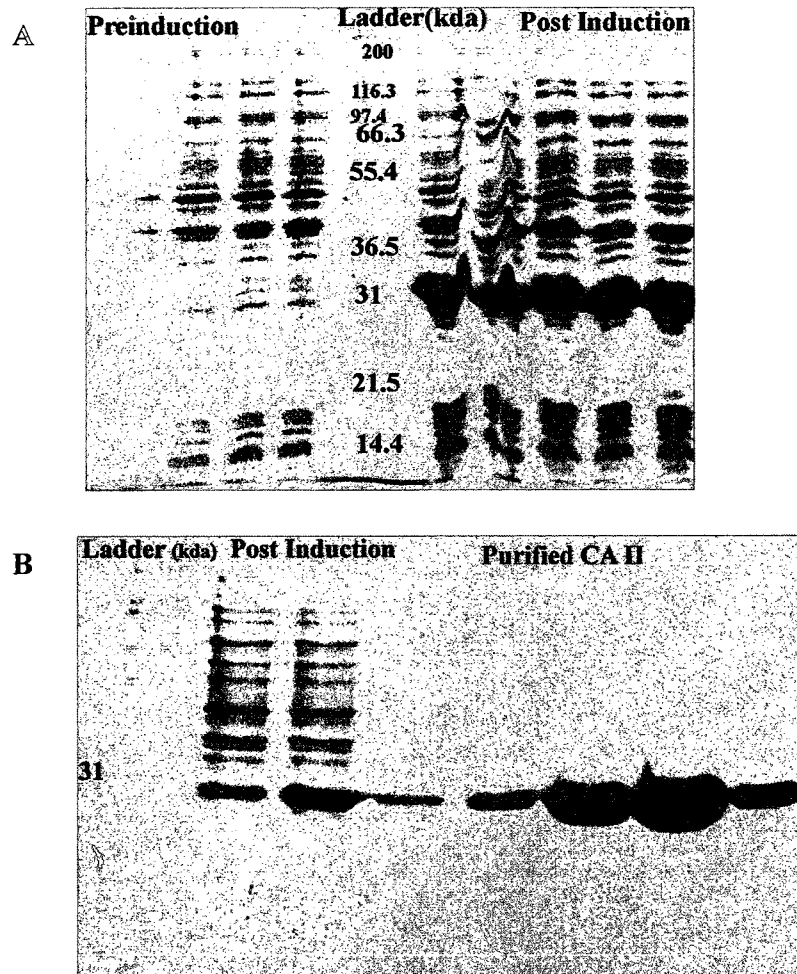


Figure 3.3. A.) SDS polyacrylamide gel showing preinduction whole cell lysate and three hour post-induction whole cell lysate of CA II expression. B.) SDS polyacrylamide gel of whole cell lysate with induced CA II and the eluted fractions of CA II after purification by ion exchange chromatography on an SP Sepharose column.

Materials

Pure analytical grade thioxolone (99% purity) and other chemicals and solvents were obtained from Sigma-Aldrich (St. Louis, MO), unless otherwise noted. The thioxolone hydrolysis product (compound **3**) was prepared by acid hydrolysis of thioxolone. A set of 13 structural analogues of thioxolone, compounds 6–18 were obtained from Specs (Delft, Netherlands). Three other thioxolone analogues, compounds 19–21, were synthesized in the James Kiddle research group, Chemistry Dept., Western Michigan University, using thioxolone as the starting compound.

Preparation of 4-mercaptobenzene-1,3-diol (Compound 3) by acid hydrolysis of thioxolone (Compound 1)

The thioxolone hydrolysis product observed in the preliminary crystal structure, 4-mercaptobenzene-1,3-diol, was not commercially available. Therefore, it was synthetically prepared from thioxolone by acid hydrolysis and purified by silica column chromatography, after initial attempts to hydrolyze it at high pH with NaOH were unsuccessful. The acid hydrolysis of thioxolone was accomplished with the help of M. Thilak Kumara, a Ph.D graduate student in the WMU Chemistry Dept. and a member of the Tripp research group. Four grams of 99% pure thioxolone (Compound **1**; 6-hydroxybenzo [d][1,3]oxathiol-2-one) were suspended in 50 ml of deionized (DI) water and dissolved by addition of 1 M sodium hydroxide in a drop-wise manner. A solution of 0.5 M sulfuric acid was then added in a drop-wise manner until a cloudy solution was generated. The resulting solution was stored at 4 °C overnight to allow crystallization to occur. The resulting white, needle-like crystals were

isolated by vacuum filtering using a Buchner funnel with Whatman No. 1 qualitative 70 mm filter paper. The recrystallized thioxolone crystals were transferred to a 500 ml three-necked round bottom flask and resuspended in 70 ml of DI water. The flask was sealed with a rubber septum and connected to a condenser. The flask and sample were purged of oxygen by flowing nitrogen gas through the system for 30 min. A volume of 30 ml of 0.5 M sulfuric acid was injected into the system through the rubber septum cap. The system was again purged with nitrogen for a further fifteen min to ensure that all of the oxygen was removed. Nitrogen purging was then stopped and a nitrogen-filled rubber balloon was connected to the top of the condenser through the rubber septum cap. The rubber balloon was observed to expand during the hydrolysis reaction, indicating the generation of a gas, most likely CO₂ resulting from release and equilibration of carbonic acid with the solvent. The system was refluxed for four hours at 100 °C and then allowed to cool down to room temperature. Needle-like crystals formed as the solution cooled; these crystals were separated and collected by vacuum filtration with a Buchner funnel with Whatman No. 1 qualitative 70 mm filter paper. The solvent fraction of the mixture was also collected and stored in a smaller 100 ml round bottom flask and stored at room temperature for further analysis.

The resulting crystals of the 4-mercaptobenzene-1,3-diol hydrolysis product were dissolved in chloroform and analyzed by thin layer chromatography (TLC) (Uniplat, Analtech Inc., Newark, DE) using 10% acetone, 90% chloroform (vol./vol.) mixture and either directly visualized with a UV light or by staining via

incubating the plate with iodine gas in a sealed container (data not shown) and liquid chromatography-mass spectrometry (LC-MS). The solvent fraction was found to contain more 4-mercaptobenzene-1,3-diol and was therefore solvent extracted in two steps using 50 ml of chloroform in each step. The solid product was concentrated and dried to solid by rotoevaporation of the chloroform. The dried compound was dissolved in 5 ml of a mixture of 5% methanol and 95% (vol./vol.) chloroform mixture.

A glass chromatography column with a porous glass frit bottom (2 cm diameter x 50 cm length) was packed with 400 Å mesh column chromatography silica gel suspended in chloroform to give a packed gel bed height of 20 cm. The hydrolysis product from the final recrystallization step was loaded onto the column and eluted isocratically with a mixture of 10% methanol and 90% chloroform. The eluting fractions were collected in 10 ml aliquots and analyzed for the presence and purity of products with TLC. The purity of products was further confirmed by LC-MS. The purified samples were then pooled and placed in a 50 ml round bottom flask for rotoevaporation. The resulting semi-solid product was then resuspended in 1 ml of methanol and transferred into a pre-weighed 5 ml glass test tube. The test tube was then placed back inside the 50 ml round bottom flask and the sample was again rotoevaporated. After all of the methanol had been evaporated, the test tube was weighed and the final mass of the sample product was then calculated. The purified 4-mercaptobenzene-1,3-diol samples were analyzed by LC-MS to insure that none of the thioxolone starting compound was present, before they were combined and

concentrated by rotoevaporation. The purified samples yielded mass-to-charge ratio (m/z) values of 139-140, corresponding to the ionized states of the final monomer product, 4-mercaptobenzene-1,3-diol, and the disulfide-linked dimer, bis-4-mercaptobenzene-1,3-diol.

Carbonic Anhydrase 4-NPA Esterase Inhibition Studies

The CA II esterase activity with 4-NPA as the substrate²¹ has provided a reliable CA II activity assay that does not require the use of dissolved CO₂. The CA-catalyzed hydrolysis of 4-NPA results in the generation of a yellow 4-nitrophenolate anion with an isobestic point at 348 nm that is readily detected with a spectrophotometer²². IC₅₀ values were determined using a 4-NPA esterase assay in 96-well microplates as previously described¹, using 100 μ l of assay solution containing 1 μ M purified CA II in 50 mM, pH 7.5 MOPS, 33 mM Na₂SO₄, 1.0 mM EDTA buffer. The EDTA was added to minimize the background rate of solvent-catalyzed hydrolysis of the substrate. Thioxolone, 4-mercaptobenzene-1,3-diol, and other structural analogues were dissolved to a final concentration of 10 mM in 100% DMSO and were serially diluted 1:2 with pure DMSO in Costar 3365 round-bottom 96-well polypropylene plates (Corning, Lowell, MA). A volume of 1 μ l of each compound was then transferred into the assay solution, using a CCS Packard PlateTrak robotic liquid handling system (PerkinElmer, Shelton, CT). The IC₅₀ assays were determined in quadruplicate. Compounds were allowed to equilibrate with the enzyme for 15 min at room temperature. On each plate, the CA II inhibitor,

acetazolamide (10 μ M final concentration), was included as a positive control (100% inhibition) and 100% DMSO was included as a negative control (0% inhibition). The reaction was initiated by addition of 10 μ l of 5.5 mM 4-NPA solution in 100% DMSO, with a Multidrop dispenser (MTX Laboratory Systems, Vienna, VA), and data collection was started. The absorbance of each well was measured at 348 nm every 15 sec for 5 min with a SpectraMax Plus³⁸⁴ microplate spectrophotometer (Molecular Devices, Sunnyvale, CA), running SoftMax Pro software (version 4.8). The initial velocities, determined by the SoftMax Pro software, were normalized to a scale of 0% to 100% inhibition with an MS Excel spreadsheet, using the controls on each plate. This data was then fit using the GraphPad Prism (Version 4.03) graphing software to determine the IC₅₀ values for each compound.

Michaelis–Menten Enzyme Kinetic Studies

A limiting concentration of enzyme was titrated against increasing concentrations of inhibitors. CA II was diluted with 50 mM pH 7.5 MOPS buffer, 33 mM Na₂SO₄, 1 mM EDTA, and 0.01% Triton X-100 in 1.5 ml disposable polystyrene cuvettes (Bio-Rad, Hercules, CA) and also in flat-bottom 96-well plates (Costar 3370), followed by addition of thioxolone (10 mM stock solution in 100% DMSO) to give a final assay enzyme concentration of 1 μ M. The enzyme and thioxolone mixture was allowed to equilibrate for 15 min at room temperature, followed by addition of the 4-NPA substrate. The hydrolysis rate of 4-NPA was monitored by absorbance readings at 348 nm (A_{348}) with a SpectraMax Plus³⁸⁴ spectrophotometer

in the kinetic data acquisition mode. Absorbance readings were collected every 9 sec for 5 min, and initial data in the range of 5 to 30 sec from each run were used to calculate the initial velocity, v_0 (Figure 3.4).

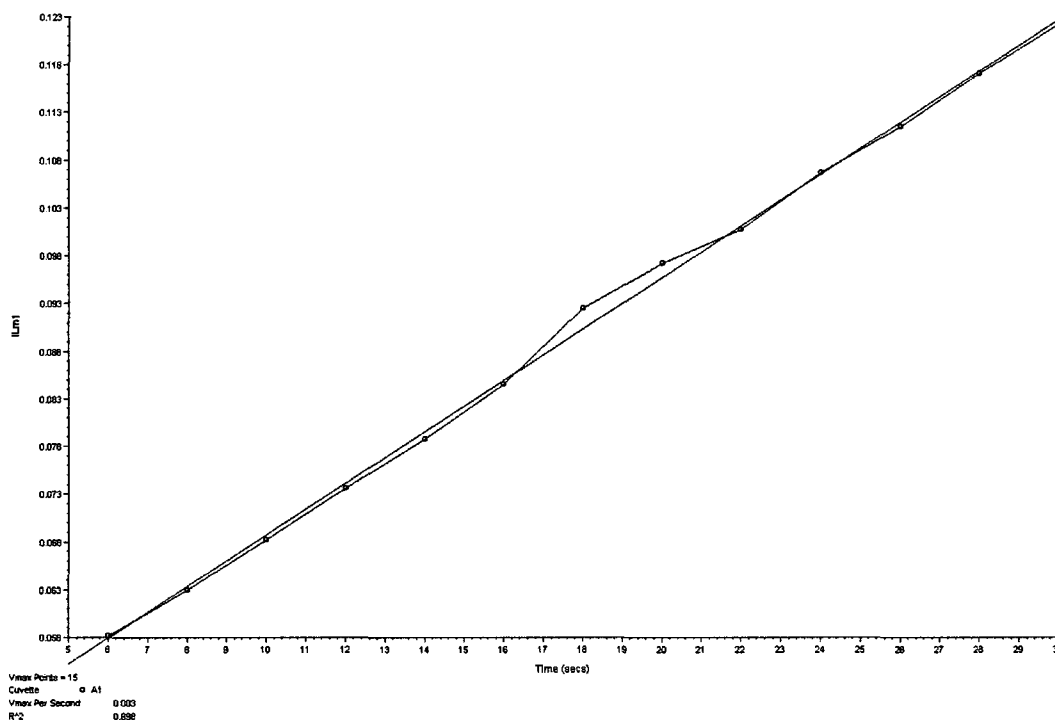


Figure 3.4. SpectraMax raw data plot, showing the time range used to calculate initial enzyme velocity from the absorbance measurements at 348 nm wavelength of the colorimetric 4-NPA esterase reaction catalyzed by CA II. The solid line is the reduced data plot and the raw data points are shown as circles.

For the preincubation time studies, the enzyme and thioxolone mixture was allowed to equilibrate for one of seven different time periods (0 sec, 1 min, 5 min, 10 min, 20 min, or 30 min), followed by rapid addition of the 4-NPA substrate with a pipettor. The hydrolysis rate of 4-NPA was then monitored by absorbance readings at 348 nm (A_{348}), with a SpectraMax Plus³⁸⁴ spectrophotometer in the kinetic data acquisition mode. Absorbance readings were collected every 2 sec for an interval of 5 min, and initial data in the range of 5 to 30 sec from each run were used to calculate the initial velocity, v_0 . The $\Delta\epsilon_{348}$ value used to calculate the 4-nitrophenolate ion product concentration at the isobestic point was $5.0 \times 10^3 \text{ M}^{-1} \text{ cm}^{-1}$ ^{23,24}. The initial substrate concentration of 4-NPA was varied from 90 μM to 1.5 mM. As reviewed previously,^{15,19} the solubility of the 4-NPA ester substrate is well below its K_m value for wild-type CA II, making it difficult to independently determine k_{cat} and K_m via a fit of the Michaelis–Menten equation. The experimentally determined estimates of K_m for this enzyme–substrate combination, which, because of the relatively low solubility of 4-NPA in aqueous solution, vary between 4 and 22 mM^{17,25}. Instead, an apparent second order rate constant, k' ($= k_{\text{cat}}/K_m$), was calculated from initial slopes corrected for the background rate of hydrolysis, using Eq. 3.1^{19,26}:

$$v_0 = k'[E_0][S_0] \quad (\text{Eq. 3.1})$$

where v_0 is the initial velocity, E_0 is total enzyme concentration at time zero, and S_0 is the initial substrate concentration. The time-dependent inhibition of CA II by thioxolone was investigated in greater detail by measuring initial rates of 4-NPA esterase hydrolysis after preincubation of the enzyme with thioxolone for varying

times (0 sec, 1 min, 5 min, 10 min, 20 min, or 30 min), at five different concentrations of inhibitor (10, 20, 50, 75, and 100 μ M thioxolone), and with 750 μ M 4-NPA initial substrate concentration. Absorbance readings were again collected every 2 sec for an interval of 5 min, and the initial data in the range of 5 to 30 sec from each run were used to calculate the initial velocity, v_0 . The apparent second order rate constant, k' ($= k_{cat}/K_m$), was again calculated from initial slopes corrected for the background rate of hydrolysis, using Eq. 3.1.

The resulting k' values were used in a nonlinear regression analysis for a single phase exponential decay model using Eq. 3.2:

$$y = k' \exp^{(-kt)} + y_{\min} \quad (\text{Eq. 3.2})$$

using GraphPad Prism 4.03) to determine the half-life of 4-NPA inhibition and the exponential decay constant. The intrinsic inactivation rate of thioxolone, k_{inact} was determined by nonlinear fitting of time-dependent data as a function of thioxolone concentration via the following Eq. 3.3:

$$k_{\text{obs}} = k_{\text{inact}}[I]/(K_I + [I]) \quad (\text{Eq. 3.3})$$

where k_{obs} is the exponential decay constant, k_{inact} is the intrinsic inactivation rate constant for thioxolone, $[I]$ is the thioxolone (inhibitor) concentration, and K_I is the equilibrium dissociation constant for the enzyme-inhibitor complex^{27,28}.

Liquid Chromatography–Mass Spectroscopic Studies

Thioxolone cleavage in the presence and absence of CA II was analyzed by liquid chromatography–mass spectrometry (LC-MS) with the help of Dr. Dutta, a postdoc in Dr. Murali's group who provided the use of their LC-MS and injected the

samples that had been prepared. The CA II-thioxolone sample was prepared by first mixing 5 μ M thioxolone (final concentration) with 5 μ M CA II (final concentration) and 50 mM MOPS, pH 7.5, 33 mM Na₂SO₄, and 1 mM EDTA buffer to bring the total volume to 5 ml in a 15 ml round-bottom centrifuge tube. After mixing by vortexing for 30 sec, the reaction was allowed to proceed at room temperature for 1 h. After 1 h, the sample was pipetted into a 2 ml 10 kDa molecular weight cut off (MWCO) Centriplus centrifugal dialysis concentrator (Millipore, Bedford, MA) and centrifuged at 4500 x g until most of the sample had passed through (approximately 1 h). The purpose of this step was to remove the CA II enzyme from any potential hydrolysis products. A stock solution of 10 mM thioxolone in 100% DMSO was diluted into 50 mM MOPS, pH 7.5, 33 mM Na₂SO₄, and 1 mM EDTA buffer to a final concentration of 5 μ M (5 ml total volume) to prepare the enzyme-free control sample. Both samples were then adjusted to an approximate pH of 3 by drop-wise addition of 1:10 diluted HCl (1.24 M), checking the pH after every few drops with pH strips to ensure that the pH was not too low. After the pH was adjusted, an equal volume of HPLC-grade chloroform was added into the tube and then vortexed vigorously for 1 min. After each tube had been vortexed once, the tubes were vortexed a second time to ensure complete mixing. The samples were then allowed to settle, resulting in phase separation of the chloroform from the aqueous layer. The aqueous layer was then removed with a Pasteur pipet. After the aqueous layer was removed, the tube was quickly vortexed for a few seconds and allowed to settle, checking for the presence of the remaining aqueous phase. This process was repeated

for each sample. After all of the aqueous layers were removed, the samples were transferred to clean small glass vials and were placed into a vacuum desiccator to remove the chloroform. Following complete removal of the chloroform, 1 ml of HPLC-grade methanol was added to each vial and samples were vortexed to resuspend the remaining residue. The samples were then filtered through a 0.2 μ M pore size sterile filter and stored in 1.5 ml microcentrifuge tubes at 4 °C, if not used immediately. The resulting thioxolone hydrolysis samples were analyzed on a Shimadzu 2010A LC-MS instrument (Shimadzu Scientific Instruments, Columbia, MD) equipped with a manual injector, LC pumps, a photo diode array (PDA) detector, and electrospray ionization (ESI) probe. All samples were dissolved in methanol. Sample introduction was achieved by direct manual injection of a 5 μ l sample solution with the methanol mobile phase pumped at an isocratic flow rate of 0.6 L/min. Sample ionization was achieved by electrospray ionization (ESI) in negative polarity mode with a 1 sec event scan time. Ionization parameters include a nebulizer gas flow rate of 2.5 L/min, a detector voltage of 1.5 kV, and a curved desolvation heater temperature of 250 °C.

Results

Structure-Activity Relationship Study

As previously reported,¹ thioxolone (compound **1**) is a relatively weak inhibitor of CA II esterase activity, with a measured IC₅₀ value of 1.77 μ M (Table 3.1). A preliminary structure-activity relationship (SAR) study was performed with a

series of small thioxolone structural analogs to examine possible mechanisms of inhibition and determine if the potency of CA II inhibition could be increased (Table 3.1). The compounds tested included the thioxolone hydrolysis product, 4-mercaptobenzene-1,3-diol (compound **3**) and two smaller structural analogs, 2-hydroxythiophenol (compound **4**) and benzenethiol (compound **5**). Two of these compounds were tested for inhibition of CA II activity, using a 4-NPA esterase assay to determine their inhibition constants. The smaller analogs (compounds **4** and **5**) had IC_{50} values of 1.05 and 1.49 μM (Figure 3.5, Table 3.1), which were slightly lower than thioxolone, with 2-hydroxythiophenol exhibiting greater potency. Thus, the two smaller aromatic thiol compounds appeared to be more potent inhibitors than the parent compound, thioxolone. The IC_{50} values were also similar to those measured for some of the other larger thioxolone analogs, discussed below (Table 3.1).

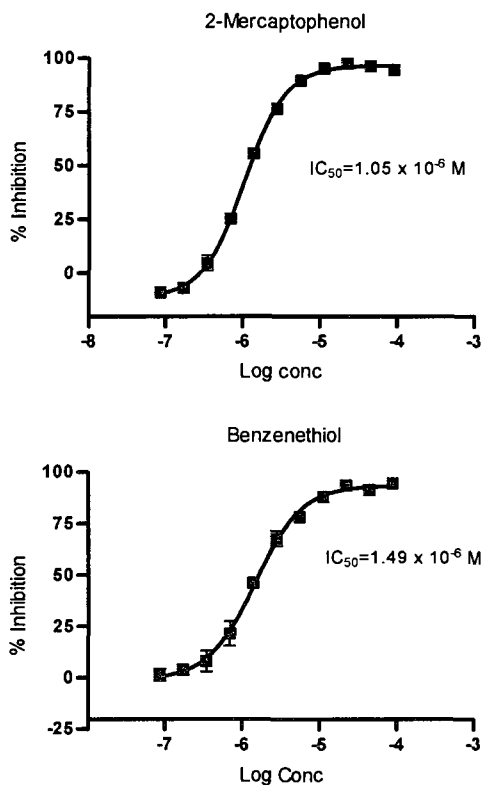


Figure 3.5. IC_{50} plots of 2-mercaptophenol (2-hydroxythiophenol, compound 4) and benzenethiol (compound 5) inhibition of CA II 4-NPA esterase activity.

Inhibition constants (K_i values) of thioxolone (compound 1), the thioxolone cleavage product, 4-mercaptobenzene-1,3-diol (compound 3), and 2-hydroxythiophenol (compound 4) were also determined for the physiologically relevant reaction of CO_2 hydration (Table 3.1), via titration of the ^{18}O exchange activity, as monitored by mass spectrometry. These ^{18}O exchange experiments were

performed by collaborator Dr. Chingkuang Tu in the lab of Prof. D.N. Silverman at the University of Florida, Gainesville, FL. This alternate method yielded K_i values of $314 \pm 69 \mu\text{M}$, $148 \pm 39 \mu\text{M}$, and $0.631 \pm 0.034 \mu\text{M}$ for compounds **1**, **3**, and **4**, respectively. These results further verified that thioxolone (compound **1**) is a relatively weak inhibitor of CA II activity, whereas the thioxolone hydrolysis product, 4-mercaptobenzene-1,3-diol (compound **3**), although still a relatively weak inhibitor, was 2-fold more potent. In contrast, 2-hydroxythiophenol (compound **4**) showed a significant ~500-fold increase in inhibition, similar in magnitude to other sulfonamide inhibitors. This result suggests that the absence of a second hydroxyl group may have greatly improved the affinity of this molecule in the active site, relative to 4-mercaptobenzene-1,3-diol (compound **3**). A closer examination of the crystal structures of the two complexes (Figures 3.6, 3.7) reveals insight into this apparent ~500-fold increase in inhibition of 2-hydroxythiophenol (compound **4**) compared to 4-mercaptobenzene-1,3-diol (compound **3**) on CA II. The additional hydroxyl group of 4-mercaptobenzene-1,3-diol (compound **3**) points toward a hydrophobic pocket in the active site of CA II (in close proximity to residues Ile 91, Phe 131, Leu 141, Val 135, and Leu 198 (not shown in Figure 3.7)). This may be the cause of the significant disparity in the affinities of the two compounds. The absence of the second hydroxyl group on the ring of 2-hydroxythiophenol (compound **4**) removes the incompatibility of the hydrophilic nature of this group in the hydrophobic pocket and therefore could explain the greatly improved affinity of this compound.

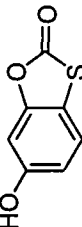
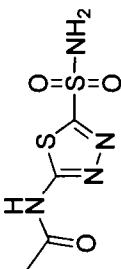
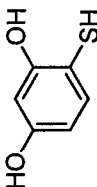
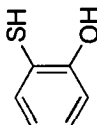
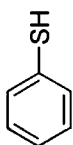
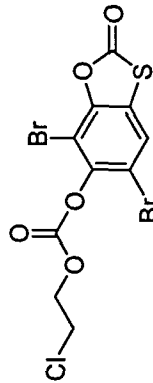
Table 3.1. Structures and apparent IC ₅₀ values for inhibition of human carbonic anhydrase II by thioxolone analogs.					
Compound Number and Name	Molecular Structure	Molecular Formula	Mol. Mass (Da)	IC ₅₀ /K _i value (μM) ^{a,b}	
1. thioxolone (6-hydroxybenzo [d][1,3]oxathiol-2-one)		C ₇ H ₄ O ₃ S	168.2	314 ± 69 ^c 1.77 ^d (1.06-2.95)	
2. acetazolamide		C ₄ H ₆ N ₄ O ₃ S ₂	222.3	0.44 (0.42-0.47)	
3. 4-mercapto-benzene-1,3-diol		C ₆ H ₆ O ₂ S	142.2	148 ± 39 ^c n.d. ^e	
4. 2-hydroxythio- phenol		C ₆ H ₆ OS	126.2	0.63 ± 0.03 ^c 1.05 (0.98-1.13)	
5. benzenethiol		C ₆ H ₆ S	110.2	1.49 (1.28-1.74)	
6. 2-chloroethyl 5,7-dibromo-2-oxobenzod[1,3] oxathiol-6-yl carbonate		C ₁₀ H ₅ Br ₂ ClO ₅ S	432.5	no inhibition ^f	

Table 3.1. - Continued

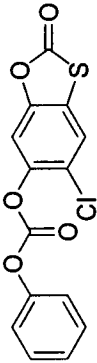
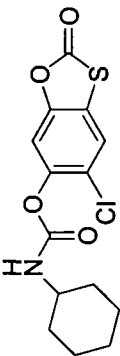
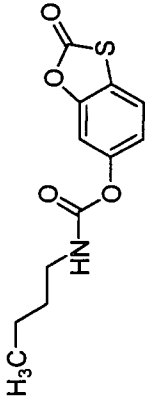
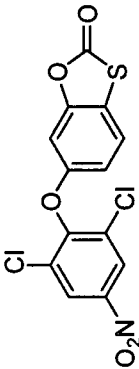
Compound Number and Name	Molecular Structure	Molecular Formula	Mol. Mass (Da)	IC ₅₀ /K _i value (μM) ^{a,b}
7. 5-chloro-2-oxobenzo[d][1,3]oxathiol-6-yl phenyl carbonate		C ₁₄ H ₇ ClO ₅ S	322.7	0.61 (0.51-0.74)
8. 5-chloro-2-oxobenzo[d][1,3]oxathiol-6-yl cyclohexyl-carbamate		C ₁₄ H ₁₄ ClNO ₄ S	327.8	0.98 (0.84-0.11)
9. 2-oxobenzo[d][1,3]oxathiol-6-yl butylcarbamate		C ₁₂ H ₁₃ NO ₄ S	267.3	2.13 (1.44-3.17)
10. 6-(2,6-dichloro-4-nitrophenoxy)benzo[d][1,3]oxathiol-2-one		C ₁₃ H ₅ Cl ₂ NO ₅ S	358.2	1.45 (0.87-2.44)

Table 3.1. - Continued

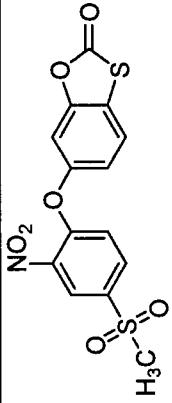
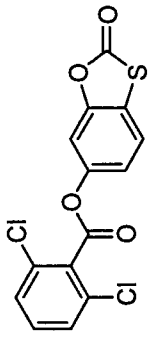
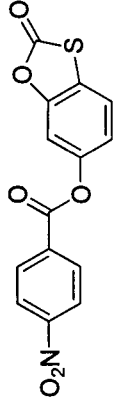
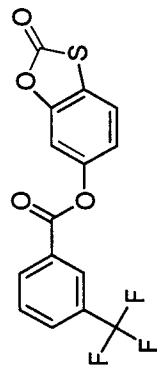
Compound Number and Name	Molecular Structure	Molecular Formula	Mol. Mass (Da)	IC ₅₀ /K _i value (μM) ^{a,b}
11. 6-(4-(methyl sulfonyl)-2-nitrophenoxy) benzo[d][1,3] oxathiol-2-one		C ₁₄ H ₉ NO ₇ S ₂	367.4	1.03 (0.85-1.25)
12. 2-oxobenzo[d] [1,3]oxathiol-6-yl 2,6-dichloro benzoate		C ₁₄ H ₆ C ₁₂ O ₄ S	341.2	0.74 (0.35-1.56)
13. 2-oxobenzo[d] [1,3]oxathiol-6-yl 4-nitrobenzoate		C ₁₄ H ₇ NO ₆ S	317.3	0.93 (0.50-1.74)
14. 2-oxobenzo[d] [1,3]oxathiol-6-yl 3(trifluoromethyl) benzoate		C ₁₅ H ₇ F ₃ O ₄ S	340.3	1.07 (0.91-1.24)

Table 3.1. - Continued

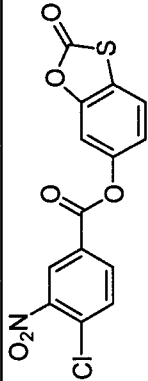
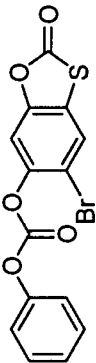
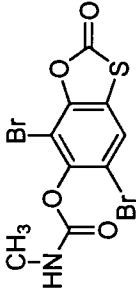
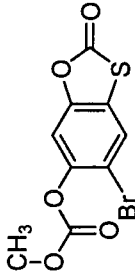
Compound Number and Name	Molecular Structure	Molecular Formula	Mol. Mass (Da)	IC ₅₀ /K _i value (μM) ^{a,b}
15. 2-oxobenzo[d][1,3]oxathiol-6-yl 4-chloro-3 nitrobenzoate		C ₁₄ H ₆ ClNO ₆ S	351.7	0.68 (0.50-0.93)
16. 5-bromo-2-oxobenzo[d][1,3]oxathiol-6-yl phenyl carbonate		C ₁₄ H ₇ BrO ₅ S	367.2	0.89 (0.57-1.37)
17. 5,7-dibromo-2-oxobenzo[d][1,3]oxathiol-6-yl methyl carbamate		C ₉ H ₅ Br ₂ NO ₄ S	383.0	No inhibition ^c
18. 5-bromo-2-oxobenzo[d][1,3]oxathiol-6-yl methyl carbonate		C ₉ H ₅ BrO ₅ S	305.1	2.01 (1.55-2.61)

Table 3.1. - Continued

Compound Number and Name	Molecular Structure	Molecular Formula	Mol. Mass (Da)	IC ₅₀ /K _i value (μM) ^{a,b}
19. 2-oxobenzo[d][1,3]oxathiol-6-yl benzoate		C ₁₃ H ₇ ClO ₅ S	334.7	0.85 (0.69-1.04)
20. 2-oxobenzo[d][1,3]oxathiol-6-yl hexanoate		C ₁₃ H ₁₄ O ₄ S	266.3	2.76 (2.18-3.50)
21. 6-(hexyloxy) benzo[d][1,3]oxathiol-2-one		C ₁₃ H ₁₆ O ₃ S	252.3	12.7 (8.6-18.8)

^a Apparent IC₅₀ values for inhibition of 4-NPA esterase kinetic rate, determined by absorbance measurements at 348 nm.^b Error range for fitted IC₅₀ value was defined as a 95% confidence interval.^c Inhibitor constants (K_i values) for these compounds were determined using ¹⁸O exchange activity studies.^d IC₅₀ data from Iyer, et al.¹. Error range for fit IC₅₀ value was defined as a 95% confidence interval.^e No data. No IC₅₀ data was determined for this compound using the 4-NPA esterase assay.^f No detectable inhibition was observed for this compound in the CA II 4-NPA esterase IC₅₀ assay.

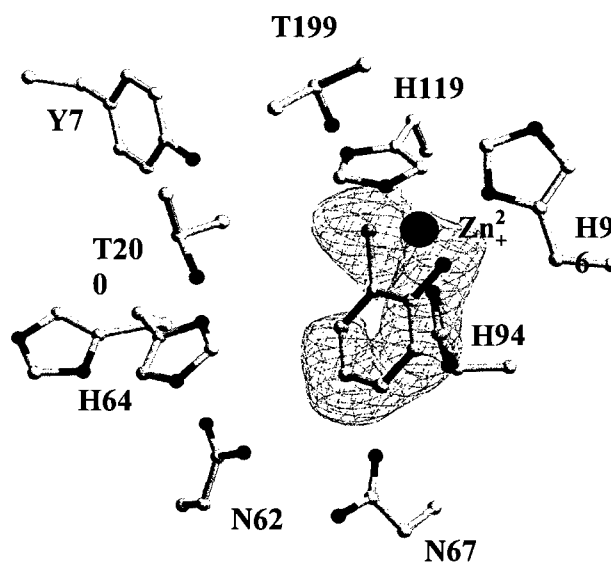


Figure 3.6. Crystal structure of CA II complexed with 2-hydroxythiophenol (compound 4). The zinc atom is shown as a black sphere, side chains are as labeled. Blue F_o-F_c electron density map shown is contoured at 2σ and was calculated without the inhibitor present. Figure was generated and rendered with BobScript and Raster3D, respectively^{29,30} by collaborator Dr. Robert McKenna at University of Florida, Gainesville.

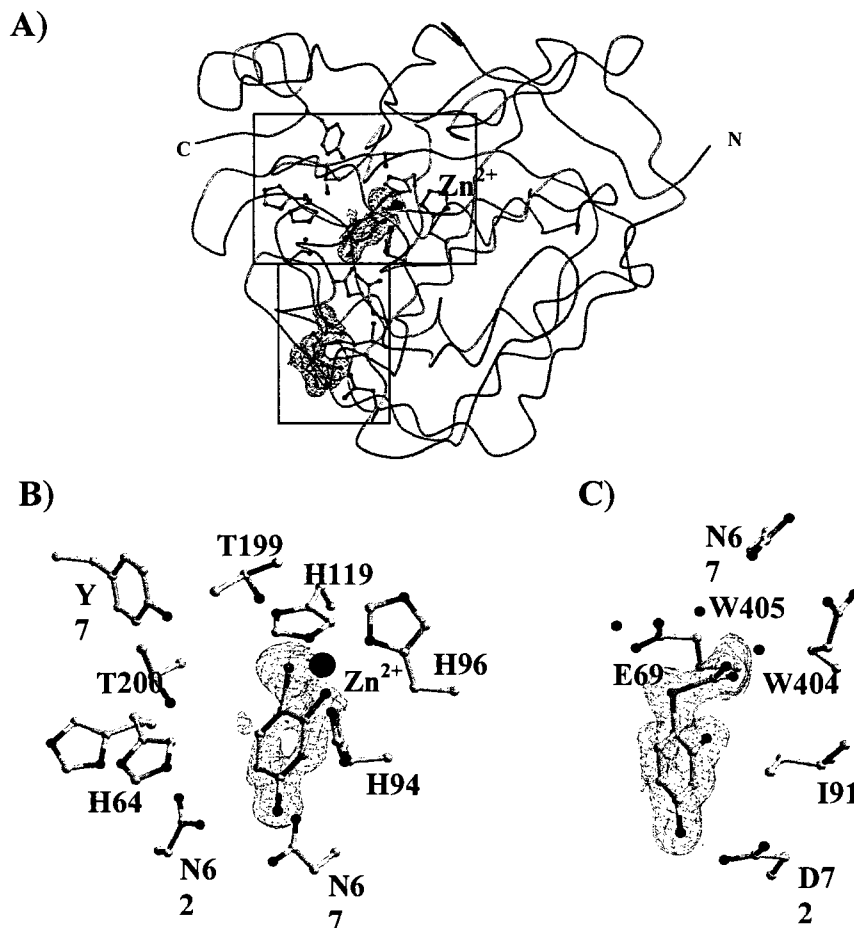


Figure 3.7. Crystal structure of CA II soaked with thioxolone. (A) Ribbon diagram of CA II complexed with (B) 4-mercaptobenzene-1,3-diol (compound **3**) and (C) S-(2,4-hydroxyphenyl)thiocarboxylic acid, (B) and (C) are close up views of the open boxes as depicted in (A). The zinc atom is shown as a black sphere, side chains are as labeled. Blue F_o-F_c electron density map shown in (B) and (C) is contoured at 2σ and was calculated without the inhibitors present. Figures were generated and rendered with BobScript and Raster3D, respectively^{29,30} by collaborator Dr. McKenna at University of Florida, Gainesville.

Another SAR study was performed on a series of 16 structural analogs of thioxolone. All 16 analogs contained the original thioxolone ring structure, but also had additional aliphatic and aromatic groups substituted at the C6 carbon hydroxyl group, using the nomenclature of Byres and Cox². Some analogs were also modified by halogenation of the C1 and/or C5 carbons. Apparent IC₅₀ values were determined for these compounds after a 15 min incubation time. The resulting ester hydrolysis products of these compounds should have similar structures to the thioxolone product, 4-mercaptobenzene-1,3-diol (compound **3**). However, inhibition first requires that the pro-drug compound can correctly bind in the CA II active site to allow activation by ester/thioester cleavage to occur. Excluding the exceptionally weak inhibitor, compound **21**, and the non-inhibitory compounds **6** and **17**, the average apparent IC₅₀ value for the remaining 13 analogs was 1.27 ± 0.65 μ M. Thus, the apparent IC₅₀ values for many of the analogs were slightly lower than, but similar in magnitude to, the IC₅₀ value of 1.77 μ M measured for thioxolone (compound **1**) after the same incubation time. These results clearly demonstrated that modification of the thioxolone structure by addition of other moieties could result in a moderately higher potency of inhibition. Five thioxolone analogs, compounds **7**, **12**, **13**, **15**, and **16**, had the lowest IC₅₀ values in the 4-NPA esterase assay, ranging from 0.6–0.9 μ M, with the lower values approaching the 0.44 μ M IC₅₀ value observed for the strong CA II inhibitor, acetazolamide (compound **2**), in the same assay. Compound **7** had the lowest IC₅₀ value of 0.61 μ M. This compound differed from thioxolone in that it had a benzyl group linked to the C6 oxygen by an ester linkage; this additional moiety

may improve its non-polar interactions with the CA II hydrophobic pocket. Compounds **8**, **10**, **11**, **14**, and **19** exhibited lower potencies of CA II inhibition, with IC_{50} values ranging from 1-2 μM . The observed differences in the inhibition properties of these compounds may result from the different groups remaining attached to the 4-mercaptobenzene-1,3-diol scaffold. The observed variations in the IC_{50} values may also be a result of differences in the initial binding affinity of the pro-drug compound of the enzyme, varying rates of CA II ester hydrolysis of each compound to generate the final product, and secondary effects of other hydrolysis compounds generated from the rest of the scaffold. All 16 of the larger thioxolone analogs tested possessed a nucleophilic oxygen attached to the C6 carbon (Table 3.1), analogous to the hydroxide group present in the original thioxolone structure (compound **1**). The majority of these analogs had a substituent attached at the C6 carbon via an ester linkage, although three compounds had an ether linkage at this position (compounds **10**, **11**, and **21**). No obvious correlation was apparent between potency of inhibition and the presence of an ester vs. ether oxygen bond at the C6 position; these three ether-bonded analogs yielded IC_{50} values ranging from 1.0-12.7 μM . However, analogs with an aromatic substituent (compounds **7**, **10**, **11**, **12**, **13**, **14**, **15**, **16**, and **19**) or cyclohexane (compound **8**) at the C6 position exhibited a higher potency of inhibition, with IC_{50} values of 0.61-1.45 μM . Conversely, analogs with aliphatic C6 hydroxyl substituents (compounds **9**, **18**, **20**, and **21**) generally exhibited weaker inhibition, with larger IC_{50} values of 2.0-12.7 μM , or no inhibition (compounds **6** and **17**); however, another factor may be responsible for the lack of

inhibition, as discussed below. Six of the thioxolone analogs were also further modified by halogenation at the C5 position on the thioxolone ring structure, either by chlorine (compounds **7** and **8**) or bromine (compounds **6**, **16**, **17**, and **18**). Two of these analogs (compounds **6** and **17**) were also modified by bromination at the C1 position. The four compounds with chlorine or bromine present only at the C5 position functioned as inhibitors, with a wide range of IC_{50} values (0.6-2.0 μ M); including the most potent inhibitor, compound **7**). In contrast, compounds **6** and **17**, with bromine attached at the C1 position, failed to exhibit any detectable inhibition of the enzyme esterase activity. This complete lack of inhibition was interpreted as a failure of these compounds to bind at the enzyme active site, an event required for subsequent ester bond cleavage and generation of the more strongly inhibitory thiol derivatives. The C1 bromine substituent is the most unique feature of these two compounds; otherwise, a wide variety of functional groups were tolerated at the C5 and C6 positions. This analysis suggests that the C1 bromine group is responsible for this behavior, possibly due to a steric effect that prevents binding of the thioxolone analog to one or more CA II active site residues. To further test this hypothesis, a computer model was generated of a bromine atom attached to carbon C1 of the thioxolone hydrolysis product, S-(2,4-thiophenyl)hydrogen thiocarbonate, using the cocrystal structure determined by the research group of Dr. McKenna at the University of Florida. This model indicated a pronounced steric clash between the C1 bromine atom and the CA II active site residue, Val 121, providing further support for this hypothesis. Furthermore, bromine present at the C1 position could also reduce the

likelihood that hydrolysis of thioxolone compounds would occur, even if binding was feasible. Residue Val 121 is one of several residues, along with Val 143, Leu 198, and Trp 209, that function as a hydrophobic pocket for substrate binding, near the zinc-bound hydroxide³¹. Several studies have shown that these residues are important for the interaction between the enzyme and the 4-NPA substrate^{20,32-34} and for specificity for different ester substrates¹⁷. Recently, the combination of the two V121A and V143A mutations was shown to greatly increase the rate of CA II hydrolysis of some long chain esters, such as paranitrophenyl valerate¹⁹. Thus, it is not unexpected that introducing substituents at certain positions, such as the C1 carbon, could alter the ability of thioxolone analogs to bind in the active site. It should be noted that none of the 16 analogs tested had any substituents at the C4 carbon. Therefore, the effect of other functional groups at this position remains to be explored, as does substitution of the reactive ester and thioester bonds with other types of atoms and chemical structures. It also remains to be determined if the addition of sulfonamide and related groups could further improve the potency of thioxolone compounds and what type of inhibition specificity is observed for other alpha class CA isozymes.

Enzyme Kinetic Studies

Michaelis–Menten kinetics was measured for the rate of 4-NPA ester hydrolysis by CA II as a function of thioxolone concentration, to determine possible mechanisms of inhibition. The upper limit of substrate concentration (0.5 mM) was within the typical range of 0.4 to 1.0 mM 4-NPA concentration used in CA activity

assays^{1,17,24} and is far in excess of the enzyme concentration (1 μ M). The substrate concentration is well below experimental estimates of K_m for this enzyme–substrate combination, which, because of the relatively low solubility of 4-NPA in aqueous solution, vary between 4 and 22 mM^{17,25}. However, the chosen range of 4-NPA substrate concentrations well below K_m should also yield good sensitivity for detection and monitoring of potentially weak competitive inhibitors of the system,³⁵ such as thioxolone. The CA II-catalyzed 4-NPA esterase reaction rate was dependent on the concentration of thioxolone (Figure 3.8); the initial reaction velocity decreased with increasing thioxolone concentration, confirming inhibition by this compound. The best-fit values of the Michaelis–Menten parameters, k_{cat} and K_m , decreased and increased, respectively, as the concentration of thioxolone was increased (Table 3.2).

Table 3.2. Michaelis-Menten kinetic parameters determined for concentration-dependence of thioxolone inhibition of 4-nitrophenyl acetate hydrolysis by carbonic anhydrase II. ^a

Thioxolone concentration	0 μM	25 μM	50 μM	99 μM
Best-fit values				
k_{cat} (sec^{-1})	2670	1530	914	734
K_{M} (mM)	1.13	1.17	1.50	2.08
Std. Error				
k_{cat} (sec^{-1})	521	1130	748	577
K_{M} (mM)	0.32	0.81	0.93	1.21
95% Confidence Intervals				
k_{cat} (sec^{-1})	1600 to 3740	-798 to 3860	-630 to 2460	-452 to 1920
K_{M} (mM)	0.48 to 1.78	-0.48 to 2.81	-0.40 to 3.39	-0.37 to 4.52
R^2	0.97	0.84	0.91	0.95

^a Kinetic measurements of thioxolone inhibition of the 4-NPA esterase reaction were performed using 1 μM CA II, as described in Experimental Procedures. GraphPad Prism version 4.03 was used to fit the data.

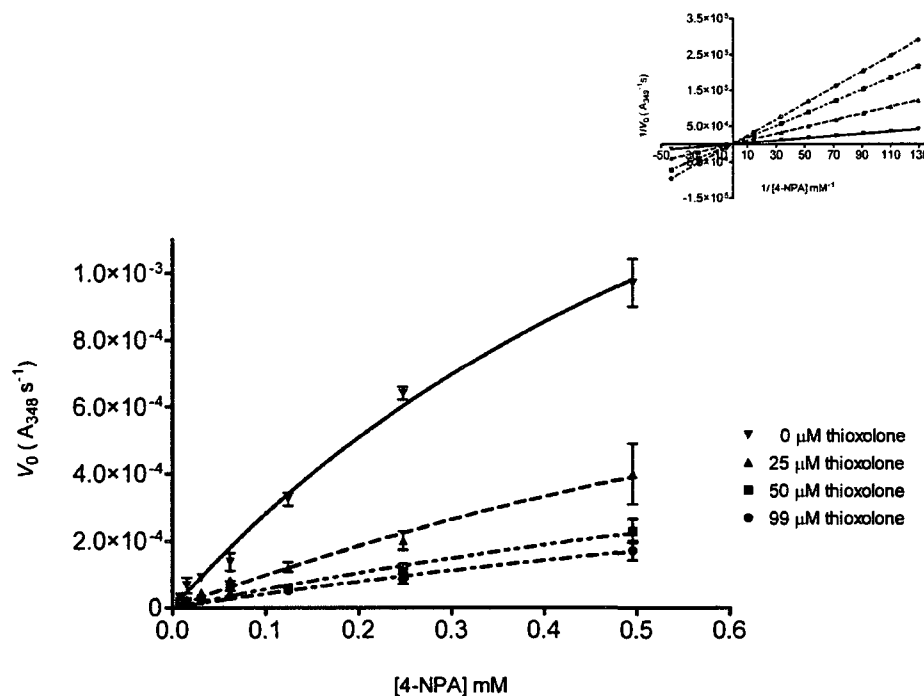


Figure 3.8. Kinetics studies of thioxolone inhibition of CA II esterase activity. The rate of 4-NPA ester hydrolysis catalyzed by CA II is plotted as a function of initial thioxolone concentration. The data was fit to the Michaelis-Menten equation using non-linear regression analysis and GraphPad Prism 4.03 software. Inset: Lineweaver-Burke plot of the Michaelis-Menten data, indicating apparent mixed inhibition behavior by thioxolone.

These results are suggestive of a mixed inhibition mode (i.e., competitive and noncompetitive), a result further supported by a Lineweaver–Burke plot analysis of the kinetic data (Figure 3.8, inset). However, these results do not exclude a purely competitive mode of inhibition, as the range of substrate concentrations used was well below the K_m value, for reasons discussed above. It should also be noted that the 4-NPA assay used a non-physiological esterase reaction with a substrate that has a

relatively large aromatic group; however, there is considerable evidence that both esterase and CO₂ hydration reactions use the same zinc hydroxide mechanisms^{17,19}. Additional kinetic studies also clearly indicated that thioxolone exhibited time-dependent inhibition of the CA II esterase reaction, but that the majority of inhibition occurred within the 15 min preincubation period used for all IC₅₀ experiments with 4-NPA substrate (Figure 3.9).

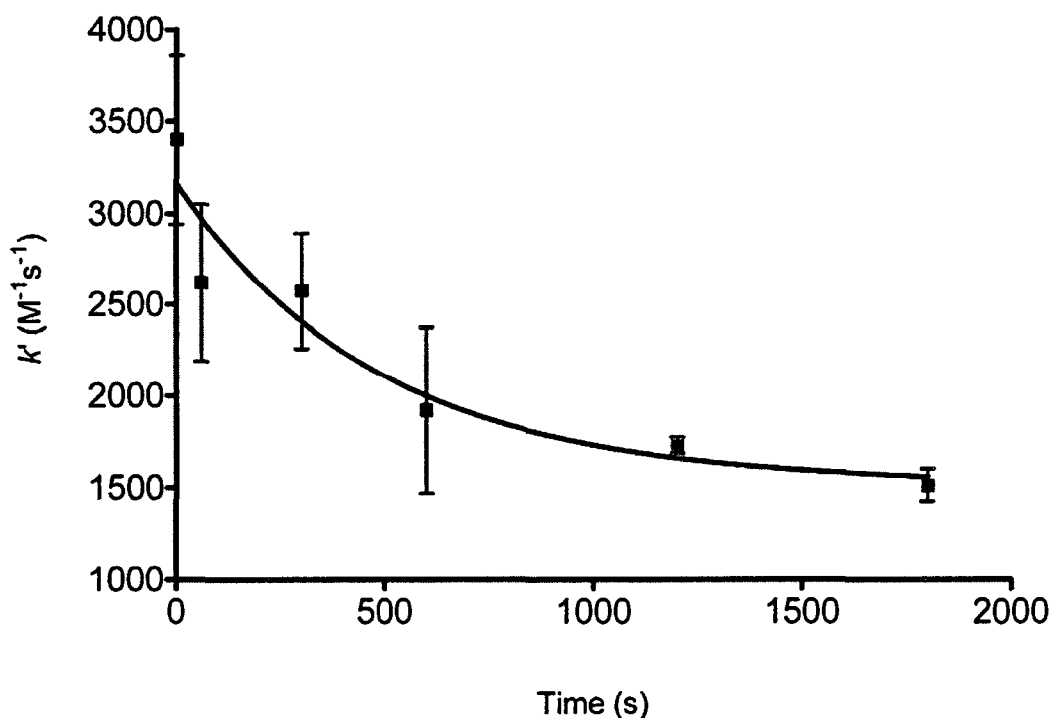


Figure 3.9. Time-dependence of thioxolone inhibition of CA II as monitored by apparent second order rate constant, k' , as a function of inhibitor incubation time. Data were fit to a single exponential decay model to yield a $t_{1/2}$ value of 340 sec. Initial assay conditions were 20 μ M thioxolone concentration, 750 μ M 4-NPA substrate concentration, and 1 μ M CA II.

A fit of the apparent second order rate constant, k' , as a function of thioxolone preincubation time, to a single exponential decay model, yielded an estimated half-life for inhibition of 4-NPA esterase activity of 340 sec. The nonlinear fit of time-dependent data as a function of thioxolone concentration is shown in Figure 3.10 and the k_{inact} and K_I values are listed in Table 3.3.

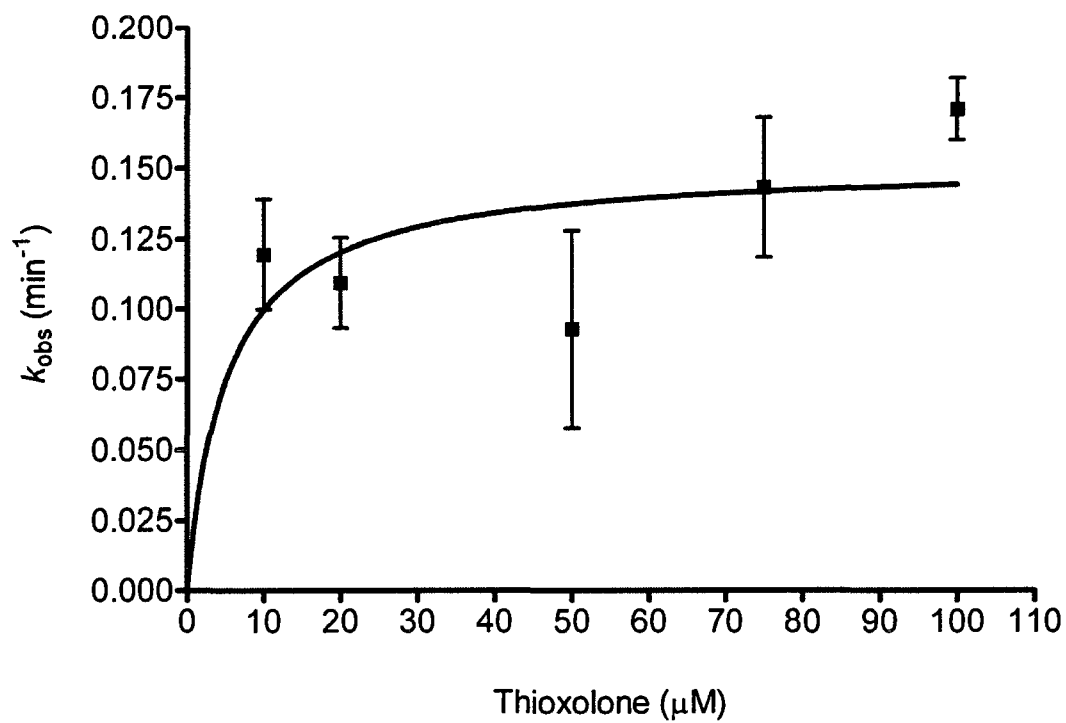


Figure 3.10. Plot of CA II activity loss versus thioxolone concentration. The data was modeled by fitting the decay constant to Eq. 3.3 via nonlinear regression analysis with GraphPad Prism (4.03). Each point is the mean of triplicate data (\pm S.D.).

Table 3.3. Mechanism-based enzyme inactivation parameters determined for thioxolone inhibition of 4-nitrophenyl acetate hydrolysis by carbonic anhydrase II. ^a	
Best-fit values	
K_{inact} (min ⁻¹)	0.15
K_I (μM)	5.21
Standard Error	
K_{inact} (min ⁻¹)	0.02
K_I (μM)	3.83
95% Confidence Interval	
K_{inact} (min ⁻¹)	0.12 to 0.19
K_I (μM)	-3.22 to 13.6
^a Measurements of thioxolone inhibition of the 4-NPA esterase reaction were performed using 1 μM CA II, 750 μM 4-NPA and the varying concentrations of thioxolone (10, 20, 50, 75, and 100 μM) . GraphPad Prism version 4.03 was used to fit the data.	

Liquid Chromatography–Mass Spectroscopy Analysis of Thioxolone and Hydrolysis Products

The analytical technique of LC-MS was used to verify that the thioxolone hydrolysis products observed in the preliminary crystal structure were generated by reaction with CA II and not due to other non-enzymatic hydrolysis events, for example, non-enzymatic cleavage by exposure to X-ray radiation. The LC-MS analysis was first performed in both the positive ionization and negative ionization modes to determine which mode would best detect thioxolone. The negative

ionization mode resulted in the detection of the deprotonated thioxolone ion with a mass-to-charge ratio (m/z) of 167, and the positive mode yielded an m/z value of 169, as expected. Comparison of the two ionization modes indicated that the negative ionization mode was more sensitive. Pure thioxolone (compound **1**) was incubated with either CA II enzyme or with enzyme-free buffer as a control; the resulting small molecule products were isolated from the protein by diafiltration and organic liquid-liquid extraction. The resulting products were then analyzed by LC-MS. When thioxolone was incubated with the enzyme, a probable hydrolysis product was isolated with an m/z value of 139 (Figure 3.11); this value is consistent with the predicted value for 4-mercaptobenzene-1,3-diol (compound **3**). The amount of 4-mercaptobenzene-1,3-diol in the sample was approximately 23% of the amount of thioxolone present when 5 μ M of thioxolone was cleaved by 1 μ M CA II. The percentage of 4-mercaptobenzene-1,3-diol to thioxolone was consistently observed in every LC-MS analysis of samples of thioxolone incubated with CA II. The lower m/z value detected was consistent with the form of 4-mercaptobenzene-1,3-diol resulting from the cleavage of a disulfide-linked dimer, bis-4-mercaptobenzene-1,3-diol. When the control samples of thioxolone without CA II were analyzed by LC-MS, the previous product, 4-mercaptobenzene-1,3-diol (compound **3**), was not detected (Figure 3.11).

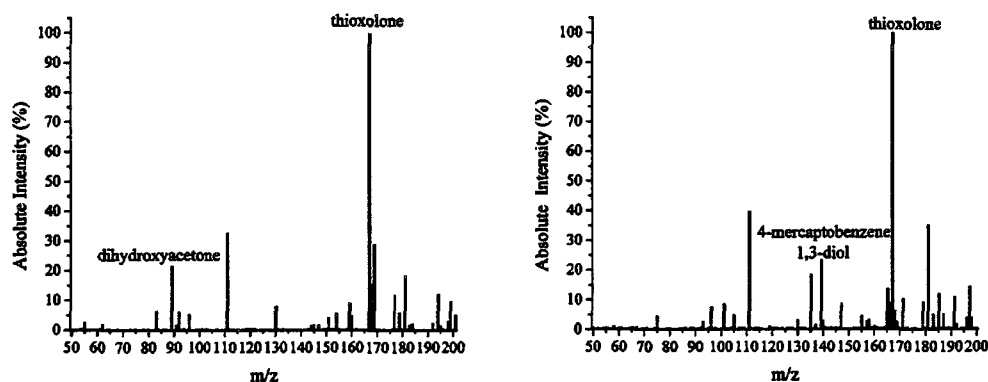


Figure 3.11. LC-MS of thioxolone products generated in the absence and presence of CA II. Left, mass spectrum of thioxolone control sample incubated in buffer only. Dihydroxyacetone was also observed in the control sample. Right, mass spectrum of thioxolone and resulting 4-mercaptobenzene-1,3-diol (compound **3**) hydrolysis product observed after thioxolone was incubated with CA II.

Discussion

The results indicate that thioxolone binds to the active site of CA II and is cleaved by successive hydrolysis of the thioester and ester bonds to form 4-mercaptobenzene-1,3- diol (compound **3**) (Figure 3.12). The 4-mercaptobenzene-1,3- diol product then binds to the CA II active site zinc ion, displacing the zinc-bound hydroxide group. Thus, thioxolone is proposed to be a prodrug inhibitor that is cleaved via a CA II zinc-hydroxide mechanism known to catalyze the hydrolysis of esters¹⁷.

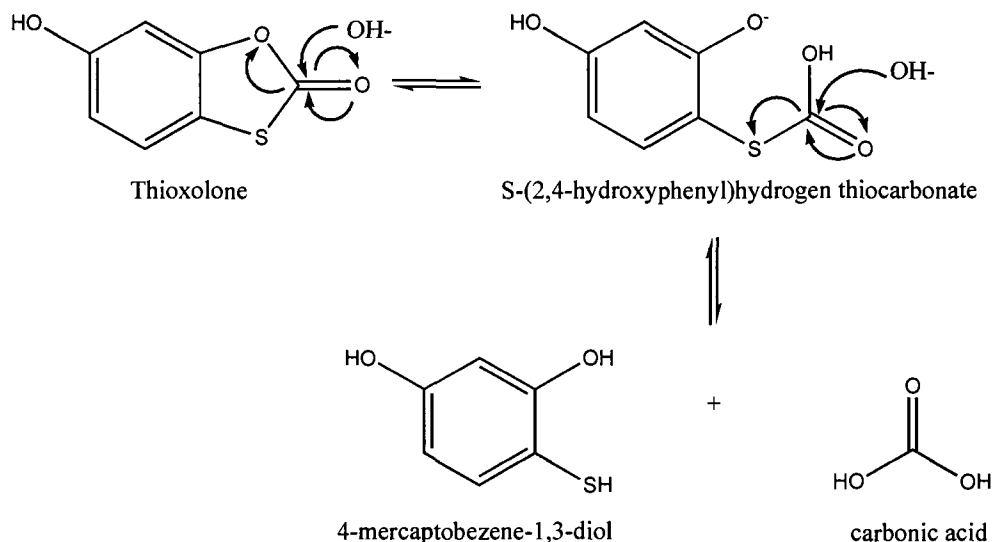


Figure 3.12. Proposed reaction mechanism of thioxolone cleavage by CA II, based on crystallographic studies. The less reactive ester bond is first enzymatically cleaved via nucleophilic attack by the active site Zn-bound hydroxide ion. A second nucleophilic attack by another activated hydroxide ion then cleaves the remaining, more reactive thioester bond, releasing the final inhibitor, 4-mercaptobenzene-1,3-diol (compound 3) and carbonic acid. The carbonic acid rapidly ionizes to form a bicarbonate ion (HCO_3^-) and CO_2 .

The mechanism of CA II inhibition by thioxolone is complex and cannot be adequately described by simple models of reversible inhibition, as indicated by the failure of Lineweaver–Burke plot analysis (Figure 3.8) to give a clear mechanistic classification. Suicide inhibitors typically inactivate the enzyme completely. However, this was not observed within the time frame of the experiment (Figure 3.9). This result may be due to competition between the 4-NPA substrate and the final

inhibition product, 4-mercaptobenzene-1,3-diol, for the active site, preventing complete CA II inactivation, as observed in other dual substrate systems^{36,37}. The proposed CA II-thioxolone inhibition mechanism requires multiple steps, some of which are irreversible, as described in the following scheme: (1) initial diffusion into the CA II active site and binding by a thioxolone prodrug molecule (compound 1); (2) subsequent cleavage of ester and thioester bonds in two successive steps; and (3) a second binding event by one of the resulting cleavage products, 4-mercaptobenzene-1,3-diol (compound 3), via a now exposed thiol group, to the active site zinc ion. The first step might be expected to involve competitive inhibition, with thioxolone competing with the 4-NPA substrate for the zinc hydroxide active site region of the enzyme. The sequential ester and thioester hydrolysis reactions in the second step represent essentially irreversible steps. It is somewhat surprising that the more stable ester bond is cleaved first, rather than the more labile thioester bond. However, thioxolone has a stereospecific group in the form of the hydroxyl group on the C6 carbon; this group may determine how the molecule binds to the CA II active site, resulting in preferential cleavage of the ester bond first by the active site hydroxyl group. The last event in the proposed mechanism could potentially involve a noncompetitive inhibition mechanism, due to the formation of a metal–thiol bond between the zinc ion and the product, 4-mercaptobenzene-1,3-diol. Some compounds that form metal–thiol bonds are frequently cited as textbook examples of noncompetitive inhibitors;³⁸ these noncompetitive inhibitor systems are sometimes known to exhibit mixed inhibition as well³⁹. It is well known that different CA

isozymes vary greatly in their ability to cleave esters; for example, CA III has very little esterase activity with 4-NPA compared to CA II⁴⁰. Because this type of prodrug inhibitor mechanism depends on activation by enzymatic cleavage of ester bonds, this class of inhibitor may have advantages in determining isozyme specificity. As noted previously, thioxolone lacks the sulfonamide, sulfamate, or related functional groups that are typically found in known CA inhibitors and could represent the starting point for a new class of CA inhibitors that may have advantages for patients with sulfonamide allergies.

Innocenti et al., from Supuran's group, recently published a follow-up study on thioxolone's potential mammalian CA isozyme specificity⁴¹. In this study, the inhibition of 13 catalytically active mammalian CA isozymes with thioxolone, 3,5-dichloro-4-hydroxybenzenesulfonamide (containing the benzenesulfonamide scaffold substituted with three groups, including one -OH in the para position to the zinc binding group like the hydrolysis product of thioxolone) and the classic clinical sulfonamide CA inhibitor, acetazolamide, was studied⁴¹. The results of this study showed that, with the exception of CA I (K_i 91 nM), all of the other mammalian CA isozymes had very similar weak inhibition constants (K_i) in the μ M range and they only varied around 4 μ M between the different CA isozymes inhibited with thioxolone⁴¹. In contrast, 3,5-dichloro-4-hydroxybenzenesulfonamide had a range of K_i from 58 nM for CA II to 78.6 μ M for CA III⁴¹. The inhibition constant range for acetazolamide inhibition was similar to that for 3,5-dichloro-4-hydroxybenzenesulfonamide. However, more potent inhibition was observed with

acetazolamide because it is a more potent CA inhibitor⁴¹. This study did not include any structural analogues of thioxolone, e.g., the Specs compounds (Table 3.1), to determine if modifications to the thioxolone structure would increase isozyme specificity.

Based on analysis of the experimental results, thioxolone is proposed to be a prodrug inhibitor that is cleaved via a CA II zinc-hydroxide mechanism known to catalyze the hydrolysis of esters. When thioxolone binds in the active site of CA II, it is cleaved and forms 4-mercaptobenzene-1,3-diol via the intermediate S-(2,4-thiophenyl)hydrogen thiocarbonate. The esterase cleavage product binds to the zinc active site via the thiol group and is therefore the active CA inhibitor, while the intermediate is located at the rim of the active-site cavity. The time-dependence of this inhibition reaction was investigated in detail. Because this type of prodrug inhibitor mechanism depends on cleavage of ester bonds, this class of inhibitors may have advantages over sulfonamides in determining isozyme specificity. A preliminary structure–activity relationship study with a series of structural analogues of thioxolone yielded similar estimates of inhibition constants for most compounds, although two compounds with bromine groups at the C1 carbon of thioxolone were not inhibitory, suggesting a possible steric effect.

References

1. Iyer, R.; Barrese, A. A., 3rd; Parakh, S.; Parker, C. N.; Tripp, B. C. Inhibition profiling of human carbonic anhydrase II by high-throughput screening of structurally diverse, biologically active compounds. *J Biomol Screen* 2006, 11, 782-91.
2. Byres, M.; Cox, P. J. The supramolecular structure of 6-hydroxy-1,3-benzoxathiol-2-one (tiocholone). *Acta Crystallogr C* 2004, 60, o395-6.
3. Wildfeuer, A. 6-hydroxy-1,3-benzoxathiol-2-one, an antipsoriatic with antibacterial and antimycotic properties. *Arzneimittelforschung* 1970, 20, 824-31.
4. Lius, V.; Sennerfeldt, P. Local treatment of acne with tiocholone. *Lakartidningen* 1979, 76, 39-41.
5. Goeth, H.; Wildfeuer, A. Antibacterial and cytostatic properties of 6-hydroxy-1,3-benzoxathiol-2-one. *Arzneimittelforschung*. 1969, 19, 1298-1304.
6. Camarasa, J. Contract dermatitis to thioxolone. *Contract Dermatitis* 1981, 7, 213-214.
7. Winum, J. Y.; Scozzafava, A.; Montero, J. L.; Supuran, C. T. New zinc binding motifs in the design of selective carbonic anhydrase inhibitors. *Mini Rev. Med. Chem.* 2006, 6, 921-36.
8. Lindskog, S. Structure and mechanism of carbonic anhydrase. *Pharmacol. Ther.* 1997, 74, 1-20.
9. Supuran, C. T. Carbonic anhydrases: novel therapeutic applications for inhibitors and activators. *Nat Rev Drug Discov* 2008, 7, 168-81.
10. Simonsson, I.; Jonsson, B.; Lindskog, S. Phenol, a competitive inhibitor of CO₂ hydration catalyzed by carbonic anhydrase. *Biochemical and Biophysical Research Communications* 1982, 108, 1406-1412.

11. Tibell, L.; Forsman, C.; Simonsson, I.; Lindskog, S. The inhibition of human carbonic anhydrase II by some organic compounds. *Biochim. Biophys. Acta* 1985, 829, 202-8.
12. Innocenti, A.; Vullo, D.; Scozzafava, A.; Supuran, C. T. Carbonic anhydrase inhibitors: interactions of phenols with the 12 catalytically active mammalian isoforms (CA I-XIV). *Bioorg Med Chem Lett* 2008, 18, 1583-7.
13. Pocker, Y.; Meany, J. E. The catalytic versatility of erythrocyte carbonic anhydrase. II. Kinetic studies of the enzyme-catalyzed hydration of pyridine aldehydes. *Biochemistry* 1967, 6, 239-46.
14. Verpoorte, J. A.; Mehta, S.; Edsall, J. T. Esterase activities of human carbonic anhydrases B and C. *J Biol Chem* 1967, 242, 4221-9.
15. Thorslund, A.; Lindskog, S. Studies of the esterase activity and the anion inhibition of bovine zinc and cobalt carbonic anhydrases. *Eur. J. Biochem.* 1967, 3, 117-23.
16. Pocker, Y.; Sarkanen, S. Carbonic anhydrase: structure catalytic versatility, and inhibition. *Adv Enzymol Relat Areas Mol Biol* 1978, 47, 149-274.
17. Elleby, B.; Sjoblom, B.; Lindskog, S. Changing the efficiency and specificity of the esterase activity of human carbonic anhydrase II by site-specific mutagenesis. *Eur J Biochem* 1999, 262, 516-21.
18. Gould, S. M.; Tawfik, D. S. Directed evolution of the promiscuous esterase activity of carbonic anhydrase II. *Biochemistry* 2005, 44, 5444-52.
19. Host, G.; Martensson, L. G.; Jonsson, B. H. Redesign of human carbonic anhydrase II for increased esterase activity and specificity towards esters with long acyl chains. *Biochim. Biophys. Acta* 2006, 1764, 1601-6.
20. Nair, S. K.; Calderone, T. L.; Christianson, D. W.; Fierke, C. A. Altering the mouth of a hydrophobic pocket. Structure and kinetics of human carbonic anhydrase II mutants at residue Val-121. *J. Biol. Chem.* 1991, 266, 17320-5.

21. Pocker , Y.; Stone, J. T. The Catalytic Versatility of erythrocyte carbonic anhydrase. III: kinetic studies of enzyme-catalyzed hydrolysis of p-nitrophenyl acetate. *Biochemistry* 1967, 3, 668-678.
22. Bergmann, F.; Rimon, S.; Segal, R. Effect of pH on the activity of eel esterase towards different substrates. *Biochem. J.* 1958, 68, 493-9.
23. Armstrong, J. M.; Myers, D. V.; Verpoorte, J. A.; Edsall, J. T. Purification and properties of human erythrocyte carbonic anhydrases. *J. Biol. Chem.* 1966, 241, 5137-49.
24. Baird, T. T., Jr.; Waheed, A.; Okuyama, T.; Sly, W. S.; Fierke, C. A. Catalysis and inhibition of human carbonic anhydrase IV. *Biochemistry* 1997, 36, 2669-78.
25. Banerjee, A. L.; Swanson, M.; Roy, B. C.; Jia, X.; Haldar, M. K.; Mallik, S.; Srivastava, D. K. Protein surface-assisted enhancement for recombinant human carbonic anhydrase II. *Journal of the American Chemical Society* 2004, 126, 10875-10883.
26. Fersht, A. Structure and mechanism in protein science: A guide to enzyme catalysis and protein folding. W. H. Freeman and Company: New York, 1999.
27. Chang, T. K.; Chen, J.; Lee, W. B. Differential inhibition and inactivation of human CYP1 enzymes by trans-resveratrol: evidence for mechanism-based inactivation of CYP1A2. *J Pharmacol Exp Ther* 2001, 299, 874-82.
28. Maurer, T.; Fung, H. L. Comparison of methods for analyzing kinetic data from mechanism-based enzyme inactivation: application to nitric oxide synthase. *AAPS PharmSci* 2000, 2, E8.
29. Esnouf, R. M. An extensively modified version of MolScript that includes greatly enhanced coloring capabilities. *J. Mol. Graph. Model.* 1997, 15, 132-4, 112-3.
30. Merritt, E. A.; Bacon, D. J. Raster3D Version 2: photorealistic molecular graphics. *Methods Enzymol.* 1997, 277, 505–524.

31. Eriksson, A. E.; Jones, T. A.; Liljas, A. Refined structure of human carbonic anhydrase II at 2.0 Å resolution. *Proteins* 1988, 4, 274-82.
32. Fierke, C. A.; Calderone, T. L.; Krebs, J. F. Functional consequences of engineering the hydrophobic pocket of carbonic anhydrase II. *Biochemistry* 1991, 30, 11054-63.
33. Krebs, J. F.; Fierke, C. A. Determinants of catalytic activity and stability of carbonic anhydrase II as revealed by random mutagenesis. *J Biol Chem* 1993, 268, 948-54.
34. Krebs, J. F.; Rana, F.; Dluhy, R. A.; Fierke, C. A. Kinetic and spectroscopic studies of hydrophilic amino acid substitutions in the hydrophobic pocket of human carbonic anhydrase II. *Biochemistry* 1993, 32, 4496-505.
35. Copeland, R. A. Mechanistic considerations in high-throughput screening. *Anal. Biochem.* 2003, 320, 1-12.
36. Wimalasena, K.; Haines, D. C. A general progress curve method for the kinetic analysis of suicide enzyme inhibitors. *Anal Biochem* 1996, 234, 175-82.
37. Moruno-Davila, M. A.; Garrido-del Solo, C.; Garcia-Moreno, M.; Havsteen, B. H.; Garcia-Sevilla, F.; Garcia-Canovas, F.; Varon, R. Kinetic analysis of enzyme systems with suicide substrate in the presence of a reversible competitive inhibitor, tested by simulated progress curves. *Int J Biochem Cell Biol* 2001, 33, 181-91.
38. Berg, J. M.; Tymoczko, J. L.; Stryer, L. *Biochemistry*. 6th ed.; W. H. Freeman: New York, 2007.
39. Boyer, R. F. *Concepts in Biochemistry*. 3rd ed.; John Wiley and Sons: Hoboken, NJ., 2006.
40. Jewell, D. A.; Tu, C. K.; Paranawithana, S. R.; Tanhauser, S. M.; LoGrasso, P. V.; Laipis, P. J.; Silverman, D. N. Enhancement of the catalytic properties of human carbonic anhydrase III by site-directed mutagenesis. *Biochemistry* 1991, 30, 1484-90.

41. Innocenti, A.; Maresca, A.; Scozzafava, A.; Supuran, C. T. Carbonic anhydrase inhibitors: thioxolone versus sulfonamides for obtaining isozyme-selective inhibitors? *Bioorg Med Chem Lett* 2008, 18, 3938-41.

CHAPTER IV

A HIGH-THROUGHPUT SCREENING ASSAY FOR DETECTING INHIBITION OF FLAGELLAR MOTILITY

Introduction

Antibiotic resistance in bacteria is currently a growing, major public health problem; bacteria may soon evolve resistance to all known antibiotics¹⁻³. Commercial research in this area has waned over the last several decades; consequently, few new classes of antibiotics have recently been developed^{1,3,4}. Bacterial signal transduction components, efflux pumps, and genes involved in motility and biofilm formation represent some of the possible targets for antibiotic drug discovery research^{5,6}. Bacterial motility frequently involves the chemotaxis-controlled rotation of extracellular protein fibers called flagella,^{7,8} which are also involved in evasion of host immunity,⁹ host colonization, and biofilm formation¹⁰. There are over 40 genes directly involved in flagellar assembly and structure, plus additional genes for the sensory apparatus. The flagellum is a complex structure composed of more than 20 component proteins⁸ and has several major features: a basal body, a trans-membrane motor, a hook structure, and an elongated helical filament. Thus, bacterial flagellar motility can potentially be inhibited at various levels including gene expression, translation, assembly of the motor or shaft, export of flagellin, motor rotation, chemotaxis components, etc. Consequently, the bacterial flagellar system represents a possible target for antimicrobial drugs. Motility inhibitors could potentially be used

with other antimicrobial compounds to prevent the spread of infectious pathogens in the environment or the host organism. A high-throughput screening (HTS) assay for detecting inhibition of flagellar motility or other types of bacterial motility, e.g. pili-mediated motility, could be used for screening compounds for antimicrobial activity in bacterial strains which are known to be motile. This type of assay could also have applications in fundamental structure function studies of genes and proteins involved in motility, i.e., in screening of mutations and compounds that inhibit or promote motility.

Experimental Procedures

Two basic techniques were combined to enable rapid screening for motility inhibitors; a bacterial swarming agar motility assay, and the use of 96-well microplates common to HTS assay methods. Two *Salmonella typhimurium* bacterial strains were used in all motility screening experiments: *S. typhimurium* strain SJW1103,¹¹ which is wild-type for flagellar motility, and non-motile *S. typhimurium* strain SJW134,¹² which has both of the *fliC* and *fliB* flagellin genes deleted, and thus cannot produce flagella fibers. For each experiment, liquid bacterial flask cultures (50 ml) of motile SJW1103 and non-motile SJW134 *S. typhimurium* strains were grown to saturation by overnight culture in LB media at 30 °C, with shaking at 150 rpm. The liquid cultures of motile and non-motile *S. typhimurium* control strains were then transferred into sterile 25 ml disposable reservoirs. A volume of 200 µl of each liquid culture was pipetted into sample or control wells of a sterile 96-well tissue culture plate with a Matrix Impact² P1250 programmable 8-channel pipettor (Matrix

Technologies Corp., Hudson, NH), for use as the source plate for inoculation of agar motility screening plates.

The 96-well motility agar screening plates were prepared in the following manner. A volume of 200 μ l of freshly prepared motility agar, composed of 1% tryptone (EM Science, Gibbstown, NJ), 0.5% NaCl (Sigma-Aldrich, St. Louis, MO) and 0.3% agar (Calbiochem, La Jolla, CA), was pipetted into each well of a sterile 96-well U-bottom plate (Linbro, Flow Laboratories, McLean, VA) using a Matrix Impact² P1250 programmable 8-channel pipettor and allowed to solidify at 4 °C overnight. This low agar media remains in a liquid state until the temperature is lowered to approximately 35 °C; hence, it can be effectively mixed with thermolabile screening compounds.

The Genesis Plus (GenPlus) library of 960 biologically active, structurally diverse compounds was obtained from MicroSource Discovery Systems (Gaylordsville, CT). A modification of the above method was used to prepare 96-well motility agar plates containing the GenPlus library of 960 compounds, prior to screening for inhibitors of bacterial growth and motility. A 3 μ l volume of each 2 mM stock compound dissolved in 100% DMSO was pipetted into each well of a 96-well tissue culture plate with a CCS Packard PlateTrak robotic pipetting station (Perkin Elmer, Shelton, CT), followed by addition of 197 μ l of liquefied motility agar media with a Matrix Impact² P1250 programmable 8-channel pipettor. This yielded a final screening compound concentration of 30 μ M, within the typical range used for screening assays¹³. The compound and media were then mixed by pipetting up and

down 5-6 times to insure even distribution of the compound within the well and allowed to solidify overnight.

For the preliminary assays on the feasibility of motility detection, a plastic, sterile, disposable 96-pin tool (V&P Scientific, Inc., San Diego, CA) was first manually dipped into the liquid bacterial culture, removed, and then carefully lowered by hand into the agar media to inoculate it. The pin tool was manually positioned above the 96-well motility agar microplates in a manner that resulted in inoculation at the approximate center of each well, a method termed “center-inoculation”. The inoculated agar plates were then incubated for 12-15 hrs at 30 °C in a humidified incubator and assayed for bacterial growth, both visually and by absorbance measurements at 550 nm wavelength (OD₅₅₀) with a SpectraMax Plus³⁸⁴ microplate spectrophotometer (Molecular Devices Corp., Sunnyvale, CA).

The final, quantitative screen of the GenPlus compound library was performed by using a novel “offset-inoculation” method with the PlateTrak instrument to precisely position the plate under a set of 96 pipet tips for inoculation with the bacterial cultures. The PlateTrak was equipped with a P250 (250 µl x 96 tip capacity) pipetting head with horizontal X- and Y-axis plate offset capability for dispensing liquid samples into 384-well plates, via 4 quadrants x 96-wells at a time. The sterile pipette tips were first lowered into the 96-well source plate containing the overnight liquid cultures and then raised, with only a small volume of liquid, i.e. ~0.5 µl, adhering to the surface of each tip by capillary forces. Each 96-well plate containing sterile motility agar was then placed under the pipetting station and laterally offset to

allow the 96 pipette tips to access the upper right quadrant of each well, corresponding to one fourth of the wells in a 384-well plate. The 96 pipette tips were then briefly lowered approximately halfway into the agar in each well (~5 mm depth) of the motility agar plate to inoculate the media and removed. Although pipette tips were used for inoculation in this study, a pin tool would function equally well, if available as an attachment on a robotic dispensing instrument. Each motility agar plate was inoculated with the motile SJW1103 *S. typhimurium* strain in the 80 screening compound wells; control wells lacking any screening compounds were inoculated with the non-motile SJW134 and motile SJW1103 strains as positive and negative controls. The plates were then incubated for 12-15 hrs at 30 °C in a humidified incubator. All absorbance measurements of inoculated 96-well plates were performed at 550 nm wavelength (OD₅₅₀) with a SpectraMax Plus³⁸⁴ spectrophotometer.

Results and Discussion

Initial feasibility studies of motility screening in 96-well plates were performed with motile and non-motile strains of *S. typhimurium*, a Gram-negative bacterial species used as a model system for flagellar motility studies¹⁴. The center-inoculated cultures of the motile *S. typhimurium* SJW1103 strain were observed to spread throughout the motility agar media after overnight incubation. In contrast, the inoculated cultures of the non-motile *S. typhimurium* SJW134 only grew in the immediate vicinity of the inoculation zone, surrounded by clear zones of media (Figure 4.1).

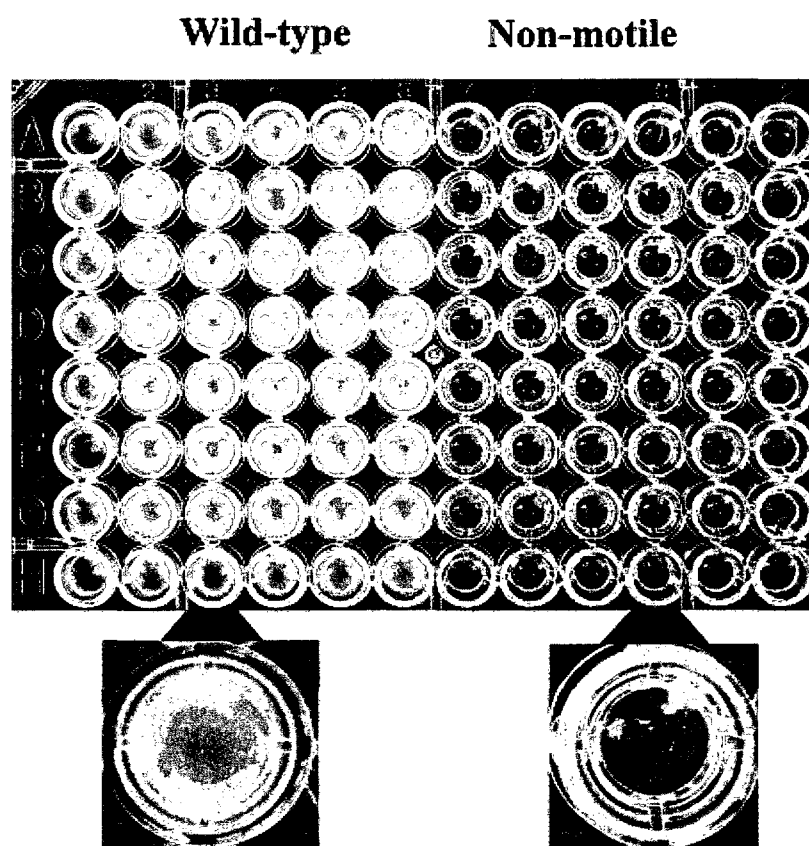


Figure 4.1. Comparison of motile and non-motile bacterial growth patterns in 96-well plate formatted motility agar. Digital camera image of entire 96-well plate containing motility agar that was offset-inoculated with motile and non-motile strains of *S. typhimurium* bacteria and enlarged images of two example wells.

These preliminary results indicated that the center-inoculation method could be used to screen compound libraries for inhibitors of bacterial growth and or motility, as the differences in the motile vs. non-motile cells were readily apparent to the human eye. However, despite the clear differences in growth patterns, no significant differences were observed in the absorbance values (OD_{550}) of the center-inoculated unknowns and motile and non-motile controls, when measured with a microplate spectrophotometer (Figure 4.2). This lack of discrimination resulted from the growth of both non-motile and motile cells to high densities in the inoculated center region of each well, combined with a narrow detection area of ~ 1 mm diameter in each well of the SpectraMax Plus³⁸⁴ plate reader. Thus, this center-inoculation method was not adaptable to simple HTS approaches for identifying inhibitors of motility with the absorbance plate reader used in this study, although it could still be useful for identifying inhibitors of bacterial growth.

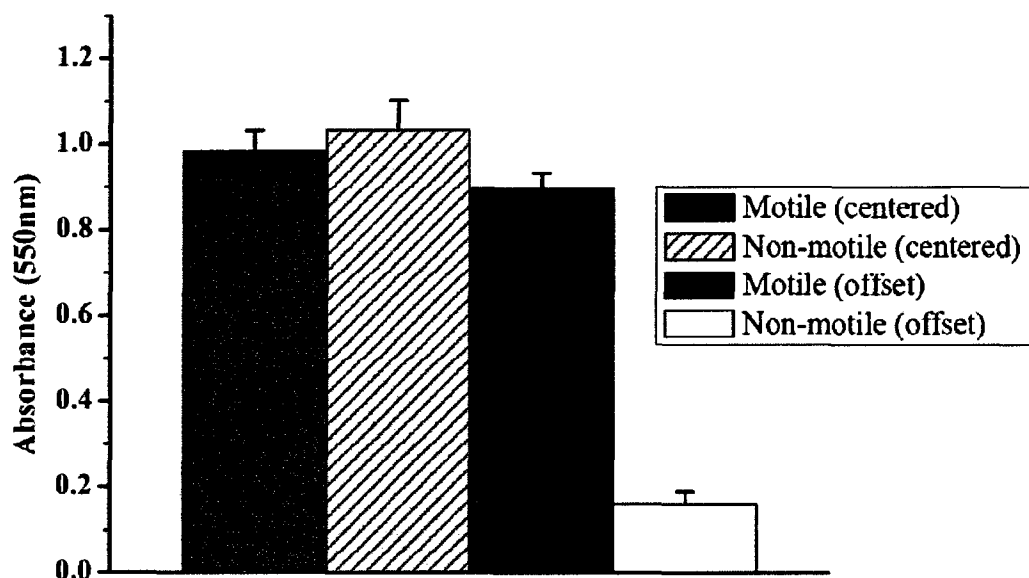


Figure 4.2. Comparison of average absorbance readings for motile and non-motile *S. typhimurium* bacterial cells.

Although the positive controls did not provide a useful reference for determining motility inhibition, it was possible to statistically analyze the absorbance data with respect to the deviation of individual sample readings from the average value of each plate for antimicrobial activity. The average (\bar{x}) and standard deviation (σ) of the OD₅₅₀ readings were computed for each of the two duplicate plates using a spreadsheet. The absorbance data in each well were analyzed with respect to the difference between each well and the average plate value. Strong inhibitors were defined by the criteria that the OD₅₅₀ of a well containing a strong inhibitor was less than the mean plate value by two times the standard deviation $\{OD_{550} < (\bar{x} -$

2σ). This cut-off criteria yielded a total of 70 compounds that significantly inhibited the growth of the bacteria. Although no previously unknown antibiotic compounds were identified among the hits, these results indicate the general validity of the screening method for detecting antimicrobial compounds, although a further improvement was possible, as demonstrated below.

A variation on the inoculation method, termed “offset-inoculation”, was developed to allow the use of an HTS-compatible plate reader for detection of inhibitors of antimicrobial growth and motility. In this technique, a PlateTrak robotic pipetting workstation was used to simultaneously inoculate one quadrant of each well of a 96-well motility agar microplate at an *off-center* location, instead of the center of each well. Although 96 sterile plastic pipet tips were used with this particular workstation to inoculate the motility agar plates, a 96-pin tool attachment would be equally effective for this purpose. Using this method, control wells inoculated with motile and non-motile cells were readily distinguished, both by visual inspection and with a plate reader in 96-well detection mode, after 10 hrs of post-incubation growth (Figures 4.1, 4.2), with 100% repeatability. As observed previously, the wild-type motile cultures spread in all directions of the motility media in the wells, while non-motile cultures only grew in the immediate vicinity of the inoculation zone (Figure 4.1). This resulted in clear, sterile media in the center of each well for non-motile cells, where absorbance is typically measured by a 96-well plate reader. This offset-inoculation method was used to measure growth curves via OD₅₅₀ measurements with a microplate spectrophotometer and was able to consistently detect a significant

difference between the growth of motile and non-motile *S. typhimurium* strains (Figure 4.3).

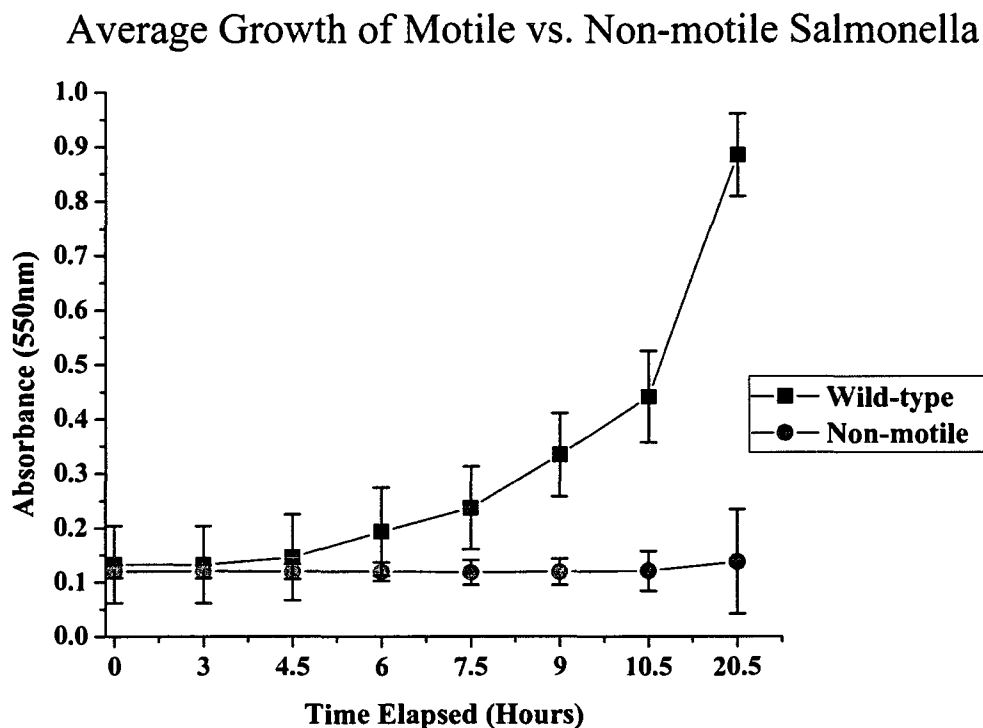


Figure 4.3. Growth curves for motile and non-motile *S. typhimurium* bacterial cells inoculated in 96-well plate-formatted motility agar. *S. typhimurium* cells, either wild type for motility (strain SJW1103) or non-motile (strain SJW134), were inoculated in the upper right quadrant of each well, as shown in Figure 4.1. The time-dependent absorbance readings (OD_{550}) from two identical 96-well plates containing six columns (48 wells) for each bacterial strain were averaged to generate each data point; the error bars represent the computed standard deviation of each set of measurements. The difference in a non-motile strain vs. a motile strain and the rate of growth of the motile strain can be readily determined with this assay method.

The hit compounds previously identified in the visual screen were used to prepare a master hit plate and retested for inhibition of growth and motility by this offset inoculation method. The absorbance at 550 nm of each well (OD_{550}) was measured with the SpectraMax Plus³⁸⁴ spectrophotometer. The reproducibility of the assay controls was determined by calculating the Z' value for the assay. The statistical assay quality was determined by calculating the Z' factor,¹⁵ given in Eq. 2.4, Chapter Two of this thesis. The average Z' value for all 12 compound plates was 0.67 ± 0.14 ; an acceptable value for HTS-format assays (Figure 4.4)¹³. Furthermore, the signal to noise ratio calculated from the positive and negative controls was 5.94 ± 1.11 , also indicative of a robust screening assay. The signal to noise ratio is an indication of the degree of confidence for which a signal can be regarded as different from the background^{13,15}. While the signal to noise ratio can be helpful in determining the effectiveness of an assay, the Z' value is the preferred standard for determining the quality of an HTS assay^{13,15}. Both the types of controls (motile and non-motile bacterial strains) and the location of inoculation contributed to the quality of the assay. An antibiotic compound such as ampicillin or kanamycin could be used as an alternative positive control instead of the non-motile strain, for assays where antimicrobial growth inhibitors is the only objective. Because of the different motile and non-motile strains of *Salmonella* used as controls, the assay was able to consistently detect a wide range of antibiotic activity, as determined by a cutoff of 50% inhibition of motility, as shown in a scatterplot (Figure 4.5) and listed in Table 4.1.

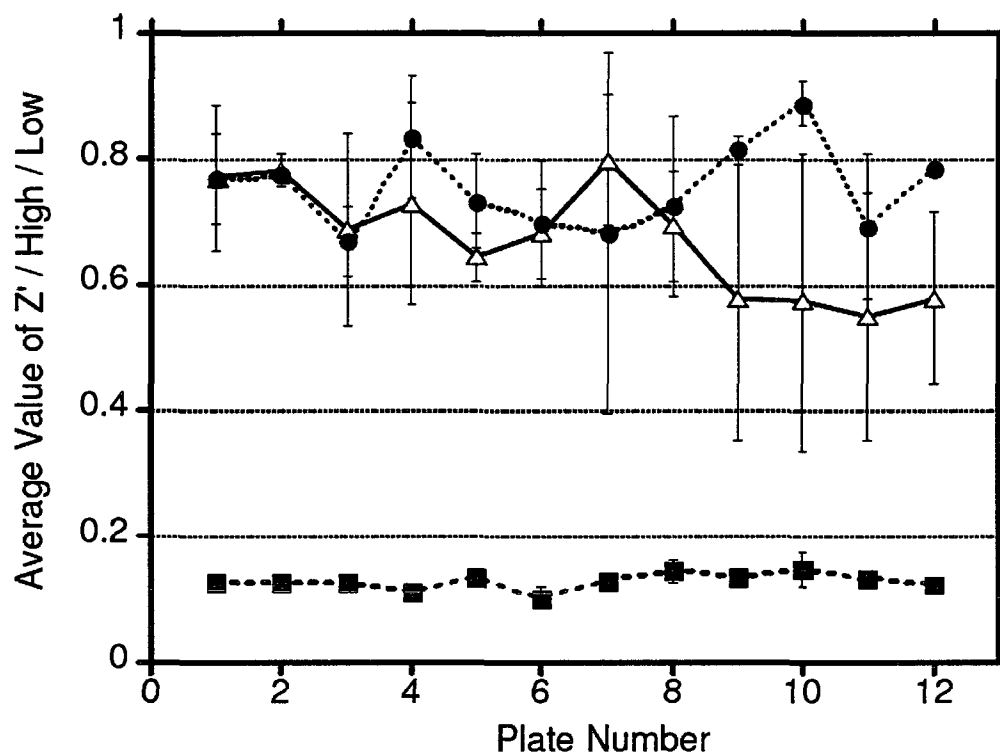


Figure 4.4. Plot of average Z' values and average absorbance (OD₅₅₀) values for positive and negative controls for each of the 12 Genesis Plus library compound plates, using the offset-inoculation method. Open triangle symbols represent the average Z' values, the closed circles represent the average high (positive) control values, closed squares represent the average low (negative) controls for each plate. Error bars represent the standard deviation computed from two duplicate experiments for each plate.

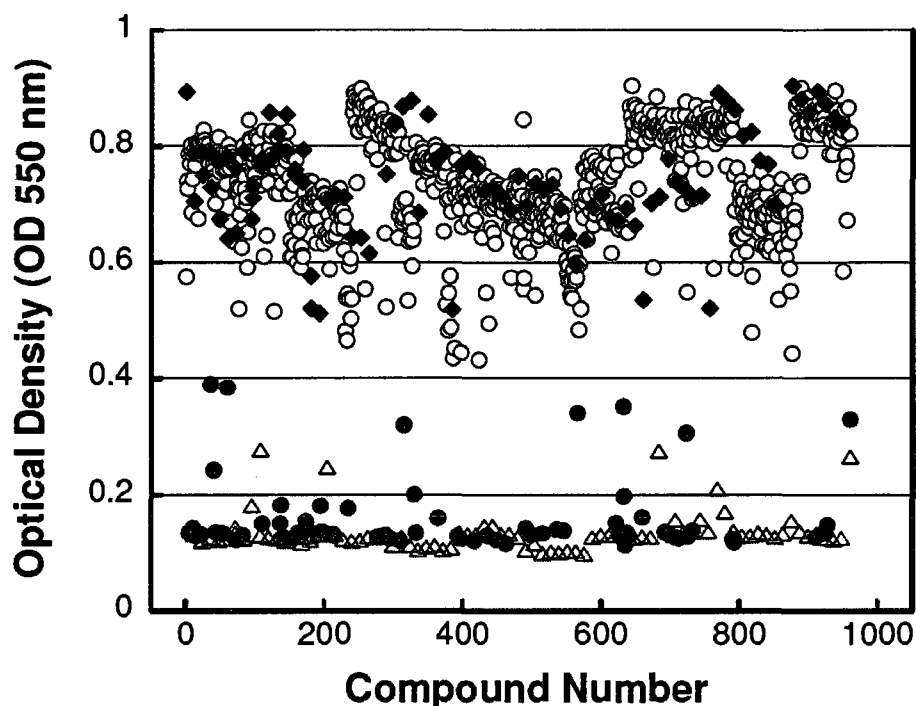


Figure 4.5. Scatter plot of results of screening the Genesis Plus library of 960 compounds for inhibitors of microbial growth and motility, using the offset-inoculation method. Filled circles (black, lower region) denote the 70 hit compounds, which exhibited 50% or higher inhibition of the spreading of the SJW1103 *S. typhimurium* strain in the motility agar wells, relative to the non-inhibited motile controls. Open circles (white, upper region) denote the non-inhibitory compounds in the Genesis Plus library. Filled diamonds (black, upper region) indicate the negative motility inhibition controls (wild-type motile SJW1103 *S. typhimurium* strain) and open triangles (white, lower region) indicate the positive motility controls (non-motile SJW134 *S. typhimurium* strain) for each individual plate of 80 compounds.

Table 4.1. Complete list of antibacterial compounds detected in screen of Genesis Plus library with offset motility detection method.

Compound name	Functional classification	Antibiotic effectiveness ^{a, b}
1. Cefoperazone sodium	antimicrobial	105.13 (\pm 4.77%)
2. Ciprofloxacin	antibacterial, fungicide	104.92 (\pm 5.12%)
3. Trimethoprim	antibacterial	104.28 (\pm 6.82%)
4. Cefamandole nafate	antimicrobial	103.81 (\pm 0.73%)
5. Chloroxine	chelating agent	102.86 (\pm 3.03%)
6. Cephaloridine	antimicrobial	102.81 (\pm 0.76%)
7. Metampicillin sodium	antimicrobial	102.72 (\pm 2.10%)
8. Lomefloxacin hydrochloride	antimicrobial	102.41 (\pm 2.40%)
9. Cefuroxime sodium	antimicrobial	102.24 (\pm 0.94%)
10. Thimerosal	anti-infective	101.95 (\pm 1.02%)
11. Ofloxacin	antimicrobial	101.82 (\pm 0.68%)
12. Ceftriaxone sodium	antibiotic	101.63 (\pm 1.99%)
13. Enoxacin	antibacterial	101.50 (\pm 2.36%)
14. Oxolinic acid	antimicrobial	101.43 (\pm 2.10%)
15. Bacampicillin hydrochloride	antibiotic	101.39 (\pm 1.70%)
16. Tetracycline hydrochloride	antibacterial	101.06 (\pm 0.41%)
17. Chlorhexidine	topical antibacterial	100.87 (\pm 2.12%)
18. Alexidine hydrochloride	antibacterial	100.81 (\pm 2.53%)
19. Cefazolin sodium	antibacterial	100.59 (\pm 0.59%)
20. Polymyxin b sulfate	antibacterial	100.27 (\pm 1.03%)
21. Floxuridine	antineoplastic	100.08 (\pm 1.12%)
22. Aureomycin	antibacterial	99.94 (\pm 0.98%)
23. Cephalirin sodium	antibacterial	99.79 (\pm 1.08%)
24. Pipemidic acid	antimicrobial	99.63 (\pm 4.69%)
25. Pyrithione zinc	antibacterial; antifungal	99.63 (\pm 0.92%)
26. Tobramycin	antibacterial	99.45 (\pm 0.59%)

Table 4.1. - Continued

Compound name	Functional classification	Antibiotic effectiveness ^{a, b}
27. Mitomycin C	antineoplastic	99.40 (± 1.91%)
28. Cefaclor	antibiotic	99.20 (± 1.68%)
29. Hexachlorophene	topical anti-infective	99.17 (± 0.95%)
30. Flumequine	antibacterial	99.15 (± 0.99%)
31. Cefotaxime sodium	antibacterial	98.94 (± 2.19%)
32. Hetacillin potassium	antibacterial	98.69 (± 0.47%)
33. Amoxicillin	antibacterial	98.29 (± 0.99%)
34. Doxycycline hydrochloride	antibacterial	98.29 (± 0.99%)
35. Norfloxacin	antibacterial	98.24 (± 0.41%)
36. Oxytetracycline	antibacterial	98.24 (± 0.40%)
37. Cefoxitin sodium	antimicrobial	98.20 (± 0.97%)
38. Nalidixic acid	antibacterial	98.04 (± 2.78%)
39. Chloramphenicol	antibacterial	98.03 (± .72%)
40. Furazolidone	antimicrobial	97.96 (± 0.49%)
41. Minocycline hydrochloride	antibacterial	97.86 (± 10.75%)
42. Meclocycline sulfosalicylate	antibacterial	97.83 (± 2.08%)
43. Cephalothin sodium	antibacterial	97.78 (± 1.62%)
44. Moxalactam disodium	antibacterial	97.67 (± 0.34%)
45. Methacycline hydrochloride	antibacterial	97.60 (± 1.95%)
46. Bergaptene	antipsoriatic	97.54 (± 2.47%)
47. Nitrofurantoin	antibacterial	97.47 (± 0.30%)
48. Erythromycin	antibacterial	97.07 (± 0.77%)
49. Phenylmercuric acetate	fungicide	96.72 (± 0.82%)
50. Cinoxacin	antibacterial	96.51 (± 2.74%)
51. Demeclocycline hydrochloride	antibacterial	96.47 (± 1.46%)
52. Zidovudine	antiviral	96.28 (± 0.65%)

Table 4.1. - Continued

Compound name	Functional classification	Antibiotic effectiveness ^{a, b}
53. 5-azacytidine	antimicrobial	96.23 (\pm 0.66%)
54. Rifampin	antibacterial	95.81 (\pm 7.69%)
55. Broxyquinoline	antiseptic; disinfectant	95.61 (\pm 1.64%)
56. Erythromycin ethylsuccinate	antibacterial	94.55 (\pm 2.36%)
57. Ciclopirox olamine	antifungal	91.41 (\pm 8.54%)
58. Penicillin g potassium	antibiotic	91.30 (\pm 2.84%)
59. Iodoquinol	anti-amebic	90.35 (\pm 3.01%)
60. Piperacillin sodium	antibacterial	90.08 (\pm 13.64%)
61. Fluorouracil	antineoplastic	89.90 (\pm 1.32%)
62. Cefmetazole sodium	antimicrobial	88.58 (\pm 0.73%)
63. Chloramphenicol hemisuccinate	antibacterial	82.38 (\pm 2.70%)
64. Thiamphenicol	antibacterial	78.77 (\pm 1.22%)
65. Fosfomycin	antimicrobial	71.09 (\pm 62.31%)
66. Tannic Acid	nonspecific enzyme blocker	68.75 (\pm 1.69%)
67. Sulfachlorpyridazine	antibacterial	65.55 (\pm 6.18%)
68. Benzethonium chloride	topical anti-infective	61.39 (\pm 27.58%)
69. Cetylpyridinium chloride	topical anti-infective	60.46 (\pm 24.75)
70. Benzalkonium chloride	topical anti-infective	60.32 (\pm 55.55%)

^a The percentage of motility inhibition for each compound, as normalized by comparison with motile and non-motile *S. typhimurium* controls on each plate. Numbers in parentheses are the standard deviation, as computed from two separate experiments.

^b Only compounds with at least 50% inhibition of the motility are listed.

Encouraged by the initial results of the offset inoculation method with previously identified hits, the entire 960 compound GenPlus library was rescreened in duplicate, using the offset inoculation method, to verify the consistency of the

previous results. The hits identified were 100% identical to those identified by the previous screening methods. The average Z' value for all 12 compound plates was 0.62 ± 0.19 , indicative of a high quality assay. These preliminary screening results with a model compound library indicate that the HTS-compatible “offset inoculation” method can be used to screen compounds for bactericidal, bacteriostatic, and motility inhibition activity.

All of the hit compounds possessed known or suspected antimicrobial activity, e.g., amoxicillin, ciprofloxacin, and rifampin. Furthermore, three distinct types of bacterial growth behavior were observed in the motility agar wells: complete spreading of the cells throughout the well, a total absence of growth in the well, and marginal growth at the region of inoculation without significant spreading of the cells (Figure 4.6). The third type of limited growth and swarming behavior was only observed for the compound hexachlorophene, a chlorinated bisphenol compound with known bacteriostatic action against gram-positive organisms,¹⁶ but less effective against gram-negative organisms¹⁷. Although no previously unknown antibiotic compounds were identified among the hits, the results obtained indicate that the offset inoculation method can be used to screen compounds for bactericidal, bacteriostatic, and motility inhibition activity. However, it should be noted that this preliminary screening method, as implemented with a plate reader, is not capable of distinguishing among these modes of inhibition; more detailed follow-up studies will be required to further characterize the mode of action of each inhibitor compound.

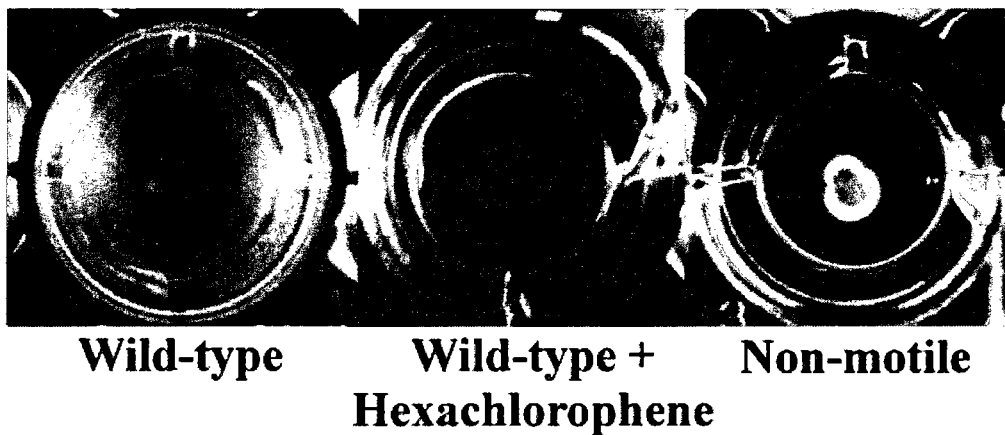


Figure 4.6. Enlarged images showing three types of growth patterns observed for *S. typhimurium* cells center-inoculated in the larger wells of the 24-well tissue culture plate. Left image: wild-type SJW1103 cells in plain LB agar. Center image: wild-type SJW1103 cells grown in the presence of 30 μ M hexachlorophene, showing partial inhibition of growth and motility. Right image: non-motile SJW134 cells grown in plain LB agar.

References

1. Fishman, N. Antimicrobial stewardship. *Am J Med* 2006, 119, S53-61; discussion S62-70.
2. Tenover, F. C. Mechanisms of antimicrobial resistance in bacteria. *Am J Med* 2006, 119, S3-10; discussion S62-70.
3. Yoneyama, H.; Katsumata, R. Antibiotic resistance in bacteria and its future for novel antibiotic development. *Biosci Biotechnol Biochem* 2006, 70, 1060-75.
4. Payne, D. J.; Gwynn, M. N.; Holmes, D. J.; Pompliano, D. L. Drugs for bad bugs: confronting the challenges of antibacterial discovery. *Nat Rev Drug Discov* 2007, 6, 29-40.
5. Danese, P. N. Antibiofilm approaches: prevention of catheter colonization. *Chem Biol* 2002, 9, 873-80.
6. Pages, J. M.; Masi, M.; Barbe, J. Inhibitors of efflux pumps in Gram-negative bacteria. *Trends Mol Med* 2005, 11, 382-9.
7. Bardy, S. L.; Ng, S. Y.; Jarrell, K. F. Prokaryotic motility structures. *Microbiology* 2003, 149, 295-304.
8. Macnab, R. M. Type III flagellar protein export and flagellar assembly. *Biochim Biophys Acta* 2004, 1694, 207-17.
9. Andersen-Nissen, E.; Smith, K. D.; Strobe, K. L.; Barrett, S. L.; Cookson, B. T.; Logan, S. M.; Aderem, A. Evasion of Toll-like receptor 5 by flagellated bacteria. *Proc Natl Acad Sci U S A* 2005, 102, 9247-52.
10. Costerton, J. W.; Stewart, P. S.; Greenberg, E. P. Bacterial biofilms: a common cause of persistent infections. *Science* 1999, 284, 1318-22.
11. Yamaguchi, S.; Fujita, H.; Sugata, K.; Taira, T.; Iino, T. Genetic analysis of H2, the structural gene for phase-2 flagellin in Salmonella. *J Gen Microbiol* 1984, 130, 255-65.

12. Williams, A. W.; Yamaguchi, S.; Togashi, F.; Aizawa, S. I.; Kawagishi, I.; Macnab, R. M. Mutations in *fliK* and *flhB* affecting flagellar hook and filament assembly in *Salmonella typhimurium*. *J Bacteriol* 1996, 178, 2960-70.
13. Walters, W. P.; Namchuk, M. Designing screens: how to make your hits a hit. *Nat Rev Drug Discov* 2003, 2, 259-66.
14. Malapaka, V. R.; Barrese, A. A.; Tripp, B. C. High-throughput screening for antimicrobial compounds using a 96-well format bacterial motility absorbance assay. *J Biomol Screen* 2007, 12, 849-54.
15. Zhang, J. H.; Chung, T. D.; Oldenburg, K. R. A simple statistical parameter for use in evaluation and validation of high-throughput screening assays. *J Biomol Screen* 1999, 4, 67-73.
16. Haley, C. E.; Marling-Cason, M.; Smith, J. W.; Luby, J. P.; Mackowiak, P. A. Bactericidal activity of antiseptics against methicillin-resistant *Staphylococcus aureus*. *J Clin Microbiol* 1985, 21, 991-2.
17. Maris, P. Resistance of 700 gram-negative bacterial strains to antiseptics and antibiotics. *Ann Rech Vet* 1991, 22, 11-23.

CHAPTER V

CARBONIC ANHYDRASE SUBCLONING, EXPRESSION, AND CO₂ HYDRATION ACTIVITY ASSAY DEVELOPMENT

Carbonic Anhydrase Isozyme Subcloning and Expression

As noted previously, the human CA II expression plasmid was obtained from Prof. Carol Fierke at the University of Michigan. However, CA II is only one member of the mammalian α -class CA isozyme family; consequently, a hypothesis was proposed that other mammalian CA isozymes might have different inhibition profiles with the GenPlus compound library than CA II. Therefore, a new research project was initiated to express and screen one or more other mammalian CA isozymes to determine if there were differences in their inhibition profile with the GenPlus library. A set of commercially-available vectors (plasmids) encoding the full-length genes for eleven of the catalytically active mammalian α -CA isozymes were purchased from Open Biosystems (Huntsville, Al). Each plasmid encoded a full-length cDNA gene for a different CA isozyme (see Table 5.1) and an *E. coli* compatible origin of replication to allow production of more plasmid DNA in suitable cloning strains, e.g. DH5-alpha *E. coli*. The plasmids were first transformed into XL-1 Blue *E. coli* cells by electroporation. A volume of 2 μ l of each plasmid encoding a CA isozyme was mixed with 48 μ l of electrocompetent XL-1 Blue *E. coli* (Stratagene) inside a cold electroporation cuvette with an electrode gap of 1 mm and pulsed once at 1.8 kV. Immediately after each sample was subjected to the electrical pulse, 950 μ l of room

temperature SOC media was added to the cuvette, followed by transfer of the entire solution to a 1.5 ml Eppendorf tube and incubation at 37 °C with shaking for an hour. The electroporated cells were then aliquoted into two Eppendorf tubes (450 µl each) and centrifuged at 14,000 g for 10 min. The SOC media was then carefully poured off and one pellet was then resuspended in 200 µl of fresh SOC media while the second pellet was stored at -20 °C overnight as a backup. Then, 20 µl of SOC cell mixture was spread onto LB plates containing the correct antibiotic (ampicillin or chloramphenicol), and after allowing the plates to dry, they were placed inside a 37 °C incubator for overnight growth. The next step was to pick a colony from the overnight plates with a sterile toothpick and culture it in the appropriate LB antibiotic media at 37 °C for ~16 hours (overnight). A Qiagen Mini-prep kit was then used to purify the plasmid DNA. A 10 µl sample of plasmid DNA at a concentration of 200 ng/ul was sent to the University of Michigan DNA Core sequence facility (Ann Arbor, MI) for confirmation of the DNA sequence. Standard T7 forward and M13 reverse primers were used to sequence the inserted CA genes in each vector, which were supplied by the sequence facility. The reason for using two different primers was due to the failure of the T7 forward primer to yield useable sequence data for five of the CA isozymes (CA I, CA III, CA V, CA VII, and CA XIV). The DNA sequencing results from the University of Michigan DNA Core sequence facility were typically acceptable. All samples were checked for DNA concentration via A₂₆₀ measurements before being submitted. Samples that did not yield any sequence data and had measurable DNA concentration were resequenced using an M13 sequencing

primer. A summary of the results of the DNA sequencing data for α -class CA clones is listed in Table 5.1; the GenBank accession numbers are given for each confirmed α -CA gene.

Table 5.1. Mammalian α -class carbonic anhydrase clone vector and sequence information.

Clone Name	Accession Number	Original Vector	Antibiotic
CA I	BC027890	pCMV-SPORT6	Ampicillin
CA III	BC004897	pOTB7	Chloramphenicol
CA IV	BC069649	pBluescriptR	Ampicillin
CA VB	BC028142	pCMV-SPORT6	Ampicillin
CA VII	BC033865	pCMV-SPORT6	Ampicillin
CA IX	BC014950	pOTB7	Chloramphenicol
CA X	BC020577	pCMV-SPORT6	Ampicillin
CA XI	BC002662	pOTB7	Chloramphenicol
CA XII	BC023981	pDNR-LIB	Chloramphenicol
CA XIII	BC052602	pCMV-SPORT6	Ampicillin
CA XIV	BC034412	pCMV-SPORT6	Ampicillin

The genes encoding the CA isozymes were previously subcloned into four different cloning vectors (Table 5.1) by Open Biosystems. None of these vectors had any useful restriction sites for cutting the gene out of its original vector and placing the gene in pET28c vector. Furthermore, they varied with respect to the type of antibiotic resistance gene required to maintain selection for the plasmid in a bacterial host (*E. coli*). Thus, an initial goal was to subclone all of the CA isozymes into a standard bacterial pET-series expression vector for ease of use. The vector pET28c was chosen to be the standard vector because it encodes kanamycin resistance and has a wide range of restriction sites to facilitate directional cloning. Kanamycin is a better antibiotic for selection than ampicillin because it is not as susceptible to degradation

during overnight growth due to changes in pH of the growth media, which occur as the bacteria excrete chemicals into the media. In addition, the pET vector is designed for high-yield bacterial expression of protein when induced by the addition of suitable amounts of IPTG to the growth media.

Human carbonic anhydrase I and carbonic anhydrase IV were chosen as the first isozymes to be subcloned in the pET28c vector because of their well-characterized behavior and previously observed differences in enzymatic activity from CA II. These two isozymes were cloned from the original vector by PCR, using the following primers. These PCR primers were designed to amplify the portion of each carbonic anhydrase gene that codes for a soluble catalytic domain of each protein. The PCR primers also encoded new restriction sites to enable insertion via directional cloning into the multiple cloning site of the pET 28c vector. The CA IV forward PCR primer sequence was 5' GGT ACT TCC CAT ATG ATG CGG ATG CTG GCG 3' and the CA IV reverse primer sequence was 5' GGC CGG TAG AAT TCT TAT CAT CGC AGG AAG CC 3'. The CA IV primers were designed to include restriction sites for EcoRI at the 3' end and NdeI at the 5' end. These PCR primers were internal to the entire wild-type CA IV sequence, and were designed to remove the signal sequence from the N-terminus and the GPI lipid anchor tail sequence from the C-terminus. These previously described modifications are required to generate a water-soluble, cytosolic active form of CA IV, which is normally expressed as a membrane-bound form¹. Pfu Turbo DNA polymerase is a high-fidelity polymerase and was used for all PCR subcloning procedures. The master PCR mix

for one reaction consisted of 5 µl Pfu Turbo buffer, 1 µl dNTPs (10 mM starting concentration), 2.5 µl of each primer (100 µM starting concentration), 0.2 µl Pfu Turbo, 1 µl of template DNA, and sterile DI H₂O to bring the reaction volume to 50 µl in a 200 µl PCR tube. A Techne Touchgene Gradient thermocycler was used for all PCR procedures. The PCR conditions were as follows. First, an initial sample heating step of 2 min at 94 °C was performed before starting the amplification cycles. Each cycle consisted of the following steps: 1. denaturing the DNA at 94 °C for 45 sec 2. annealing the primers to each DNA strand at 55 °C for 40 sec, and 3. extension of the new DNA product by the DNA polymerase at 72 °C for 2 min. This procedure was repeated for a total of 30 cycles. This was followed by a final extension step at 72 °C for 10 min to fill in any remaining short PCR products. At the end of the PCR run, the product tubes were stored overnight at 4 °C.

After the first PCR run with CA IV gene, the resulting PCR product was checked by gel electrophoresis on a 1% agarose gel stained with ethidium bromide. The initial PCR product was observed to have a smeared pattern of DNA, indicating multiple PCR products with a range of molecular masses. Different PCR conditions were tried and the conditions given above were the final ones which yielded a clean PCR product (Figure 5.1).

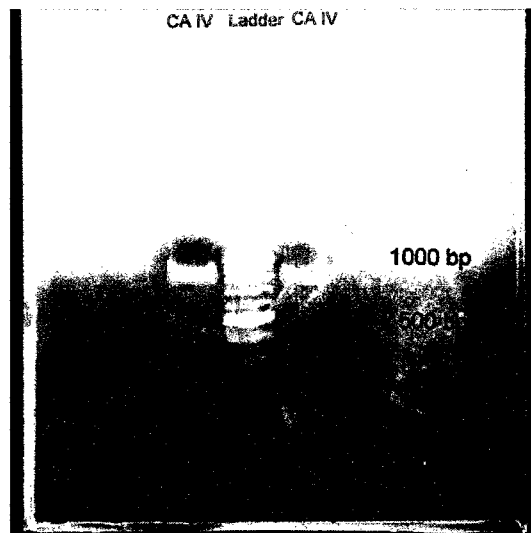


Figure 5.1. Agarose gel electrophoresis analysis of Pfu Turbo PCR product for the subcloned CA IV gene.

After optimization of the PCR conditions for each CA gene, the DNA bands corresponding to each amplified CA gene were cut out of the agarose gel using a clean razor blade under long wavelength UV light and were purified with a Qiagen PCR purification kit, using the directions provided with the kit. The ends of the purified linear CA IV gene fragment were then cut at the introduced restriction sites with the appropriate restriction enzymes (EcoRI, NdeI). The corresponding restriction sites in the target pET28c vector were also cut with the same restriction enzymes. The restriction enzymes used in the digestion of the CA IV PCR product and pET28c plasmid digest were then heat inactivated for 20 min at 65 °C and the resulting DNA products were stored at -20 °C. The digested pET28c samples were purified by

electrophoresis on a 0.8% agarose gel for 70 min at 50 volts to separate the small cut fragment from the larger linear plasmid DNA. Afterwards, the larger DNA band was gel purified using the Qiagen gel purification kit and stored at -20 °C.

The two linear fragments of DNA (CA gene and pET28c fragment) were ligated together using T4 ligase during an overnight ligation at 16 °C. The reaction mixture contained the following: 4 µl of ligation buffer, 8 µl of CA IV insert, 5 µl of pET28c vector, 2 µl of T4 ligase (which was added last), and 1 µl of sterile dH₂O. Following ligation, the ligase was heat inactivated for ten min at 65 °C and 1 µl of the ligation product was transformed by electroporation into 49 µl of DH5-alpha *E. coli*. Following application of the electrical pulse, 950 µl of room temperature SOC media was added to the electroporation cuvette and the solution was transferred to a 1.5 ml Eppendorf tube and placed into the 37 °C incubator with shaking for 1 hour. The cells were then plated onto LB kanamycin plates. The transformed cells were grown overnight at 37 °C until visible colonies were obtained and several colonies were picked with sterile toothpicks for plasmid isolation using a Qiagen Mini-prep kit. The purified plasmid DNA was sequenced by the University of Michigan DNA Core facility to confirm that the CA IV gene had been correctly inserted in the pET28c.

The same procedure used for CA IV above was repeated with the CA I gene to subclone it into the same pET28c plasmid. For CA I, the forward primer was 5' CCA TGG CAA GTC CAG ACT GG 3' and the CA I reverse primer was 5' GCG GAT CCT TAT CAA AAT GAA GCT CTC ACT GTT CTG 3'. In this case, the full-length CA I gene was amplified as it is already expressed as a soluble enzyme, and

new NcoI and BamHI restriction sites were introduced at opposite ends of the PCR product. The master PCR mix for one reaction consisted of 5 µl Pfu Turbo buffer, 1 µl dNTPs (10 mM starting concentration), 2.5 µl of each primer (100 µM starting concentration), 0.2 µl Pfu Turbo, 1 µl of template DNA, and sterile DI H₂O to bring reaction volume to 50 µl. The PCR conditions were as follows: an initial 2 min at 94 °C before starting the cycle and 94 °C for 45 sec, 55 °C for 40 sec, and 72 °C for 2 min, repeated for a total of 30 cycles, followed by a final extension step of 72 °C for 10 min. At the end of the PCR run the tubes were stored overnight at 4 °C. After the PCR run, the resulting PCR product was checked by gel electrophoresis on a 1% agarose gel stained with ethidium bromide and was found to be a single band. The final pET28c-CA I plasmid was submitted to the University of Michigan DNA Core sequence facility to confirm that the CA I gene had been correctly inserted. The sequencing results confirmed that CA I and CA IV had been inserted in the pET28c vector (Table 5.2, Table 5.3, and Table 5.4). A plasmid map for pET28c-CA I and pET28c-CA IV is shown in Figures 5.2 and 5.3 and the translated protein sequences are shown in Table 5.5. In Tables 5.6 and 5.7, an NCBI blastx search sequence alignment is shown to indicate how the pET28c-CA I and the pET28c-CA IV plasmid DNA sequences compare to the wild-type CA I and CA IV protein sequences.

Table 5.2. Sequencing results for the pET28c-CA I and pET28c-CA IV.

CA I	GCNTTNNGTGACCTATAGNAAAAGTTTGTACAAAAAAGCAG GCTGGTACCGGTCCGGAATTCCCGGGATCAGTCCTCAGGTGC AACCCCCTGCGTGGTCCTCTGTGGCAGCCTTCTCTCATTTCAG AGCTAAAAAGAAAACTCAGTAGAAGATAATGGCAAGTCCAG ACTGGGGATATGATGACAAAAATGGTCCTGAACAATGGAGC AAGCTGTATCCCATTGCCAATGGAAATAACCAGTCCCCTGTT GATATTAAAACCAGTGAAACCAAACATGACACCTCTCTGAA ACCTATTAGTGTCTCCTACAACCCAGCCACAGCCAAAGAAAT TATCAATGTGGGGCATTTCCTTCCATGTAAATTTTGAGGACAA CGATAACCGATCAGTGCTGAAAGGTGGTCCTTTCTCTGACAG CTACAGGCTCTTTCAGTTCCATTTTCACTGGGGCAGTACAAA TGAGCATGGTTCAGAACATACAGTGGATGGAGTCAAATATT CTGCCGAGCTTCACGTAGCTCACTGGAATTCTGCAAAGTACT CCAGCCTTGCTGAAGCTGCCTCAAAGGCTGATGGTTTGGCAG TTATTGGTGTTTTGATGAAGGTTGGTGAGGCCAACCCAAAGC TGCAGAAAGTACTTGATGCCCTCCAAGCAATTAAAACCAAG GGCAAACGAGCCCCATTCACAAATTTTGACCCCTCTACTCTC CTTCCTTCATCCCTGGATTTCTGGACCTACCCTGGCTCTCTGA CTCATCCTCCTCTTTATGAGAGTGTAACCTGGATCATCTGTAA G NNTTTTCCGNAGGTTAAGCCCCGAGTCCTCNACTACCCCTGC TTGGTGCCAGTCAAGTGGGGTGGAACTGCCAGAAGGACCG CCAGTCCCCCATCAACATCGTCACCACCAAGGCAAAGGTGG ACAAAAAACTGGGACGCTTCTTCTTCTCTGGCTACGATAAGA AGCAAACGTGGACTGTCCAAAATAACGGGCACTCAGTGATG ATGTTGCTGGAGAACAAGGCCAGCATTCTGGAGGAGGACT GCCTGCCCCATACCAGGCCAAACAGTTGCACCTGCACTGGTC CGACTTGCCATATAAGGGCTCGGAGCACAGCCTCGATGGGG AGCACTTTGCCATGGAGATGCACATAGTACATGAGAAAGAG AAGGGGACATCGAGGAATGTGAAAGAGGGCCAGGACCCTGA AGACGAAATTGCGGTGCTGGCCTTTCTGGTGGAGGCTGGAA CCCAGGTGAACGAGGGCTTCCAGCCACTGGTGGAGGCACTG TCTAATATCCCCAAACCTGAGATGAGCACTACGATGGCAGA GAGCAGCCTGTTGGACCTGCTCCCCAAGGAGGAGAACTGA GGCACTACTTCCGCTACCTGGGCTCACTCACCACACCGACCT GCGATGAGAAGGTCGTCTGGACTGTGTTCCGGGAGCCCATTC AGCTTCACAGAGAACAGATCCTGGCATTCTCTCAGAAGCTGT ACTACGACAAGGAACAGACAGTGAGCATGAAGGACAATGTC AGGCCCTGCAGCAGCTGGGGCAGCGCACCGTGATCAAGAG CTAAGAATTCTTAGGGCCCAACNNNNNNNTNNNA
CA IV	

Table 5.3. Partial blastx search results with CA I DNA sequence results.

Accession	Description	Max score	Total score	Query coverage	E value	Max ident
BC027890.1	Homo sapiens carbonic anhydrase I, mRNA (cDNA clone MGC:34628 IMAGE:5222602), complete cds	1341	1341	91%	0.0	100%
NM_001128830.1	Homo sapiens carbonic anhydrase I (CA1), transcript variant 3, mRNA	1251	1251	85%	0.0	99%
NM_001128831.1	Homo sapiens carbonic anhydrase I (CA1), transcript variant 4, mRNA	1230	1230	83%	0.0	100%
NM_001128829.1	Homo sapiens carbonic anhydrase I (CA1), transcript variant 1, mRNA	1230	1352	91%	0.0	100%
NM_001738.2	Homo sapiens carbonic anhydrase I (CA1), transcript variant 2, mRNA	1230	1342	91%	0.0	100%

Table 5.4. Partial blastx search results with CA IV DNA sequence results.

Accession	Description	Max score	Total score	Query coverage	E value	Max ident
NM_000717.3	Homo sapiens carbonic anhydrase IV (CA4), mRNA	1395	1395	94%	0.0	99%
BC074768.2	Homo sapiens carbonic anhydrase IV, mRNA (cDNA clone MGC:103808 IMAGE:30915189), complete cds	1395	1395	94%	0.0	99%
BC057792.1	Homo sapiens carbonic anhydrase IV, mRNA (cDNA clone MGC:71638 IMAGE:30331755), complete cds	1395	1395	94%	0.0	99%
CR541766.1	Homo sapiens full open reading frame cDNA clone RZPDo834A0430D for gene CA4, carbonic anhydrase IV; complete cds, incl. stop codon	1395	1395	94%	0.0	99%
AY893416.1	Synthetic construct Homo sapiens clone FLH131004.01X carbonic anhydrase IV (CA4) mRNA, complete cds	1395	1395	94%	0.0	99%

Table 5.5. The translated peptide sequence for the subcloned carbonic anhydrase I and IV genes in the pET 28c-CA I and pET 28c-CA IV plasmids.^a

CA I: 5'3' Frame 1	MASPDWGYDDKNGPEQWSKLYPIA NGNNQSPVDIKTSETKHDTSLKPISV SYNPATAKEIINVGHSHFVNFDND NRSVLKGGPFSDSYRLFQFHFHWGS TNEHGSEHTVDGVKYSaelHVAHW NSAKYSSLAEAAASKADGLAVIGVLM KVGEANPKLQKVLDALQAIKTKGKR APFTNFDpstLLPSSLDfWtYPGSLT HPPLYESVTWIICKESISVSSEQLAQF RSLLSNVEGDNAVPMQHNNRPTQPL KGRTVRASF Stop
CA IV: 5'3' Frame 1 ^b	AESHWCYEVQAESSNYPCLVPVKW GGNCQKDRQSPINIVTTKAKVDKKL GRFFFSGYDKKQTWTVQNNGHSVM MLLENKASISGGGLPAPYQAKQLHL HWSDLPYKGSEHSLDGEHFAMEMHI VHEKEKGTsrNVKEAQDPEDeIAVL AFLVEAGTQVNEGfQPLVEALSNIP KPEMSTTMAESSLLDLLPKEEKL RH YFRYLGSLLTPTCDEKVVWTVFREPI QLHREQILAFS QKLYYDKEQT VSMK DNVRPLQQLGQRTVIKS Stop

^a. The DNA sequences were translated using the ExPASy proteomics server (<http://www.expasy.ch/tools/>).

^b. The 18 amino acid signal sequence and the 27 amino acid sequence for attachment of the GPI anchor have been removed.

Table 5.6. Comparison of the translated CA I pET28c-CA I plasmid DNA sequence to the wild-type protein sequence. ^a		
ref	NP_001729.1	carbonic anhydrase I [Homo sapiens]
ref	NP_001122301.1	carbonic anhydrase I [Homo sapiens]
ref	NP_001122302.1	carbonic anhydrase I [Homo sapiens]
Length=309		
GENE ID: 759 CA1 carbonic anhydrase I [Homo sapiens]		
Score = 540 bits (1390), Expect = 2e-158		
Identities = 261/261 (100%), Positives = 261/261 (100%), Gaps = 0/261 (0%)		
Frame = +3		
Query	51	MASPDWGYDDKNGPEQWSKLYPIANGNNQSPVDIKTSETKHDTSLKPIISVSNPATAKEI 230
		MASPDWGYDDKNGPEQWSKLYPIANGNNQSPVDIKTSETKHDTSLKPIISVSNPATAKEI
Sbjct	49	MASPDWGYDDKNGPEQWSKLYPIANGNNQSPVDIKTSETKHDTSLKPIISVSNPATAKEI 108
Query	231	INVGHSHVNFEDNDNRSVLKGGPFSDSYRLFQFHFWGSTNEHGSEHTVDGVKYSSELH 410
		INVGHSHVNFEDNDNRSVLKGGPFSDSYRLFQFHFWGSTNEHGSEHTVDGVKYSSELH
Sbjct	109	INVGHSHVNFEDNDNRSVLKGGPFSDSYRLFQFHFWGSTNEHGSEHTVDGVKYSSELH 168
Query	411	VAHWNSAKYSSSLAEAAASKADGLAVIGVLMKVGEANPKLQKVLDAQAIAIKTKGRAPFTNF 590
		VAHWNSAKYSSSLAEAAASKADGLAVIGVLMKVGEANPKLQKVLDAQAIAIKTKGRAPFTNF
Sbjct	169	VAHWNSAKYSSSLAEAAASKADGLAVIGVLMKVGEANPKLQKVLDAQAIAIKTKGRAPFTNF 228
Query	591	DPSTLLPSSLDFTWYPGSLTHPPLYESVTWII CKESISVSSEQLAQFRSLLSNVEGDNAV 770
		DPSTLLPSSLDFTWYPGSLTHPPLYESVTWII CKESISVSSEQLAQFRSLLSNVEGDNAV
Sbjct	229	DPSTLLPSSLDFTWYPGSLTHPPLYESVTWII CKESISVSSEQLAQFRSLLSNVEGDNAV 288
Query	771	PMQHNNRPTQPLKGRTVRAS 833
		PMQHNNRPTQPLKGRTVRAS
Sbjct	289	PMQHNNRPTQPLKGRTVRAS 309
^a NCBI blastx search sequence alignment: http://blast.ncbi.nlm.nih.gov/Blast.cgi .		

Table 5.7. Comparison of pEt 28c-CA IV plasmid DNA sequence to the wild-type CA IV sequence. ^a			
ref AAH57792.1	Carbonic anhydrase IV [Homo sapiens]		
ref CH471109.2	Carbonic anhydrase IV isoform CRA_b [Homo sapiens]		
Length=312			
GENE ID: 762 CA IV			
Score = 547 bits (1410), Expect = 1e-160			
Identities = 266/266 (100%), Positives = 266/266 (100%), Gaps = 0/266 (0%)			
Frame = +1			
Query	7	AESHWCYEVQAESSNYPCLVPVKWGGNCQKDRQSPINIVTTAKAVDKKLGRFFSGYDKK	186
		AESHWCYEVQAESSNYPCLVPVKWGGNCQKDRQSPINIVTTAKAVDKKLGRFFSGYDKK	
Sbjct	19	AESHWCYEVQAESSNYPCLVPVKWGGNCQKDRQSPINIVTTAKAVDKKLGRFFSGYDKK	78
Query	187	QWTWVNNGHVSVMMLLENKASISGGGLPAPYQAKQLHLHWSDLPYKGSEHSLDGEHFAME	366
		QWTWVNNGHVSVMMLLENKASISGGGLPAPYQAKQLHLHWSDLPYKGSEHSLDGEHFAME	
Sbjct	79	QWTWVNNGHVSVMMLLENKASISGGGLPAPYQAKQLHLHWSDLPYKGSEHSLDGEHFAME	138
Query	367	MHIVHEKEKGTSRNVKEAQDPEDEIAVLAFVLVEAGTQVNEGFPQPLVEALSNIPKPEMSTT	546
		MHIVHEKEKGTSRNVKEAQDPEDEIAVLAFVLVEAGTQVNEGFPQPLVEALSNIPKPEMSTT	
Sbjct	139	MHIVHEKEKGTSRNVKEAQDPEDEIAVLAFVLVEAGTQVNEGFPQPLVEALSNIPKPEMSTT	198
Query	547	MAESSLLDLLPKEEKLRHYFRYLGSLTTPTCDEKVVVWTVVFREPIQLHREQILAFSQKLYY	726
		MAESSLLDLLPKEEKLRHYFRYLGSLTTPTCDEKVVVWTVVFREPIQLHREQILAFSQKLYY	
Sbjct	199	MAESSLLDLLPKEEKLRHYFRYLGSLTTPTCDEKVVVWTVVFREPIQLHREQILAFSQKLYY	258
Query	727	DKEQTVSMKDNVRPLQQLGQRTVIKS	804
		DKEQTVSMKDNVRPLQQLGQRTVIKS	
Sbjct	259	DKEQTVSMKDNVRPLQQLGQRTVIKS	284

^a NCBI blastx search sequence alignment: <http://blast.ncbi.nlm.nih.gov/Blast.cgi>.

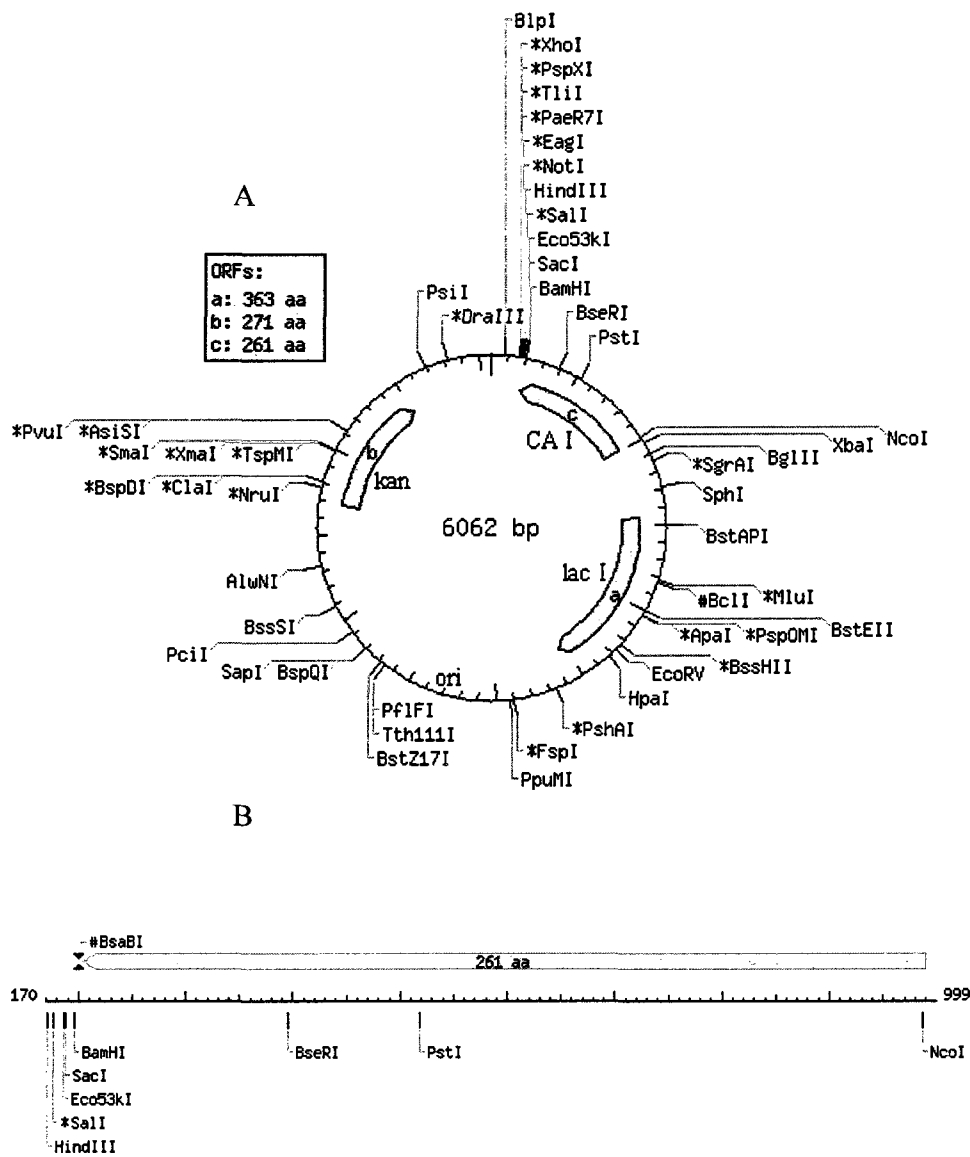


Figure 5.2. A. Plasmid map of pET28c-CA I, showing the CA I gene, the kanamycin resistance gene, and the lac I gene. Some of the restriction enzyme cut sites found within the plasmid are shown as well. B. This is the linear cut away of the CA I gene and the two (HindIII and NcoI) restriction enzyme sites that were introduced via PCR primers to facilitate directional cloning into the pET28c vector. Figure produced using NEBcutter V2.0 at <http://tools.neb.com/NEBcutter2/>.

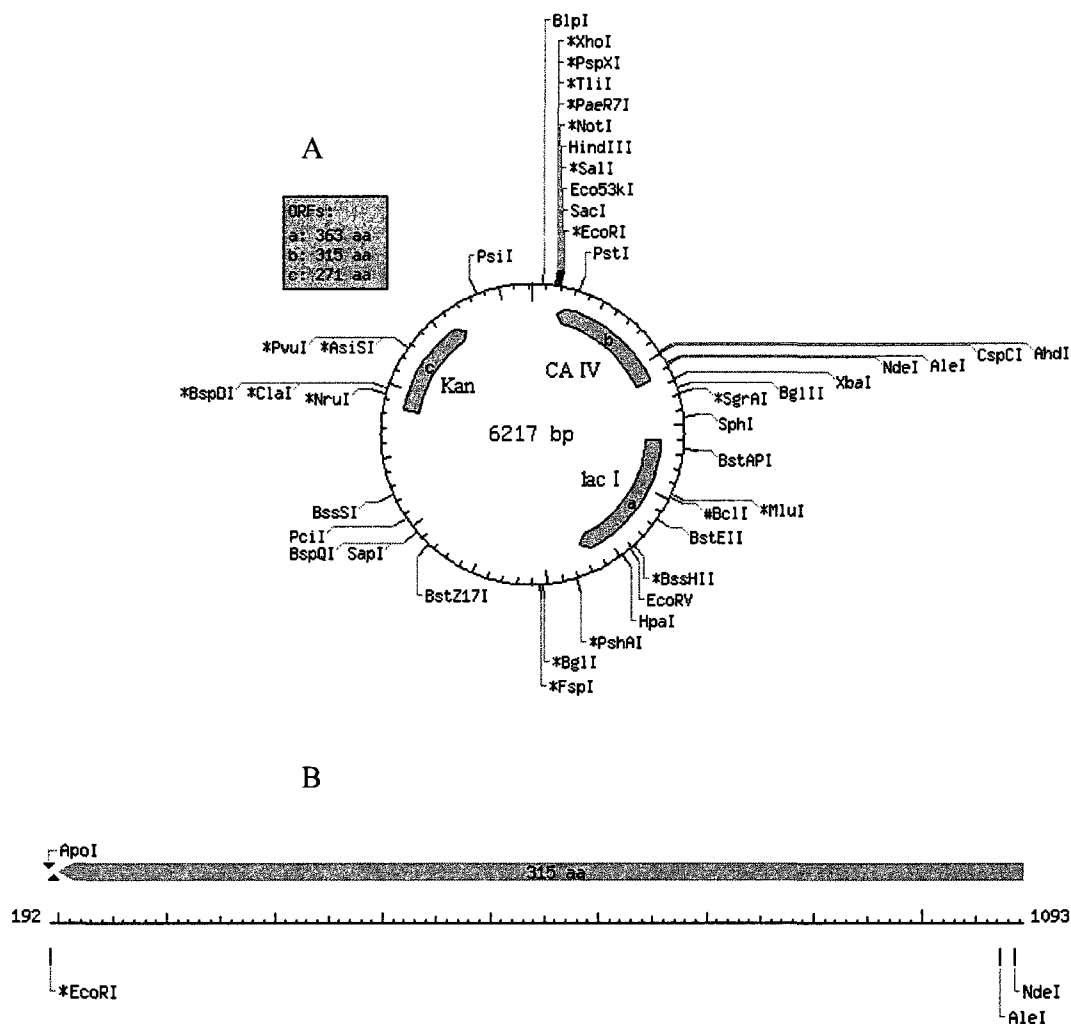


Figure 5.3. A. Plasmid map of pET28c-CA IV, showing the CA IV gene, the kanamycin resistance gene, and the lac I gene. Some of the restriction enzyme cut sites found within the plasmid are shown as well. B. This is the linear cut away of the CA IV gene and the two (EcoRI and NdeI) restriction enzyme sites that were introduced via PCR primers to facilitate directional cloning into the pET28c vector. Figure produced using NEBcutter V2.0 at <http://tools.neb.com/NEBcutter2/>.

The next step in this research project was to evaluate the level of CA isozyme protein expression in *E. coli*. Each pET28c-CA I and pET28c-CA IV plasmid was transformed into the BL21-AI One Shot® chemically competent expression strain of *E. coli* (Invitrogen). An aliquot of 50 µl of the BL21-AI *E. coli* cells were first pipetted into a 1.5 ml Eppendorf tube and then 5 µl of plasmid (pET28c-CA I or pET28c-CA IV) was added. The cells and plasmid were then allowed to incubate on ice for 30 min before being subjected to heat shock at 42 °C for 30 sec in a heat block. Immediately after the heat shock procedure, 250 µl of room temperature SOC media was added to the Eppendorf tube and the tube was placed in a 37 °C incubator with shaking for 1 hr. Volumes of 50 µl and 100 µl of the transformed *E. coli* cells were then plated onto LB plates containing 50 µg/ml kanamycin. Different volumes of transformed cell media were plated to insure that single colonies could be obtained on the plates after overnight growth. The next day, four colonies were picked from each plate (pET28c-CA I and pET28c-CA IV) with sterile toothpicks and placed into separate 15 ml culture tubes containing LB media with 50 µg/ml kanamycin and zinc sulfate (500 µM final concentration). The zinc was added to the media to condition the *E. coli* cells to grow in the presence of extra zinc. Zinc is required as a cofactor to obtain active forms of the CA I and CA IV zinc metalloenzymes during protein expression. The cultures were grown overnight with shaking at 37 °C. The following day, 100 µl of *E. coli* cells was transferred to fresh culture tubes containing 5 ml of the same LB-kanamycin media used previously. The freshly inoculated cultures were grown with shaking at 37 °C until an O.D.₅₅₀ reading of 0.5-0.8 was obtained. Then, a

1 ml pre-induction sample was collected from each tube and 0.8 M IPTG was added to each tube to give a final concentration of 0.8 mM IPTG to induce protein expression. The bacterial cultures were then grown at 37 °C with shaking for four additional hrs to allow protein expression, followed by collection of a 1 ml post-induction sample. All of the pre-induction and post-induction samples were centrifuged at 4 °C at ~14,000 x g in a Marathon Micro A table top centrifuge for 30 sec. Afterwards, the supernatant was removed and the cell pellets were stored at -20 °C until analysis by SDS-PAGE was performed. The samples for the protein gel were prepared by adding 200 µl of 2X SDS loading dye to each sample, vortexing to resuspend the pellets and then heated using a bench top heat block for 20 min at 90 °C. Afterwards, the samples were allowed to cool to room temperature before loading. The samples were loaded onto a 15% acrylamide gel and run for 90 min at an initial setting of 180 volts and 30 milliamps. The results of the gel are shown in Figure 5.4. The predicted size of the expressed CA I and CA IV proteins is approximately 30 kDa, consistent with the observed molecular mass for the expressed proteins.

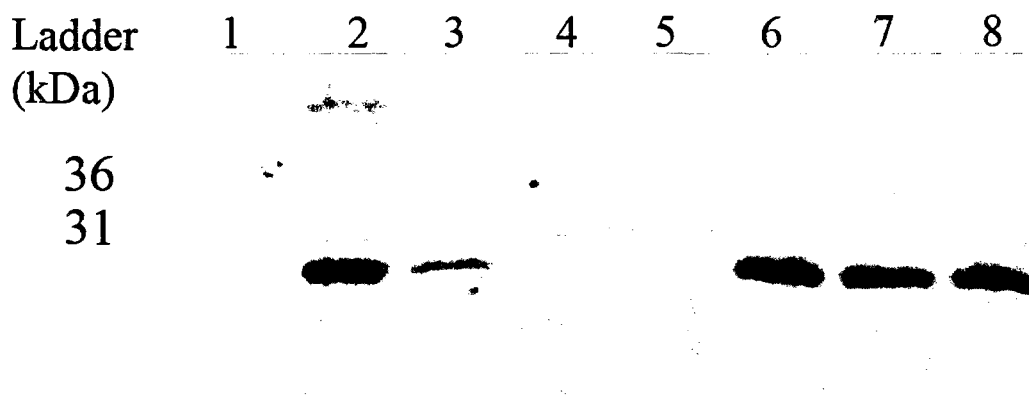


Figure 5.4. SDS-PAGE analysis of CA I and CA IV protein expression using the BL21-AI strain of *E. coli*. Lane 1 is a preinduction sample of *E. coli* pET28c-CA I whole cell lysate. Lanes 2, 3 and 4 are postinduction CA I whole cell lysate. Lane 5 is a preinduction sample of *E. coli* pET28c-CA IV whole cell lysate. Lanes 6, 7, and 8 are postinduction CA IV whole cell lysate.

Following successful subcloning and bacterial expression of both CA I and CA IV enzymes, the next step was to develop purification methods for each CA isozyme. The CA IV plasmid was again transformed into BL21-AI *E. coli*, using the previously described culture and induction procedures. Following plating and overnight growth, two colonies were picked using sterile toothpicks and used to inoculate two separate sterile 150 ml flasks that contained 50 ml of LB-kanamycin 0.5 mM ZnSO₄ media, and cultured overnight at 37 °C with shaking at 225 rpm. The next morning, 1 ml of the overnight growth from each flask was transferred to sterile 150 ml flasks containing 50 ml of LB-kanamycin media with 0.5 mM ZnSO₄ and cultured to an O.D.₅₅₀ of 0.5 - 0.8. After a suitable O.D.₅₅₀ was achieved, 50 µl of 0.8

M IPTG was added to each flask (0.8 mM final concentration), followed by an additional 4 hours of growth with shaking at 225 rpm to induce expression of the CA IV protein. After 4 hours, the cells were transferred to four 50 ml conical tubes (25 ml per tube), pelleted by centrifugation for 30 min at 3500 rpm, the supernatant was carefully poured off, and the pellets were stored at -80°C .

The tubes containing the frozen *E. coli* cells CA IV pellets were allowed to sit at room temperature until the pellets were thawed (about 10 min), and then the pellets were resuspended in 20 ml of 20 mM MOPS (pH 7.5) buffer by carefully pipetting up and down until all cells were resuspended. The resuspended cell solution was transferred to a 50 ml beaker which was placed on ice and the cells were sonicated for 5 min with a 10 sec on pulse followed by 10 sec off. After sonication, Dnase I (1 mg/ml) was added to the beaker and the sonicated cell lysate was gently stirred with a magnetic stir bar on ice for 30 min. After 30 min the solution was transferred to a round bottom 40 ml white polypropylene Oak Ridge centrifuge tube (20 ml) and a second tube was filled with 20 ml of water for balancing. These tubes were then centrifuged at 8000 RPM in a Sorvall RC 5B Plus centrifuge using a Sorvall SS-34 rotor for 20 min. An initial small-scale purification of the bacterially expressed CA IV proteins was attempted with a 1 ml SP Sepharose FF anion exchange column on an ÄKTA™ FPLC instrument (GE Healthcare, formerly Amersham Biosciences).

The ExPASy proteomics site program ProtParam

(<http://www.expasy.ch/tools/protparam.html>) was used to calculate the theoretical isoelectric point (pI) of CA IV from the modified amino acid sequence (Swiss-Prot

accession number - P22748), which does not include the signal sequence or the GPI anchor sequence. The calculated pI for CA IV was 6.40 and the calculated pI for CA II was 6.87. The similar isoelectric points for the two CA isozymes suggested that the SP Sepharose FF ion exchange chromatography column previously used to purify CA II might also be used to purify CA IV in the same manner. In a paper by Baird, et al. by the Fierke group, the same truncated form of CA IV was expressed in both Chinese hamster ovary (CHO) cells and in *E. coli* and they used the affinity purification resin benzenesulfonamide to purify CA IV following a method published in a paper by Waheed, et al²⁻⁴.

The clarified cell lysate supernatant from the previous centrifugation step was carefully removed using a sterile 25 ml syringe and needle. This step was performed to collect as much of the 20 ml clarified cell lysate without disturbing the pellet and avoid having to go back for a second collection attempt. Afterwards, the needle was removed and the syringe was used to load the column via a 50 ml Superloop sample loading accessory (Amersham Biosciences). The FPLC UNICORNTM software settings were configured for the correct column upper pressure limit for the 1 ml SP Sepharose FF column. The 20 ml sample of soluble protein was loaded onto the column using a 1 ml/min flow rate, and washed with 2 CV of 20 mM MOPS, pH 7.5 buffer (buffer A). The bound CA protein was then eluted with a linear gradient of 20 mM MOPS (pH 7.5) 1 M NaCl buffer (buffer B) from 0% to 100%, applied over 10 CV. The wash fractions were collected in sterile plastic disposable 50 ml conical tubes (45 ml/tube) and the elution fractions were collected in sterile plastic 15 ml

disposable conical tubes (10 ml/tube). The eluting proteins were detected via absorbance at 280 nm (A_{280}). A plot of the eluting sample A_{280} absorbance data, fraction tubes and other parameters for the chromatography run are shown in Figure 5.5. Samples from the wash collection tube X1 and the sample elution collection tubes A1 and A2 were prepared for SDS-PAGE analysis using the same methods as those used to prepare the CA I and CA IV protein induction samples described earlier in this chapter. The samples were loaded on a 15% acrylamide gel and run for 90 min at 180 volts and 30 milliamps. The gel was then stained using Coomassie Brilliant Blue dye. No CA IV protein was observed in either A1 or A2 fractionation collection samples corresponding to the small elution peak.

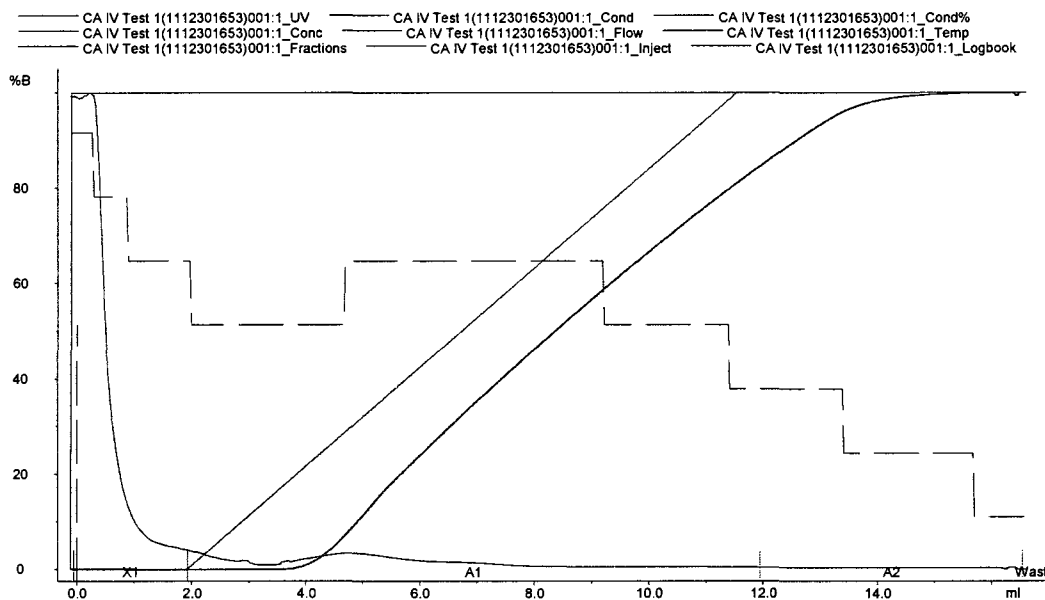


Figure 5.5. Plot of the initial FPLC purification run of CA IV protein using the ÄKTA™ FPLC instrument with the FPLC UNICORN™ software. The small hill-shaped peak that may have been CA IV is seen starting at the 4 ml mark and ending around 6 ml mark. The linear concentration gradient of buffer B (20 mM MOPS (pH 7.5) 1 M NaCl buffer) used to elute any bound proteins is indicated by the line increasing linearly starting at the 2 ml mark.

The same procedures described above for the expression of CA IV were used for the bacterial expression of CA I, using the pET28c-CA I plasmid. The theoretical isoelectric point of CA I is 6.59, which was determined using the ExPASy proteomics site program ProtParam (<http://www.expasy.ch/tools/protparam.html>) and the amino acid sequence for CA I (Swiss-Prot accession number – P00915). This isoelectric point was also similar to the theoretical CA II isoelectric point of 6.87. Therefore, the same chromatography purification method using a 50 ml SP Sepharose FF cation exchange column was investigated for protein purification of CA I. The results of the

initial purification run are shown in Figure 5.6. Samples from the sample elution collection tubes B5 and C4 were prepared for SDS-PAGE analysis using the same methods as those used to prepare the CA I and CA IV protein induction samples described earlier in this chapter. The samples were loaded on a 15% acrylamide gel and run for 90 min at 180 volts and 30 milliamps. The gel was then stained using Coomassie Brilliant Blue dye to identify the purified CA I fractions.

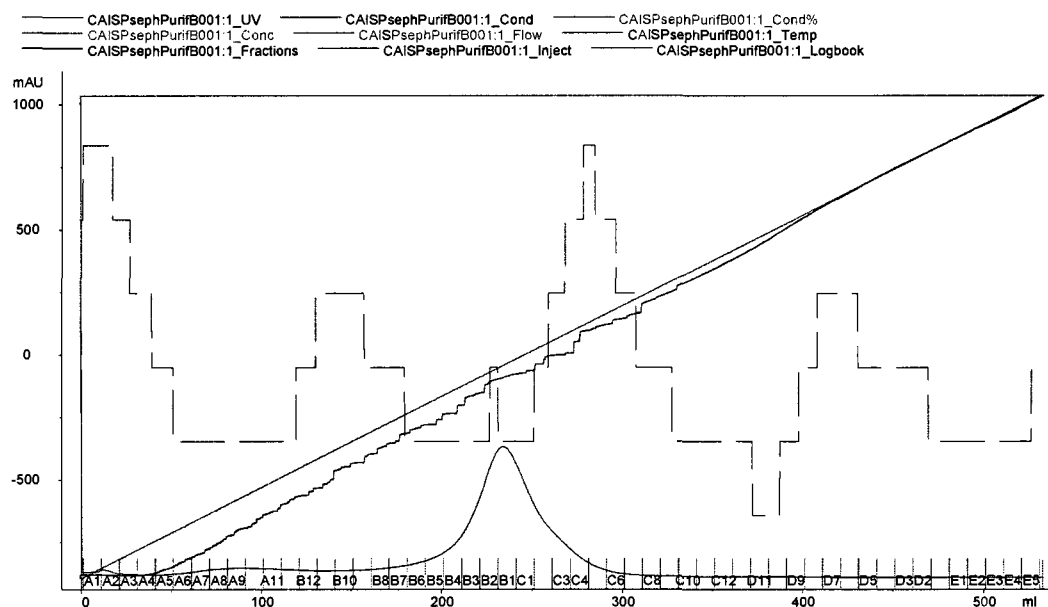


Figure 5.6. Plot of the FPLC purification run of CA I protein using the ÄKTA™ FPLC instrument with the FPLC UNICORN™ software and a 50 ml SP Sepharose FF column. The small hill shaped peak that was CA I is seen starting around the 200 ml mark and ending near the 300 ml mark. The increasing concentration of buffer B (20 mM MOPS (pH 7.5) 1 M NaCl buffer) is the line increasing linearly starting near the 0 ml mark.

Expression and Purification of γ -class Carbonic Anhydrase (Cam)

The pCAM-AC plasmid is modified version of the pBA1416NB plasmid that contains two unique BanII and BsrGI restriction sites, and is derived from plasmid pT7-7⁵. This plasmid also contains a 34-amino acid deletion from the N-terminal sequence, which has properties characteristic of a secretory signal peptide leader sequence⁵. The process of transforming BL 21 Star *E. coli* strain with Cam was the same as described earlier in this chapter for CA I and CA IV, except the antibiotic ampicillin (100 μ g/ml final concentration) was used. Following plating and overnight growth, two colonies were picked using sterile toothpicks and placed into separate sterile 250 ml flasks that contained 150 ml of LB-ampicillin 0.5 mM ZnSO₄ media for overnight growth at 37 °C with shaking at 225 rpm. The next morning, 30 ml of the overnight growth culture from each flask was transferred to four sterile 2 L flasks containing 1 L of LB- ampicillin media with 0.5 mM ZnSO₄ and cultured to an O.D.₅₅₀ of 0.5 - 0.8. After the correct O.D.₅₅₀ was achieved, 1 ml of 0.8 M IPTG was added to each flask (0.8 mM final concentration), followed by an additional 3.5 hours of growth with shaking at 225 rpm to induce the Cam protein. After 3.5 hours, the cells were transferred to four 1 L flasks, balanced by weight and spun down for 30 min at 5000 rpm, and then the liquid was carefully poured off and the pellets were stored at – 80 °C.

The flasks containing the frozen *E. coli* cell pellets were thawed at room temperature (ca. 10 min), and then the pellets were resuspended in 40 ml of 20 mM

MOPS (pH 7.5) buffer per flask by carefully pipetting up and down until all cells were resuspended. The resuspended cell solution from each flask was transferred to a 200 ml beaker which was placed inside a bucket of ice and the cells were sonicated for 5 min with a 10 sec on pulse followed by 10 sec off. After sonication, 500 μ l of Dnase I (1 mg/ml) was added to the beaker and the sonicated cell lysate was gently stirred with a magnetic stir bar on ice for 30 min. After 30 min the solution was transferred to round bottom 40 ml white polypropylene Oak Ridge centrifuge tube (40 ml) and again balanced by weight. These tubes were then centrifuged at 3000 g in a Sorvall RC 5B Plus centrifuge using a Sorvall SS 34 rotor for 20 min. After 20 min the liquid was carefully poured from the Oak Ridge tubes into a clean plastic 250 graduated cylinder for loading onto the Q-Sepharose anion exchange column on an ÄKTA™ FPLC instrument (GE Healthcare, formerly Amersham Biosciences) for the first step of purification. The Q-Sepharose column is a cationic (+) quaternary amine resin that binds and exchanges anions (Cl^- , SO_4^{2-} , etc).

The FPLC UNICORN™ software settings were configured for the correct column upper pressure limit for the 50 ml 2.6 cm diameter Q-Sepharose FF column. The 160 ml sample of soluble protein was loaded onto the column using a 5 ml/min flow rate, and washed with 2 CV of 20 mM MOPS, pH 7.5 buffer (buffer A). The bound CA protein was then eluted with an increasing linear gradient of 20 mM MOPS (pH 7.5) 1 M NaCl buffer (buffer B) from 0% to 100%, applied over 10 CV. The wash fractions were collected in sterile plastic disposable 50 ml conical tubes (45 ml/tube) and the elution fractions were collected in sterile plastic 15 ml disposable

conical tubes (10 ml/tube). After this step, samples were taken from each tube corresponding to an elution peak (Figure 5.7) to be analyzed by SDS-PAGE gel electrophoresis to check for the presence of Cam. Afterwards the tubes that contained Cam were mixed with an equal amount of 3 M $(\text{NH}_4)_2\text{SO}_4$ for a final salt concentration of 1.5 M in a clean plastic 250 graduated cylinder and loaded onto a 50 ml 2.6 cm diameter Phenyl Sepharose hydrophobic interaction chromatography column using a 5 ml/min flow rate. The bound CA protein was then eluted with a decreasing ionic strength linear gradient from 0% buffer B (20 mM MOPS (pH 7.5) 1.5 M $(\text{NH}_4)_2\text{SO}_4$, buffer) to 100% buffer B (20 mM MOPS (pH 7.5) buffer, 0.0 M $(\text{NH}_4)_2\text{SO}_4$), applied over 10 CV. The wash fractions were collected in sterile plastic disposable 50 ml conical tubes (45 ml/tube) and the elution fractions were collected in sterile plastic 15 ml disposable conical tubes (10 ml/tube). Samples were collected from the elution tubes corresponding to the absorbance peak (Figure 5.8) for analysis by SDS-PAGE gel electrophoresis. Afterwards, the purified Cam was aliquoted into 1.5 ml Eppendorf tubes (1 ml/tube) and flash frozen in liquid nitrogen and stored at -80°C .

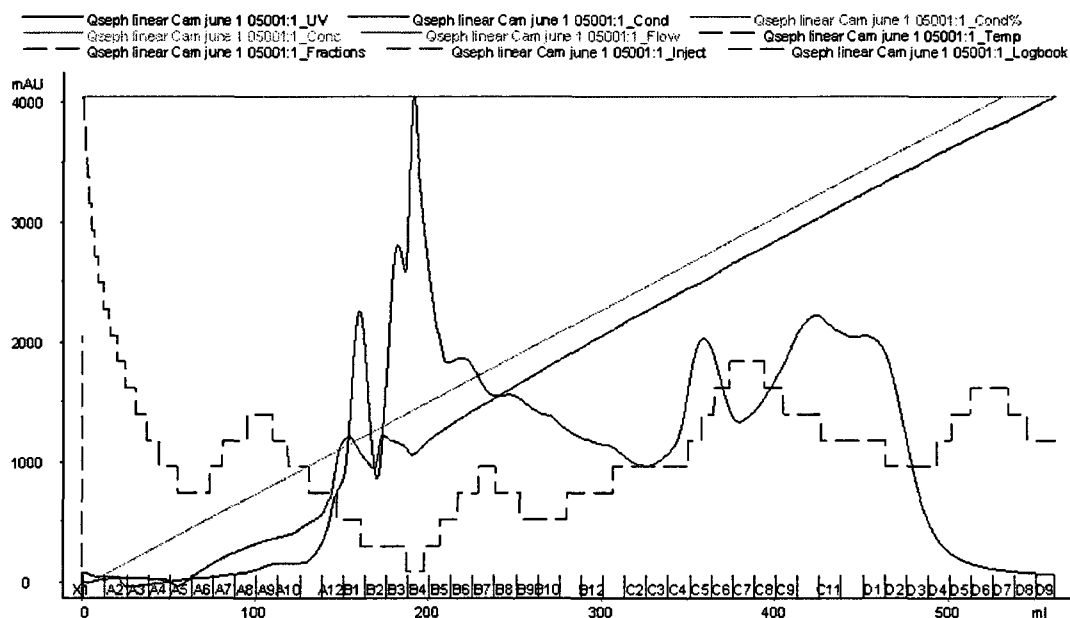


Figure 5.7. Plot of the first step of the FPLC purification of Cam protein using the ÄKTA™ FPLC instrument with the FPLC UNICORN™ software. This first step involved the use of a Q-sepharose anion exchange column to purify Cam (isoelectric point of 4.18) and other negatively charged proteins from clarified *E. coli* crude cell lysate. Cam was found in the fractions from B3 to B5.

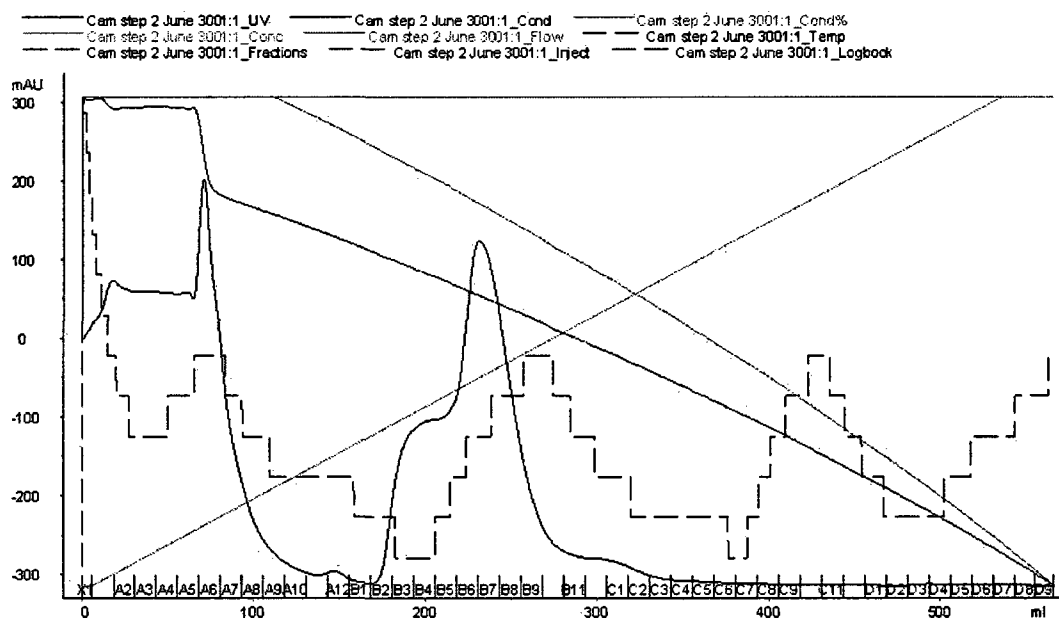


Figure 5.8. Plot of the second step of the FPLC purification of Cam protein via hydrophobic interaction chromatography. This step involved the use of a phenyl sepharose column to purify Cam from the other proteins collected during the previous Q-sepharose anion exchange chromatography step. Cam eluted in the fractions from B5 to B9.

Sodium Bicarbonate pH Assay

Ideally, a colorimetric assay could be used with all CA isozymes for screening compounds for potential inhibitors and any subsequent kinetic assays. The non-physiological substrate, 4-NPA, was nearly ideal for screening of CA II, despite a high background rate of hydrolysis. However, some alpha-class CA isozymes, e.g. CA III, have very low rates or no detectable hydrolysis of 4-NPA^{4,6-8}. To overcome this potential assay problem, a different type of colorimetric pH assay was investigated using sodium bicarbonate as the enzyme substrate and phenol red as a

colorimetric pH indicator. The solution pH should increase as the bicarbonate is converted to CO₂ until equilibrium is reached. This method appeared to be more advantageous over the reverse CO₂ hydration assay, because it only required weighing out of a bicarbonate salt for substrate, *versus* bubbling CO₂ gas through water to obtain a saturated solution of this compound as a substrate.

The experimental design of this HTS-microplate format sodium bicarbonate assay was based to some extent on the previously described CA II esterase assay from Chapter Two of this thesis. The final volume of the assay was 111 µl and the initial assay conditions consisted of 1 µM purified CA II enzyme in 50 mM, pH 7.0 MOPS, 33 mM Na₂SO₄, 1.0 mM EDTA buffer. The buffer was dispensed into flat-bottom polystyrene 96-well plates (Costar 3370) with a Matrix Impact² P1250 electronic programmable 8-channel pipettor (Matrix Technologies Corp., Hudson, NH). A stock solution of 10 mM phenol red dye (pH indicator range 6.4-8.0) was made by weighing out 35.4 mg of phenol red and carefully transferring it into a 15 ml plastic disposable conical tube. Then, 10 ml of MOPS pH 7.0 buffer was added, the lid was sealed, and the contents were dissolved and mixed by hand shaking. To arrive at the final assay concentration of 100 µM, 1.11 µl of the stock solution was added to the buffer solution from above before dispensing into 96-well plates. When performing the test screening it was noticed that consistent results could not always be achieved with the control inhibitor, acetazolamide, and that a 2X difference in the inhibited and uninhibited kinetic rate data, i.e., signal to background ratio, could not be consistently obtained with the MultiDrop 8-channel peristaltic pump dispensing method. This 2X

difference is a minimum standard for defining a useful drug-screening assay. Several attempts were made to correct this problem, including adjusting the concentration of the bicarbonate substrate between 10 mM and 100 mM to find the best concentration for the substrate, as well as varying the enzyme concentration from 1 μ M to 2 μ M. A sample of the results using this assay is given in Figures 5.9 and 5.10.

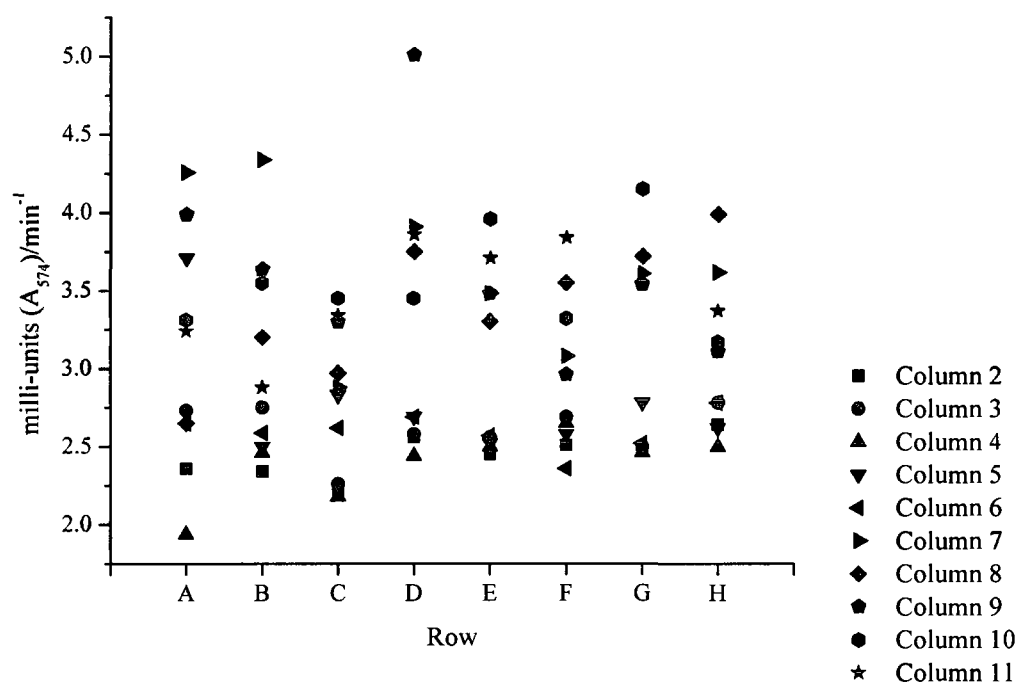


Figure 5.9. Bicarbonate dehydration kinetic absorbance assay results for CA II - 10 mM NaHCO₃ pH assay. Columns 2-6 had a final concentration of 100 μ M acetazolamide CA inhibitor added and columns 7-11 had no acetazolamide added. The absorbance was detected at a wavelength of 574 nm with a SpectraMax Plus384 microplate spectrophotometer running SoftMax Pro software. The assay was run for 5 min; with absorbance readings collected every 15 sec.

As shown in Figure 5.9, columns two through six, which contained acetazolamide, had only a slight difference in the measured rate of pH increase from columns seven thru eleven, which contained CA II with no inhibitor. The average value for columns two through six (CA II was inhibited) was 2.56 ± 0.26 milliAbs₅₇₄ min⁻¹ and for columns seven thru eleven (uninhibited CA II), the average value was 3.54 ± 0.46 milliAbs₅₇₄ min⁻¹. These results do not show a statistically significant 2X difference between inhibited and uninhibited rates of enzyme catalysis in this assay. Figure 5.10 shows the results for a 60 mM concentration of the substrate, for which a difference between from the inhibited and uninhibited enzyme was visible to the eye. The average value for inhibited CA II was 9.98 ± 1.31 milliAbs₅₇₄ min⁻¹ and for uninhibited CA II the average value was 14.14 ± 1.52 milliAbs₅₇₄ min⁻¹.

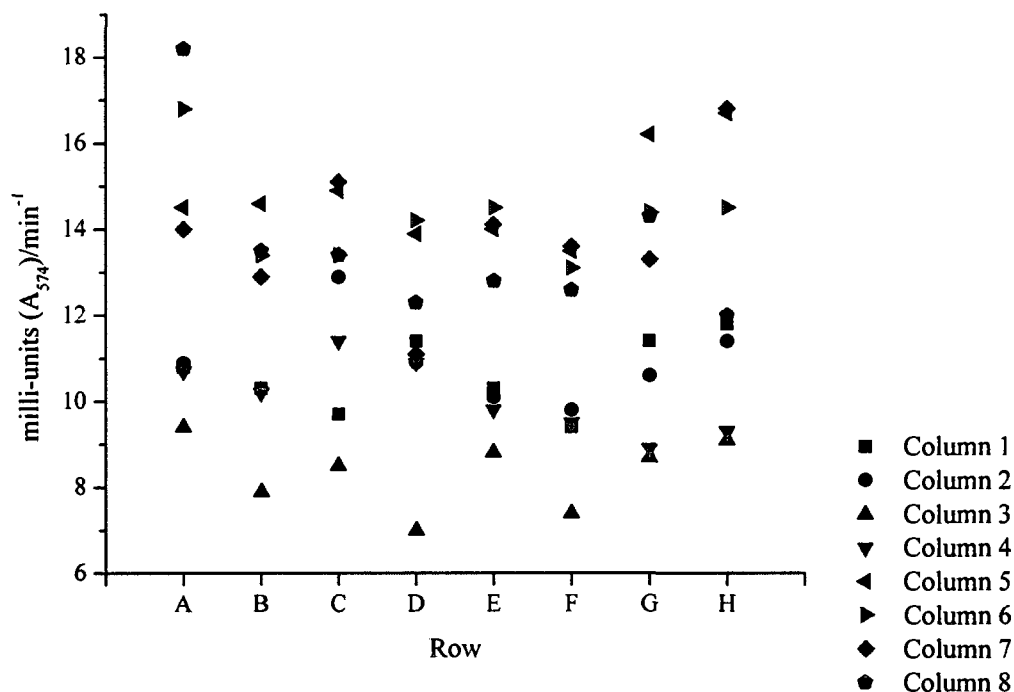


Figure 5.10. Bicarbonate dehydration kinetic assay results for CA II - 60 mM NaHCO₃ pH assay. CA II was inhibited with acetazolamide at a final concentration of 100 μ M. Absorbance was detected at a wavelength of 574 nm with a SpectraMax Plus384 microplate spectrophotometer running SoftMax Pro software for a total assay time of 5 min, with absorbance readings collected every 15 sec.

After testing a wide range of sodium bicarbonate concentrations, the minimum concentration that showed a difference between inhibited and uninhibited was found to be 50 mM. Concentrations below 50 mM did not show much difference between inhibited and uninhibited. The next test was to perform an actual screening of Cam with inhibitors to see if the same inconsistent results were seen. The

inhibitors that were chosen were based on the results of a recent paper published by Zimmerman, who tested the classic sulfonamide inhibitors of carbonic anhydrase against Cam⁹.

As shown in Figure 5.11, each inhibitor was represented in two rows and for all four inhibitors there were some large differences in the results at most concentrations. The average value for acetazolamide was 9.60 ± 4.43 milli-units(A_{560})/min⁻¹, for ethoxycarbolamide the average value was 7.28 ± 2.73 milli-units(A_{560})/min⁻¹, for sulfanilamide the average value was 7.40 ± 3.06 milli-units(A_{560})/min⁻¹, and for methazolamide the average value was 8.29 ± 2.52 milli-units(A_{560})/min⁻¹. In addition, there was no significant increase in activity as the inhibitor concentration decreased. For both of these reasons a different approach to the pH assay was pursued.

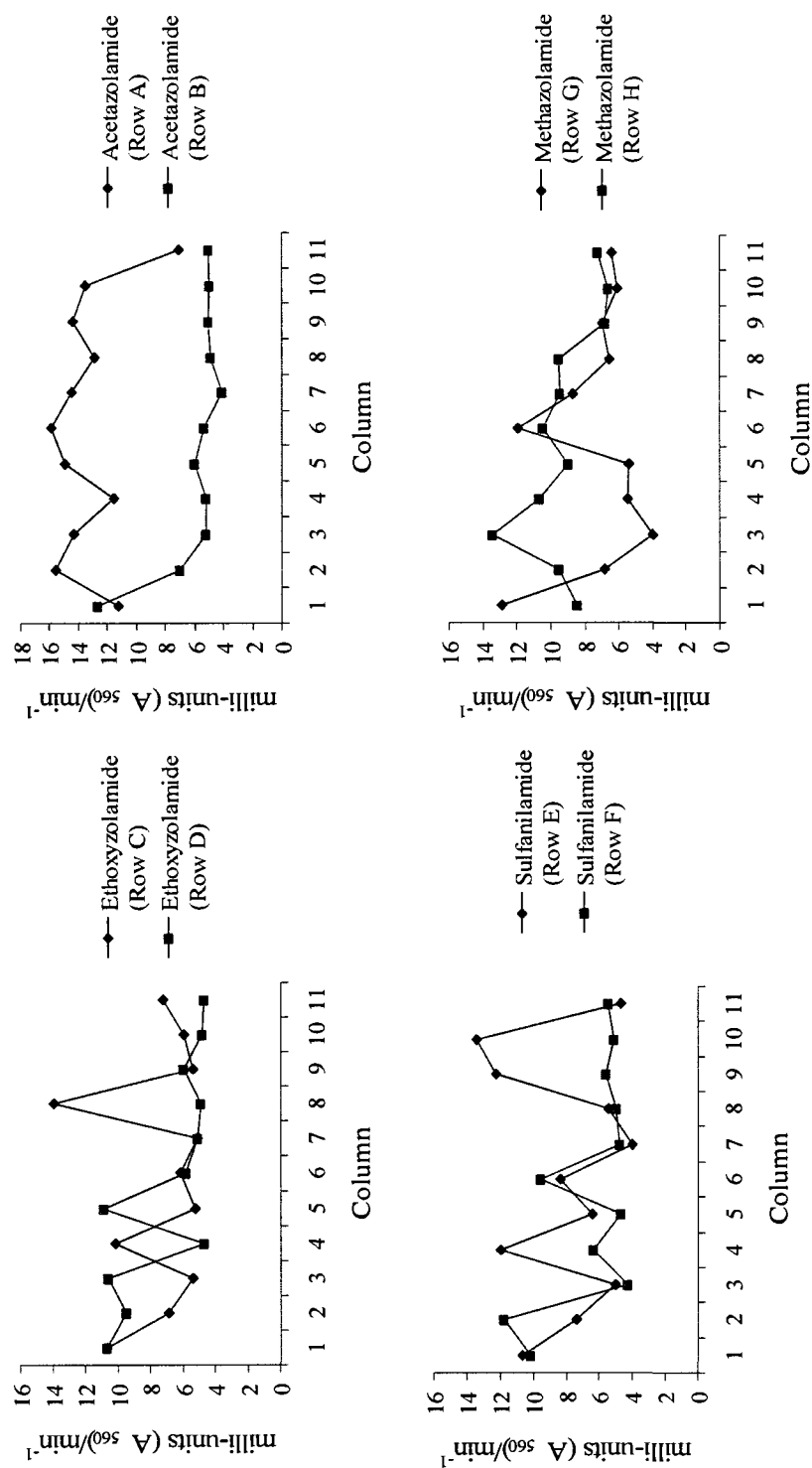


Figure 5.11. Bicarbonate dehydration kinetic assay results for Cam - 60 mM NaHCO_3 pH assay with serial dilution of Cam inhibitors. The highest concentration of each inhibitor was in column 1 (final concentration was 90 μM) and is diluted 1:2 until column 11. Absorbance was detected at a wavelength of 560 nm with a SpectraMax Plus³⁸⁴ microplate spectrophotometer running SoftMax Pro software. The assay was performed for 5 min, with absorbance readings collected every 15 sec.

A series of preliminary assay feasibility experiments were performed using the physiological substrate, dissolved CO₂, for use in screening human CA II for inhibitors, using a MultiDrop 8-channel peristaltic pump to rapidly dispense the CO₂ substrate solution into the enzyme solution in 96-well microplates.

Carbon dioxide gas was bubbled into sterile DI water for at least an hour at room temperature (~25 °C) to saturate it with CO₂. This CO₂ substrate solution was rapidly dispensed using a MultiDrop 8-channel peristaltic pump dispenser into a clear polystyrene 96-well plate containing 100 µl of CA enzyme (1 µM final concentration), para-nitrophenol (pNP) pH indicator dye at final concentration of 100 µM, and 50 mM MOPS buffer (pK_a 7.20, and pH 7.0) immediately before performing the assay. The total volume of the assay was initially 111 µl and the absorbance of each plate was read at a wavelength of 400 nm with a SpectraMax Plus³⁸⁴ microplate spectrophotometer running SoftMax Pro software and the total time of each kinetic experiment was 3 min. The wavelength of 400 nm is typically used to monitor absorbance changes in the pNP indicator, which is yellow at pH 7.0 and becomes colorless as the pH drops to pH 5.0. In between each run, fresh CO₂-saturated water was loaded into the MultiDrop 8-channel peristaltic pump tubing after the old water was removed. This was to insure that the water was fully saturated with carbon dioxide for each kinetic screening experiment. In addition, care was taken to insure that no large, i.e., visible, bubbles entered into tubing of the MultiDrop 8-channel peristaltic pump dispenser. Any bubbles that entered were removed before the substrate had been dispensed into the plate by further priming of the tubing and as the

final step in the assay preparation. Inhibitor dilution experiments were performed to evaluate the feasibility of this new pH assay, and to determine how the data compared when analyzed in the same manner as the esterase IC_{50} data was analyzed. For this experiment, the inhibitor acetazolamide was used in the usual 1:2 dilution ratio starting from a 10 mM stock concentration, which yielded a 90 μ M final concentration in a 111 μ l total assay volume. Figure 5.12 shows the microplate format CO_2 hydration pH assay graph on the top and the esterase IC_{50} graph of acetazolamide on the bottom. After the graphs, two tables (Table 5.8 and Table 5.9) give the statistical analysis of the data presented in the graphs. As shown below in Figure 5.12, the pH assay result for the IC_{50} value was approximately five times higher than the esterase assay IC_{50} value. In addition, there were more data points that had to be excluded for the pH assay than the esterase assay.

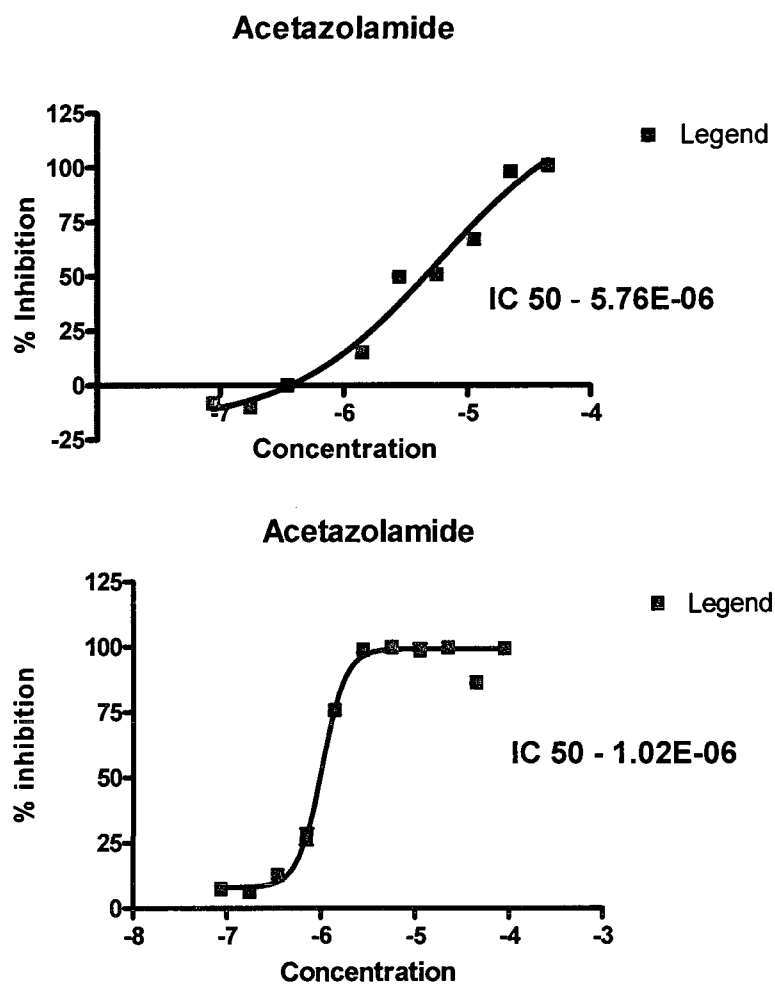


Figure 5.12. Comparison of CA II microplate format CO₂ hydration pH assay IC₅₀ vs. standard IC₅₀ esterase assay with 1:2 diluted acetazolamide. Microplate format CO₂ hydration pH assay is the top graph and standard esterase assay IC₅₀ is the bottom graph.

Table 5.8. Results of non-linear fit of standard CA II esterase assay IC ₅₀ data using Graph Pad Prism 4.0 sigmoidal dose-response model/curve fit.					
	Bottom	Top	Log_{ec50}	Hill Slope	EC₅₀
Best-fit values	7.929	99.28	-5.99	3.444	1.02E-06
Std. Error	1.248	0.9095	0.01255	0.2567	
95% Confidence Intervals	5.398 to 10.46	97.43 to 101.1	-6.015 to -5.965	2.924 to 3.965	9.6508e-007 to 1.0850e-006
Goodness of Fit	Degrees of Freedom	R²	Absolute Sum of Squares	Sy.x	
	37	0.9916	574.2	3.939	
Data	Number of X values	Number of Y replicates	Total number of values	Number of missing values	
	11	4	41	3	

Table 5.9. Results of non-linear fit for microplate format CA II CO ₂ hydration pH assay IC ₅₀ data using Graph Pad Prism 4.0 sigmoidal dose-response model/curve fit.					
	Bottom	Top	Log_{ec50}	Hill Slope	EC₅₀
Best-fit values	-17.55	130.4	-5.24	0.7297	5.76E-06
Std. Error	14.9	41.47	0.3116	0.3717	
95% Confidence Intervals	-55.84 to 20.75	23.78 to 237.0	-6.041 to -4.439	-0.2259 to 1.685	9.1028e-007 to 3.6422e-005
Goodness of Fit	Degrees of Freedom	R²	Absolute Sum of Squares	Sy.x	
	5	0.977	347.4	8.336	
Data	Number of X values	Number of Y replicates	Total number of values	Number of missing values	
	11	3	9	24	

The first modification to this assay was to increase the total reaction volume. The total sample volume in each well of the 96-well microplate was increased, first to 200 μ l, and then to 300 μ l. When the reaction volume was first increased, the results indicated that the buffer concentration should also be increased. Upon addition of the increased amount of saturated CO₂ water, the pH of each sample rapidly decreased below 5, as indicated by the pNP becoming colorless. Furthermore, the CA II did not show any activity because all wells stayed colorless, which most likely meant that the CA II was inactivated due to the low pH. To prevent the pH of the solution from becoming too low and denaturing the enzyme, the buffer concentration was also increased from 50 mM, first to 100 mM, and then to 150 mM, to determine which buffer concentrations gave the best results. In addition, another modification explored was to use different types of amino acid “Good” buffers to potentially find a better buffer for the assay. The following buffers were used: Tris (pK_a 8.1, and initial assay pH of 8.0), and the pH indicator thymol blue (pH range 8.0-9.6 and it was used at the same final concentration for PNP 100 μ M), MES (pK_a 6.10, and initial pH 6.5), and sodium acetate (pK_a 4.76, and initial pH 5.0). The goal was to identify an optimal set of assay conditions, including buffer species, ionic strength, and pH conditions that would allow good discrimination between active and inhibited CA enzyme in the CO₂ hydration assay, using the relatively slow MultiDrop 8-channel peristaltic pump to dispense the substrate at the start of each assay. Ideally, the appropriate species and concentration of buffer would resist changes in the initial pH of the solution, but still allow good discrimination between the increased change in pH due to the CA II

enzyme and the significant background rate of CO₂ hydration in water. The Tris pH 8.0 buffer appeared to be the best buffer for this assay, but by the end of the 3 min kinetic run, the difference between inhibited and uninhibited CA II was not as clear as initially seen at the start of the kinetic run. Shortening the kinetic run to 2 min improved the difference between inhibited and uninhibited but not enough to make this assay useful.

Another possible problem with the assay was a potential lack of precision in the amount of substrate dispensed by the MultiDrop 8-channel peristaltic pump. To rule this possibility out, 10 µl of fluorescein dye (10 mM stock solution), was dispensed with the MultiDrop 8-channel peristaltic pump into black 96-well microplates containing 90 µl of MOPS buffer (pH 7.0). The plates were then read in a fluorescent plate reader (BMG fluorescent plate reader) using the 470 nm filter for excitation and the 485 nm filter for emission. The results shown in Figure 5.13 and in Table 5.10 indicated that the MultiDrop 8-channel peristaltic pump exhibited good precision. For a liquid assay, the coefficient of variation (CV) should be less than ten percent and the results for the MultiDrop 8-channel peristaltic pump were well within that amount. It should also be noted that the equilibration time for the background CO₂ hydration rate in the absence of CA enzyme in this type of assay is on the order of 60-90 sec, and that this type of assay is typically performed for CAs with a sealed stopped-flow rapid injection spectrophotometer system. No stopped-flow rapid-injection system compatible with 96-well plate systems was available for this type of colorimetric assay at the time this research was performed at WMU.

Table 5.10. Statistical results of fluorescein MultiDrop 8-channel peristaltic test for three successive dispensing operations into 96-well microplates.

Column	Average	Standard deviation	Coefficient of Variation
1	63565	811	1.28%
2	62501	1128	1.80%
3	61985	527	0.85%
4	60752	1180	1.94%
5	60805	1303	2.14%
6	60759	754	1.24%
7	60651	552	0.91%
8	60756	803	1.32%
9	60581	827	1.37%
10	61040	647	1.06%
11	60428	1401	2.32%
12	61228	840	1.37%

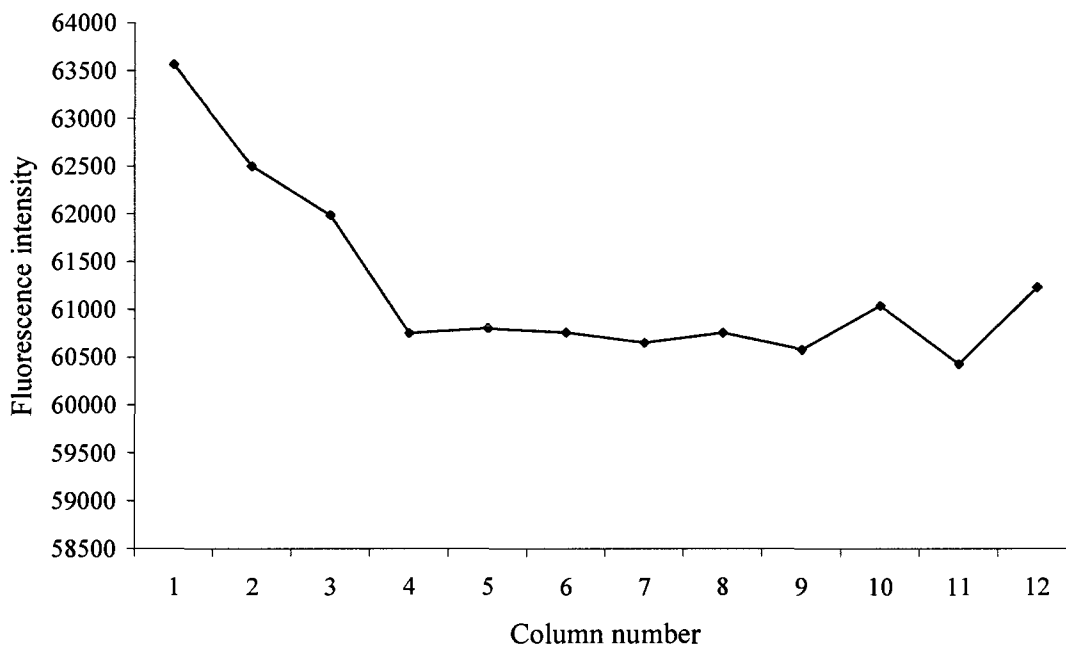
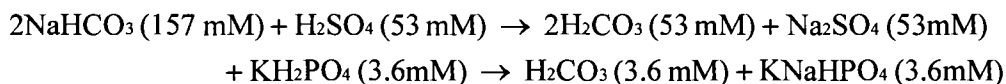


Figure 5.13. Average fluorescein fluorescence emission value for each column. Three 96-well plates were dispensed back to back with 10 μ l of fluorescein into 90 μ l of MOPS buffer (pH 7.0). Results were determined with a BMG fluorescent plate reader using the 470 nm filter for excitation and the 485 nm filter for emission.

In January of 2007 after a conversation with Dr. Tripp, a literature search was undertaken to look for information on a CA II histochemical staining procedure that involved a black cobalt precipitate. The literature search yielded six articles on the histochemistry of carbonic anhydrase by cobalt sulphide precipitation, a method first described by Holger Hannson¹⁰⁻¹⁵. To obtain the reactive solution in this method, two solutions are mixed (solutions A and B). Solution A consists of an aqueous solution of sulphuric acid, cobalt sulphate, and potassium dihydrogen phosphate and solution B is an aqueous solution of sodium bicarbonate. The stoichiometry for this reaction is shown below in Eq. 5.1. Table 5.11 lists the reagents in this reaction and their concentrations right after mixing.



Eq. 5.1

Table 5.11. The concentration of reagents right after mixing the aqueous solution of sulphuric acid, cobalt sulphate, and potassium dihydrogen phosphate with an aqueous solution of sodium bicarbonate. ^a

Reagents	Concentrations (mM)
Na ⁺	157
HCO ₃ ⁻	47
SO ₄ ²⁻	53
PO ₄ ³⁻	3.6
K ⁺	3.6
COSO ₄	2-10
H ⁺	10-3
CO ₂	34

^a Table was adapted from the paper by Thomas Maren¹².

There is 47 mM NaHCO_3 left in the solution and at the instant of mixing there is 56.6 mM H_2CO_3 and no CO_2 ¹² The rate of $\text{H}_2\text{CO}_3 \rightarrow \text{CO}_2$ dehydration is 14 s^{-1} ¹² at room temperature. Of all the CO_2 that is formed (56.6 mM), only 34 mM is soluble in water. In this reaction, carbonic acid is dehydrated to form CO_2 and attains the equilibrium ratio of 400 CO_2 : 1 H_2CO_3 rather quickly¹² in water, while the remaining CO_2 is lost as a gas and therefore the solution reaches equilibrium with an initial pH of 6.14¹². When the pH of the solution reaches pH 6.8 the precipitate appears first as an insoluble cobalt salt, probably a phosphate or hydroxy phosphate, and then is converted to the insoluble cobalt sulphide by reaction with H_2S or $(\text{NH}_4)_2\text{S}$ ¹². In the absence of carbonic anhydrase this precipitate will still form, because it is the alkalinization of the solution that is causing the precipitate to form. However, the presence of carbonic anhydrase greatly increases the rate of alkalinization of the solution¹².

Initial experiments were undertaken with large scale beaker experiments that followed the exact concentrations written above to confirm the pH at which the precipitate forms. After observing formation of a black precipitate in the solution, it was apparent that the Hannon method would not be feasible for detection of CA activity with a spectrophotometer. The black precipitate in the wells caused inconsistent results when the plate reader was used. Instead of using the Hannon method, carbonic acid dehydrating to CO_2 via sulphuric acid and sodium bicarbonate could be used to replace the bubbling CO_2 gas in water to generate the carbonic acid as described earlier in this chapter. The concentrations for sulphuric acid and sodium

bicarbonate from the Hannson method were kept exactly as previously written and were used to develop a new assay solution B. For solution A: 1 μ l CA II, 50 mM MES (pH 5.8 and pka 6.1), 33 mM Na₂SO₄, 1 mM EDTA, and the pH indicating dye 4-nitrophenol (pH range 5.4-7.5, pK_a 7.1) (Table 5.12).

Table 5.12. CA II carbonic acid dehydrating to CO ₂ pH assay. Assay components and concentrations.			
Assay basis - volume per well in 96-well plate (μ l):	100		
Actual final volume per well (μ l):	111		
Total plate volume (x100 samples per plate) [ml]:	12		
Total stock solution volume [ml]:	24		
CA-II enzyme stock soln [M]:	1.76E-05		
Final Buffer + Enzyme Assay Solution (Solution A)		Final Sample Conc. [M]	Volume to add (ml)
MES pH 5.8 stock soln [M]	1	0.050	1.2
Na ₂ SO ₄ stock soln [M]:	1	0.033	0.792
EDTA stock soln [M]:	0.50	0.001	0.048
Total vol of buffer			2.04
Final volume dH ₂ O to add			20.36
4-nitrophenol [M]:	0.01	0.0001	0.240
Final Diluted CA-II Enzyme stock soln [M]:	1.76 E-05	1.0E-06	1.364
Solution B ((substrate) (total solution volume [ml]))	45		
H ₂ SO ₄ [M]	1	0.053	2.385
NaCO ₃ [M]	1	0.157	7.065
Final volume dH ₂ O to add			35.55

This assay was then tested with CA II and three strong CA inhibitors: acetazolamide, ethoxzolamide, and sulfanilamide. Each inhibitor (10 mM stock solution) was diluted 1:2 in a 96-well plate. One μl from each well of the diluted inhibitor plate was then added to 60 μl of enzyme-assay buffer using a CCS PlateTrak and allowed to incubate for 15 min. The final pH of solution B was 6.13 and 40 μl of this was dispensed with the MultiDrop 8-channel peristaltic pump. The detection wavelength was 400 nm and there was a 1 sec shake cycle between readings (performed by the plate reader) and the assay was run for 10 min. Once solution B was prepared, it was useable for several 96-well plates; however, it was replaced with fresh solution when the activity of CA II started to decline in the uninhibited control wells. Acetazolamide was included in duplicate on each assay plate at 100 μM concentration as a positive control (100% inhibition).

Analysis of the data in Table 5.13 and Figure 5.14 indicated that the results for the CA II carbonic acid dehydrating to CO_2 pH assay were reasonably close to those obtained with the standard 4-NPA esterase CA II screening assay.

Table 5.13. Comparison of standard 4-nitrophenyl acetate CA II esterase assay vs. CA II carbonic acid dehydrating to CO_2 pH assay.

Compound	1 μM CA II IC_{50} Value (μM) ^a	1 μM CA II IC_{50} Value (μM) ^b
1. Acetazolamide	0.312	0.713
2. Ethoxzolamide	0.209	0.48
3. Sulfanilamide	2.71	11.5

^a Results from Chapter 2, Table 2.1 esterase screening assay.

^b Results from CA II carbonic acid dehydrating to CO_2 pH assay.

^c GraphPad Prism 4.3 was used to calculate IC_{50} plots.

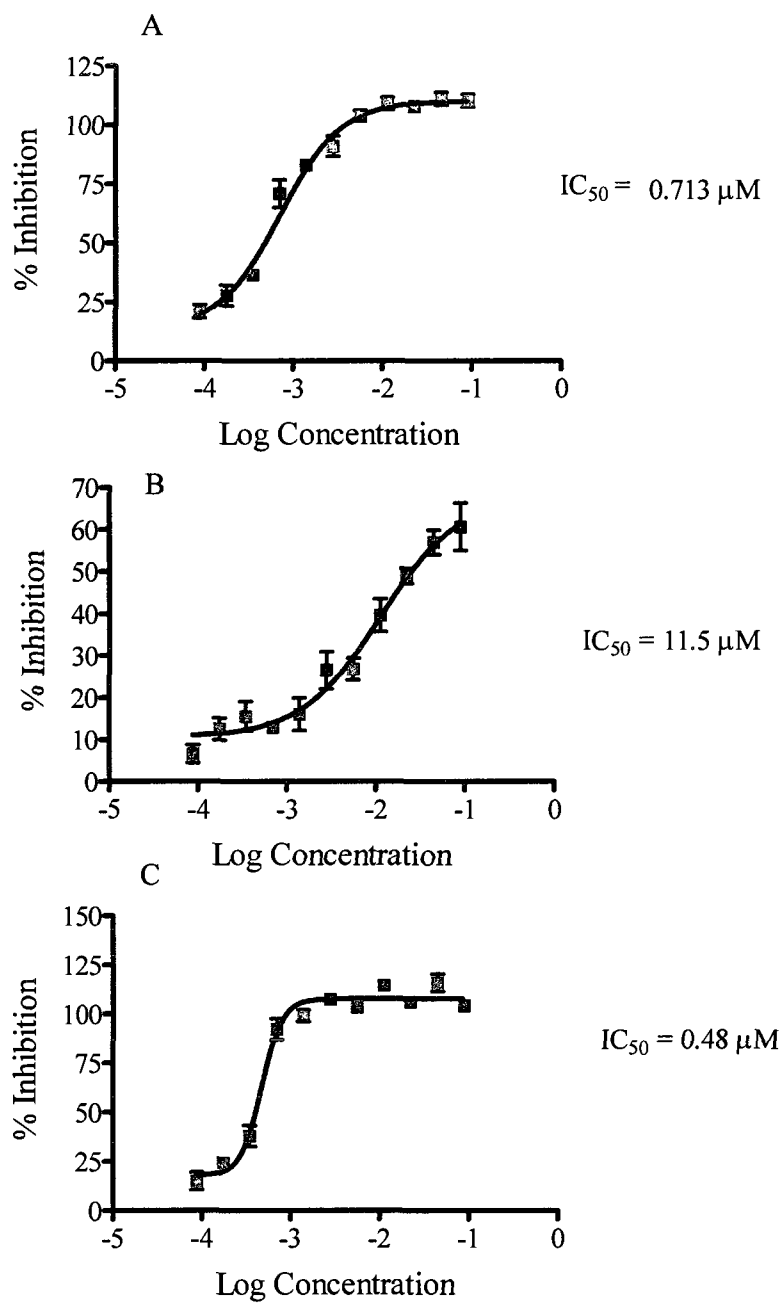


Figure 5.14. IC₅₀ plots for A. acetazolamide, B. sulfanilamide, and C. ethoxycarbazamide using the CA II carbonic acid dehydrating to CO₂ pH assay. GraphPad Prism 4.3 was used to generate the graphs.

As shown in Table 5.13, the IC_{50} values obtained by both methods were similar, with acetazolamide IC_{50} values of 0.312 μM for CA II esterase assay vs. 0.713 μM IC_{50} for acetazolamide from the CA II carbonic acid dehydrating to CO_2 pH assay. The IC_{50} for ethoxzolamide from the CA II esterase assay was 0.209 μM and from the CA II carbonic acid dehydrating to CO_2 pH assay the IC_{50} was 0.48 μM . For these first two inhibitors the IC_{50} values were slightly more than double the CA II esterase assay IC_{50} values. However, for sulfanilamide, the IC_{50} from the CA II esterase assay was 2.71 μM and from the CA II carbonic acid dehydrating to CO_2 pH assay the IC_{50} was 11.5 μM . Looking at Figure 5.15b, it is apparent that there was more error in the graph, which implies more inconsistency between the duplicate rows for this inhibitor. While it was not performed, repeating the kinetic run with sulfanilamide may give a better IC_{50} value that would then be closer to the CA II esterase value or just slightly over double that value, similar to the other two inhibitors tested in this assay.

It was noticed that when the 4-nitrophenol was added to the MES buffer, a faint yellow color developed, which also happens in the standard esterase assay when 4-NPA is added to MOPS. However, the deep yellow color typically observed at the end of the standard 4-NPA esterase assay in uninhibited samples was not observed in samples at the end of the CA II carbonic acid dehydrating to CO_2 pH assay. This lack of a deep color difference between inhibited and non inhibited CA might explain the difference in IC_{50} results between the two assays (Table 5.13). Consequently, using a different pH indicator dye that has a different color for each end of its pH range may

help make this assay perform more accurately and give results similar to the CA II esterase assay. The first alternative pH indicator is bromocresol purple which has a pH range from 5.2 to 6.8 and changes color from yellow to purple. Another potential pH indicator that could be used with MES buffer is chlorophenol red, which has a pH range from 5.4 to 6.8 and changes color from yellow to red.

Of the three different pH assays presented in this chapter, CA II carbonic acid dehydrating to CO₂ pH assay is the one with the most potential and least amount of problems to resolve. Preliminary results using that assay already show that the assay works and can generate similar results to the CA II esterase IC₅₀ assay.

References

1. Okuyama, T.; Waheed, A.; Kusumoto, W.; Zhu, X. L.; Sly, W. S. Carbonic anhydrase IV: role of removal of c-terminal domain in glycosylphosphatidylinositol anchoring and realization of enzyme activity. *Arch Biochem Biophys* 1995, 320, 315-22.
2. Waheed, A.; Okuyama, T.; Heyduk, T.; Sly, W. S. Carbonic anhydrase IV: purification of a secretory form of the recombinant human enzyme and identification of the positions and importance of its disulfide bonds. *Arch Biochem Biophys* 1996, 333, 432-8.
3. Okuyama, T.; Sato, S.; Zhu, X. L.; Waheed, A.; Sly, W. S. Human carbonic anhydrase IV: cDNA cloning, sequence comparison, and expression in COS cell membranes. *Proc Natl Acad Sci U S A* 1992, 89, 1315-9.
4. Baird, T. T., Jr.; Waheed, A.; Okuyama, T.; Sly, W. S.; Fierke, C. A. Catalysis and inhibition of human carbonic anhydrase IV. *Biochemistry* 1997, 36, 2669-78.
5. Tripp, B. C.; Tu, C.; Ferry, J. G. Role of arginine 59 in the gamma-class carbonic anhydrases. *Biochemistry* 2002, 41, 669-78.
6. Kim, G.; Selengut, J.; Levine, R. L. Carbonic anhydrase III: the phosphatase activity is extrinsic. *Arch Biochem Biophys* 2000, 377, 334-40.
7. Cabiscol, E.; Levine, R. L. The phosphatase activity of carbonic anhydrase III is reversibly regulated by glutathiolation. *Proc Natl Acad Sci U S A* 1996, 93, 4170-4.
8. Pocker, Y.; Stone, J. T. The catalytic versatility of erythrocyte carbonic anhydrase. III: kinetic studies of the enzyme-catalyzed hydrolysis of p-nitrophenyl acetate. *Biochemistry* 1967, 6, 668-678.
9. Zimmerman, S. A.; Ferry, J. G.; Supuran, C. T. Inhibition of the archaeal beta-class (Cab) and gamma-class (Cam) carbonic anhydrases. *Curr. Top. Med. Chem.* 2007, 7, 901-8.

10. Hansson, H. P. Histochemical demonstration of carbonic anhydrase activity. *Histochemie* 1967, 11, 112-28.
11. Dermietzel, R.; Leibstein, A.; Siffert, W.; Zamboglou, N.; Gros, G. A fast screening method for histochemical localization of carbonic anhydrase. Application to kidney, skeletal muscle, and thrombocytes. *J Histochem Cytochem* 1985, 33, 93-8.
12. Maren, T. H. Kinetics, equilibrium and inhibition in the Hansson histochemical procedure for carbonic anhydrase: a validation of the method. *Histochem J* 1980, 12, 183-90.
13. Brown, D.; Zhu, X. L.; Sly, W. S. Localization of membrane-associated carbonic anhydrase type IV in kidney epithelial cells. *Proc Natl Acad Sci U S A* 1990, 87, 7457-61.
14. Riehl, B.; Schlue, W. R. Localization of carbonic anhydrase in identified glial cells of the leech central nervous system: application of histochemical and immunocytochemical methods. *J Histochem Cytochem* 1990, 38, 1173-8.
15. Sender, S.; Decker, B.; Fenske, C. D.; Sly, W. S.; Carter, N. D.; Gros, G. Localization of carbonic anhydrase IV in rat and human heart muscle. *J Histochem Cytochem* 1998, 46, 855-61.

CHAPTER VI

FUTURE WORK

In Chapter Two the development of a novel high-throughput screening assay and subsequent screening of two compound libraries (Gen Plus and NCI) was explored. From those studies, four compounds were identified as CAIs that did not possess any sulfonamide-related structural groups: tannic acid, cevadine, thioxolone, and merbromin. Cevadine failed to show significant inhibition in the initial hit confirmation studies and was dropped from further studies, while thioxolone was studied further. This leaves tannic acid and merbromin from the GenPlus library for further investigation as to their CA inhibitory mechanisms and as lead candidates for further SAR studies. However, the follow-up studies suggested that the tannic acid was acting as a promiscuous inhibitor; it may not warrant further study.

The screen of the NCI library yielded two compounds (compounds **39** and **40**, Table 2.3) with internal sulfonamide groups. These two compounds could be further investigated using 4-NPA esterase kinetics, X-ray crystallography, LC-MS, NMR, and other methods that were used to examine the mechanism of thioxolone. There are also three compounds (**2**, **4**, and **14**, Table 2.3) with multiple sulfonamide groups that could be investigated by X-ray crystallography to determine their mode of binding in the active site of CA II. Additional studies of these aforementioned compounds could also involve the use of an alternate screening assay, such as a colorimetric or fluorescence assay of pH changes, using sodium bicarbonate or CO₂

as the enzyme substrate, instead of 4-NPA (Refer to Chapter Five for additional information on sodium bicarbonate or CO₂ assays). These alternate assays will require further development for microplate format, or will require implementation of the established stopped-flow methods. Furthermore, structurally related compounds could be purchased from commercial sources, if available, or synthesized *de novo* by a collaborating synthetic chemist, to further define the SAR properties of these novel CAIs.

In Chapter Three, the mechanism of thioxolone inhibition of CA II was determined, and the results indicated that thioxolone binds to the active site of CA II and is cleaved by successive hydrolysis of the thioester and ester bonds to form 4-mercaptobenzene-1,3-diol. As reviewed in Chapter Three, Innocenti et al.¹ from the Supuran research group tested the hypothesis of thioxolone having advantages over sulfonamides in determining isozyme specificity for carbonic anhydrase inhibition and found that, with the exception of CA I, all of the remaining carbonic anhydrase isozymes had a very narrow range of inhibition. However, there are modifications that can be made to the thioxolone structure that could potentially improve carbonic anhydrase inhibition and isozyme specificity. In Chapter Three, this hypothesis was explored in a preliminary manner with a series of commercially-available Specs compounds (Table 3.1). Further studies with the remaining carbonic anhydrase isozymes and various thioxolone analogues would be able to test that hypothesis. It would also be possible with the collaboration of a synthetic chemist to further generate additional variations of thioxolone compounds based on the results of the

above study to generate isozyme specificity.

Chapter Four also explored the development of a novel high-throughput screening assay and use of 96-well microplates to grow bacterial cultures. This assay was then used to screen for motility inhibition of bacterial flagella. While no motility inhibitors were found, the assay did identify many compounds with known antimicrobial activity (Table 4.1). The GenPlus compound library was not the only compound library screened with this assay, the NCI compound library was also screened. Because there was not enough of the compound library left after the initial screen follow up studies to confirm the initial hits could not be performed. The initial screen identified three compounds with antimicrobial activity that have not been reported as antimicrobial compounds. These NCI compounds were NSC 69343, NSC 207895, and NSC 321237. Further studies are needed to confirm the antimicrobial activity of these compounds and to determine the minimum inhibition concentration. This assay could also be used with larger compound libraries to further investigate the initial hypothesis of finding a motility inhibitor for bacterial flagella or even other possible novel antibiotic compounds.

In 2004, the NIH started a “Roadmap for Medical Research” initiative to address roadblocks in research that would span all areas of health and disease research and cross boundaries of NIH Institutes and Centers. There were twelve roadblocks that were grouped into three themes by the NIH: new pathways to discovery, research teams of the future, and reengineering the clinical research enterprise. Under the theme of pathways to discovery, the NIH set up approximately

10 specialized screening centers and a small molecule repository that maintains a 300,000 chemically diverse small molecule compound library. The screen centers can then request portions of the chemical library as needed. The goal was for each center to apply their particular HTS assay expertise to screen the compound library for interactions with a user-submitted target cell or molecule, by adapting a previously developed, validated assay. For more information, see the following website:

<http://nihroadmap.nih.gov/molecularlibraries/>.

This approach would be one possible way to screen larger compound libraries without the expense of having to purchase larger compound libraries for use in the HTS bacterial screening assay. However, it will require the technical capabilities and willingness of a supported center to implement this assay on a large scale.

The CA isozyme screening project in Chapter Five only described the subcloning of CA I and CA IV; therefore, other mammalian CA isozymes could also be subcloned into pET28c or another suitable expression vector as a continuation of the project. Furthermore, the purification of bacterially expressed CA I and CA IV enzymes was not successfully accomplished and could be pursued further. In Chapter Five, the preliminary attempt to purify CA IV was described; however, additional work on developing purification methods for CA IV and CA I was not pursued due to additional studies on the thioxolone inhibition mechanism being required for publication at the time. The addition of an affinity tag (e.g. His-tag) to facilitate purification could also be investigated with any of the CA isozymes, because this peptide tag is already present in many pET vectors. Each CA isozyme would simply

need to be subcloned into the correct location on a suitable pET vector to have it present on one end of the expressed protein. In addition, if the other mammalian CA isozymes were subcloned, they could be bacterially expressed, purified, and screened against the GenPlus or other compound libraries for novel CA inhibitors. Any known or future lead CA inhibitor compounds could then be profiled for their relative affinities and specificities against the different CA isozymes, and explored as potential therapeutic drugs for the treatment of relevant diseases.

References

1. Innocenti, A.; Maresca, A.; Scozzafava, A.; Supuran, C. T. Carbonic anhydrase inhibitors: thioxolone versus sulfonamides for obtaining isozyme-selective inhibitors? *Bioorg Med Chem Lett* **2008**, 18, 3938-41.

Appendix

Recombinant DNA Biosafety Approval

Recombinant DNA Biosafety Committee

Project Approval Certification

For rDNA Biosafety Committee Use Only

Project Title: Engineering and Display of Enzymes and Proteins on Bacterial Flagella Fibers

Principal Investigator: Brian Tripp

IBC Project Number: 09-BTa

Date Received by the rDNA Biosafety Committee: 2/27/2009

☒ Reviewed by the rDNA Biosafety Committee

☒ Approved

☐ Approval not required

1 Silvia Repbach 2/27/2009
Chair of rDNA Biosafety Committee Signature Date

Revised 5/02 WMU RDBC
All other copies obsolete

Western Michigan University

Recombinant DNA Biosafety Committee

Registration for Recombinant Research - 2009

This form must be submitted for all research involving recombinant DNA molecules. Renewal of approval is required annually.

In this form, *Guidelines* means: *Guidelines for Research Involving Recombinant DNA Molecules (NIH Guidelines)*.

General Registration Information

Principal Investigator: Brian C. Tripp, Ph.D. Associate Professor

Office Phone: 269 387-4166 Laboratory Phone: 269 387-1955 Department: BIOS

Electronic Mail Address: brian.tripp@wmich.edu

Office Address: Room 3435, Building: Wood Hall

Laboratory Where Research is to be Conducted:

Building: Haenicke Hall

Room: 4007H, 4009H, 2022H

Project Title: Engineering and Display of Enzymes and Proteins on Bacterial Flagella Fibers

Project Start Date: 04/01/02

Current status (check one):

- | | |
|--|-----------------------------------|
| <input type="checkbox"/> Initiated | Date: |
| <input type="checkbox"/> Will be initiated | Date: |
| <input checked="" type="checkbox"/> Continuing (no changes) | Current Project Number: 06-04-BTa |
| <input type="checkbox"/> Continuing (modifications) | Current Project Number: 06- |
| <input type="checkbox"/> Will not be initiated or will be discontinued | |
| <input type="checkbox"/> Completed | Date: |

If Part of a Grant Proposal, List Agency/Agencies: DoD, NIH, NSF, WMU-FRACAS

WMU Proposal Tracking Number (if applicable):

Class of Covered Experiments and Containment

1. Which class of the *Guidelines* for covered experiments apply to the proposed experiments (see section III of the *Guidelines*). Check only one:
- ☐ III-A. Experiments that require Recombinant DNA Biosafety Committee (RDBC) approval, Recombinant DNA Advisory Committee (RAC) review, and NIH Director approval before initiation
- ☐ III-B. Experiments that require NIH/OBA (Office of Biotechnology Activities) and RDBC approval before initiation
- ☐ III-C. Experiments that require RDBC and Human Subjects Institutional Review Board (HSIRB) approvals and NIH/OBA registration before initiation.
- ☒ III-D. Experiments that require RDBC approval before initiation (see items III-D-1 through III-D-6 in the *Guidelines*). Check all that apply to III-D:
- ☒ a. Use of other than a risk group 1 agent as a host-vector system. State risk group: RG2
- ☒ b. Use of other than a risk group 1 agent as a DNA source. State risk group: RG2
- ☐ c. A viral vector (other than risk group 1) will be used:
1. Will less than 2/3 of a genome be used? ☐ Yes ☐ No
2. With helper virus? ☐ Yes ☐ No
3. May your experiment enhance pathogenicity (e.g. insertion of oncogene, extend host range)? ☐ Yes ☐ No
- ☐ d. Whole animals or plants will be used as host.
- ☐ e. Experiments will involve more than 10 liters of culture.
- All checks need to be explained on a separate page.
- ☐ III-E. Experiments that require RDBC notice simultaneous with initiation (experiments not included in III-A, III-B, III-C, III-D and III-F)
- ☐ III-F. Exempt experiments that require RDBC notice simultaneous with initiation (see items III-F-1 through III-F-6 in the *Guidelines*)
2. Which physical containment level applies to this proposal (Appendix G, section II in the *Guidelines*)? Check one: ☐ BL-1 ☒ BL-2 ☐ BL-3
3. State brief reason for choosing class and containment and cite appropriate sections of the *Guidelines*.

A. Pathogenic Risk Group 2 Salmonella Strains.

The experiments covered under this registration form involve the use of several strains of the Risk Group 2 (RG2) bacterial agent, *Salmonella typhimurium*. *Salmonella typhimurium* is a known bacterial pathogen known to cause food poisoning when ingested and is widely present in the environment, sometimes associated with reptiles, birds and amphibians.

The section entitled *Appendix B-II - Risk Group 2 (RG2) Agents* of the April 2002 version of the *NIH Guidelines* gives the definition of RG2 agents: "RG2 agents are associated with human disease which is rarely serious and for which preventive or therapeutic interventions are often available."

Appendix B-II-A of the *NIH Guidelines* lists Risk Group 2 (RG2) - Bacterial Agents including Chlamydia, which includes the statement "—*Salmonella* including *S. arizonae*, *S. choleraesuis*, *S. enteritidis*, *S. gallinarum-pullorum*, *S. meleagridis*, *S. paratyphi*, A, B, C, *S. typhi*, *S. typhimurium*."

B. Non-Pathogenic E. coli Strains.

Other experiments in these recombinant DNA protocols involve the use of standard, non-pathogenic *E. coli* K-12 Host-plasmid systems such as DH5-alpha, NEB-alpha, and BL21-DE3 strains, including derivative strains, BL21(DE3)-Star, C41(DE3) and C43(DE3), which are considered exempt from the *NIH Guidelines*. As stated in the *NIH Guidelines, Appendix C-II. Escherichia coli K-12 Host-Vector Systems*: "Experiments which use *Escherichia coli* K-12 host-vector systems, with the exception of those experiments listed in *Appendix C-II-A*, are exempt from the *NIH Guidelines* provided that: (i) the *Escherichia coli* host does not contain conjugation proficient plasmids or generalized transducing phages; or (ii) lambda or lambdoid or Ff bacteriophages or non-conjugative plasmids (see *Appendix C-VII Footnotes and References of Appendix C, Footnotes and References of Appendix C*) shall be used as vectors. However, experiments involving the insertion into *Escherichia coli* K-12 of DNA from prokaryotes that exchange genetic information (see *Appendix C-VII. Footnotes and References of Appendix C, Footnotes and References of Appendix C*) with *Escherichia coli* may be performed with any *Escherichia coli* K-12 vector (e.g., conjugative plasmid). When a non-conjugative vector is used, the *Escherichia coli* K-12 host may contain conjugation-proficient plasmids either autonomous or integrated, or generalized transducing phages. For these exempt laboratory experiments, Biosafety Level (BL) 1 physical containment conditions are recommended. For large-scale fermentation experiments, the appropriate physical containment conditions need be no greater than those for the host organism unmodified by recombinant DNA techniques; the Institutional Biosafety Committee can specify higher containment if deemed necessary."

C. Bacterial Cell Culture Volumes.

The experimental procedures described in this protocol involve bacterial cell culture of Exempt or potential RG1 *E. coli* K-12 strains and RG2 *Salmonella typhimurium* cells in volumes ranging from 1 ml to 5 liters. As noted in *Appendix C-II-A. Exceptions of the Guidelines*, "The following categories are not exempt from the *NIH Guidelines*: ... (iv) large-scale experiments (e.g., more than 10 liters of culture), ...". Thus, the cell culture procedures in this protocol do not use volumes of cell culture that exceed more than 50% of the volumes considered to be in the category of "large-scale" by the *NIH Guidelines*.

Description of Recombinant DNA Experiments

1. Summary of project (1 or 2 paragraphs). Include purpose and manner in which recombinant DNA will be used in the project. Please define acronyms and abbreviations.

The proposed primary research is a continuation of a research project that involves the investigation of the export and folding pathways of bacterial flagella fibers, with the goal of displaying foreign enzymes and proteins as genetic fusions to flagellin proteins attached to the surface of bacteria, for possible use as sensors and in nanotechnology applications. This flagellin-oriented research also involves research on the construction of novel nanomaterials using flagellin proteins as a novel nanomaterial fiber to bind or induce precipitation of other inorganic nanomaterials. Some gene fusion experiments involve the well-characterized green fluorescent protein originally cloned from *Aequoria Victoria*, Pacific jellyfish, which will be inserted in various ways into *Salmonella*, *E. coli* and *Aquifex pyrophilus* flagellin proteins. Additional cloning experiments will involve the same techniques and approaches applied to the extracellular display of human carbonic anhydrase II on bacterial flagellin. Carbonic anhydrase II is a well-characterized enzyme with easily detected catalytic activity. Another area of current research involves the engineering and optimization of a particular structural class of bacterial left-handed beta helical acyltransferase and carbonic anhydrase enzymes to perform novel catalytic functions, and the catalytic engineering of flagellins to a) mimic the carbonic anhydrase active site and catalytic function and b) contain an internal fusion of the human carbonic anhydrase enzyme. These areas of research will involve investigating the effect of various mutations, foreign gene insertions and gene rearrangements on function of the corresponding proteins. The catalytic activity of mutated enzymes, level of recombinant protein production in *E. coli*, extracellular protein export, and the flagella-mediated bacterial motility of *E. coli* and *Salmonella typhimurium* strains will be studied as a function of mutations in the corresponding genetic DNA. Thus, recombinant DNA will be used as a template for the introduction of amino acid and polypeptide substitutions into the corresponding proteins. Genes encoding various proteins and enzymes will individually be subjected to random mutagenesis, site-directed mutagenesis, gene insertion and gene shuffling. Standard molecular biology techniques, such as polymerase chain reaction (PCR) will be used to introduce mutations in the DNA, while other cutting and ligation procedures will be performed with restriction enzymes and T4 ligase enzyme. Molecular biology and cell culture procedures are performed in the PI's laboratory in 4007 and 4009 Haenicke Hall. Other physiological experiments involve the use of a laser tweezer-optical microscope instrument to measure the motility, i.e. ability to swim, of *E. coli* and *Salmonella* bacteria. This instrument is installed as part of a W. M. Keck Nanotechnology facility presently located in room 2022 Haenicke Hall on the main WMU campus.

An interrelated enzymology research project that involves the investigation of catalytic function and screening small molecules for inhibition of mammalian, bacterial and archaeal carbonic anhydrases and several structurally related left-handed beta helical acyltransferase enzymes. Cloning experiments will involve structure-function studies of the relationships between catalytic rate, substrate recognition and binding by various types of inhibitors. Initial studies involve human carbonic anhydrase II, which is a well-characterized enzyme with easily detected catalytic activity. Another part of this current research involves the engineering and optimization of alpha and gamma-class class carbonic anhydrase enzymes to perform novel catalytic functions. These areas of research will involve investigating the effect of various mutations, foreign gene insertions and gene rearrangements on function of the corresponding proteins. The catalytic activity of wild-type and mutated enzymes, inhibition by small molecules, and the level of recombinant protein production in *E. coli* will be studied as a function of mutations in the corresponding genetic DNA. Thus, recombinant DNA will be used as a template for the introduction of amino acid and polypeptide substitutions into the corresponding proteins. Genes encoding various carbonic anhydrase and related enzymes may individually be subjected to random mutagenesis, site-directed mutagenesis, gene insertion and gene shuffling. Standard molecular biology techniques, such as polymerase chain reaction (PCR) will be used to introduce mutations in the DNA, while other cutting and ligation procedures will be performed with restriction enzymes and T4 ligase enzyme. Preliminary experiments on the bacterial expression and biochemical function of several *E. coli* membrane proteins, the ammonia transport protein, AmB, and aquaporin, are also underway, using expression plasmids and strains described below.

2. Host strain(s) used, including genus, species, parent strains, and class of each agent.

Only prokaryotic bacterial microorganisms will be used in this research: *E. coli* and *Salmonella enterica* serovar Typhimurium LT2 (*Salmonella typhimurium*). Host strains to be used include: *E. coli* K-12 strains (exempt class) XL-1 Red, XL-1 Blue, DH5-alpha, BL21(DE3)Gold (Stratagene, La Jolla, CA), TOP10, G1724, G1826, BL23(DE3)star, BL21(DE3)pLysS, BL21(DE3)pLysE, BL21(DE3)AI (Invitrogen, Carlsbad, CA), NEB-5-alpha (New England Biolabs, Beverly, MA), C41(DE3), C43(DE3), and AVB99 containing pBirAcm, an engineered pACYC184 plasmid with an IPTG inducible birA gene to over express the biotin ligase enzyme (Avidity, Denver, CO). Three *Salmonella typhimurium* strains (Class III-D, risk group 2/BL-2) will also be used: SJW1103 (wild-type for flagellar-mediated motility and

plasmids for use in *E. coli*. Plasmid vectors containing the other eleven human carbonic anhydrase genes are either pCMV-SPORT6, pOTB7 or pBlueScriptR and were obtained from Open Biosystems, Huntsville, AL.

5. Will an attempt be made to obtain expression of a foreign gene? ☒ Yes ☐ No
If so, what protein will be produced?

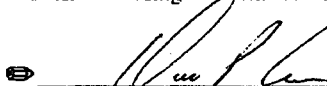
Eubacterial *E. coli*, *Salmonella typhimurium*, and *Aquifex pyrophilus* wild-type, partially deleted flagellin proteins, and hybrids of flagellin and green fluorescent protein (GFP), including soluble-modified GFP, hybrids of *E. coli* thioredoxin and flagellin ("FliTrx"), the *E. coli* biotin ligase enzyme, BirA, hybrids of streptavidin and flagellin and hybrids of flagellin and mammalian (human) carbonic anhydrase isozymes will be expressed in both *E. coli* and *Salmonella typhimurium*. Streptavidin, archaeal carbonic anhydrase, acyltransferase enzymes including Cam, LpxA, DapD, GlnU, and Val(D), and membrane proteins AmB and AqpZ will also be expressed as soluble proteins in *E. coli*. CA II and other previously described isozymes of human carbonic anhydrases CA I, CA II, CA IV, CA VB, CA VII, CA IX, CA X, CA XI, CA XII, CA XIII, CA XIV will be cloned into pET vectors and expressed in *E. coli* for use as controls in flagellin fusion-protein experiments and in catalytic engineering of flagellin. It is anticipated that several integral membrane proteins from *E. coli*, AmB and aquaporin, will also be expressed in suitable *E. coli* expression strains for preliminary experiments for future proposal resubmission.

Statements of Certification

I certify that I have read and understood the *Western Michigan University Policy for Recombinant DNA Biosafety* including the description of my role and responsibilities as Principal Investigator on this project. I agree to abide by the *Guidelines for Research Involving Recombinant DNA Molecules (NIH Guidelines)* in conducting all work using recombinant DNA molecules.

 Feb. 2, 2009
Principal Investigator Signature Date

I have read the description of this proposed research involving recombinant DNA molecules. I have determined that the facilities and procedures proposed in this project registration form are adequate for the safe conduct of this research and the safety of other personnel – faculty, staff, and visitors – using the facilities within which this research is to be conducted.

 2 Feb 09
Department Chair/Unit Head Signature Date

Submit the original plus 7 copies to the research compliance coordinator, 251W Walwood Hall. (Be sure to make and keep another copy for your files.) Contact the research compliance coordinator at 387-8293 for additional information.

Western Michigan University

Recombinant DNA Biosafety Committee

Registration for Recombinant Research - 2010

This form must be submitted for all research involving recombinant DNA molecules. Renewal of approval is required annually.

In this form, *Guidelines* means: *Guidelines for Research Involving Recombinant DNA Molecules (NIH Guidelines)*.

General Registration Information

Principal Investigator: Brian C. Tripp, Ph.D. Associate Professor

Office Phone: (269) 387-4166 Laboratory Phone: (269) 387-1955 Department: BIOS

Electronic Mail Address: brian.tripp@wmich.edu

Office Address: Room 3435, Building: Wood Hall

Laboratory Where Research is to be Conducted:

Building: Haenicke Hall

Room: 4007, 4009, 2022

Project Title: Engineering and Display of enzymes and Proteins on Bacterial Flagella Fibers

Project Start Date: 04/01/02

Current status (check one):

- | | | |
|-------------------------------------|---|-------------------------------|
| <input type="checkbox"/> | Initiated | Date: |
| <input type="checkbox"/> | Will be initiated | Date: |
| <input checked="" type="checkbox"/> | Continuing (no changes) | Current Project Number:)6-04 |
| <input type="checkbox"/> | Continuing (modifications) | Current Project Number: |
| <input type="checkbox"/> | Will not be initiated or will be discontinued | |
| <input type="checkbox"/> | Completed | Date: |

If Part of a Grant Proposal, List Agency/Agencies: DoD, NIH, NSF, WMU-FRACAS

WMU Proposal Tracking Number (if applicable):

Class of Covered Experiments and Containment

1. Which class of the *Guidelines* for covered experiments apply to the proposed experiments (see section III of the *Guidelines*). Check only one:
- ☐ III-A. Experiments that require Recombinant DNA Biosafety Committee (RDBC) approval, Recombinant DNA Advisory Committee (RAC) review, and NIH Director approval before initiation
- ☐ III-B. Experiments that require NIH/OBA (Office of Biotechnology Activities) and RDBC approval before initiation
- ☐ III-C. Experiments that require RDBC and Human Subjects Institutional Review Board (HSIRB) approvals and NIH/OBA registration before initiation.
- ☒ III-D. Experiments that require RDBC approval before initiation (see items III-D-1 through III-D-6 in the *Guidelines*). Check all that apply to III-D:
- ☒ a. Use of other than a risk group 1 agent as a host-vector system. State risk group: RG2
- ☒ b. Use of other than a risk group 1 agent as a DNA source. State risk group: RG2
- ☐ c. A viral vector (other than risk group 1) will be used:
1. Will less than 2/3 of a genome be used? ☐ Yes ☐ No
2. With helper virus? ☐ Yes ☐ No
3. May your experiment enhance pathogenicity (e.g. insertion of oncogene, extend host range)? ☐ Yes ☐ No
- ☐ d. Whole animals or plants will be used as host.
- ☐ e. Experiments will involve more than 10 liters of culture.
- All checks need to be explained on a separate page.
- ☐ III-E. Experiments that require RDBC notice simultaneous with initiation (experiments not included in III-A, III-B, III-C, III-D and III-F)
- ☐ III-F. Exempt experiments that require RDBC notice simultaneous with initiation (see items III-F-1 through III-F-6 in the *Guidelines*)
2. Which physical containment level applies to this proposal (Appendix G, section II in the *Guidelines*)? Check one: ☐ BL-1 ☒ BL-2 ☐ BL-3
3. State brief reason for choosing class and containment and cite appropriate sections of the *Guidelines*.

Class of Covered Experiments and Containment

1. Which class of the *Guidelines* for covered experiments apply to the proposed experiments (see section III of the *Guidelines*). Check only one:

- ☐ III-A. Experiments that require Recombinant DNA Biosafety Committee (RDBC) approval, Recombinant DNA Advisory Committee (RAC) review, and NIH Director approval before initiation
- ☐ III-B. Experiments that require NIH/OBA (Office of Biotechnology Activities) and RDBC approval before initiation
- ☐ III-C. Experiments that require RDBC and Human Subjects Institutional Review Board (HSIRB) approvals and NIH/OBA registration before initiation.
- ☒ III-D. Experiments that require RDBC approval before initiation (see items III-D-1 through III-D-6 in the *Guidelines*). Check all that apply to III-D:
- ☒ a. Use of other than a risk group 1 agent as a host-vector system. State risk group: RG2
- ☒ b. Use of other than a risk group 1 agent as a DNA source. State risk group: RG2
- ☐ c. A viral vector (other than risk group 1) will be used:
1. Will less than 2/3 of a genome be used? ☐ Yes ☐ No
2. With helper virus? ☐ Yes ☐ No
3. May your experiment enhance pathogenicity (e.g. insertion of oncogene, extend host range)? ☐ Yes ☐ No
- ☐ d. Whole animals or plants will be used as host.
- ☐ e. Experiments will involve more than 10 liters of culture.

All checks need to be explained on a separate page.

- ☐ III-E. Experiments that require RDBC notice simultaneous with initiation (experiments not included in III-A, III-B, III-C, III-D and III-F)
- ☐ III-F. Exempt experiments that require RDBC notice simultaneous with initiation (see items III-F-1 through III-F-6 in the *Guidelines*)
2. Which physical containment level applies to this proposal (Appendix G, section II in the *Guidelines*)? Check one: ☐ BL-1 ☒ BL-2 ☐ BL-3
3. State brief reason for choosing class and containment and cite appropriate sections of the *Guidelines*.

- A. Pathogenic Risk Group 2 Salmonella Strains.
The experiments covered under this registration form involve the use of several strains of the Risk Group 2 (RG2) bacterial agent, *Salmonella typhimurium*. *Salmonella typhimurium* is a known bacterial pathogen known to cause food poisoning when ingested and is widely present in the environment, sometimes associated with reptiles, birds and amphibians. The section entitled Appendix B-II - Risk Group 2 (RG2) Agents of the Sept. 2009 version of the NIH Guidelines for Research Involving Recombinant DNA Molecules gives the definition of RG2 agents: "RG2 agents are associated with human disease which is rarely serious and for which preventive or therapeutic interventions are often available." Appendix B-II-A of the NIH Guidelines lists Risk Group 2 (RG2) - Bacterial Agents Including Chlamydia, which includes the statement "--Salmonella including *S. arizonae*, *S. choleraesuis*, *S. enteritidis*, *S. gallinarum-pullorum*, *S. meleagridis*, *S. paratyphi*, A, B, C, *S. typhi*, *S. typhimurium*."
- B. Non-Pathogenic *E. coli* Strains.
Other experiments in these recombinant DNA protocols involve the use of standard, non-pathogenic (RG1) *E. coli* K-12 derivative host-vector systems or *E. coli* B strain-vector systems in which the host does not contain conjugation proficient plasmids. These strains include DH5-alpha, and NEB-alpha, which are considered exempt from the NIH Guidelines. As stated in Section III-F-6: The DNA does "not present a significant risk to health or the environment...", as listed in Appendix C of the Guidelines. Some protein expression experiments will also use commercially available non-pathogenic *E. coli* B strain derivatives that are also presumably classified as RG1 or possibly as RG2, such as the BL21-DE3 strain and derivative strains, BL21(DE3)-Star, C41(DE3) and C43(DE3). For these exempt laboratory experiments, Biosafety Level (BL) 1 physical containment conditions are recommended. For large-scale fermentation experiments, the appropriate physical containment conditions need be no greater than those for the host organism unmodified by recombinant DNA techniques; the Institutional Biosafety Committee can specify higher containment if deemed necessary."
- C. Bacterial Cell Culture Volumes.
The experimental procedures described in this protocol involve bacterial cell culture of exempt or potential RG1 *E. coli* K-12 and B strains and RG2 *Salmonella typhimurium* cells in volumes ranging from of 1 ml to 5 liters. As noted in Appendix C-II-A. Exceptions of the Guidelines, "The following categories are not exempt from the NIH Guidelines: ... (iv) large-scale experiments (e.g., more than 10 liters of culture), ...". Thus, the cell culture procedures in this protocol do not use volumes of cell culture that exceed more than 50% of the volumes considered to be in the category of "large-scale" by the NIH Guidelines.

Description of Recombinant DNA Experiments

1. Summary of project (1 or 2 paragraphs). Include purpose and manner in which recombinant DNA will be used in the project. Please define acronyms and abbreviations.

The proposed primary research is a continuation of a research project that involves the investigation of the export and folding pathways of bacterial flagella fibers, with the goal of displaying foreign enzymes and proteins as genetic fusions to flagellin proteins attached to the surface of bacteria, for possible use as sensors and in nanotechnology applications. This flagellin-oriented research also involves research on the construction of novel nanomaterials using flagellin proteins as a novel nanomaterial fiber to bind or induce precipitation of other inorganic nanomaterials. Some gene fusion experiments involve the well-characterized green fluorescent protein originally cloned from *Aequoria victoria*, Pacific jellyfish, which will be inserted in various ways into *Salmonella*, *E. coli* and *Aquifex pyrophilus* flagellin proteins. Additional cloning experiments will involve the same techniques and approaches applied to the extracellular display of human carbonic anhydrase II on bacterial flagellin. Carbonic anhydrase II is a well-characterized enzyme with easily detected catalytic activity. Another area of current research involves the engineering and optimization of a particular structural class of bacterial left-handed beta helical acyltransferase and carbonic anhydrase enzymes to perform novel catalytic functions, and the catalytic engineering of flagellins to a) mimic the carbonic anhydrase active site and catalytic function and b) contain an internal fusion of the human carbonic anhydrase enzyme. These areas of research will involve investigating the effect of various mutations, foreign gene insertions and gene rearrangements on function of the corresponding proteins. The catalytic activity of mutated enzymes, level of recombinant protein production in *E. coli*, extracellular protein export, and the flagella-mediated bacterial motility of *E. coli* and *Salmonella typhimurium* strains will be studied as a function of mutations in the corresponding genetic DNA. Thus, recombinant DNA will be used as a template for the introduction of amino acid and polypeptide substitutions into the corresponding proteins. Genes encoding various proteins and enzymes will individually be subjected to random mutagenesis, site-directed mutagenesis, gene insertion and gene shuffling. Standard molecular biology techniques, such as polymerase chain reaction (PCR) will be used to introduce mutations in the DNA, while other cutting and ligation procedures will be performed with restriction enzymes and T4 ligase enzyme. Molecular biology and cell culture procedures are performed in the PI's laboratory in 4007 and 4009 Haenicke Hall. Other physiological experiments involve the use of a laser tweezer-optical microscope instrument to measure the motility, i.e. ability to swim, of *E. coli* and *Salmonella* bacteria. This instrument is installed as part of a W. M. Keck Nanotechnology facility presently located in room 2022 Haenicke Hall on the main WMU campus.

An interrelated enzymology research project that involves the investigation of catalytic function and screening small molecules for inhibition of mammalian, bacterial and archaeal carbonic anhydrases and several structurally related left-handed beta helical acyltransferase enzymes. Cloning experiments will involve structure-function studies of the relationships between catalytic rate, substrate recognition and binding by various types of inhibitors. Initial studies involve human carbonic anhydrase II, which is a well-characterized enzyme with easily detected catalytic activity. Another part of this current research involves the engineering and optimization of alpha and gamma-class class carbonic anhydrase enzymes to perform novel catalytic functions. These areas of research will involve investigating the effect of various mutations, foreign gene insertions and gene rearrangements on function of the corresponding proteins. The catalytic activity of wild-type and mutated enzymes, inhibition by small molecules, and the level of recombinant protein production in *E. coli* will be studied as a function of mutations in the corresponding genetic DNA. Thus, recombinant DNA will be used as a template for the introduction of amino acid and polypeptide substitutions into the corresponding proteins. Genes encoding various carbonic anhydrase and related enzymes may individually be subjected to random mutagenesis, site-directed mutagenesis, gene insertion and gene shuffling. Standard molecular biology techniques, such as polymerase chain reaction (PCR) will be used to introduce mutations in the DNA, while other cutting and ligation procedures will be performed with restriction enzymes and T4 ligase enzyme. Preliminary experiments on the bacterial expression and biochemical function of several *E. coli* membrane proteins, the ammonia transport protein, AmtB, and aquaporin, are also underway, using expression plasmids and strains described below.

2. Host strain(s) used, including genus, species, parent strains, and class of each agent.

Only prokaryotic bacterial microorganisms will be used in this research: *E. coli* and *Salmonella enterica* serovar Typhimurium LT2 (*Salmonella typhimurium*). Host strains to be used include: *E. coli* K-12 strains (exempt class) XL-1 Red, XL-1 Blue, DH5-alpha, and commonly used laboratory *E. coli* B strains BL21(DE3)Gold (Stratagene, La Jolla, CA), TOP10, GI724, GI826, BL23(DE3)star, BL21(DE3)pLysS, BL21(DE3)pLysE, BL21(DE3)AI (Invitrogen, Carlsbad, CA), NEB-5-alpha (New England Biolabs, Beverly, MA), C41(DE3), C43(DE3), and AVB99 containing pBirAcm, an engineered pACYC184 plasmid with an IPTG inducible birA gene to over express the biotin ligase enzyme (Avidity, Denver, CO). Three *Salmonella typhimurium* strains (Class III-D, risk group 2/BL-2) will also be used: SJW1103 (wild-type for flagellar-mediated motility and chemotaxis), SJW134, which has the two genes for flagellin deleted (flc and

fljB) and is therefore non-motile unless foreign flagellin genes are added via plasmid transformation, and JR501 (r-m⁺) which is used to convert *E. coli* grown plasmids for compatibility in other *Salmonella* strains. These bacterial strains will be used for host-vector plasmid production and also for bacterial protein expression.

3. Source(s) and nature of inserted DNA sequences. Include size, gene name(s) and function of gene(s), and sequence(s), if known.

The PI, Dr. Tripp, has a number of genes encoded in plasmid vectors suitable for transformation into *E. coli* or *Salmonella* bacteria. These include:

1. The *Aequoria victoria* green fluorescent protein, (gene size: 720 b.p.) an autofluorescent protein used as a biological probe/label, encoded in the pGLO plasmid purchased from Bio-Rad, Hercules, CA.
2. Three plasmids encoding wild-type *Salmonella* fliC flagellin gene pTH810 (gene size 1491 b.p.), pTH890 (gene size 1501 b.p.), and pMM1501 (gene size 1501 b.p.), were obtained from Prof. Robert Macnab at Yale University, New Haven CT.
3. Four plasmids containing green fluorescent protein variants were obtained from Doug Sheridan & Thomas R. Hughes, Yale University: pBNJ24.6, pBNJ26.3, pBNJ28.2, pBNJ37.2 (GFP gene size 720 b.p.).
4. Two plasmids containing fragments of the marine hyperthermophilic bacterium, *Aquifex pyrophilus* flagellin gene, approx. 1500 b.p. pRU1650 and pRU1651 were obtained from Prof. Dr. Rudiger Schmitt at the University of Regensburg, Germany.
5. One plasmid, pUC8-SZ, containing the full-length gene encoding the biotin-binding protein, streptavidin cloned from *Streptomyces avidinii*, was obtained from Dr. Takeshi Sano, Harvard Medical School.
6. Twelve plasmids encoding most of the catalytically active human carbonic anhydrase (CA) genes. The human CA II gene is encoded in the pACA plasmid (gene size: 784 DNA base pairs). Other plasmids from the mammalian gene collection containing full length human carbonic anhydrase isozyme genes (approximate length 800 b.p. each) were purchased from Open Biosystems, Huntsville, AL. The Open Biosource clone catalog numbers for each CA gene are: CA I - MHS1010-7430110, CA III - MHS1011-60292, CA IV - EHS1001-7498723, CA VB - MHS1010-7507834, CA VII - MHS1010-7508192, CA IX - MHS1011-76616, CA X - MHS1010-7429536, CA XI - MHS1011-60412, CA XII - MHS1011-7509335, CA XIII - EHS1001-6903676, CA XIV - MHS1010-7507617.
7. Five plasmids encoding five left-handed beta-helical enzymes: gamma-class carbonic anhydrase (Cam) from the archaeon *Methanosarcina thermophila* (gene size: 639 DNA base pairs), *E. coli* UDP-N-acetylglucosamine 3-O-acyltransferase (LpxA, gene size 786 b.p.), *Mycobacterium bovis* tetrahydridipicolinate N-succinyltransferase (DapD, gene size 822 b.p.), streptogramin acetyltransferase from *Enterococcus faecium* (ValD, gene size: 624 b.p.), and N-acetylglucosamine-1-phosphate pyrophosphorylase (GlmU, gene size: 1368 b.p.). The latter four genes were obtained from Prof. Steven Roderick at the Albert Einstein College of Medicine, Bronx, NY.
8. Two plasmids (pET series) encoding full-length genes for *E. coli* integral membrane proteins, ammonia transport channel B (AmtB) in pET29b vector and aquaporin Z (AqpZ) in vector pET 28b vector were provided in Feb. 2008 by Dr. William Harries in the lab of Prof. Larry Miercke at the Membrane Protein Expression Center & Center for Structures of Membrane Proteins Macromolecular Structure Group, Biochemistry & Biophysics Department, University of California San Francisco (UCSF), San Francisco, CA.
9. Plasmid pSMGFP, cloning vector containing gene for soluble-modified green fluorescent protein mutant obtained from The Arabidopsis Biological Resource Center (ABRC) at The Ohio State University
10. Plasmid pBirAcm, an engineered pACYC184 plasmid with an IPTG inducible birA gene to over express the *E. coli* biotin ligase enzyme birA, obtained from Avidity, LLC, Denver, CO.

4. Vector(s) to be used. Include source.

Vectors to be used include pUC18, pUC19, pET15b, pET28a,b,c, pET29b, pET34, pET35b, pET37b, pET38b (purchased from Novagen, Madison, WI), pLEX, pLEX-lacZ, pFliTrx (purchased from Invitrogen, Carlsbad, CA), pGLO (pBAD-GFPuv), (purchased from Bio-Rad, Hercules, CA), pACA (T7-promotor vector obtained from Prof. Carol Fierke, Dept. of Chemistry, University of Michigan), pBirAcm, an engineered pACYC184 plasmid with an IPTG inducible birA gene, purchased from Avidity, LLC, Denver, CO, Cloning vector pSMGFP soluble-modified green fluorescent protein (smGFP) gene, purchased from The Arabidopsis Biological Resource Center (ABRC) at The Ohio State University, three vectors obtained from Prof. Robert Macnab, Dept. of Molecular Biophysics and Biochemistry, Yale University: pTH810 (fliC flagellin gene in pTrc99A), pTH890 (N-his tag fliC gene in pTrc99A vector) and pMM1501 (N-his tag fliC gene in pET19b vector), four vectors obtained from Doug Sheridan & Thomas R. Hughes, Yale University: pBNJ24.6, pBNJ26.3, pBNJ28.2, pBNJ37.2. Two vectors pRU1650 and pRU1651 (*Aquifex pyrophilus* FlaA flagellin gene fragments) were obtained from Prof. Dr. Rudiger Schmitt at the University of Regensburg, Germany. These gene fragments have been subcloned into the pTrc and pET8b expression plasmids for use in *E. coli*. Plasmid vectors

containing the other eleven human carbonic anhydrase genes are either pCMV-SPORT6, pOTB7 or pBlueScriptR and were obtained from Open Biosystems, Huntsville, AL.

5. Will an attempt be made to obtain expression of a foreign gene? ☒ Yes ☐ No

If so, what protein will be produced? Eubacterial *E. coli*, *Salmonella typhimurium*, and *Aquifex pyrophilus* wild-type, partially deleted flagellin proteins, and hybrids of flagellin and green fluorescent protein (GFP), including soluble-modified GFP, hybrids of *E. coli* thioredoxin and flagellin ("FitTrx"), the *E. coli* biotin ligase enzyme, BirA, hybrids of streptavidin and flagellin and hybrids of flagellin and mammalian (human) carbonic anhydrase isozymes will be expressed in both *E. coli* and *Salmonella typhimurium*. Streptavidin, archaeal carbonic anhydrase, acyltransferase enzymes including Cam, LpxA, DapD, GlnU, and Val(D), and membrane proteins AmtB and AqpZ will also be expressed as soluble proteins in *E. coli*. CA II and other previously described isozymes of human carbonic anhydrases CA I, CA III, CA IV, CA VB, CA VII, CA IX, CA X, CA XI, CA XII, CA XIII, CA XIV will be cloned into pET vectors and expressed in *E. coli* for use as controls in flagellin fusion-protein experiments and in catalytic engineering of flagellin. It is anticipated that several integral membrane proteins from *E. coli*, AmtB and aquaporin, will also be expressed in suitable *E. coli* expression strains for preliminary experiments for future proposal resubmission.

Statements of Certification

I certify that I have read and understood the *Western Michigan University Policy for Recombinant DNA Biosafety* including the description of my role and responsibilities as Principal Investigator on this project. I agree to abide by the *Guidelines for Research Involving Recombinant DNA Molecules (NIH Guidelines)* in conducting all work using recombinant DNA molecules.

 1-28-2010
Principal Investigator Signature Date

I have read the description of this proposed research involving recombinant DNA molecules. I have determined that the facilities and procedures proposed in this project registration form are adequate for the safe conduct of this research and the safety of other personnel – faculty, staff, and visitors – using the facilities within which this research is to be conducted.

 29 Jan 10
Department Chair/Unit Head Signature Date

Submit the original plus 9 copies to the research compliance coordinator, 251W Walwood Hall, mailstop 5456. (Be sure to make and keep another copy for your files.) Contact the research compliance coordinator at 387-8293 for additional information.